Non-covalent Interactions in the Gas Phase: Infrared Spectroscopy and Nanocalorimetry of Ion-Biomolecule Complexes

by

Jeremy Thomas O'Brien

A dissertation submitted in partial satisfaction of the
requirements for the degree of
Doctor of Philosophy

in

Chemistry

in the

Graduate Division
of the
University of California, Berkeley

Committee in charge:

Professor Evan Williams, Chair
Professor Richard Mathies
Professor Robert Glaeser

Spring 2012

The dissertation of Jeremy Thomas O'Brien, titled Non-covalent Interactions in the Gas Phase: Infrared Spectroscopy and Nanocalorimetry of Ion-Biomolecule Complexes, is approved:

Chair Date

Date

Date

University of California, Berkeley

Non-covalent Interactions in the Gas Phase: Infrared Spectroscopy and Nanocalorimetry of Ion-Biomolecule Complexes

Abstract

Non-covalent Interactions in the Gas Phase: Infrared Spectroscopy and Nanocalorimetry of Ion-Biomolecule Complexes

by

Jeremy Thomas O'Brien
Doctor of Philosophy in Chemistry

University of California, Berkeley

Professor Evan Williams, Chair

In this dissertation, experiments investigating the effects of non-covalent interactions on the structure and reactivity of gas-phase, ion-containing clusters, including ion-amino acid and ion-water complexes, are presented and discussed. Ions generated using electrospray ionization and analyzed using Fourier transform ion cyclotron resonance mass spectrometers at the University of California, Berkeley, and the FOM Institute for Plasma Physics Rijnhuizen in Nieuwegein, The Netherlands, are investigated using infrared photodissociation/infrared multiple photon dissociation (IRPD/IRMPD) spectroscopy, collision-induced dissociation, and electron capture dissociation (ECD). Using ion nanocalorimetry, the effect of varying the potential which controls the kinetic energy of the thermally generated electrons used for ECD experiments is determined to be minimal under typical experimental conditions. The results indicate that only a small population of electrons with near zero velocity relative to the trapped hydrated ions are captured and result in the observed ECD products. IRMPD spectra of proton-bound heterodimers containing valine and basic amines indicate that the structure of the heterodimer changes with increasing basicity of the amine suggesting that the structure of an amino acid in a proton-bound dimer may be different than in isolation which breaks an assumption made in the determination of gas-phase basicities using the kinetic method. IRMPD spectra of ion-amino acid complexes reported here reveal the effects of gas-phase acidity, ion polarity/charge state and ion size on the relative zwitterionic stability of the amino acids. The coordination numbers (CN) of hydrated divalent transition metals are determined using IRPD spectroscopy and photodissociation kinetics measurements. The CN of Cu^{2+} is lower than the other metal ions (CN = 4) due to Jahn-Teller effects brought about by the d^9 electronic configuration of the ion. IRPD spectra of ${SO_4}^{2-}$ with up to 80 water molecules attached indicate that the structure induced by the dianion dominates over the intrinsic water-water interactions for clusters with up to 43 water molecules, well beyond the first solvation shell. The roles of ion charge state and cluster size in the structure of gas-phase "nanodrops" are investigated for the largest mass-selected ionic clusters for which IRPD spectra have been reported. Effects of ion charge state are observed for nanodrops containing up to ∼250 water molecules in contrast with recent reports that only the first solvation shell is affected by ions in aqueous solution.

For my family: my beautiful wife, Rachel, my parents Tony and Joan, and my brother Charlie

Contents

List of Figures

List of Tables

Acknowledgments

I would like to thank my advisor, Prof. Evan Williams, from whom I have learned much about how to conduct, present, and publish world-class research and whose guidance has been critical to my success and my growth as a scientist.

My wife, Rachel, has been an incredible support and source of joy throughout my time at Berkeley. She is a wonderfully creative person with an excellent scientific mind, and is a constant source of inspiration for me.

My parents, Tony and Joan O'Brien have my deepest gratitude and admiration for encouraging and supporting my academic pursuits over so many years and for helping me to seek out new experiences and to explore! I thank my brother, Charlie, for whose love, competitiveness, and faith in my abilities I am truly grateful.

I have had many colleagues and mentors during my time at Berkeley and their friendship, instruction, and scientific collaboration have been invaluable. In particular, I thank Dr. Matthew Bush for training me, introducing me to the wide variety of Berkeley cuisine, and for sharing his interests, both the scientific and the fun. Dr. Ryan Leib is an invaluable friend and colleague. We bonded over late nights, shared interests, and a passion for science. Dr. James Prell is a dear friend who has taught me more about science, language, math and music than I will ever learn. Most of this research is the result of a true collaboration with him, a sharing of inspiration, hard work, and insights. Also, I sincerely thank Dr. Andy Lemoff, Dr. Mariam ElNaggar, Dr. Alex Donald, Dr. Harry Sterling, Maria Demireva, Tawnya Flick, Terry Chang, Dr. Sam Merenbloom, Catherine Cassou, Dr. Anne Holm, Dr. Jeffrey Steill and Thiago Correra. I acknowledge the generous financial support from the National Science Foundation which made this research all possible.

I thank Prof. Peter Armentrout and Prof. Jos Oomens for their collaboration, helpful reviews, and insightful questions at conferences. I am grateful for the technical support and advice of Dr. Kathy Durkin, Phil Simon, and Eric Granlund. I also wish to acknowledge the many professors and teachers who have challenged and inspired me throughout the years. In particular, I thank Dr. Craig Herb, Prof. Demetrios Sarantites, Prof. George Pepe, and Mr. Robert Mitchell whose energy, drive and brilliance I will forever hold as an inspiration.

Finally, I would like to thank my dissertation committee members, Prof. Richard Mathies and Prof. Robert Glaeser.

Chapter 1

Introduction

1.1 Non-covalent Interactions: Bridging gas-phase to solution

Non-covalent interactions are ubiquitous and critical to biochemistry. The delicate balance of inter- and intramolecular interactions is crucial to protein folding, macromolecular assembly, and the effects of hydration on biomolecules. Ions, proteins and water molecules form complex and dynamic systems which are built up from components interacting though many individual, non-covalent interactions. Remarkable constructs are present in nature; ion channels mimic the hydration of specific ions to transport only those ions across cell membranes and some proteins drastically alter their structure when binding just a few metal ions. Our knowledge and understanding of these systems is gained through two general approaches; the observation and investigation of large-scale or macromolecular phenomena which can be simplified to fundamental interactions, and the study of the small-scale, fundamental interactions and phenomena which can then be built up to explain more complex systems.

This division in conceptual approach is mirrored by the division in experimental approach between solution-phase and gas-phase studies. In solutions, macromolecular properties such as solubility, visocisty, concentration, and chemical reactivity can be investigated in complex systems. Techniques such as liquid chromatography (LC), X-ray diffraction, gel electrophoresis, calorimetry, and UV/Vis spectroscopy are powerful tools for the investigation of biomolecules in solution. In the gas phase, molecular properties such as proton affinity, binding energies, ion mobility, and relative conformation energies are obtained for specific systems under highly controlled conditions. Mass spectrometry often plays a crucial role in the investigation of these properties; the capability to measure the mass-to-charge ratios (m/z) of ions produced in gas-phase experiments has opened many fields of study and can greatly enhance the chemical information gained from other techniques, such as gas chromatography, by providing the molecular masses. Mass spectrometry enables the detailed study of specific interactions isolated from the often complex conditions present in solution. However, a key challenge for many gas-phase studies is relating the results and conclusions determined from gas-phase experiments to the solution phase, where most biological interactions occur. A well established example of the differences between gas- and solution-phase behavior is the observation that in the gas phase, all naturally occurring amino acids, the building blocks of proteins, are nonzwitterionic, i.e. have no local charges. However in the solution phase, these amino acids are all zwitterionic with both a positive and a negative charge present within each molecule.

A promising route to the bridge needed to link these gas- and solution-phase results can be found in the investigation of hydrated clusters. Typically, ions generated from solution for detection using mass spectrometry are de-solvated to enable accurate determination of the m/z of the analyte of interest. Especially for mixtures, hydration can greatly complicate the interpretation of the resulting mass spectra. However, hydrated clusters represent a bridge between the gas and solution phases. Through investigation of biomolecules complexed with progressively more water molecules, the effects of hydration on the molecules of interest can be observed as a function of the cluster size until solution-phase behavior and characteristics

are obtained. Using mass spectrometry techniques to isolate the clusters of interest, the interactions of ions with water molecules can be observed in the absence of counter-ions which can complicate the interpretation of results and are always present in solution-phase experiments.

1.2 The Hofmeister Series

In the 1880's, Franz Hofmeister observed that salts affect the solubility of proteins and ordered a series of ions based on their tendency to precipitate hen-egg albumin in aqueous solutions.[1-3] This "Hofmeister series", which ranks how ions affect protein solubility, is remarkably reproducible for a wide variety of salts and proteins and has been observed for other chemical properties such as salt solubilities,[4] cloud points of nonionic surfactants,[5] and transport through ion channels.[6] Ions in the Hofmeister series are often referred to as 'chaotropes' (structure breakers) or 'kosmotropes' (structure makers) according to their tendency to increase or decrease aqueous protein solubility, respectively. A standard Hofmeister series is shown in Figure 1. Ammonium sulfate, a highly kosmotropic salt, has such a strong effect on protein solubility that it is commonly used in protein purification procedures.

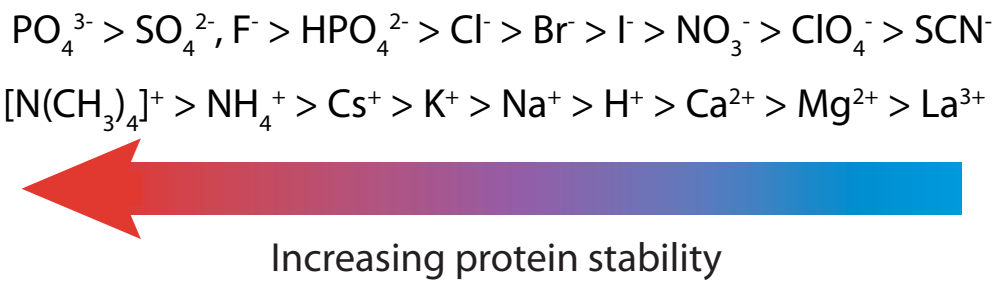

Figure 1.1: Typical Hofmeister Series Ions

Hofmeister series effects have been investigated using many methods including X-ray absorption spectroscopy,[7] nuclear magnetic resonance,[8] sum-frequency generation (SFG) spectroscopy,[9] computational chemistry,[10,11] and static vibrational spectroscopy.[11,12] Despite over 120 years of research subsequent to its discovery, the physical origin of the Hofmeister series is still debated.[4,7-20] Two classes of noncovalent interactions have been proposed to drive the ordering of the Hofmeister series; direct ion-protein interactions, and effects of ions on water structure. Results supporting direct ion-protein interactions[4,7-10,15] and effects of ions on solvent structure[11,16-19] have been reported, but no clear consensus has been reached as to what extent either of these effects are responsible for the Hofmeister series.

Results from static vibrational spectroscopy,[11,12] femtosecond IR spectroscopy,[21-24] and terahertz dielectric relaxation spectroscopy[23,24] indicate that ions do not strongly affect the hydrogen bond (H-bond) network of water beyond the first solvation shell for salt solutions with high ionic strengths (2-12 M). Bakker and co-workers have reported, based on water

reorientation dynamics, that ion-water interactions only extend beyond the first solvation shell in solutions where both ion and counterion are strongly hydrated (i.e. $MgSO_4$).[23,24] They suggest that the physical origin of the Hofmeister series is related to cooperative structure-making effects between ions and charges present on biomolecules.[24]

This concept of cooperative structure making effects is similar to the "Law of Matching Water Affinities" proposed by Collins and co-workers which states that oppositely charged ions with matching water affinities, i.e. chaotrope-chaotrope and kosmotrope-kosmotrope, will form contact ion pairs in solution whereas those with differing water affinities will tend to separate.[25] Based on X-ray diffraction and neutron scattering studies, which provide radial distribution functions of the distance between an ion and oxygen atoms, and size exclusion chromatography, which orders ions based on the time required to pass through a size-exclusion column, Collins concludes that "weakly" hydrated ions only affect water molecules in the first solvation shell and that "strongly" hydrated ions affect the first solvation shell and some water molecules in the second shell of the ion. Hofmeister effects on proteins are reported to arise from the direct interaction of anions with water molecules in the second solvation shell of proteins.[25] Anions with high water affinity reduce the availability of water molecules to solvate the protein stabilizing the protein and encouraging it to crystallize or precipitate.

The effects of salts on water structure at aqueous interfaces have also been linked to the Hofmeister series due to the large dielectric difference at both the liquid-vapor and the protein-water interfaces.[16] Sum frequency generation (SFG) spectroscopy is a second-order optical technique and is sensitive to the structure of the first few layers of water molecules at the liquid-vapor interface. Linear spectroscopies have poor sensitivity to surface water molecules due to the overwhelming signal from the bulk. Results from SFG,[26,27] electrospray ionization,[20] and molecular dynamics simulations[28] indicate that some ions including Br^- and I^- are highly surface active,[26,28] whereas other ions, including Cl^- [26] and SO_4^{2-},[27] have lower surface activity, suggesting that the ranking for ion surface activities is similar to the Hofmeister series.

The effects of ions on water structure are very important to the debate over the physical origins of the Hofmeister series and solution phase studies are complicated by the presence of counterions and the high concentrations necessary to perform the experiments. This is an ideal challenge for gas-phase studies of hydrated clusters which enable the detailed analysis of the effects of ions on solvating water molecules.

1.3 Gas-Phase Ion Structures Obtained with Infrared Photodissociation Spectroscopy

Infrared absorption spectra provide direct information about the vibrational modes of ions and molecules which can be related to their structures. The frequency and absorption cross-section of infrared-active vibrational modes, particularly OH and NH bending and stretching modes, are highly sensitive to differences in ion structure. The density of ions in gas-phase experiments is typically too low for IR absorption spectroscopy with current

detection techniques due to the electrostatic repulsion between the charges on each ion. Infrared photodissociation (IRPD) spectroscopy is an action spectroscopy where vibrational modes of the precursor ions are excited by IR photons and this absorption is observed from the dissociation of the precursor ions, i.e. photodissociation. Photodissociation occurs if enough photons are absorbed to cause dissociation before the photons can be re-emitted. The rate of photodissociation is much faster when the photon energy is resonant with vibrational modes of the ion complex. Using tunable IR lasers, photodissociation rates can be measured across a range of photon energies. With sufficiently low laser power, the absorption of two or more photons simultaneously becomes improbable and photons may be absorbed sequentially such that each photon's energy is statistically redistributed throughout the ion complex resulting in slow heating.

Under typical experimental conditions, the absorption of the first photon is the rate-limiting step in the photodissociation process and the rate of photodissociation depends linearly on laser power. For ion complexes whose structure, and therefore absorption spectrum, do not change significantly with heating, the IRPD spectrum obtained by plotting the photodissociation rate versus photon energy is similar to an infrared absorption spectrum. If absorption of multiple photons is necessary to produce measureable photodissociation, this technique is called "infrared multiple photon dissociation (IRMPD) spectroscopy."

1.4 Amino Acids and Peptide-Ion Complexes

IR(M)PD spectroscopy is a powerful tool for understanding ion-protein and ion water interactions because the vibrational resonances of many functional groups are highly sensitive to their chemical environment. Hydrogen stretching modes (OH, NH), bending vibrations (OH, NH, and CH), and the carbonyl stretches of carboxylic acid and carboxylate groups are IR-active and provide significant structural information. OH and NH stretching modes occur at relatively high energies ($\sim$3600 – 3750 cm^{-1}, and $\sim$3300 – 3500 cm^{-1}, respectively) when not donating a hydrogen bond, but can shift to significantly lower energies, as low as 840 cm^{-1},[29] when part of a shared proton bond, also called an ionic hydrogen bond. Smaller red shifts can occur for these modes either when donating a non-ionic hydrogen bond or due to Stark shifts resulting from alignment of the vibrational mode with the electric field of local charges. The frequency of the stretching mode of the hydroxyl group of a carboxylic acid depends on the conformation of the acid. Also, the carbonyl stretch of a carboxylic acid group occurs at a higher frequency ($\sim$1750 cm^{-1}) than the symmetric and asymmetric carbonyl stretches of a carboxylate group ($\sim$1450 and 1625 cm^{-1}, respectively). This difference is particularly useful in determining if cationized/anionized amino acids and peptides adopt predominantly zwitterionic (carboxylate) or nonzwitterionic (carboxylic acid) structures in the gas phase.

The interactions of metal cations with amino acids and peptides, the building blocks of proteins, have been extensively investigated using IR(M)PD spectroscopy.[30-51] IR(M)PD spectra have been reported for amino acids complexed with mono-,[32-51] di-, [30,31,41-44] and even trivalent cations. In isolation in the gas phase, all naturally occurring amino acids are nonzwitterionic, but the zwitterionic form can be preferentially stabilized by the addition of a metal cation. Effects of metal ion size,[32-38,42-47] charge state, [30,31,41-44,52] amino acid

basicity/acidity,[32-34,44,53-57] and peptide length/sequence on the relative stability of zwitterionic structures have been studied extensively. These studies indicate that for some amino acids, zwitterionic structures are preferentially stabilized with increasing metal ion size,[36-38,42,45] higher charge state,[30,31,42,44] and with increasing amino acid basicity,[32-34,44,53-57] although other factors can compete to stabilize nonzwitterionic forms.[33,34,56] Trp,[31] His,[42] Arg, Gln, Pro, Ser, Val,[30] and Glu[44] complexed with Ba^{2+} are zwitterionic, but nonzwitterionic structures have been reported for some doubly charged complexes, including His•Ca^{2+}[42] and Asn•Ba^{2+}.[43]

In contrast to results for cations, much less is known about anion interactions with amino acids and peptides and whether anions can stabilize zwitterionic structures. Attachment of an excess electron has been reported to stabilize the zwitterionic form of Arg[58,59] and complexes of oxalic and malonic acid dianions with the zwitterionic glycine were each found to be metastable with relatively low barriers to dissociation, based on computational modelling.[60] IRMPD spectra of deprotonated amino acids (Asp, Cys, Glu, Phe, Ser, Trp, and Tyr) have been reported and the spectra show only bands corresponding to carboxylate stretching modes.[61] For Glu and Asp, the IRMPD spectra have very broad, poorly resolved bands which are attributed to the sharing of a proton between the side chain and C-terminal carboxylate groups. In Chapter 5, IRMPD spectra for Glu•X-, His•X-, and Arg•X-, where X = Cl, Br, or I, are reported and these spectra clearly indicate that the nonzwitterionic form of the amino acid is dominant for Glu•X- and His•X-, but that Arg is zwitterionic in these complexes.

Similarly, the zwitterionic forms of some amino acids can be preferentially stabilized when attached to other protonated molecules. For example, the zwitterionic forms of Arg and Pro are more stable than the nonzwitterionic form when proton-bound to another Arg[62,63] or Pro[64] molecule, respectively, but Gly is nonzwitterionic when in a protonated dimer.[62-67] This can create complications in the investigation of certain physical properties of amino acids, such as proton affinities or gas-phase basicities, which involve formation of protonated dimers,[68-70] because the form of an amino acid present in the dimer can be different than in isolation. In Chapter 3, we investigate the role of gas-phase basicity on the structure of protonated heterodimers containing Val and a series of primary and secondary amine bases using IRMPD spectroscopy and theory.

1.5 Hydrated Ion Clusters

Gas-phase studies of hydrated ion clusters have the advantage that the effects of a single ion or electron on water structure can be investigated as a function of hydration extent for up to hundreds of water molecules attached,[71-74] and any competing effects of counterions can be eliminated. The structures of many hydrates of small mono-[19,74-93], di-[18,19,90-100] and tri-valent[19,71,101] ions have been investigated using IRPD spectroscopy. The hydrogen-stretch region (2300 – 4000 cm^{-1}) is especially useful for investigating how ions affect water structure because the frequencies of OH stretching modes are very sensitive to their H-bonding environment. Water structure investigated as a function of cluster size can provide evidence for the formation of hydration shells or other uniquely stable structures, such as

clathrates, for some ion-containing water clusters. For example, IRPD spectra of hydrated Ca^{2+} indicates that the coordination number (CN) of Ca^{2+}, or the number of water molecules in the first hydration shell, increases from ∼6 at smaller cluster size to ∼8 for clusters with a least a partial second solvation shell.[95,97] The larger CN is consistent with the range of values reported for bulk aqueous Ca^{2+}. As the cluster size increases, the IRPD spectra of $Ca^{2+}(H_2O)_n$, n = 11 - 69, become more like the infrared spectrum of bulk water suggesting that the hydrogen bonding environment of the interior water molecules is approaching that of bulk water.[97] These results demonstrate the development of solution phase ion properties with increasing hydration state. For Cu^{2+}, it is widely assumed that the metal ion has a CN of six, however coordination numbers ranging from 4 to 6 have been indicated from results of solution phase studies.[102-107] Hydration of Cu^{2+} is especially interesting because the d^9 electronic configuration results in Jahn-Teller distortion characterized by two elongated axial bonds in octahedral structures. There may be no clearly preferred structure, but rather rapidly interconverting structures that have coordination numbers ranging from 4 to 6.[102] In Chapters 6 and 7, the CN's of Cu^{2+}, Fe^{2+}, Co^{2+}, Mn^{2+}, Ni^{2+}, and Zn^{2+} are investigated using IRPD spectroscopy of hydrated metal ion clusters.

IRPD spectra of small hydrated ion clusters[76-100] indicate that many ions can have strong effects on the structure of water molecules in the first solvation shell. However, for some ions, such as tetramethylammonium[75] and Cs^+,[80] water-water hydrogen bonding is favored over ion-water interactions even at small cluster size and these ions have little effect on the hydration structure. IRPD spectra of seventeen different hydrated ions with charge states between -1 and +3 at fixed cluster size (35 – 37 water molecules) show spectral differences attributable to various extents of ion-induced patterning of the water network, providing further evidence of long-range ion effects on hydration structure.[19]

Ion polarity can play a key role in the structure of solvating water molecules. Cations tend to pattern adjacent water molecules so that the OH groups point away from the ion whereas for anions, the H atoms generally interact with the anion or oxygen atoms of other water molecules so that the OH groups point inwards, or are at least tangent to the ion. This difference in water orientation can result in significant differences between the IRPD spectra of cations and anions, especially in the free-OH spectral region. A free OH-band occurs for cations at all cluster sizes. In contrast, there is no free-OH band for many smaller hydrated anion clusters, including I^-, Cl^-, and Br^- with three water molecules and SO_4^{2-} with up to at least 14 water molecules.[83,96,108] Many water molecules at the surface of bulk solutions have free-OH groups and so a benchmark for the extent of water patterning is at what size does the surface of hydrated anion clusters show free-OH groups. In Chapters 8 and 9, using IRPD spectroscopy, we investigate the hydration structure of $SO_4^{2-}(H_2O)_n$ with up to 80 water molecules attached and compare the IRPD spectra of hydrated ions with charge states between 2- and 3+ at large cluster size, ∼250 water molecules attached.

1.6 Ion Nanocalorimetry

Mass spectrometry is generally well suited for measuring thermodynamics of endothermic reactions because known quantities of energy can be deposited into a gas-phase ion under

controlled conditions using photons or collisions until dissociation is observed. However, measurements of exothermic processes can be far more challenging because the abundance and identity of the products of the reaction do not inherently provide information regarding amount of energy released during the reaction. Using bulk systems, the thermodynamics of exothermic reactions can be measured using a technique called calorimetry where the energy released by a reaction is measured indirectly by a well-characterized endothermic process, such as heating a water bath. An analog of this technique exists for the gas phase where the extent of energy deposition can be measured using "chemical thermometers" which are ions that have fragmentation pathways with known activation energies and entropies. For example, the appearance energies for fragments of $Fe(CO)_5^{+\bullet}$ are known, and occur with similar entropies so that the quantity of internal energy deposited is directly reflected by the fragment ion abundances and has been used to measure the energy deposition of collision induced dissociation and surface induced dissociation.[109]

Recently, hydrated cluster ions have been demonstrated as excellent "nanocalorimeters" that can be used to measure the internal energy deposited into these ions upon activation by the capture of a free electron[44,71,73,110-115] or by absorption of a photon.[116,117] After ion activation, water molecules evaporate from the ion cluster until the energy of the reaction has been dissipated. The number of water molecules that evaporate provide a measurement of the thermodynamics of the reaction and can be calibrated directly using photons of known energy or indirectly using binding energy measurements or modeled values. Ion nanocalorimetry has been used to obtain thermodynamic information previously considered experimentally unobtainable such as the value of the absolute standard hydrogen electrode potential[44,114,115] and the absolute solvation free energy and enthalpy of the proton.[71,112,115] Many factors contribute to the ultimate accuracy of the nanocalorimetry technique and for ion activation by capture of a free electron, two important factors are the effects of the electron kinetic energy and ion-electron inelastic collisions. In Chapter 1, we investigate the effects of electron kinetic energy and the role of inelastic ion-electron collisions on the internal energy deposited into hydrated ion clusters as measured by ion nanocalorimetry.

1.7 References

(1) Hofmeister, F. *Arch. Exp. Pathol. Pharmacol.* **1888**, *25*, 1-30.

(2) Hofmeister, F. *Arch. Exp. Pathol. Pharmacol.* **1887**, *24*, 247-260.

(3) Kunz, W.; Henle, J.; Ninham, B. W. *Curr. Opin. Colloid Interface Sci.* **2004**, *9*, 19-37.

(4) Collins, K. D. *Biophys. J.* **1997**, *72*, 65-76.

(5) Schott, H. *J. Colloid Interface Sci.* **1973**, *43*, 150-155.

(6) Grigorjev, P. A.; Bezrukov, S. M. *Biophys. J.* **1994**, *67*, 2265-2271.

(7) Uejio, J. S.; Schwartz, C. P.; Duffin, A. M.; Drisdell, W. S.; Cohen, R. C.; Saykally, R. J. *Proc. Natl. Acad. Sci. U. S. A.* **2008**, *105*, 6809-6812.

(8) Freire, M. G.; Neves, C. M. S. S.; Silva, A. M. S.; Santos, L. M. N. B. F.; Marrucho, I. M.; Rebelo, L. P. N.; Shah, J. K.; Maginn, E. J.; Coutinho, J. A. P. *J. Phys. Chem. B* **2010**, *114*, 2004-2014.

(9) Chen, X.; Yang, T.; Kataoka, S.; Cremer, P. S. *J. Am. Chem. Soc.* **2007**, *129*, 12272-12279.

(10) Algaer, E. A.; van der Vegt, N. F. A. *J. Phys. Chem. B* **2011**, *115*, 13781-13787.

(11) Smith, J. D.; Saykally, R. J.; Geissler, P. L. *J. Am. Chem. Soc.* **2007**, *129*, 13847-13856.

(12) Lin, Y. S.; Auer, B. M.; Skinner, J. L. *J. Chem. Phys.* **2009**, *131*, 144511.

(13) Baldwin, R. L. *Biophys. J.* **1996**, *71*, 2056-2063.

(14) Cacace, M. G.; Landau, E. M.; Ramsden, J. J. *Q. Rev. Biophys.* **1997**, *30*, 241-277.

(15) Collins, K. D. *Methods* **2004**, *34*, 300-311.

(16) Pegram, L. M.; Record, M. T. *J. Phys. Chem. B* **2007**, *111*, 5411-5417.

(17) Flick, T. G.; Merenbloom, S. I.; Williams, E. R. *J. Am. Soc. Mass Spectrom.* **2011**, *22*, 1968-1977.

(18) O'Brien, J. T.; Prell, J. S.; Bush, M. F.; Williams, E. R. *J. Am. Chem. Soc.* **2010**, *132*, 8248-8249.

(19) Prell, J. S.; O'Brien, J. T.; Williams, E. R. *J. Am. Chem. Soc.* **2011**, *133*, 4810-4818.

(20) Cheng, J.; Vecitis, C. D.; Hoffmann, M. R.; Colussi, A. J. *J. Phys. Chem. B* **2006**, *110*, 25598-25602.

(21) Omta, A. W.; Kropman, M. F.; Woutersen, S.; Bakker, H. J. *J. Chem. Phys.* **2003**, *119*, 12457-12461.

(22) Omta, A. W.; Kropman, M. F.; Woutersen, S.; Bakker, H. J. *Science* **2003**, *301*, 347-349.

(23) Tielrooij, K. J.; Garcia-Araez, N.; Bonn, M.; Bakker, H. J. *Science* **2010**, *328*, 1006-1009.

(24) Tielrooij, K. J.; van der Post, S. T.; Hunger, J.; Bonn, M.; Bakker, H. J. *J. Phys. Chem. B* **2011**, *115*, 12638-12647.

(25) Collins, K. D.; Neilson, G. W.; Enderby, J. E. *Biophys. Chem.* **2007**, *128*, 95-104.

(26) Liu, D. F.; Ma, G.; Levering, L. M.; Allen, H. C. *J. Phys. Chem. B* **2004**, *108*, 2252-2260.

(27) Gopalakrishnan, S.; Jungwirth, P.; Tobias, D. J.; Allen, H. C. *J. Phys. Chem. B* **2005**, *109*, 8861-8872.

(28) Jungwirth, P. *Faraday Discuss.* **2009**, *141*, 9-30.

(29) Roscioli, J. R.; McCunn, L. R.; Johnson, M. A. *Science* **2007**, *316*, 249-254.

(30) Bush, M. F.; Oomens, J.; Saykally, R. J.; Williams, E. R. *J. Am. Chem. Soc.* **2008**, *130*, 6463-6471.

(31) Dunbar, R. C.; Polfer, N. C.; Oomens, J. *J. Am. Chem. Soc.* **2007**, *129*, 14562-14563.

(32) Bush, M. F.; Forbes, M. W.; Jockusch, R. A.; Oomens, J.; Polfer, N. C.; Saykally, R. J.; Williams, E. R. *J. Phys. Chem. A* **2007**, *111*, 7753-7760.

(33) Bush, M. F.; Oomens, J.; Saykally, R. J.; Williams, E. R. *J. Phys. Chem. A* **2008**, *112*, 8578-8584.

(34) Bush, M. F.; Oomens, J.; Williams, E. R. *J. Phys. Chem. A* **2009**, *113*, 431-438.

(35) Armentrout, P. B.; Armentrout, E. I.; Clark, A. A.; Cooper, T. E.; Stennett, E. M. S.; Carl, D. R. *J. Phys. Chem. B* **2010**, *114*, 3927-3937.

(36) Armentrout, P. B.; Rodgers, M. T.; Oomens, J.; Steill, J. D. *J. Phys. Chem. A* **2008**, *112*, 2248-2257.

(37) Bush, M. F.; O'Brien, J. T.; Prell, J. S.; Saykally, R. J.; Williams, E. R. *J. Am. Chem. Soc.* **2007**, *129*, 1612-1622.

(38) Carl, D. R.; Cooper, T. E.; Oomens, J.; Steill, J. D.; Armentrout, P. B. *Phys. Chem. Chem. Phys.* **2010**, *12*, 3384-3398.

(39) Drayss, M. K.; Blunk, D.; Oomens, J.; Gao, B.; Wyttenbach, T.; Bowers, M. T.; Schäfer, M. *J. Phys. Chem. A* **2009**, *113*, 9543-9550.

(40) Drayss, M. K.; Blunk, D.; Oomens, J.; Schäfer, M. *J. Phys. Chem. A* **2008**, *112*, 11972-11974.

(41) Polfer, N. C.; Oomens, J.; Moore, D. T.; von Helden, G.; Meijer, G.; Dunbar, R. C. *J. Am. Chem. Soc.* **2006**, *128*, 517-525.

(42) Dunbar, R. C.; Hopkinson, A. C.; Oomens, J.; Siu, C. K.; Siu, K. W. M.; Steill, J. D.; Verkerk, U. H.; Zhao, J. F. *J. Phys. Chem. B* **2009**, *113*, 10403-10408.

(43) Heaton, A. L.; Bowman, V. N.; Oomens, J.; Steill, J. D.; Armentrout, P. B. *J. Phys. Chem. A* **2009**, *113*, 5519-5530.

(44) Donald, W. A.; Leib, R. D.; O'Brien, J. T.; Bush, M. F.; Williams, E. R. *J. Am. Chem. Soc.* **2008**, *130*, 3371-3381.

(45) Forbes, M. W.; Bush, M. F.; Polfer, N. C.; Oomens, J.; Dunbar, R. C.; Williams, E. R.; Jockusch, R. A. *J. Phys. Chem. A* **2007**, *111*, 11759-11770.

(46) Polfer, N. C.; Oomens, J.; Dunbar, R. C. *Phys. Chem. Chem. Phys.* **2006**, *8*, 2744-2751.

(47) Rodgers, M. T.; Armentrout, P. B.; Oomens, J.; Steill, J. D. *J. Phys. Chem. A* **2008**, *112*, 2258-2267.

(48) Kamariotis, A.; Boyarkin, O. V.; Mercier, S. R.; Beck, R. D.; Bush, M. F.; Williams, E. R.; Rizzo, T. R. *J. Am. Chem. Soc.* **2006**, *128*, 905-916.

(49) Kapota, C.; Lemaire, J.; Maitre, P.; Ohanessian, G. *J. Am. Chem. Soc.* **2004**, *126*, 1836-1842.

(50) Polfer, N. C.; Oomens, J.; Dunbar, R. C. *Chemphyschem* **2008**, *9*, 579-589.

(51) Polfer, N. C.; Paizs, B.; Snoek, L. C.; Compagnon, I.; Suhai, S.; Meijer, G.; von Helden, G.; Oomens, J. *J. Am. Chem. Soc.* **2005**, *127*, 8571-8579.

(52) Prell, J. S.; Flick, T. G.; Oomens, J.; Berden, G.; Williams, E. R. *J. Phys. Chem. A* **2010**, *114*, 854-860.

(53) Prell, J. S.; O'Brien, J. T.; Steill, J. D.; Oomens, J.; Williams, E. R. *J. Am. Chem. Soc.* **2009**, *131*, 11442-11449.

(54) Prell, J. S.; Demireva, M.; Oomens, J.; Williams, E. R. *J. Am. Chem. Soc.* **2009**, *131*, 1232-1242.

(55) Wyttenbach, T.; Witt, M.; Bowers, M. T. *J. Am. Chem. Soc.* **2000**, *122*, 3458-3464.

(56) Julian, R. R.; Jarrold, M. F. *J. Phys. Chem. A* **2004**, *108*, 10861-10864.

(57) Lemoff, A. S.; Bush, M. F.; Williams, E. R. *J. Am. Chem. Soc.* **2003**, *125*, 13576-13584.

(58) Skurski, P.; Rak, J.; Simons, J.; Gutowski, M. *J. Am. Chem. Soc.* **2001**, *123*, 11073-11074.

(59) Xu, S. J.; Zheng, W. J.; Radisic, D.; Bowen, K. H. *J. Chem. Phys.* **2005**, *122*, 091103.

(60) Kass, S. R. *J. Am. Chem. Soc.* **2005**, *127*, 13098-13099.

(61) Oomens, J.; Steill, J. D.; Redlich, B. *J. Am. Chem. Soc.* **2009**, *131*, 4310-4319.

(62) Price, W. D.; Jockusch, R. A.; Williams, E. R. *J. Am. Chem. Soc.* **1997**, *119*, 11988-11989.

(63) Strittmatter, E. F.; Williams, E. R. *J. Phys. Chem. A* **2000**, *104*, 6069-6076.

(64) Wu, R. H.; McMahon, T. B. *J. Am. Chem. Soc.* **2007**, *129*, 4864-4865.

(65) Rajabi, K.; Fridgen, T. D. *J. Phys. Chem. A* **2008**, *112*, 23-30.

(66) Raspopov, S. A.; McMahon, T. B. *J. Mass Spectrom.* **2005**, *40*, 1536-1545.

(67) Oh, H. B.; Lin, C.; Hwang, H. Y.; Zhai, H. L.; Breuker, K.; Zabrouskov, V.; Carpenter, B. K.; McLafferty, F. W. *J. Am. Chem. Soc.* **2005**, *127*, 4076-4083.

(68) McLuckey, S. A.; Cameron, D.; Cooks, R. G. *J. Am. Chem. Soc.* **1981**, *103*, 1313-1317.

(69) McLuckey, S. A.; Cooks, R. G.; Fulford, J. E. *Int. J. Mass Spectrom. Ion Processes* **1983**, *52*, 165-174.

(70) Cooks, R. G.; Wong, P. S. H. *Acc. Chem. Res.* **1998**, *31*, 379-386.

(71) Donald, W. A.; Leib, R. D.; Demireva, M.; O'Brien, J. T.; Prell, J. S.; Williams, E. R. *J. Am. Chem. Soc.* **2009**, *131*, 13328-13337.

(72) Griffin, G. B.; Young, R. M.; Ehrler, O. T.; Neumark, D. M. *J. Chem. Phys.* **2009**, *131*, 194302.

(73) Donald, W. A.; Leib, R. D.; Demireva, M.; Negru, B.; Neumark, D. M.; Williams, E. R. *J. Phys. Chem. A* **2011**, *115*, 2-12.

(74) Mizuse, K.; Mikami, N.; Fujii, A. *Angew. Chem.-Int. Edit.* **2010**, *49*, 10119-10122.

(75) Prell, J. S.; Williams, E. R. *J. Am. Chem. Soc.* **2009**, *131*, 4110-4119.

(76) Chang, H. C.; Wang, Y. S.; Lee, Y. T. *Int. J. Mass Spectrom.* **1998**, *180*, 91-102.

(77) Choi, J. H.; Kuwata, K. T.; Cao, Y. B.; Okumura, M. *J. Phys. Chem. A* **1998**, *102*, 503-507.

(78) Headrick, J. M.; Diken, E. G.; Walters, R. S.; Hammer, N. I.; Christie, R. A.; Cui, J.; Myshakin, E. M.; Duncan, M. A.; Johnson, M. A.; Jordan, K. D. *Science* **2005**, *308*, 1765-1769.

(79) Iino, T.; Ohashi, K.; Inoue, K.; Judai, K.; Nishi, N.; Sekiya, H. *J. Chem. Phys.* **2007**, *126*, 194302.

(80) Miller, D. J.; Lisy, J. M. *J. Am. Chem. Soc.* **2008**, *130*, 15381-15392.

(81) Miyazaki, M.; Fujii, A.; Ebata, T.; Mikami, N. *Science* **2004**, *304*, 1134-1137.

(82) Nicely, A. L.; Miller, D. J.; Lisy, J. M. *J. Mol. Spectrosc.* **2009**, *257*, 157-163.

(83) Robertson, W. H.; Johnson, M. A. *Annu. Rev. Phys. Chem.* **2003**, *54*, 173-213.

(84) Shin, J. W.; Hammer, N. I.; Diken, E. G.; Johnson, M. A.; Walters, R. S.; Jaeger, T. D.; Duncan, M. A.; Christie, R. A.; Jordan, K. D. *Science* **2004**, *304*, 1137-1140.

(85) Walters, R. S.; Pillai, E. D.; Duncan, M. A. *J. Am. Chem. Soc.* **2005**, *127*, 16599-16610.

(86) Ayotte, P.; Bailey, C. G.; Weddle, G. H.; Johnson, M. A. *J. Phys. Chem. A* **1998**, *102*, 3067-3071.

(87) Ayotte, P.; Weddle, G. H.; Bailey, C. G.; Johnson, M. A.; Vila, F.; Jordan, K. D. *J. Chem. Phys.* **1999**, *110*, 6268-6277.

(88) Beck, J. P.; Lisy, J. M. *J. Chem. Phys.* **2011**, *135*, 044302.

(89) Cabarcos, O. M.; Weinheimer, C. J.; Lisy, J. M.; Xantheas, S. S. *J. Chem. Phys.* **1999**, *110*, 5-8.

(90) Bandyopadhyay, B.; Duncan, M. A. *Chem. Phys. Lett.* **2012**, *530*, 10-15.

(91) Carnegie, P. D.; Bandyopadhyay, B.; Duncan, M. A. *J. Phys. Chem. A* **2008**, *112*, 6237-6243.

(92) Carnegie, P. D.; Bandyopadhyay, B.; Duncan, M. A. *J. Chem. Phys.* **2011**, *134*, 014302.

(93) Carnegie, P. D.; Bandyopadhyay, B.; Duncan, M. A. *J. Phys. Chem. A* **2011**, *115*, 7602-7609.

(94) Bush, M. F.; O'Brien, J. T.; Prell, J. S.; Wu, C. C.; Saykally, R. J.; Williams, E. R. *J. Am. Chem. Soc.* **2009**, *131*, 13270-13277.

(95) Bush, M. F.; Saykally, R. J.; Williams, E. R. *ChemPhysChem* **2007**, *8*, 2245-2253.

(96) Bush, M. F.; Saykally, R. J.; Williams, E. R. *J. Am. Chem. Soc.* **2007**, *129*, 2220-2221.

(97) Bush, M. F.; Saykally, R. J.; Williams, E. R. *J. Am. Chem. Soc.* **2008**, *130*, 15482-15489.

(98) Cooper, T. E.; O'Brien, J. T.; Williams, E. R.; Armentrout, P. B. *J. Phys. Chem. A* **2010**, *114*, 12646-12655.

(99) O'Brien, J. T.; Williams, E. R. *J. Phys. Chem. A* **2008**, *112*, 5893-5901.

(100) O'Brien, J. T.; Williams, E. R. *J. Phys. Chem. A* **2011**, *115*, 14612-14619.

(101) Bush, M. F.; Saykally, R. J.; Williams, E. R. *J. Am. Chem. Soc.* **2008**, *130*, 9122-9128.

(102) Chaboy, J.; Muñoz-PÁez, A.; Merkling, P. J.; Marcos, E. S. *J. Chem. Phys.* **2006**, *124*, 064509.

(103) Garcia, J.; Benfatto, M.; Natoli, C. R.; Bianconi, A.; Fontaine, A.; Tolentino, H. *Chem. Phys.* **1989**, *132*, 295-307.

(104) Frank, P.; Benfatto, M.; Szilagyi, R. K.; D'Angelo, P.; Della Longa, S.; Hodgson, K. O. *Inorg. Chem.* **2005**, *44*, 1922-1933.

(105) Beagley, B.; Eriksson, A.; Lindgren, J.; Persson, I.; Pettersson, L. G. M.; Sandström, M.; Wahlgren, U.; White, E. W. *J. Phys.: Condens. Matter* **1989**, *1*, 2395-2408.

(106) Salmon, P. S.; Neilson, G. W. *J. Phys.: Condens. Matter* **1989**, *1*, 5291-5295.

(107) Pasquarello, A.; Petri, I.; Salmon, P. S.; Parisel, O.; Car, R.; Tóth, E.; Powell, D. H.; Fischer, H. E.; Helm, L.; Merbach, A. E. *Science* **2001**, *291*, 856-859.

(108) Zhou, J.; Santambrogio, G.; Brummer, M.; Moore, D. T.; Meijer, G.; Neumark, D. M.; Asmis, K. R. *J. Chem. Phys.* **2006**, *125*, 111102.

(109) Dekrey, M. J.; Kenttamaa, H. I.; Wysocki, V. H.; Cooks, R. G. *Org. Mass Spectrom.* **1986**, *21*, 193-195.

(110) Donald, W. A.; Demireva, M.; Leib, R. D.; Aiken, M. J.; Williams, E. R. *J. Am. Chem. Soc.* **2010**, *132*, 4633-4640.

(111) Donald, W. A.; Leib, R. D.; O'Brien, J. T.; Holm, A. I. S.; Williams, E. R. *Proc. Natl. Acad. Sci. U. S. A.* **2008**, *105*, 18102-18107.

(112) Donald, W. A.; Williams, E. R. *J. Phys. Chem. B* **2010**, *114*, 13189-13200.

(113) Donald, W. A.; Williams, E. R. *J. Am. Soc. Mass Spectrom.* **2010**, *21*, 615-625.

(114) Donald, W. A.; Williams, E. R. *Pure and Appl. Chem.* **2011**, *83*, 2129-2151.

(115) Donald, W. A.; Leib, R. D.; O'Brien, J. T.; Williams, E. R. *Chem. Eur. J.* **2009**, *15*, 5926-5934.

(116) Donald, W. A.; Leib, R. D.; Demireva, M.; Negru, B.; Neumark, D. M.; Williams, E. R. *J. Am. Chem. Soc.* **2010**, *132*, 6904-6905.

(117) Donald, W. A.; Leib, R. D.; Demireva, M.; Williams, E. R. *J. Am. Chem. Soc.* **2011**, *133*, 18940-18949.

Chapter 2

Effects of Electron Kinetic Energy and Ion-Electron Inelastic Collisions in Electron Capture Dissociation Measured using Ion Nanocalorimetry

Jeremy T. O'Brien, James S. Prell, Anne I. S. Holm and Evan R. Williams

Journal of the American Chemical Society, 2010, 132, 8248–8249

2.1 Introduction

Capture of an electron by a multiply charged protein can result in extensive backbone fragmentation from which information about the sequence,[1–3] sites of posttranslational modifications[3–7] and even tertiary structure can be obtained.[2,8,9] Since the introduction of this electron capture dissociation (ECD) method by Zubarev and colleagues.[1] who combined thermally generated electrons with trapped ions in a Fourier-transform ion cyclotron resonance (FT/ICR) mass spectrometer, others have demonstrated that similar fragmentation pathways can be obtained when the electron is captured from an atom[10,11] or from molecular anions.[12,13] These methods provide a new route to obtain structural information from intact proteins and large peptides, making applications such as "top-down" proteomics[7] feasible.

Ion-electron recombination or electron capture (EC) is exothermic by a value corresponding to the recombination energy (RE).[14,15] This energy can partition into internal modes of the precursor ion and into translational, rotational, and vibrational modes of the dissociation products. The extent of internal energy deposition upon ion activation can be measured using "chemical thermometers," which are ions that have fragmentation pathways with known activation energies and entropies. For example, Cooks and coworkers used $Fe(CO)_5^{+\bullet}$ to compare the energy deposition of collision induced dissociation and surface induced dissociation.[16] The appearance energies for fragments of $Fe(CO)_5^{+\bullet}$ are known, and their formation occurs with similar entropies so that the internal energy deposition is directly reflected by the fragment ion abundances. A measure of the internal energy deposition into molecular ions of *n*-butylbenzene molecules can be obtained from the relative abundance of fragment ions at m/z 91 and 92.[17–19] The appearance potential of the former is higher, but so is the entropy, making it the favored process when more internal energy is deposited into the molecular ion. Rate constants can be measured using thermal activation methods, such as blackbody infrared radiative dissociation (BIRD),[20–23] and these values can be used to establish "effective" temperatures of ions activated by other methods.[20]

We recently demonstrated that hydrated cluster ions are ideal "nanocalorimeters" that can be used to accurately measure the internal energy deposited into these ions upon activation.[24–27] This nanocalorimetry method has been used to measure the internal energy deposited by EC with thermally generated electrons as a function of cluster size and cation identity.[24–27] For sufficiently large hydrated clusters containing divalent or trivalent ions, EC results in loss of multiple water molecules from the reduced precursor. For example, EC by $[Ru(NH_3)_6(H_2O)_{55}]^{3+}$ results in formation of $[Ru(NH_3)_6(H_2O)_n]^{2+}$, $n = 36$, 37 and 38, corresponding to the loss of 17 – 19 water molecules from the reduced precursor ion.[26]

For these large clusters, all the available recombination energy is deposited into internal modes of the ion and the dissociation is statistical. In contrast, dissociation of much smaller clusters in which loss of a hydrogen atom and water molecules occurs can be nonstatistical.[25]

For large clusters where the dissociation is statistical, the RE can be obtained from the average number of water molecules lost from the reduced precursor. To obtain the RE, the threshold dissociation energy for the loss of each water molecule from the reduced precursor must be known. Values for clusters of the size typically investigated have not been measured, but these values can be obtained from the Thomson liquid drop model.[28,29] Various implementations of this model have been recently evaluated by comparison to experimental data for both monovalent and divalent ions.[29] A recently introduced discrete implementation of the Thomson model that takes into account ion size appears to fit most experimental and quantum chemical data accurately.[29] Energy can also partition into translational, rotational, and vibrational modes of each water molecule that is lost and can be accounted for using a simple statistical model. A more detailed description about how RE values can be accurately obtained from the number of water molecules lost, including effect of energy partitioning, is presented elsewhere.[27]

Unlike some methods, such as photoionization spectroscopy, which can be used to obtain vertical ionization energies, the RE values obtained from this experiment are adiabatic values and correspond to the adiabatic ionization energy of the reduced precursor.[26,27] Although the initial electron capture may be a vertical process, solvent reorganization is fast (few picoseconds) compared with the time scale of these nanocalorimetry experiments (tens to hundreds of milliseconds). Energy released upon solvent reorganization will appear as internal energy in these clusters and is reflected by the number of water molecules that evaporate from the reduced clusters.

An emerging application of this nanocalorimetry method is measuring physical properties of ions in bulk solution that are difficult to obtain by other methods. For example, reduction potentials of red-ox active species in bulk solution are measured on a relative basis where the potential of one half-cell is measured relative to that of another. Such measurements result in a ladder of thermochemical values anchored to that of the standard hydrogen electrode, which is arbitrarily assigned a value of exactly 0 V. We have recently reported the use of our ion nanocalorimetry method to obtain absolute solution-phase reduction potentials.[26,27] By comparing these values to relative values measured in solution, an absolute value for the standard hydrogen potential of 4.2 $\pm$0.4 V is obtained.[27]

Many factors contribute to the ultimate accuracy of the nanocalorimetry method. Two important factors are the roles of the electron kinetic energy and ion-electron inelastic collisions on values of the RE obtained by ion nanocalorimetry. Here, we demonstrate that the internal energy deposited into hydrated clusters does not depend on the cathode voltage, which can be used to vary the electron kinetic energy, over the range of values typically used in an ECD experiment. In addition, we show that inelastic ion-electron collisions occur, but that these collisions do not significantly affect the internal energy deposition reported in these nanocalorimetry experiments under typical experimental conditions.

2.2 Experimental

Experiments were performed in a 2.75 Tesla FT/ICR mass spectrometer, equipped with a nanoelectrospray ion source,[30] a temperature controlled ion cell,[31] and a heated metal cathode.[25] (Figure 1). The cylindrical ion cell (10 cm long and 7 cm in diameter) consists of four copper mesh excite/detect plates separated from two beryllium-copper trapping plates by macor rings. The trapping plates are solid except for a central 1.0-cm hole and are wound with thin copper wire to ensure a uniform electric field across the hole. An oxygen-free copper jacket surrounds the cell and a controlled flow of liquid nitrogen is introduced into the copper jacket by means of a solenoid regulated by a temperature controller (Model No. CN-i3222, Omega Engineering, Inc., Stamford, CT, USA). The cell is allowed to equilibrate to a temperature of –140.0 ºC for at least 8 h before conducting these experiments.

The nanoelectrospray ion source, with which extensively hydrated ion clusters are generated, is described in detail elsewhere.[30] Briefly, borosilicate capillaries with tips pulled to an inner diameter of about1 μm are filled with 4 mM aqueous solution of calcium chloride (Fisher Scientific, Fair Lawn, NJ, USA). A platinum wire is placed in direct contact with the solution and held at a potential of about 450 V relative to the approximately 90 ºC heated metal capillary entrance to the mass spectrometer. Ions are guided through five stages of differential pumping and trapped in the ion cell. A 7-s pulse of nitrogen gas, which raises the cell pressure to about 5×10^{-7} Torr, is used to assist in trapping and thermalizing the ions. A mechanical shutter is closed at all other times to prevent additional ions from entering the cell. The trapped ions are allowed to reach a steady state internal energy distribution by exchange of photons with the blackbody radiation field inside the cell.[21–23] over a period of 8 s, during which time the cell pressure returns to $\sim10^{-8}$ Torr. Except where noted, the trapping plate potentials were held at 8.5 V (source side) and 9.5 V (far side) during ion accumulation, stepped down gradually during the 8-s delay to 2.0 V, and held at this potential for the remainder of the experimental sequence.

Clusters of interest are isolated using stored waveform inverse Fourier transforms (SWIFTs), followed by a 50 ms delay. This is followed by either electron irradiation or BIRD. Electrons are thermally generated using a 1.0 cm diameter barium scandate-impregnated cathode (HeatWave Laboratories, Watsonville, CA, USA) mounted axially 20 cm away from the cell center. A direct current of 3 A is used to heat the cathode to a temperature of about 950 ºC. To introduce electrons into the cell, the potential of the cathode housing is pulsed from +10.0 V to values between 0.0 and –10.0 V. A value of –1.5 V for the cathode potential during electron irradiation resulted in maximum ECD efficiency, and this setting was used in all experiments where cathode potential was not a variable. Electrons that pass through the cell should be reflected back through the cell due to the ion-injection optics that are maintained at high negative potentials.[22] For BIRD experiments, the heated cathode potential was kept at +10.0 V to prevent electrons from entering the cell. In all experiments, a potential of +9 V was applied to a copper-wire mesh mounted 0.5 cm in front of the cathode. All potentials are referenced to instrumental ground.

A mobile instrumentation data aquisition system (MIDAS)[32] was used to acquire 32 K data point transients. Ion abundances were obtained by subtracting the average noise in

an approximately 30 m/z signal-free region near the precursor. For ECD experiments, the average number of water molecules lost from a cluster upon reduction was calculated as the weighted average of reduced product cluster abundances and corrected for background dissociation from BIRD by subtracting the water loss due to BIRD, as measured with no electrons present in the cell. Experimental error was propagated assuming a distribution of noise that is uniform and uncorrelated with respect to m/z in the mass spectral regions investigated, and normal with respect to intensity. The standard deviation in noise intensity over the aforementioned signal free region was propagated through all calculations to estimate error.

2.3 Results and Discussion

2.3.1 Electron Kinetic Energy

In these ECD experiments, the electron kinetic energy is poorly defined and depends on a number of experiment parameters, including, for example, position inside the ion cell; trapping plate potentials; cell geometry; cathode voltage, temperature, and location; and electron current. Electrons produced from the heated cathode should have an initial velocity spread given by a Maxwell-Boltzmann distribution at the cathode temperature. At 950 ºC, the temperature of the heated cathode in these experiments, the average electron velocity is 1.9 $\times 10^5$ m/s, corresponding to a kinetic energy of 0.1 eV. In addition to the thermal distribution, electron-electron repulsion at the high electron currents typically used in these experiments will result in an even broader distribution of electron kinetic energies.

To study possible effects of electron kinetic energy on the internal energy deposition into ions upon EC, the potential of the cathode can be varied while keeping all other parameters constant. However, there is a limited range over which the cathode potential can be varied (about –1.2 to –2.0 V in these experiments) and ECD products observed. To investigate the origin of this effect, $[Ca(H_2O)_{15}]^{2+}$ was isolated in the cell and the precursor abundance was measured as a function of cathode potential with electron irradiation times of 120 ms (Figure 2). With symmetric trapping potentials of 2.0 V during ECD and ion detection, rapid loss of the precursor is observed when the cathode potential is varied from 0 to –1.0 V (Figure 2; solid black squares). A local maximum in precursor intensity occurs at about –1.5 V and the precursor intensity rapidly decreases at cathode potentials more negative than –2.0 V. Another local maximum in precursor intensity is observed at –8.0 V. To investigate effects of trapping plate potentials on this phenomenon, asymmetric trapping potentials of 8.3 and 9.2 V were used during ECD (2.0 V during ion detection). With these higher trap potentials, precursor ion loss is significantly reduced at low cathode potentials, but otherwise the trapping potentials during ECD have little effect (Figure 2; open circles). Similar results to the higher trapping plate data have been reported by Lioe and O'Hair, who irradiated singly charged ions with electrons and concluded that the loss of signal was due to neutralization.[33] However, no singly charged ions were observed in our experiments with cathode potentials between –3.0 and –7.0 V, indicating that ion-electron recombination is not the origin of precursor loss. Marshall and colleagues demonstrated that manipulation

of the trapping potentials during and immediately after the ECD event or the use of single-pass versus reflected electron configurations can shift the peak in ECD efficiency as a function of cathode potential.[34] High electron currents can reduce the effective potential inside the cell, which could result in loss of positively charged ions, consistent with retention of ion signal with high trap potentials when the cathode potential is low. However, the maximum observed at –1.5 V with 2.0-V trap potentials suggests that other effects, such as inelastic or elastic collisions with electrons which could "push" the ions out of the cell, may occur.

2.3.2 Effects of Cathode Potential on ECD Spectra

To determine how the electron kinetic energy affects the internal energy deposition upon EC, ECD spectra of $[Ca(H_2O)_{32}]^{2+}$ and $[Ca(H_2O)_{15}]^{2+}$ were measured as a function of cathode potential. ECD of the former results exclusively in loss of either 10 or 11 water molecules from the reduced precursor, whereas ECD of the latter results in loss of an H atom and 8 or 9 water molecules, resulting in formation of hydrated calcium hydroxide with a single charge. For $[Ca(H_2O)_{32}]^{2+}$, there is no discernable trend in the average number of water molecules lost from the reduced precursor for cathode potentials ranging from –1.2 to –2.0 V (Figure 3). The average number of water molecules lost over this range is 10.26 ±0.04. Extrapolation of these data to a cathode housing potential of 0.0 V results in a value of 10.2 ±0.2 water molecules. If the electron kinetic energy were deposited into internal modes of the ion, the ECD spectra should reflect a 0.80 eV (18.4 kcal/mol) change in internal energy deposition over this 0.80 V range of cathode potentials. Because ∼0.4 eV (∼9 kcal/mol) is required to evaporate a water molecule from a monovalent cluster of this size,[29] if the entire electron kinetic energy had been deposited into the ion, the average number of water molecules that evaporate from these clusters should have changed by approximately 0.80/0.4 = 2.0 water molecules over the 0.80 V range in cathode potentials. The insensitivity of the ECD spectra to cathode voltage clearly indicates that the internal energy deposited into these hydrated clusters is not a function of the electron kinetic energy over the range of cathode potentials typically used in ECD experiments.

Similar results are obtained for $[Ca(H_2O)_{15}]^{2+}$ where, again, there is no discernable trend in the average number of water molecules lost as a function of the cathode housing potential over a range of –1.4 to –2.0 V with an average value of 8.26 ±0.04 (Figure 3). Extrapolation of these data to a cathode potential of 0.0 V results in a value of 8.4 ±0.1. As was the case for $[Ca(H_2O)_{32}]^{2+}$, the cathode potential and thus inital electron kinetic energy have no effect on the internal energy deposited into this ion. Zubarev et al. reported that the fragmentation patterns in ECD spectra of 11+ ubiquitin ions did not change over a 0.0 to –0.4 V range of cathode potentials and concluded that the electron kinetic energy was minor compared to the energy released upon EC.[35] Our results show that changing cathode potentials does not affect ECD energy deposition in the low electron energy regime. However, different fragment ions have been observed in "hot" ECD experiments where the electron kinetic energy is > 5 eV.[36,37]

Trapping plate potentials during ECD also influence the electron kinetic energy inside the ion cell. To investigate the effects of trap potentials in these experiments, an ECD spectrum

of $[Ca(H_2O)_{32}]^{2+}$ was measured using asymmetric trap potentials of 8.3 and 9.2 V (source side and far side, respectively) during ECD. An average of 10.25 ±0.01 water molecules is lost from the reduced precursor, essentially the same number observed when the spectrum was acquired with a symmetric trapping potential of 2.0 V. These results indicate that the trapping potentials do not influence the internal energy deposited into ions upon ECD over the range of values typically used in these experiments.

Although these results may seem counterintuitive, it is important to consider that the capture of an electron is most efficient when the relative velocity between an ion and an electron is zero. The relative velocities of positive ions and electrons can be carefully controlled by merging the corresponding ion beams in ion storage rings.[38–41] From such experiments, accurate recombination cross sections as a function of relative ion-electron velocity can be obtained. The cross section for dissociative recombination when a protonated water molecule captures an electron increases by about 5 orders of magnitude as the center-of-mass kinetic energy decreases from 30 eV to 0.001 eV.[40] The EC cross section for $D^+(D_2O)_2$ increases by about 3 orders of magnitude when the ion-electron center-of-mass kinetic energy decreases from 0.01 to 0.001 eV.[41]

In the ECD experiments described here, the spread of electron velocities is very broad. Contributing further to the broadening is electron-electron repulsion, which is significant at the high electron currents used in these experiments. In addition, inelastic ion-electron collisions that do not result in electron capture can result in lower electron kinetic energies. All of these factors could result in a small fraction of electrons with near zero kinetic energies inside the ion cell, and these electrons should be the most efficiently captured by the slow moving positive ions in our experiment.

2.3.3 Effects of Inelastic Ion-Electron Collisions on ECD Spectra

Inelastic ion-electron collisions can deposit energy into either the intact precursor or the fragment ions, resulting in ion heating that could contribute to the extent of dissociation observed. A method to fragment organic ions based on this phenomenon has been implemented previously in FT/ICR mass spectrometers by Freiser and Beauchamp[42] and has been affectionately called ***e***lectron ***i***mpact ***e***xcitation of ***i***ons from ***o***rganics or EIEIO.[43] This method has been used to dissociate singly charged peptides.[33,44]

To investigate the extent to which inelastic ion-electron collisions occur and influence the internal energy deposition in these experiments, $[Ca(H_2O)_{15}]^{2+}$ was isolated, and ECD experiments were performed as a function of electron irradiation time from 40 to 200 ms with a cathode potential of –1.5 V. These data are corrected for contributions to ion heating by BIRD originating from the heated cathode and the cooled cell and surroundings. The average number of water molecules lost from the reduced precursor as a function of electron irradiation time is shown in Figure 4. There is a slight trend in the average number of water molecules lost as a function of electron irradiation time. Average numbers of water molecules lost at 40, 80, and 120 ms irradiation times are indistinguishable within experimental error; the average of these three values is 8.24 ±0.03. Values at 160 and 200 ms are slightly higher and outside experimental error, indicating that inelastic ion-electron collisions do play a

minor role in ion heating at these longer irradiation times. Extrapolation of these data to zero irradiation time should give the number of water molecules lost solely due to EC in the absence of any heating from inelastic ion-electron collisions; this value is 8.18 ±0.05. From these results, we conclude that, although inelastic ion-electron collisions occur, they contribute negligibly to the internal energy of the ions when the electron irradiation is less than 120 ms. At longer irradiation times, this effect can be measured but continues to be negligible at least up to 200 ms.

2.3.4 Effects of Inelastic Ion-Electron Collisions on Precursor Heating

In separate experiments, effects of precursor heating due to inelastic ion-electron collisions were obtained for both $[Ca(H_2O)_{17}]^{2+}$ and for $[Ca(H_2O)_{32}]^{2+}$ by measuring the extent of water loss from the precursor ions as a function of electron irradiation time. For both ions, loss of one or two water molecules from the precursor are the only products observed in addition to singly charged product ions due to ECD. In these experiments, blackbody infrared radiative dissociation occurs[21–23] that can be directly attributed to the heated cathode that is located 20 cm away from the cell center.[25] Effects of precursor ion heating due to inelastic ion-electron collisions can be obtained from differences in the extent of water loss with and without electrons introduced into the cell. To do this, the cathode remains at ∼950 °C in both experiments, but for the blackbody comparison, the cathode potential is +10 V at all times so that no electrons enter the cell. Differences in the water loss from the precursor ion measured in these two experiments can be directly attributed to inelastic electron-ion collisions. The water loss from the precursor ions, corrected for loss of the precursor due to ECD, as a function of electron irradiation time is shown in Figure 5. For $[Ca(H_2O)_{17}]^{2+}$, there is no significant difference in the fragmentation rate with or without electron irradiation up to 200 ms, but at longer times, more fragmentation occurs when electrons are introduced into the ion cell (Figure 5a). This result indicates that inelastic ion-electron collisions result in heating of the precursor ion over this longer time frame. The induction period at times below about 200 ms indicates that the precursor ions require some initial heating to a steady state temperature before pseudo first-order kinetics are observed, analogous to preheating in laser dissociation kinetic studies.[45]

In contrast, there is no observable effect of inelastic ion-electron collisions for the complex $[Ca(H_2O)_{32}]^{2+}$ (Figure 5b) for times up to 400 ms. In these experiments, the initial internal energy of this larger cluster is approximately twice that of the smaller cluster as are the rates of radiative absorption and emission. However, the threshold dissociation energies for loss of a water molecule from these two different size clusters are nearly the same. These experiments indicate that the rate of ion heating due to inelastic ion-electron collisions is negligible compared to that from radiative absorption (and emission) at this cluster size. Thus, for the cluster sizes typically used in nanocalorimetry experiments, heating of the ions due to inelastic ion-electron collisions is negligible under typical experimental conditions.

2.4 Conclusions

Ion nanocalorimetry is an accurate and highly sensitive method for measuring how much internal energy is deposited into ions upon activation.[24–27] This method has been recently applied to measuring absolute reduction potentials of red-ox couples in bulk solution.[26,27] In order to improve the accuracy with which these values can be obtained, effects of electron kinetic energy and inelastic ion-electron collisions on the internal energy deposition in ECD must be known. In typical ECD experiments done in FT/ICR mass spectrometry, the relative kinetic energies of the electrons generated by heated metal cathodes and the trapped ions vary over a relatively wide range and are poorly defined. The kinetic energy of electrons in these ECD experiments can be precisely varied by changing the heated cathode potential. Under typical experimental conditions, varying the cathode potential has no measurable effect on the internal energy deposited into ions that capture electrons. These results are consistent with the presence of some small fraction of electrons with near zero kinetic energy inside the cell. Such low energy electrons can be produced by effects of electron-electron repulsion in the high-density electron beam and/or by inelastic ion-electron collisions that occur inside the ion cell. Capture cross sections for EC are significantly higher when the relative ion-electron velocity approaches zero, and it is capture of this small population of low-energy electrons that results in the observed ECD. These results may explain in part the poor absolute cross section for ion-electron recombination in these experiments.

With electron irradiation times up to 200 ms, no discernable effects of inelastic ion-electron collisions are observed. At longer irradiation times, some ion heating due to inelastic ion-electron collisions is measurable for small nanoclusters but this effect is negligible for the larger size clusters typically used in nanocalorimetry experiments. These results indicate that the cathode potential, trapping plate potential, and inelastic ion-electron collisions do not play a significant role in the internal energy deposition in ECD under typical experimental conditions.

2.5 References

(1) Zubarev, R. A.; Kelleher, N. L.; McLafferty, F. W. *J. Am. Chem. Soc.* **1998**, *120*, 3265-3266.

(2) Breuker, K.; Oh, H. B.; Horn, D. M.; Cerda, B. A.; McLafferty, F. W. *J. Am. Chem. Soc.* **2002**, *124*, 6407-6420.

(3) Stensballe, A.; Jensen, O. N.; Olsen, J. V.; Haselmann, K. F.; Zubarev, R. A. *Rapid Commun. Mass Spectrom.* **2000**, *14*, 1793-1800.

(4) Mirgorodskaya, E.; Roepstorff, P.; Zubarev, R. A. *Anal. Chem.* **1999**, *71*, 4431-4436.

(5) Sze, S. K.; Ge, Y.; Oh, H. B.; McLafferty, F. W. *Proc. Natl. Acad. Sci. U. S. A.* **2002**, *99*, 1774-1779.

(6) Kelleher, N. L.; Zubarev, R. A.; Bush, K.; Furie, B.; Furie, B. C.; McLafferty, F. W.; Walsh, C. T. *Anal. Chem.* **1999**, *71*, 4250-4253.

(7. Ge, Y.; Lawhorn, B. G.; ElNaggar, M.; Strauss, E.; Park, J. H.; Begley, T. P.; McLafferty, F. W. *J. Am. Chem. Soc.* **2002**, *124*, 672-678.

(8) Robinson, E. W.; Leib, R. D.; Williams, E. R. The role of conformation on electron capture dissociation of ubiquitin. *J. Am. Soc. Mass Spectrom.* **2006**, *17*, 1469-1479.

(9) Breuker, K.; Oh, H. B.; Lin, C.; Carpenter, B. K.; McLafferty, F. W. *Proc. Natl. Acad. Sci. U. S. A.* **2004**, *101*, 14011-14016.

(10) Hvelplund, P.; Liu, B.; Nielsen, S. B.; Tomita, S. *Int. J. Mass Spectrom.* **2003**, *225*, 83-87.

(11) Hvelplund, P.; Liu, B.; Nielsen, S. B.; Tomita, S.; Cederquist, H.; Jensen, J.; Schmidt, H. T.; Zettergren, H. *Eur. Phys. J. D* **2003**, *22*, 75-79.

(12) Coon, J. J.; Shabanowitz, J.; Hunt, D. F.; Syka, J. E. P. *J. Am. Soc. Mass Spectrom.* **2005**, *16*, 880-882.

(13) Syka, J. E. P.; Coon, J. J.; Schroeder, M. J.; Shabanowitz, J.; Hunt, D. F. *Proc. Natl. Acad. Sci. U. S. A.* **2004**, *101*, 9528-9533.

(14) Iavarone, A. T.; Paech, K.; Williams, E. R. *Anal. Chem.* **2004**, *76*, 2231-2238.

(15) Zubarev, R. A. *Mass Spectrom. Rev.* **2003**, *22*, 57-77.

(16) Dekrey, M. J.; Kenttämaa, H. I.; Wysocki, V. H.; Cooks, R. G. *Org. Mass Spectrom.* **1986**, *21*, 193-195.

(17) Griffiths, I. W.; Harris, F. M.; Mukhtar, E. S.; Beynon, J. H. *Int. J. Mass Spectrom. Ion Processes* **1981**, *41*, 83-88.

(18) Baer, T.; Dutuit, O.; Mestdagh, H.; Rolando, C. *J. Phys. Chem.* **1988**, *92*, 5674-5679.

(19) Chen, J. H.; Hays, J. D.; Dunbar, R. C. *J. Phys. Chem.* **1984**, *88*, 4759-4764.

(20) Schnier, P. D.; Jurchen, J. C.; Williams, E. R. *J. Phys. Chem. B* **1999**, *103*, 737-745.

(21) Price, W. D.; Schnier, P. D.; Jockusch, R. A.; Strittmatter, E. F.; Williams, E. R. *J. Am. Chem. Soc.* **1996**, *118*, 10640-10644.

(22) Price, W. D.; Schnier, P. D.; Williams, E. R. *Anal. Chem.* **1996**, *68*, 859-866.

(23) Price, W. D.; Williams, E. R. *J. Phys. Chem. A* **1997**, *101*, 8844-8852.

(24) Leib, R. D.; Donald, W. A.; O'Brien, J. T.; Bush, M. F.; Williams, E. R. *J. Am. Chem. Soc.* **2007**, *129*, 4894-4895.

(25) Leib, R. D.; Donald, W. A.; Bush, M. F.; O'Brien, J. T.; Williams, E. R. *J. Am. Soc. Mass Spectrom.* **2007**, *18*, 1217-1231.

(26) Leib, R. D.; Donald, W. A.; O'Brien, J. T.; Bush, M. F.; Williams, E. R. *J. Am. Chem. Soc.* **2007**, *129*, 7716-7717.

(27) Donald, W. A.; Leib, R. D.; O'Brien, J. T.; Bush, M. F.; Williams, E. R. *J. Am. Chem. Soc.* **2008**, *130*, 3371-3381.

(28) Holland, P. M.; Castleman, A. W. *J. Phys. Chem.* **1982**, *86*, 4181-4188.

(29) Donald, W. A.; Williams, E. R. *J. Phys. Chem. A* **2008**, *112*, 3515-3522.

(30) Bush, M. F.; Saykally, R. J.; Williams, E. R. *Int. J. Mass Spectrom.* **2006**, *253*, 256-262.

(31) Wong, R. L.; Paech, K.; Williams, E. R. *Int. J. Mass Spectrom.* **2004**, *232*, 59-66.

(32) Senko, M. W.; Canterbury, J. D.; Guan, S. H.; Marshall, A. G. *Rapid Commun. Mass Spectrom.* **1996**, *10*, 1839-1844.

(33) Lioe, H.; O'Hair, R. A. J. *Anal. Bioanal. Chem.* **2007**, *389*, 1429-1437.

(34) McFarland, M. A.; Chalmers, M. J.; Quinn, J. P.; Hendrickson, C. L.; Marshall, A. G. *J. Am. Soc. Mass Spectrom.* **2005**, *16*, 1060-1066.

(35) Zubarev, R. A.; Horn, D. M.; Fridriksson, E. K.; Kelleher, N. L.; Kruger, N. A.; Lewis, M. A.; Carpenter, B. K.; McLafferty, F. W. *Anal. Chem.* **2000**, *72*, 563-573.

(36) Chan, T. W. D.; Ip, W. H. H. *J. Am. Soc. Mass Spectrom.* **2002**, *13*, 1396-1406.

(37) Kjeldsen, F.; Haselmann, K. F.; Budnik, B. A.; Jensen, F.; Zubarev, R. A. *Chem. Phys. Lett.* **2002**, *356*, 201-206.

(38) Adams, N. G.; Poterya, V.; Babcock, L. M. *Mass Spectrom. Rev.* **2006**, *25*, 798-828.

(39) Al Khalili, A.; Thomas, R.; Ehlerding, A.; Hellberg, F.; Geppert, W. D.; Zhaunerchyk, V.; af Ugglas, M.; Larsson, M.; Uggerud, E.; Vedde, J.; Adlhart, C.; Semaniak, J.; Kamińska, M.; Zubarev, R. A.; Kjeldsen, F.; Andersson, P. U.; Österdahl, F.; Bednarska, V. A.; Paal, A. *J. Chem. Phys.* **2004**, *121*, 5700-5708.

(40) Neau, A.; Al Khalili, A.; Rosen, S.; Le Padellec, A.; Derkatch, A. M.; Shi, W.; Vikor, L.; Larsson, M.; Semaniak, J.; Thomas, R.; Någård, M. B.; Andersson, K.; Danared, H.; af Ugglas, M. *J. Chem. Phys.* **2000**, *113*, 1762-1770.

(41) Någård, M. B.; Pettersson, J. B. C.; Derkatch, A. M.; Al Khalili, A.; Neau, A.; Rosen, S.; Larsson, M.; Semaniak, J.; Danared, H.; Kallberg, A.; Österdahl, F.; af Ugglas, M. *J. Chem. Phys.* **2002**, *117*, 5264-5270.

(42) Freiser, B. S.; Beauchamp, J. L. *Chem. Phys. Lett.* **1976**, *42*, 380-382.

(43) Cody, R. B.; Freiser, B. S. *Anal. Chem.* **1979**, *51*, 547-551.

(44) Wang, B. H.; McLafferty, F. W. *Org. Mass Spectrom.* **1990**, *25*, 554-556.

(45) Jockusch, R. A.; Paech, K.; Williams, E. R. *J. Phys. Chem. A* **2000**, *104*, 3188-3196.

2.6 Figures

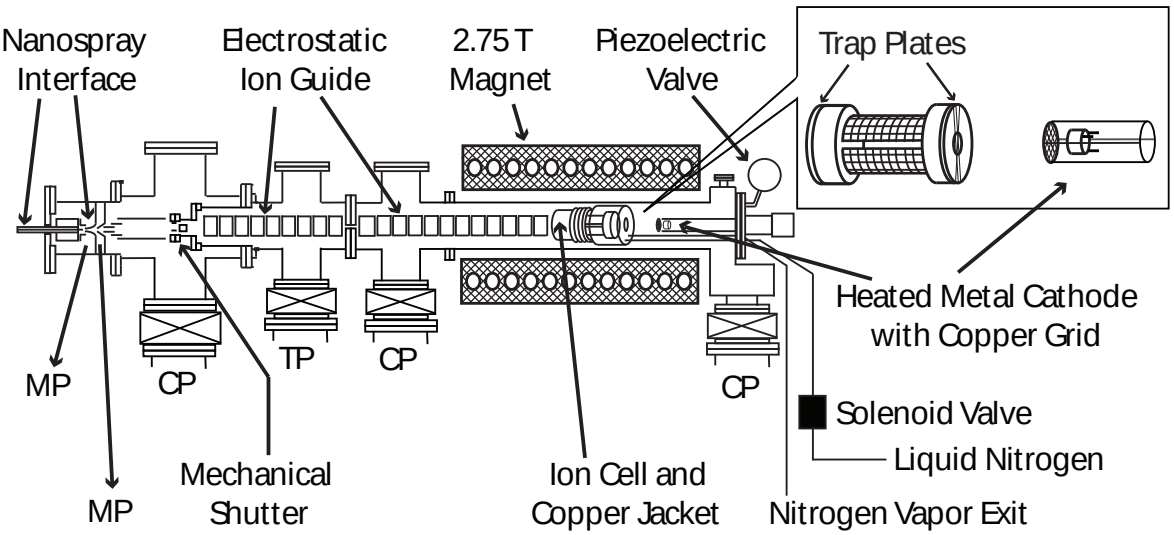

Figure 2.1: Schematic of the 2.75 T FT/ICR mass spectrometer used in these experiments. The inset shows details of the ion cell and heated metal cathode with copper grid. The heated metal cathode is mounted on the central axis of the vacuum chamber and is positioned 20 cm from the center of the ion cell. MP, CP and TP indicate mechanical pump, cryopump and turbopump, respectively.

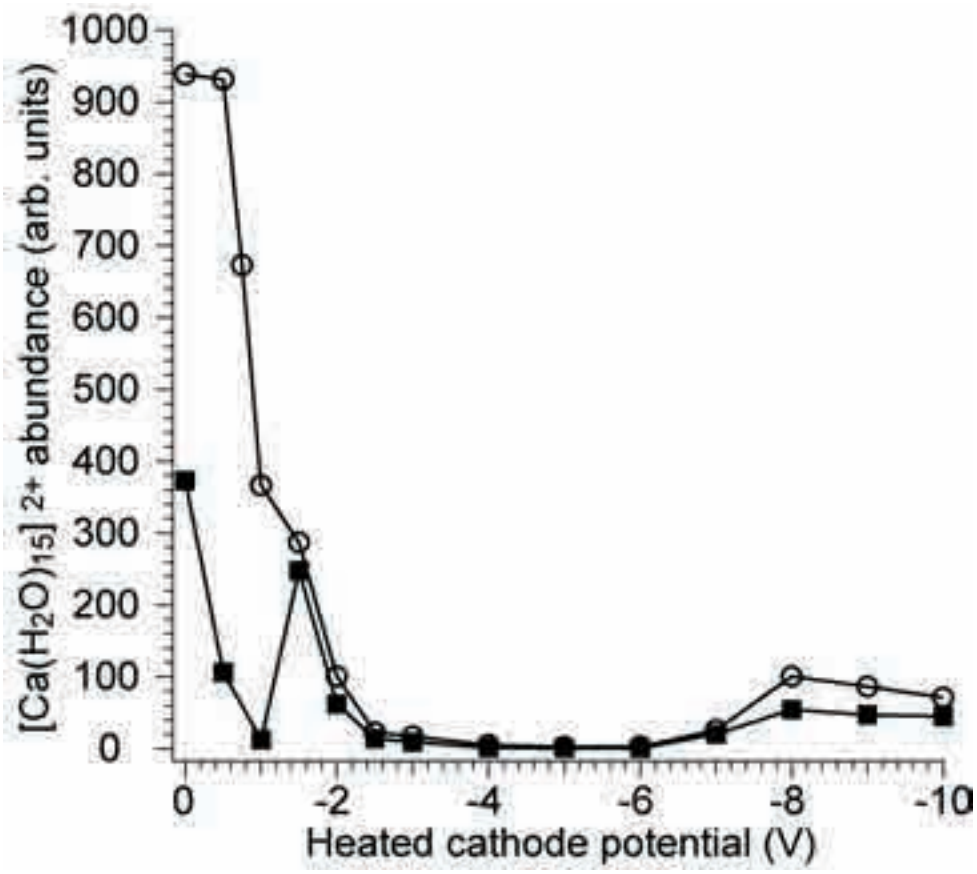

Figure 2.2: $[Ca(H_2O)_{15}]^{2+}$ precursor abundance after 120 ms of electron irradiation as a function of heated cathode potential, measured with two different trapping plate potential conditions: a symmetric 2.0 V trap potential during electron irradiation and ion detection (solid squares); and asymmetrical 8.3/9.2 V source-side/far-side trap potentials during electron irradiation, 2.0 V during ion detection (open circles).

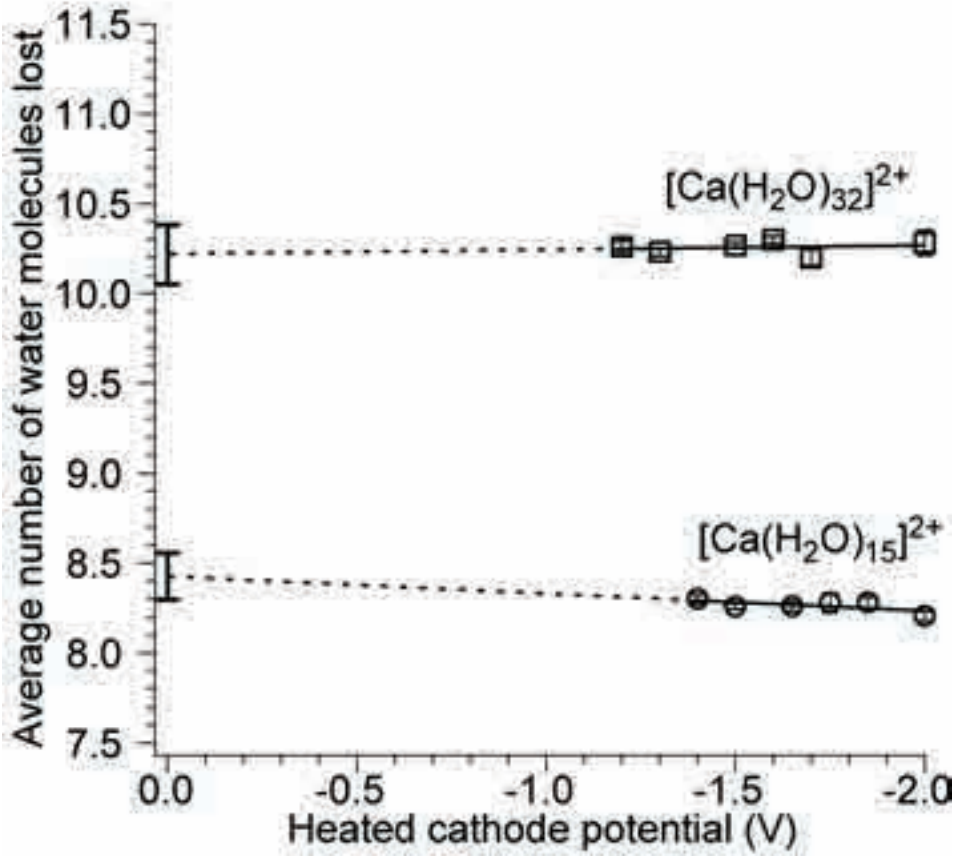

Figure 2.3: Average number of water molecules lost upon reduction of $[Ca(H_2O)_{15}]^{2+}$ and $[Ca(H_2O)_{32}]^{2+}$ as a function of heated cathode potential. Dashed lines indicate extrapolated least squares fits of the data, and the error bars at 0.0 V indicate the propagated error in the intercept.

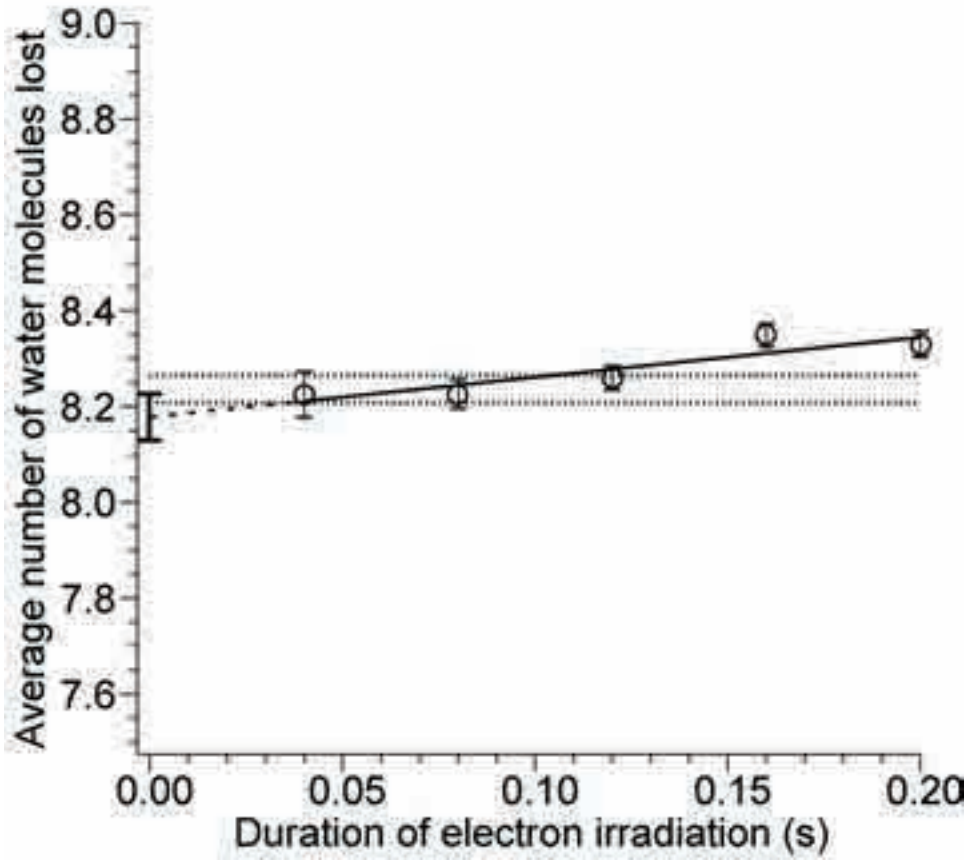

Figure 2.4: Average number of water molecules lost from reduced $[Ca(H_2O)_{15}]^{2+}$ due to EC as a function of electron irradiation time. The dashed line indicates the extrapolated least squares fit to the data, and the error bars at 0.0 s indicate the propagated error in the intercept. The dotted lines represent one standard deviation above and below the average value of the data at 40, 80, and 120 ms.

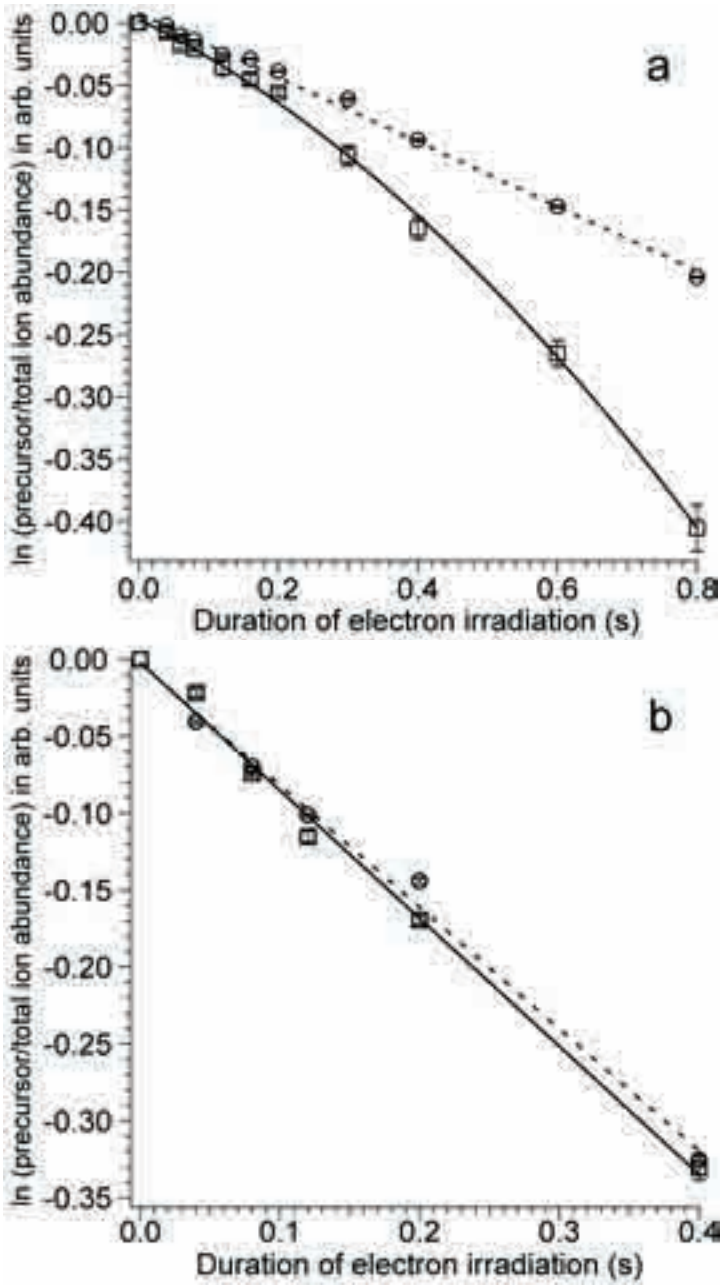

Figure 2.5: Dissociation kinetics of (a) $[Ca(H_2O)_{17}]^{2+}$ and (b) $[Ca(H_2O)_{32}]^{2+}$with (squares, cathode potential –1.5 V) and without (circles, cathode potential +10.0 V) electron irradiation as a function of electron irradiation time. The dashed lines are least squares fits to the data obtained with the heated cathode potential at +10.0 V, and the solid lines are a parabolic ($[Ca(H_2O)_{17}]^{2+}$) and least squares fit ($[Ca(H_2O)_{32}]^{2+}$) to the data with a heated cathode potential of –1.5 V.

Chapter 3

Changes in Binding Motif of Protonated Heterodimers Containing Valine and Amines Investigated Using IRMPD Spectroscopy between 800 and 3700 cm^{-1} and Theory

Jeremy T. O'Brien, James S. Prell, Jeffrey D. Steill, Jos Oomens, and Evan R. Williams

Journal of the American Chemical Society, 2009, 131, 3905–3912

3.1 Introduction

Ionic interactions play an important role in molecular reactivity and structure. Salt bridges, in which a deprotonated acidic residue interacts with a protonated basic residue, can either stabilize or destabilize protein conformations and are often found in protein-protein interfaces.[1–6] Because water, solvent, or other molecules can stabilize ions, salt-bridges and zwitterions are common in condensed phases. However, these ionic interactions can also be stable even without solvent or other molecules. The nonzwitterionic forms of isolated amino acids are more stable for all the naturally occurring amino acids in the gas phase, but the zwitterionic forms of some amino acids can be preferentially stabilized by cationization with metal ions,[7–26] attachment of an electron,[27,28] or when bound to other protonated molecules.[29–33] For example, the nonzwitterionic form of arginine is more stable than the zwitterionic form, but attachment of an electron,[27,28] larger alkali metal ions (Na, K, Rb, Cs),[10–13,23] or even another protonated arginine molecule[29,30] can result in the zwitterionic form being more stable. Similarly, proline itself is not zwitterionic, but the zwitterionic form can be most stable when cationized by a metal cation[23–25] or when bound to protonated proline.[32] In contrast, glycine is not zwitterionic when monocationized[19,20,34–37] or in protonated dimers,[29–32,38,39] but the zwitterionic form can be stabilized by attachment of dications.[9,18–22]

Investigating some physical properties of amino acids or other similar molecules can be made more complicated because the form of an amino acid present in a protonated or cationized dimer can be different from that of the amino acid in isolation. For example, proton affinities or gas-phase basicities are often measured using either the kinetic method or by bracketing, which both involve formation of protonated dimers. In the kinetic method,[40–42] products formed by dissociation of protonated dimers consisting of the molecule of interest and a reference base of known basicity are measured as a function of the basicity of the reference base. In the bracketing method, these same proton-bound dimers are formed by ion-molecule reactions. In each case, if the form of the molecule in the protonated dimer is different from that in isolation, the results of these experiments may not accurately reflect the physical properties of the isolated molecule. Metal ion affinity measurements can also be affected by the structure of the amino acid in a complex. For example, lithiated proline is zwitterionic,[23,25] but results from dissociation of heterodimers consisting of lithiated proline and proline methyl ester suggest that proline is nonzwitterionic, a result attributed to destabilization of the zwitterionic form of proline in the heterodimer.[23]

Wu and McMahon recently investigated the structures of the amino acids Gly, Ala, Val, Leu, Ile, Ser and Pro in protonated dimers with ammonia, methylamine, diethylamine,

and triethylamine.[43] They reported that, for the amino acids with alkyl side chains, the zwitterionic form of the amino acid is increasingly stable with increasing basicity of the amino acid, consistent with earlier results for metal-cationized amino acids with alkyl side chains.[8,25] They also found that the stabilities of the zwitterionic forms of these amino acids decrease with increasing basicity of the base.[43]

Infrared multiple photon dissociation (IRMPD) spectroscopy has emerged as a powerful method to obtain structural information, and this method has been applied to many different protonated dimers.[31−33,38,44−48] Elegant experiments of Johnson and coworkers showed that the frequency of the asymmetric stretching band of a shared proton between two molecules depends strongly on the relative proton affinities of the two molecules.[48] IRMPD spectroscopy has been used to investigate zwitterionic structures of amino acids in the gas phase.[12−16,26,32,33,49−52] IRMPD spectra and other results for protonated glycine dimer indicates that glycine is not zwitterionic.[30−32,38,47,53] On the basis of these data, two different structures have been proposed. In one structure, the protonated N-terminus of one glycine hydrogen bonds to the N-terminus of the other glycine in its nonzwitterionic form.[31] In the other structure, the shared proton is between the protonated N-terminus of one glycine and the carbonyl oxygen of the other nonzwitterionic glycine.[32,38,47] On the basis of IRMPD spectra measured in the 1150 to 2000 cm^{-1} region, Wu and McMahon conclude that, in Gly•NH_4^+, structures in which Gly is either zwitterionic or nonzwitterionic are equally populated even though ammonia is ∼32 kJ/mol less basic than Gly.[33]

Here, the structures and reactivities of protonated dimers consisting of valine and 11 basic molecules that are either primary or secondary amines with GB values bracketing that of valine are investigated using IRMPD spectroscopy, collisionally activated dissociation, and theory. In contrast to earlier results[43] and to theory at MP2/6-31++G** and B3LYP/6-31++G** levels, the IRMPD spectra clearly show that valine is not zwitterionic with any of these bases, but rather the protonated dimers undergo a gradual change in structure with increasing GB from one in which protonated base interacts with the N-terminus of nonzwitterionic valine to one in which the protonated base interacts with the C-terminus of nonzwitterionic valine.

3.2 Experimental

3.2.1 Mass Spectrometry

All sustained off-resonance irradiation collisional activation dissociation (SORI-CAD) and spectroscopy experiments in the frequency range between 2800 and 3700 cm^{-1} were performed on a 2.75 T Fourier transform ion cyclotron resonance (FT-ICR) mass spectrometer at Berkeley.[12,54] Methanol, isopropylamine, *n*-butylamine, *sec*-butylamine, *tert*-butylamine, hexylamine, ethylmethylamine, diethylamine as well as hydrochloride salts of methylamine, ethylamine, propylamine, dimethylamine, and L-valine were purchased from Sigma Chemical Co. All chemicals were used without further purification. Protonated heterodimers were formed by electrospray ionization of aqueous solutions of 4 mM valine and 1 – 4 mM base, except for the Val•H^+•ethylmethylamine and Val•H^+•diethylamine heterodimers, which

were formed from 50/50 water/methanol solutions. Ions were trapped and accumulated in a cylindrical ion cell for 3 s during which time nitrogen gas was pulsed into the chamber at a pressure of $\sim 10^{-6}$ Torr to enhance trapping and thermalization. This cell is surrounded by a copper jacket that is resistively heated to 351 K. The vacuum chamber pressure returned to $\sim 10^{-8}$ Torr after a pump-down delay of 3.5 s before to ion isolation. Protonated dimers were isolated using a stored waveform inverse Fourier transform (SWIFT) and then irradiated with 300 pulses (30 s at 10 Hz) of IR radiation from a tunable OPO/OPA (Laser Vision). Transients of 64 kB were acquired using a MIDAS data station.[55] IR laser-induced photodissociation rates as a function of frequency were obtained from the relative abundances of precursor and product ions following laser irradiation and were corrected for both laser power and blackbody infrared radiative dissociation.

For SORI-CAD experiments, ions of interest were isolated and excited using a 500-ms, 8 V_{pk-pk} waveform applied at a frequency 5000 Hz below the cyclotron frequency of the ion of interest, providing a maximum laboratory-frame translational energy of 1.0 – 1.5 eV, depending on the m/z of the precursor ion. Nitrogen gas was introduced into the vacuum chamber for 2 s at a pressure of $\sim 10^{-6}$ Torr to increase the number of collisions. The pressure returned to $\sim 10^{-8}$ Torr after a 3 s delay before ion detection. Under these conditions, the percentage of the precursor dissociated ranged from ∼90 % for methylamine to ∼99 % for diethylamine.

IRMPD spectra between 800 and 1900 cm^{-1} were obtained using a 4.7 T FT-ICR mass spectrometer at the FOM Institute for Plasma Physics.[56,57] Briefly, the protonated dimers were formed by electrospray ionization from 50/50 water/methanol solutions of 1 mM valine and 4 mM methylamine, or 2 mM valine and 4 mM diethylamine, infused at a rate of 10 μL/min. Precursor ions were mass selected using SWIFT and subsequently irradiated for 2.5 to 3 s using tunable irradiation from the free-electron laser. For these experiments, IRMPD spectra are obtained from the sum of the photodissociation product ion intensities divided by the total ion intensity measured as a function of photon energy and linearly power-corrected.[57]

3.2.2 Computational Methods

Candidate low-energy structures for Val•H^+•B, where B = methylamine, ethylamine, hexylamine, and diethylamine, were obtained by Monte Carlo conformational searching using the MMFF94 force field in Macromodel 8.1 (Schrödinger, Inc.). At least 5000 conformations were generated for protonated dimers with methylamine, ethylamine and hexylamine, and 10,000 conformers were generated for diethylamine. Starting structures for Val•H^+•B, B = propylamine, isopropylamine, *n*-butylamine, *sec*-butylamine, or *tert*-butylamine, were generated by substituting the corresponding alkyl groups into the low-energy candidate structures obtained for B = ethylamine. Because the relatively short alkyl chains of these primary amines do not interact significantly with the valine molecule, conformational searching for each base was not performed. Initial structures for Val•H^+•B, where B = dimethylamine and ethylmethylamine, were similarly generated by alkyl group substitution into the candidate structures identified for diethylamine.

Geometries of candidate low-energy structures were subsequently optimized with Jaguar v. 6.5 (Schrödinger, Inc.) at the B3LYP/6-31G* level of theory. The resulting low-energy structures were then optimized further at B3LYP/6-31++G** using Q-Chem 3.0 (Q-Chem, Inc.),[58] and harmonic vibrational frequencies and intensities were calculated analytically. Each final structure was found to have all positive frequency vibrational modes, indicating that these structures are local minima. Energies were obtained using B3LYP/6-31++G**, with zero-point energy corrections calculated using unscaled vibrational frequencies. For comparisons with the experimental data, calculated vibrational frequencies between 2800 and 3700 cm^{-1} were scaled by 0.956. This scaling factor has been used previously in an IR study in this region to compare experimental IR action spectra of lithiated valine water cluster to spectra calculated at the same level of theory as used in this study.[59] Calculated spectra in this frequency region were convolved using 20 and 30 cm^{-1} full-width at half-maximum (fwhm) Lorentzian peak shapes for the free OH and hydrogen bonded features, respectively, which provide a good fit to the observed peak shapes. Vibrational frequencies between 800 and 1900 cm^{-1} were scaled by 0.975, which has been used previously in other IR studies in this region to compare experimental IR action spectra and spectra calculated at similar levels of theory as used in this study.[14–17,50,60] In this region, the calculated spectra were convolved with a 50 cm^{-1} fwhm Lorentzian peak shape to approximate the width of the observed bands.

Additional calculations were performed for methylamine and diethylamine. Geometry optimization and frequency calculations using the B3LYP/6-311++G** level of theory were performed on the 6-31++G** optimized structures. In addition, MP2/6-31++G** single point energies were calculated for the B3LYP/6-31++G** optimized structures. The zero-point energy and temperature corrections from the B3LYP/6-31++G** calculations were added to the MP2 single point energies to obtain relative Gibbs free energies at the temperature of the experiments.

3.3 Results and Discussion

3.3.1 Dissociation Pathways

Dissociation of Val•H^+•B with SORI-CAD at low energy results in formation of either Val•H^+ or B•H^+ and the corresponding neutral molecule. For Val•H^+•MeA, predominantly Val•H^+ is observed, consistent with the 15 kJ/mol higher basicity of Val. For bases with GB values greater than that of hexylamine, only protonated base is observed. The ratio of protonated valine to protonated base product intensities changes for Val•H^+•B between B = methylamine and hexylamine (Figure 1a). The ratio of $[Val•H]^+$ to $[EtA•H]^+$ is 75:25, indicating that valine is more basic than ethylamine. On the basis of the results of these SORI-CAD experiments, the gas-phase basicity and proton affinity of valine are ∼880 kJ/mol and ∼914 kJ/mol, respectively. In contrast, results from both bracketing[61] and prior kinetic method[62] experiments indicate that ethylamine is more basic than valine. On the basis of these and other results, proton affinity values ranging from 900 to 912 kJ/mol have been reported.[63,64] Changing the maximum laboratory-frame translational energy in these SORI-

CAD experiments from 1.5 to 4.4 eV, resulted in a decrease in the [Val•H^+]:[EtA•H^+] ratio from 75:25 to 45:55, respectively. These results are consistent with those of Li and Harrison, who measured the effects of collision energy in kinetic method experiments and found that the ratio of protonated ethylamine to protonated valine increased with increasing energy indicating that formation of EtA•H^+ is entropically favored.[62] The higher basicity value of valine determined in our experiments is consistent with a much lower internal energy deposition in these SORI-CAD experiments and the relative entropy for dissociation by the two channels differing markedly. There is an intramolecular hydrogen bond from the hydroxyl group of the C terminus to the nitrogen of the N-terminus of valine that hinders rotation about the N–C_α bond (*vide infra*). This hydrogen bond is significantly stronger for Val•H^+ than for neutral valine. Formation of EtA•H^+ and neutral valine are likely entropically favored because neutral valine can more freely rotate around the N-C_α bond than can Val•H^+.

The same products formed by SORI-CAD are observed by photodissociation, although the ratio of products can differ. For Val•H^+•EtA, the ratio of protonated valine to protonated ethylamine is ∼90:10, indicating that basicity of valine is slightly higher than 880 kJ/mol and that the energy deposition and resulting effective temperatures in these photodissociation experiments are even lower than those in the SORI-CAD experiments. The branching ratio of the photodissociation products does not depend on photon energy.

3.3.2 IRMPD Spectra

IRMPD action spectra of protonated valine-base heterodimers were measured for each of 11 different bases (Table 1) at a cell temperature of 351 K in the frequency range from 2800 to 3700 cm^{-1} (Figure 2). These protonated dimers dissociate more readily at elevated cell temperatures as a result of their interaction with the surrounding blackbody radiation field that increases their internal energy. The temperature was chosen so that, after 30 s of exposure to just blackbody radiation, about 5 – 12% of the precursor ions dissociate. Under these conditions, absorption of even a single IR photon from the laser is expected to increase the rate of dissociation, although sequential absorption of multiple IR photons also occurs. Laser-induced photodissociation rates were between 0 and 150% of the respective blackbody infrared radiative dissociation rates.

The spectral range from 2800 to 3700 cm^{-1} can be roughly divided into three regions corresponding to free OH stretches (3500 – 3600 cm^{-1}), NH stretches (3200 – 3500 cm^{-1}) and a region with both CH stretches and hydrogen-bonded OH and NH stretches (2800 – 3200 cm^{-1}). CH stretches can appear as weak bands in IR action spectra because of the weak transition dipole moment for this mode.[12,31,59]

For complexes containing a base with a primary amine, there are three bands in the NH stretch region at roughly 3275, 3335 and 3420 cm^{-1}, although the band at 3275 cm^{-1} is not resolved from the band at 3335 cm^{-1} for methylamine and ethylamine. The IR action spectra of complexes containing bases with secondary amines (dimethylamine, methylethylamine, and diethylamine) have bands at ∼3275 and ∼3420 cm^{-1}, but no band at ∼3335 cm^{-1}. These spectra are consistent with the IR action spectra of other cationized amino acids that

have NH stretch bands between 3250 and 3450 cm^{-1}.[12,65]

All the IR action spectra have a distinct band at ~3540 cm^{-1} consistent with the free OH stretch of a carboxylic acid group (Figure 2), although this is only a minor feature for diethylamine. A plot of the intensity of the band at ~3420 cm^{-1} relative to the intensity of the band at ~3540 cm^{-1} as a function of the GB of the amine is shown in Figure 1b. The relative intensities of these bands change only slightly for bases that have GB values less than 20 kJ/mol greater than valine, indicating that the population of structures that have free OH stretches does not change significantly for these bases. In contrast, this ratio increases significantly for bases that are 20 kJ/mol or more basic than valine. This indicates that the relative population of structures with free OH stretches decreases significantly for complexes with these more basic bases. These results are consistent with a transition in structure from one in which the base is coordinated to the N-terminus to one in which it is coordinated to the C-terminus. When the base coordinates to the C-terminus, either the OH group of nonzwitterionic valine forms a hydrogen bond and the OH stretch vibration occurs at a much lower frequency, or valine is zwitterionic and does not have an OH stretching mode.

Spectra of Val•H^+•MeA and Val•H^+•Et_2A were also measured at room temperature using tunable radiation at lower energies, ~ 850 – 1850 cm^{-1}, generated by a free electron laser (Figures 3 and 4). This spectral range covers carbonyl stretching modes, as well as NH and OH bending modes, which can provide structural information complementary to that obtained from the higher photon energy range. The bands in the IRMPD spectra of Val•H^+•MeA and Val•H^+•Et_2A are relatively broad and weak between ~850 and 1850 cm^{-1} (Figures 3 and 4). Similarly broad features are observed in the IR action spectrum of Gly•NH_4^+ measured in this same spectral region.[33] The bands at ~1700 cm^{-1} are likely an overlap of a carbonyl stretching mode and NH bending modes. The carbonyl stretch of a carboxylic acid group has been observed to occur between ~1740 and 1790 cm^{-1} for protonated amino acids,[13,16,50] and between 1700 and 1800 cm^{-1} for metal cationized amino acids.[13–17,24,49,50,52,57] and Gly•NH_4^+.[33] NH bending modes are reported to occur between 1500 and 1700 cm^{-1}.[13–17,33,50,57] The bands near 1400 cm^{-1} are consistent with the OH bend of a carboxylic acid that is weakly hydrogen bonded to the N-terminus as observed for some cationized amino acids.[13–17,49,50,52] The weak bands at ~975 and 1175 cm^{-1} are consistent with CH bending modes coupled with OH and NH bends.

The spectra of Val•H^+•MeA and Val•H^+•Et_2A are similar between 850 and 1850 cm^{-1}. The structural difference clearly indicated by the spectra in the higher frequency range (2800 – 3700 cm^{-1}) is not apparent from the lower frequency data, although the relatively poor signal-to-noise of these data may obscure any differences.

3.3.3 Calculated Low-Energy Structures

For each of the protonated heterodimers, the lowest-energy structures fall into three structural families, all of which consist of formally neutral valine and a protonated base. These structural families are illustrated for methylamine and diethylamine in Figures 3 and 4, respectively. In structure NZ-N, the protonated base coordinates to the N-terminus of

nonzwitterionic valine, where it forms an ionic hydrogen bond to the nitrogen. A structure in which protonated valine donates an ionic hydrogen bond to the neutral base is calculated to be stable only for methylamine. Surprisingly, calculations predict that this structure is 28 kJ/mol higher in energy (351 K) than the NZ-N structure in which methylamine is protonated, despite the 12 kJ/mol higher basicity of valine compared to that of methylamine (i.e., the proton is predominantly associated with the less basic molecule in this dimer). Similarly, in recently reported calculations for Gly•NH_4^+, ammonia is protonated in the three most stable reported structures despite the much higher (+33 kJ/mol) basicity of glycine.[33]

In the other non-zwitterionic structure, NZ-C, the protonated base donates a single hydrogen bond to the carbonyl oxygen of valine, and there is an intramolecular hydrogen bond between the acidic hydrogen and the nitrogen of valine. In the zwitterionic structure, Z-C, the protonated base coordinates to the carboxylate group of zwitterionic valine, donating a hydrogen bond to each oxygen atom. For all structures, one position of the side chain is consistently calculated to be lowest in energy. In this preferred position, both methyl groups of the side chain are gauche relative to the N-terminal amine group (Figures 3 and 4). Other orientations of the valine side chain are generally 3 – 8 kJ/mol higher in energy. These results are consistent with the low-energy structures reported by Wu and McMahon for protonated valine alkyl-ammonium complexes.[43]

The B3LYP/6-31++G** relative Gibbs free energies at 0/351 K are given in Table 1. The relative energies of these three structures are similar for each amine base, spanning a range of less than 20 kJ/mol for each protonated heterodimer. A plot of the 351 K relative energies of these three structures as a function of the gas-phase basicity of the base is shown in Figure 1c. At this level of theory, the NZ-C structures are calculated to be lowest in energy at 351 K for all the protonated heterodimers except for those with methylamine and ethylamine, for which the Z-C structures are most stable. The 0 K relative energies are similar, typically within 5 kJ/mol of the 351 K values. There is no other apparent trend in the relative energies of these three structures with the GB of the base at either 0 or 351 K. These results are surprising because zwitterionic structures of valine are calculated to be stable for the two least basic bases at this level of theory. Calculations at both B3LYP/6-311+G* and MP2(full)/6-311++G** by Wu and McMahon also indicate that the Z-C structure is most stable for Val•H^+•MeA.[43]

To investigate the effect of basis set size and MP2 correlation on the observed trends, calculations were done on the protonated heterodimers consisting of the least basic (methylamine) and most basic (diethylamine) at the B3LYP/6-311++G** level of theory and, using the B3LYP/6-31++G** optimized geometries, MP2/6-31++G** single-point energies were also obtained (Table 1). The B3LYP/6-311++G** relative energies are within 2 kJ/mol of the 6-31++G** energies indicating the larger basis set has little effect on the relative energies. The MP2 results for methylamine indicate the Z-C structure is again most stable and the relative energies of the NZ-C and NZ-N structures are almost equal. For diethylamine, the Z-C structure is favored with MP2 and the NZ-C structure with B3LYP. Calculated spectra for these structures are shown for methylamine and diethylamine in Figures 3 and 4, respectively. The calculated spectra for the other primary amine heterodimers are very similar to the corresponding spectra of Val•H^+•MeA structures, although the vibrational

frequencies vary slightly for each base within a roughly ± 15 cm^{-1} range.

3.3.4 IRMPD and Calculated Spectra of Val•H^+•MeA

Calculated spectra for each of the candidate low-energy structures of Val•H^+•MeA are shown in Figure 3, along with the IRMPD spectra of these respective ions in both the 800 – 1850 and 2800 – 3700 cm^{-1} regions. For Val•H^+•MeA, the strong band at ∼3540 cm^{-1} clearly indicates the presence of a free carboxylic acid OH stretch. Only structures such as NZ-N with the amine coordinated to the N-terminus of nonzwitterionic valine have a free carboxylic acid OH stretch (3570 cm^{-1}). An NZ-N structure in which valine is protonated instead of methylamine also has a free carboxylic acid OH stretch but this structure cannot be distinguished from the NZ-N structure with protonated methylamine based on their very similar calculated spectra. The OH band in NZ-C is substantially red-shifted owing to hydrogen bonding to the amine nitrogen and is calculated to occur around 2900 cm^{-1}. Despite very large calculated intensities, hydrogen bonded features are often observed as relatively weak broad bands in IRMPD spectra.[66,67] Many factors can contribute to this discrepancy including peak broadening, calculation uncertainties, and anharmonicity. Structure Z-C does not have a carboxylic acid OH band, and this structure can be eliminated on the basis of the absence of this band.

The symmetric and asymmetric stretches of the free methylamine NH bonds for NZ-N are at 3315 and 3375 cm^{-1}, consistent with the broad band between 3260 and 3400 cm^{-1} in the experimental spectrum. The band at 3410 cm^{-1} in the IRMPD spectrum is consistent with the asymmetric stretch of the free NH bonds of the N-terminus, which is calculated to occur at 3400 cm^{-1}.

Bands for NZ-C at 3300, 3370, and 3450 cm^{-1} correspond to the symmetric NH stretch of methylamine, an overlap of the symmetric NH stretch of the N-terminus and the asymmetric NH stretch of methylamine, and the asymmetric stretch of the free NH bonds of the N-terminus, respectively. The absence of both this latter band and a carboxylic acid free OH stretch above 3500 cm^{-1} indicates that this structure is not significantly populated.

In the lower frequency region of the spectrum, the band at ∼1700 cm^{-1} is consistent with the asymmetric carbonyl stretch of a carboxylic acid group. The frequency of this stretch for a carboxylate group is lower and occurs at ∼1625 cm^{-1} for Z-C. This result, along with the carboxylic acid OH stretch, clearly indicates that valine is not zwitterionic in this complex. NZ-C has a band at 1400 cm^{-1} corresponding to the OH bend of the carboxylic acid group. The presence of a distinct band at 1400 cm^{-1} in the IRMPD spectrum suggests that a small population of NZ-C may be present.

These results clearly indicate that valine is not zwitterionic in the protonated dimer with methylamine. The IRMPD spectrum in the hydrogen stretch region is most consistent with the NZ-N structure, but the lower frequency data indicate that a minor population of NZ-C could be present as well. In contrast with these experimental results, calculations using both B3LYP and MP2 methods including MP2(full)/6-311++G** values reported by Wu and McMahon indicate that Z-C is the most stable.[43]

3.3.5 IRMPD and Calculated Spectra of Val•H^+•Et_2A

Calculated spectra for each of the candidate low-energy structures Val•H^+•Et_2A are shown in Figure 4, along with the IRMPD spectra in both the 800 – 1850 and 2700 – 3700 cm^{-1} regions. The presence of a small band at ∼3540 cm^{-1} indicates that a small population of structures that have a free carboxylic acid OH stretch, such as NZ-N, must be present. The calculated NH stretching bands at 3410 and 3260 cm^{-1}, respectively, and the carboxylic acid stretch at 3570 cm^{-1} are consistent with those in the measured spectrum, but the low intensity of the carboxylic acid stretch indicates that the majority of the ion population must have structures where the base is coordinated to the C-terminus of valine.

As was the case for Val•H^+•MeA, the substantial photodissociation observed at 1700 cm^{-1} is consistent with the carbonyl stretch of a carboxylic acid (1710 cm^{-1} for NZ-C) and not of a carboxylate (1660 cm^{-1} for Z-C). The separation between the two NH stretching bands (3415 and 3275 cm^{-1}) in the experimental spectrum is ∼140 cm^{-1}, and the separation in the corresponding bands in the calculated spectra of the NZ-C and Z-C structures is ∼150 and 80 cm^{-1}, respectively. Thus, structure NZ-C appears to be the best fit to the experimental spectrum. There is significant photodissociation intensity at ∼3000 cm^{-1} consistent with the calculated intramolecularly hydrogen-bonded carboxylic acid OH stretch in NZ-C. The intensity is consistent with previous studies in which hydrogen-bonded features have been observed as very broad, weak features despite the high intensity of the calculated bands.[66,67] Band intensities are calculated using a double harmonic approximation that results in attendant uncertainties in comparing with experimental spectra. CH stretches also occur in this region, but these bands are typically very weak. The lack of significant photodissociation intensity in this region of the IRMPD spectrum of Val•H^+•MeA provides additional support for the assignment of a NZ-N structure for Val•H^+•MeA. For Val•H^+•Et_2A, the weak band in the free OH stretch region indicates that a small population of the NZ-N structure is present, but the strong bonded OH feature indicates that the dominant structure is NZ-C.

In electrospray ionization, large protein ions can be kinetically trapped and can retain a "memory" of their solution-phase structures.[68–70] In aqueous solution, valine is zwitterionic whereas valine is nonzwitterionic in these protonated dimers, and thus kinetic trapping of higher-energy structures is unlikely in these experiments.

3.4 Conclusions

The structure and reactivities of proton-bound dimers consisting of valine and basic primary and secondary amines of varying gas-phase basicity were investigated using IRMPD spectroscopy between 800 and 3700 cm^{-1}, collisionally activated dissociation, and theory. Low-energy dissociation of these dimers results in a sharp transition from formation of protonated valine for bases with GB values below 880 kJ/mol to protonated base for bases with GB values above 880 kJ/mol, but the ratio of these products for bases with similar GB to valine depends on ion internal energy. The results from these experiments at low internal energy indicate that the GB of valine is approximately 880 kJ/mol, which is slightly higher than previously reported values.[63]

The IRMPD spectra clearly indicate a transition in structure with increasing basicity of the base, but this transition occurs only for bases that are ∼20 kJ/mol more basic than valine. Quantum chemical calculations indicate that the lowest-energy structure of protonated heterodimers of valine and methylamine is a salt-bridge structure in which protonated methylamine interacts with the carboxylate group of the zwitterionic form of valine. This result is consistent with previous computational results, including MP2(full)/6-311++G** results for Val•H^+•MeA and calculations for Gly•NH_4^+.[33,43] However, the IRMPD spectra in the higher frequency region clearly rule out this form of the complex. Spectroscopic data are most consistent with a structure in which methylamine coordinates to neutral valine via a strong ionic hydrogen bond at the N-terminus. For the most basic bases, a gradual structural transition occurs. For protonated heterodimers of valine and diethylamine, the most basic amine in this study, the predominant structure is one in which protonated diethylamine hydrogen bonds to the carbonyl oxygen of neutral valine and an internal hydrogen bond between the carboxylic acid hydrogen and the N-terminus of valine is formed. However, even for this cluster, a small population of structures in which the base is N-terminally bound is present.

The binding energies of proton bound dimers are greatest when the proton affinities of the two molecules are similar.[71] In the NZ-N structure, the proton is shared between the most basic sites in each molecule, and this is the predominant structure when the proton affinity of the basic molecule is within 20 kJ/mol of that of valine. The change from an N-terminally bound to a C-terminally bound structure with bases that have even higher proton affinities can be attributed to a destabilization of the NZ-N structure because of the larger difference in proton affinities of the two constituent molecules. This difference is even greater for the NZ-C structure, where the proton is not shared with the most basic site of valine. However, an intramolecular hydrogen bond between the N- and C- termini of valine stabilizes this structure. The stability gained from this neutral hydrogen bond becomes more important as the difference in the proton affinities of the two molecules increases and the stability of the ionic hydrogen bond decreases.

Calculations show that the most favorable protonation site in these dimers is on the base, even for bases with GB values that are lower than valine. However, the calculations incorrectly predict that the zwitterionic form of valine is most stable for protonated dimers with methylamine, the least basic base in this study. The calculations also do not correctly account for the change in structure of these protonated dimers with increasing GB of the base that is clearly observed from the changes in the IRMPD spectra in the higher frequency region. These results suggest that structural conclusions based on calculations of similar protonated complexes may not be reliable at this level of theory. These results also clearly demonstrate the complimentary structural information obtained in the high and low frequency regions of the IRMPD spectra.

Because valine is nonzwitterionic in isolation and also in these protonated dimers with a base, even when the GB of the base is greater than valine by 40 kJ/mol, the kinetic method, with the caveats noted previously by others,[42,72–75] should provide reliable information about the basicity and proton affinity of this and other aliphatic amino acids. For more basic amino acids, such as arginine, which has a greater propensity to form zwitterionic structures in the

presence of a charge, the structure of the amino acid in the protonated dimers may be significantly different from that in isolation. IRMPD spectroscopy should provide detailed information about the structures of these complexes and could provide useful information about how major structural differences of the form of a molecule in a protonated dimer vs in isolation may influence results from kinetic method experiments.

3.5 References

(1) Anderson, D. E.; Becktel, W. J.; Dahlquist, F. W. *Biochemistry* **1990**, 29, 2403-2408.

(2) Errington, N.; Doig, A. J. *Biochemistry* **2005**, 44, 7553-7558.

(3) Hendsch, Z. S.; Tidor, B. *Protein Sci.* **1994**, 3, 211-226.

(4) Horovitz, A.; Serrano, L.; Avron, B.; Bycroft, M.; Fersht, A. R. *Journal of Molecular Biology* **1990**, 216, 1031-1044.

(5) Lee, W. S.; Park, C. H.; Byun, S. M. *J. Biochem.* **2004**, 135, 93-99.

(6) Marqusee, S.; Sauer, R. T. *Protein Sci.* **1994**, 3, 2217-2225.

(7) Wyttenbach, T.; Witt, M.; Bowers, M. T. *Int. J. Mass Spectrom.* **1999**, 182 – 183, 243-252.

(8) Wyttenbach, T.; Witt, M.; Bowers, M. T. *J. Am. Chem. Soc.* **2000**, 122, 3458-3464.

(9) Bertran, J.; Rodriguez-Santiago, L.; Sodupe, M. *J. Phys. Chem. B* **1999**, 103, 2310-2317.

(10) Jockusch, R. A.; Price, W. D.; Williams, E. R. *J. Phys. Chem. A* **1999**, 103, 9266-9274.

(11) Cerda, B. A.; Wesdemiotis, C. *Analyst* **2000**, 125, 657-660.

(12) Bush, M. F.; O'Brien, J. T.; Prell, J. S.; Saykally, R. J.; Williams, E. R. *J. Am. Chem. Soc.* **2007**, 129, 1612-1622.

(13) Forbes, M. W.; Bush, M. F.; Polfer, N. C.; Oomens, J.; Dunbar, R. C.; Williams, E. R.; Jockusch, R. A. *J. Phys. Chem. A* **2007**, 111, 11759-11770.

(14) Bush, M. F.; Oomens, J.; Saykally, R. J.; Williams, E. R. *J. Phys. Chem. A* **2008**, 112, 8578-8584.

(15) Bush, M. F.; Oomens, J.; Saykally, R. J.; Williams, E. R. *J. Am. Chem. Soc.* **2008**, 130, 6463-6471.

(16) O'Brien, J. T.; Prell, J. S.; Steill, J. D.; Oomens, J.; Williams, E. R. *J. Phys. Chem. A* **2008**, 112, 10823-10830.

(17) Polfer, N. C.; Oomens, J.; Dunbar, R. C. *Phys. Chem. Chem. Phys.* **2006**, 8, 2744-2751.

(18) Constantino, E.; Rodriguez-Santiago, L.; Sodupe, M.; Tortajada, J. *J. Phys. Chem. A* **2005**, 109, 224-230.

(19) Ai, H. Q.; Bu, Y. X.; Li, P.; Li, Z. Q.; Hu, X. Q.; Chen, Z. D. *J. Phys. Org. Chem.* **2005**, 18, 26-34.

(20) Ai, H. Q.; Bu, Y. X.; Han, K. L. *J. Chem. Phys.* **2003**, 118, 10973-10985.

(21) Marino, T.; Toscano, M.; Russo, N.; Grand, A. *J. Phys. Chem. B* **2006**, 110, 24666-24673.

(22) Strittmatter, E. F.; Lemoff, A. S.; Williams, E. R. *J. Phys. Chem. A* **2000**, 104, 9793-9796.

(23) Talley, J. M.; Cerda, B. A.; Ohanessian, G.; Wesdemiotis, C. *Chem.-Eur. J.* **2002**, 8, 1377-1388.

(24) Kapota, C.; Lemaire, J.; Maitre, P.; Ohanessian, G. *J. Am. Chem. Soc.* **2004**, 126, 1836-1842.

(25) Lemoff, A. S.; Bush, M. F.; Williams, E. R. *J. Phys. Chem. A* **2005**, 109, 1903-1910.

(26) Dunbar, R. C.; Polfer, N. C.; Oomens, J. *J. Am. Chem. Soc.* **2007**, 129, 14562-14563.

(27) Xu, S. J.; Zheng, W. J.; Radisic, D.; Bowen, K. H. *J. Chem. Phys.* **2005**, 122, 091103.

(28) Skurski, P.; Rak, J.; Simons, J.; Gutowski, M. *J. Am. Chem. Soc.* **2001**, 123, 11073-11074.

(29) Strittmatter, E. F.; Williams, E. R. *J. Phys. Chem. A* **2000**, 104, 6069-6076.

(30) Price, W. D.; Jockusch, R. A.; Williams, E. R. *J. Am. Chem. Soc.* **1997**, 119, 11988-11989.

(31) Oh, H. B.; Lin, C.; Hwang, H. Y.; Zhai, H. L.; Breuker, K.; Zabrouskov, V.; Carpenter, B. K.; McLafferty, F. W. *J. Am. Chem. Soc.* **2005**, 127, 4076-4083.

(32) Wu, R. H.; McMahon, T. B. *J. Am. Chem. Soc.* **2007**, 129, 4864-4865.

(33) Wu, R.; McMahon, T. B. *J. Mass Spectrom.* **2008**, 43, 1641-1648.

(34) Hoyau, S.; Ohanessian, G. *J. Am. Chem. Soc.* **1997**, 119, 2016-2024.

(35) Shoeib, T.; Rodriquez, C. F.; Siu, K. W. M.; Hopkinson, A. C. *Phys. Chem. Chem. Phys.* **2001**, 3, 853-861.

(36) Hoppilliard, Y.; Ohanessian, G.; Bourcier, S. *J. Phys. Chem. A* **2004**, 108, 9687-9696.

(37) Rodriguez-Santiago, L.; Sodupe, M.; Tortajada, J. *J. Phys. Chem. A* **2001**, 105, 5340-5347.

(38) Rajabi, K.; Fridgen, T. D. *J. Phys. Chem. A* **2008**, 112, 23-30.

(39) Raspopov, S. A.; McMahon, T. B. *J. Mass Spectrom.* **2005**, 40, 1536-1545.

(40) McLuckey, S. A.; Cameron, D.; Cooks, R. G. *J. Am. Chem. Soc.* **1981**, 103, 1313-1317.

(41) McLuckey, S. A.; Cooks, R. G.; Fulford, J. E. *Int. J. Mass Spectrom. Ion Processes* **1983**, 52, 165-174.

(42) Cooks, R. G.; Wong, P. S. H. *Acc. Chem. Res.* **1998**, 31, 379-386.

(43) Wu, R.; McMahon, T. B. *J. Am. Chem. Soc.* **2008**, 130, 3065-3078.

(44) Fridgen, T. D.; MacAleese, L.; Maitre, P.; McMahon, T. B.; Boissel, P.; Lemaire, J. *Phys. Chem. Chem. Phys.* **2005**, 7, 2747-2755.

(45) Fridgen, T. D.; MacAleese, L.; McMahon, T. B.; Lemaire, J.; Maitre, P. *Phys. Chem. Chem. Phys.* **2006**, 8, 955-966.

(46) Fridgen, T. D.; McMahon, T. B.; MacAleese, L.; Lemaire, J.; Maitre, P. **2004**, 108, 9008-9010.

(47) Atkins, C. G.; Rajabi, K.; Gillis, E. A. L.; Fridgen, T. D. **2008**, 112, 10220-10225.

(48) Roscioli, J. R.; McCunn, L. R.; Johnson, M. A. *Science* **2007**, 316, 249-254.

(49) Armentrout, P. B.; Rodgers, M. T.; Oomens, J.; Steill, J. D. *J. Phys. Chem. A* **2008**, 112, 2248-2257.

(50) Bush, M. F.; Forbes, M. W.; Jockusch, R. A.; Oomens, J.; Polfer, N. C.; Saykally, R. J.; Williams, E. R. *J. Phys. Chem. A* **2007**, 111, 7753-7760.

(51) Bush, M. F.; Prell, J. S.; Saykally, R. J.; Williams, E. R. *J. Am. Chem. Soc.* **2007**, 129, 13544-13553.

(52) Rodgers, M. T.; Armentrout, P. B.; Oomens, J.; Steill, J. D. *J. Phys. Chem. A* **2008**, 112, 2258-2267.

(53) Price, W. D.; Schnier, P. D.; Williams, E. R. *J. Phys. Chem. B* **1997**, 101, 664-673.

(54) Schnier, P. D.; Jurchen, J. C.; Williams, E. R. *J. Phys. Chem. B* **1999**, 103, 737-745.

(55) Senko, M. W.; Canterbury, J. D.; Guan, S. H.; Marshall, A. G. *Rapid Commun. Mass Spectrom.* **1996**, 10, 1839-1844.

(56) Valle, J. J.; Eyler, J. R.; Oomens, J.; Moore, D. T.; van der Meer, A. F. G.; von Helden, G.; Meijer, G.; Hendrickson, C. L.; Marshall, A. G.; Blakney, G. T. *Rev. Sci. Instrum.* **2005**, 76, 023103.

(57) Polfer, N. C.; Oomens, J.; Moore, D. T.; von Helden, G.; Meijer, G.; Dunbar, R. C. *J. Am. Chem. Soc.* **2006**, 128, 517-525.

(58) Shao, Y. *et al. Phys. Chem. Chem. Phys.* **2006**, 8, 3172-3191.

(59) Kamariotis, A.; Boyarkin, O. V.; Mercier, S. R.; Beck, R. D.; Bush, M. F.; Williams, E. R.; Rizzo, T. R. *J. Am. Chem. Soc.* **2006**, 128, 905-916.

(60) Prell, J. S.; Demireva, M.; Oomens, J.; Williams, E. R. *J. Am. Chem. Soc.* **2008**, 131, 1232-1242.

(61) Gorman, G. S.; Speir, J. P.; Turner, C. A.; Amster, I. J. *J. Am. Chem. Soc.* **1992**, 114, 3986-3988.

(62) Li, X. P.; Harrison, A. G. *Org. Mass Spectrom.* **1993**, 28, 366-371.

(63) Hunter, E. P. L.; Lias, S. G. *J. Phys. Chem. Ref. Data* **1998**, 27, 413-656.

(64) Bleiholder, C.; Suhai, S.; Paizs, B. *J. Am. Soc. Mass Spectrom.* **2006**, 17, 1275-1281.

(65) Stearns, J. A.; Mercier, S.; Seaiby, C.; Guidi, M.; Boyarkin, O. V.; Rizzo, T. R. *J. Am. Chem. Soc.* **2007**, 129, 11814-11820.

(66) Bush, M. F.; Saykally, R. J.; Williams, E. R. *ChemPhysChem* **2007**, 8, 2245-2253.

(67) O'Brien, J. T.; Williams, E. R. *J. Phys. Chem. A* **2008**, 112, 5893–5901.

(68) Gross, D. S.; Zhao, Y.; Williams, E. R. *J. Am. Soc. Mass Spectrom.* **1997**, 8, 519-524.

(69) Myung, S.; Badman, E. R.; Lee, Y. J.; Clemmer, D. E. *J. Phys. Chem. A* **2002**, 106, 9976-9982.

(70) Robinson, E. W.; Williams, E. R. *J. Am. Soc. Mass Spectrom.* **2005**, 16, 1427-1437.

(71) Meot-Ner, M. *Chem. Rev.* **2005**, 105, 213-284.

(72) Armentrout, P. B. *J. Mass Spectrom.* **1999**, 34, 74-78.

(73) Armentrout, P. B. *J. Am. Soc. Mass Spectrom.* **2000**, 11, 371-379.

(74) Cooks, R. G.; Koskinen, J. T.; Thomas, P. D. *J. Mass Spectrom.* **1999**, 34, 85-92.

(75) Drahos, L.; Vekey, K. *J. Mass Spectrom.* **1999**, 34, 79-84.

3.6 Tables and Figures

molecule	gas-phase basicity kJ/mol*	NZ-C kJ/mol	NZ-N kJ/mol	Z-C kJ/mol
valine	880			
methylamine	864.5	4/7 (4/7)	11/15 (2/6)	0/0 (0/0)
ethylamine	878	0/4	10/14	$\sim$ 0/0
propylamine	883.9	0/0	12/11	5/3
butylamine	886.6	0/0	7/4	2/5
isopropylamine	889	1/0	6/10	0/6
hexylamine	893.5	0/0	10/18	7/16
sec-butylamine	895.7	0/0	7/12	$\sim$ 0/13
dimethylamine	896.5	0/0	11/12	7/8
tert-butylamine	899.9	0/0	10/16	3/9
methylethylamine	910	0/0	9/10	5/$\sim$0
diethylamine	919.9	0/0 (7/5)	14/12 (5/5)	9/7 (0/0)

*Basicity values except for valine from ref 63. Valine value from this work.

Table 3.1: Relative Energies at 0/351 K, B3LYP/6-31++G** (MP2/6-31++G** Single Point Energies with B3LYP ZPE and entropy corrections)

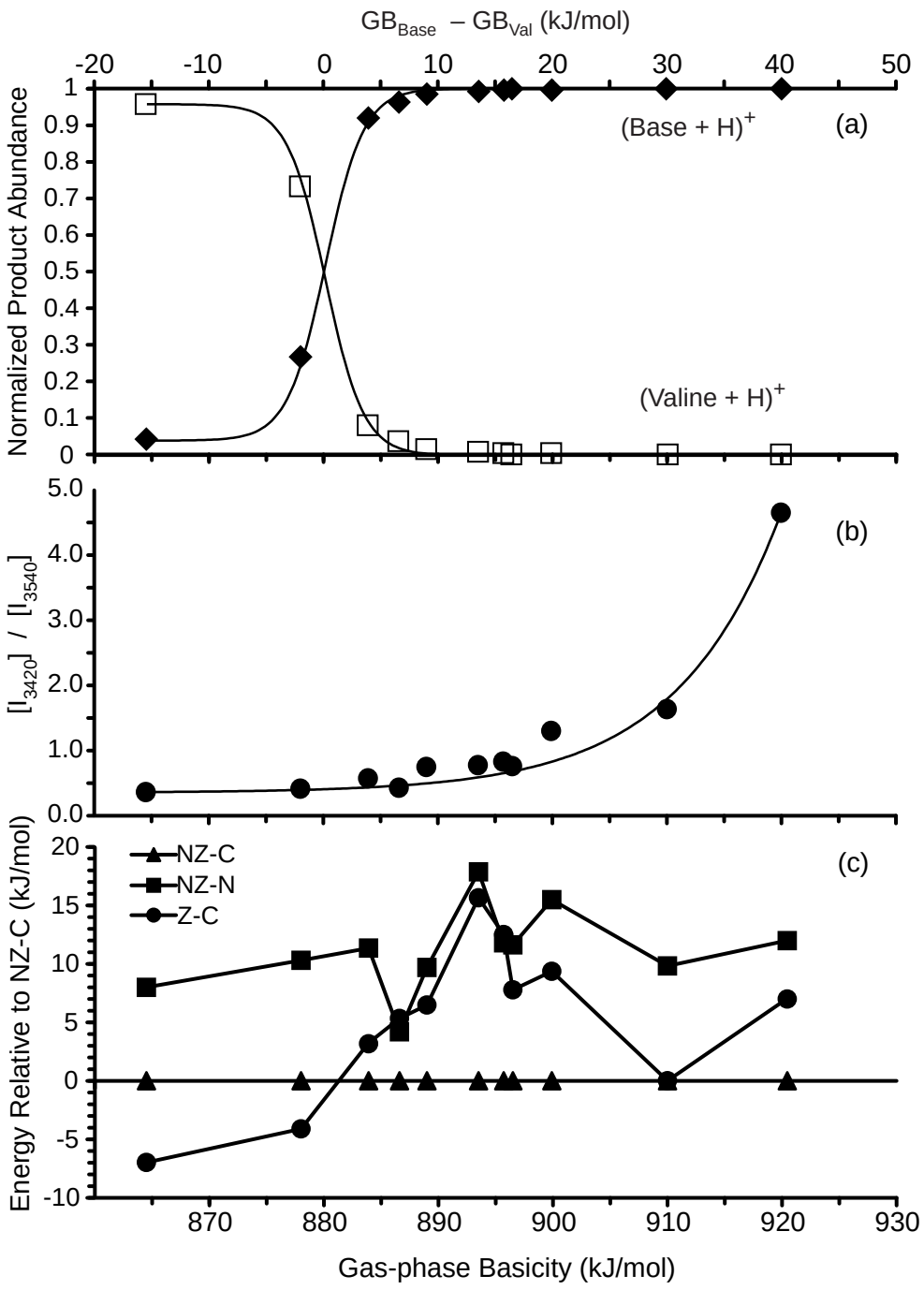

Figure 3.1: (a) SORI-CAD product ion abundances for dissociation of Val•H+•B (b) ratio of the band intensity at 3420 cm^{-1}, [I_{3420}], to the intensity at 3540 cm^{-1}, [I_{3540}], from the IRMPD spectra of the proton bound valine-base dimers (c) Gibbs free energies of the NZ-N and Z-C structures relative to NZ-C at 351 K calculated at the B3LYP/6-31++G** level of theory as a function of the gas-phase basicity of the base. The GB_{Base} – GB_{Val} values are based on a GB_{Val} = 880 kJ/mol.

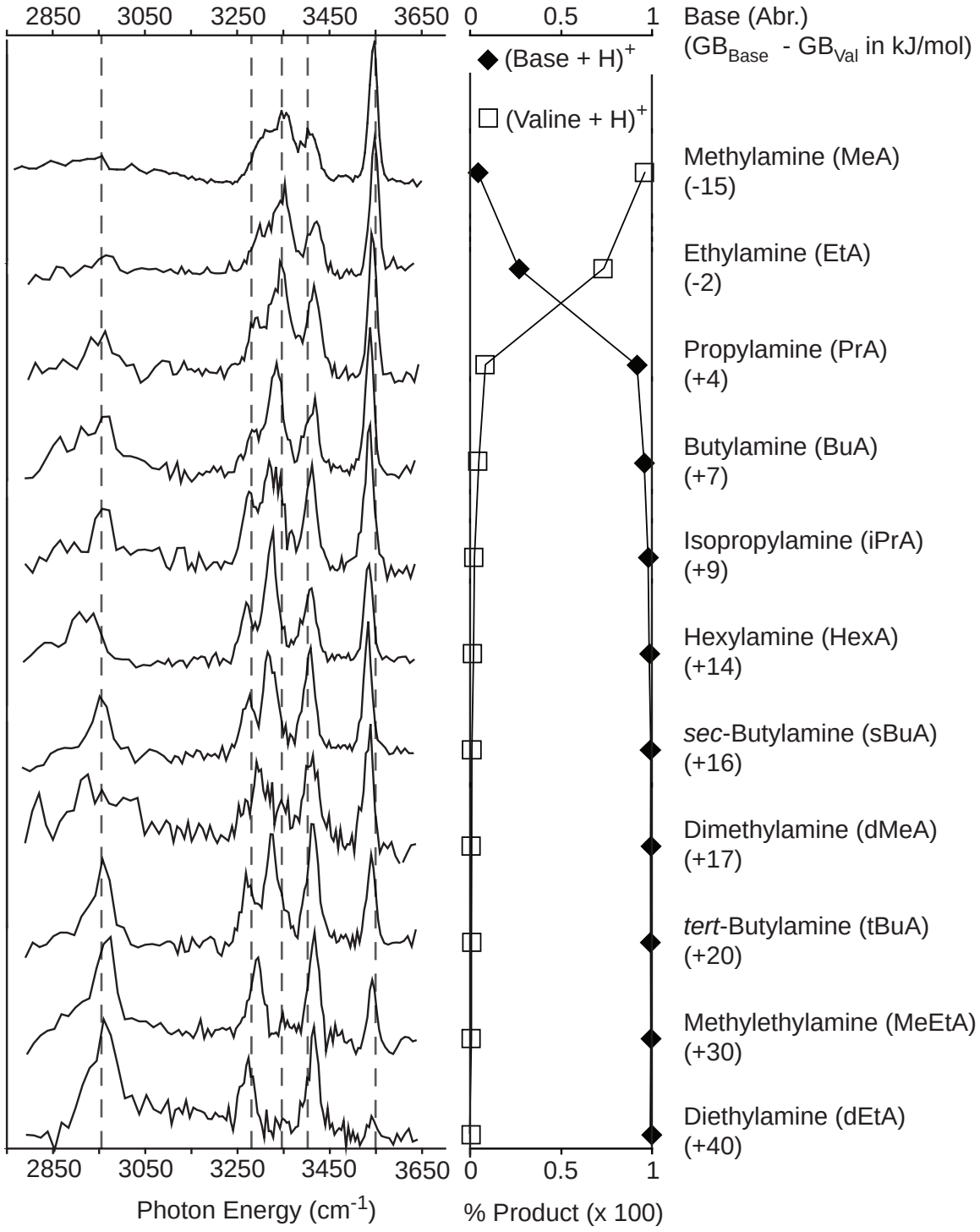

Figure 3.2: Dissociation of Val•H$^+$•B: IRMPD spectra from 2750 to 3700 cm^{-1} (left) and SORI-CAD product ratios (right). The identities of B and GB_{Base} – GB_{Val} are indicated to the right of the experimental data.

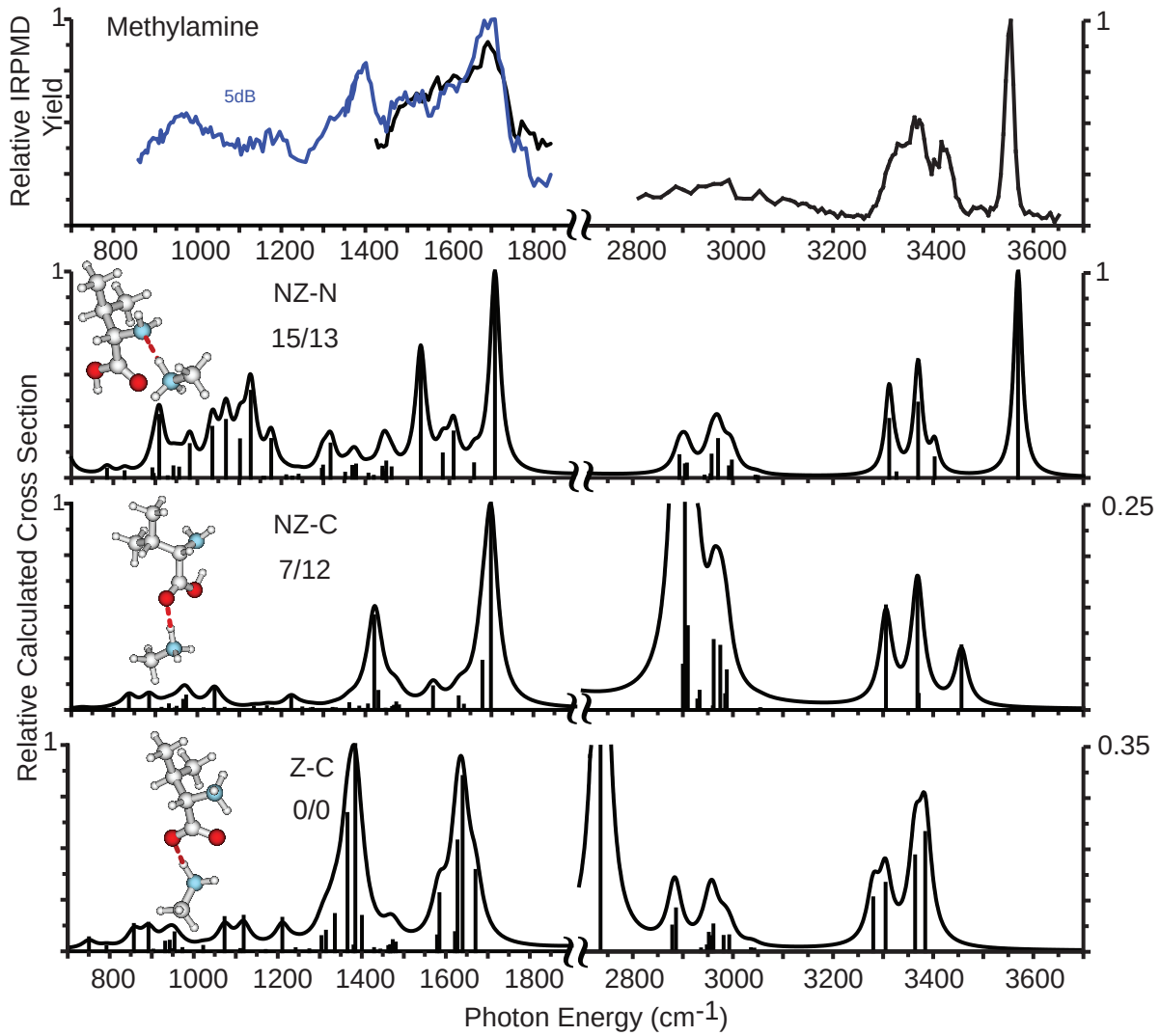

Figure 3.3: IRMPD spectra of Val•H^+•MeA from 800–1900 cm^{-1} and 2800–3700 cm^{-1} obtained at 298 K and 351 K, respectively, and calculated absorption spectra for three low-energy structures, NZ-N, NZ-C and Z-C, at the B3LYP/6-31++G** level of theory. The relative Gibbs free energies at 351 K at the (B3LYP/6-31++G**)/(MP2//B3LYP/6-31++G**) levels of theory are reported.

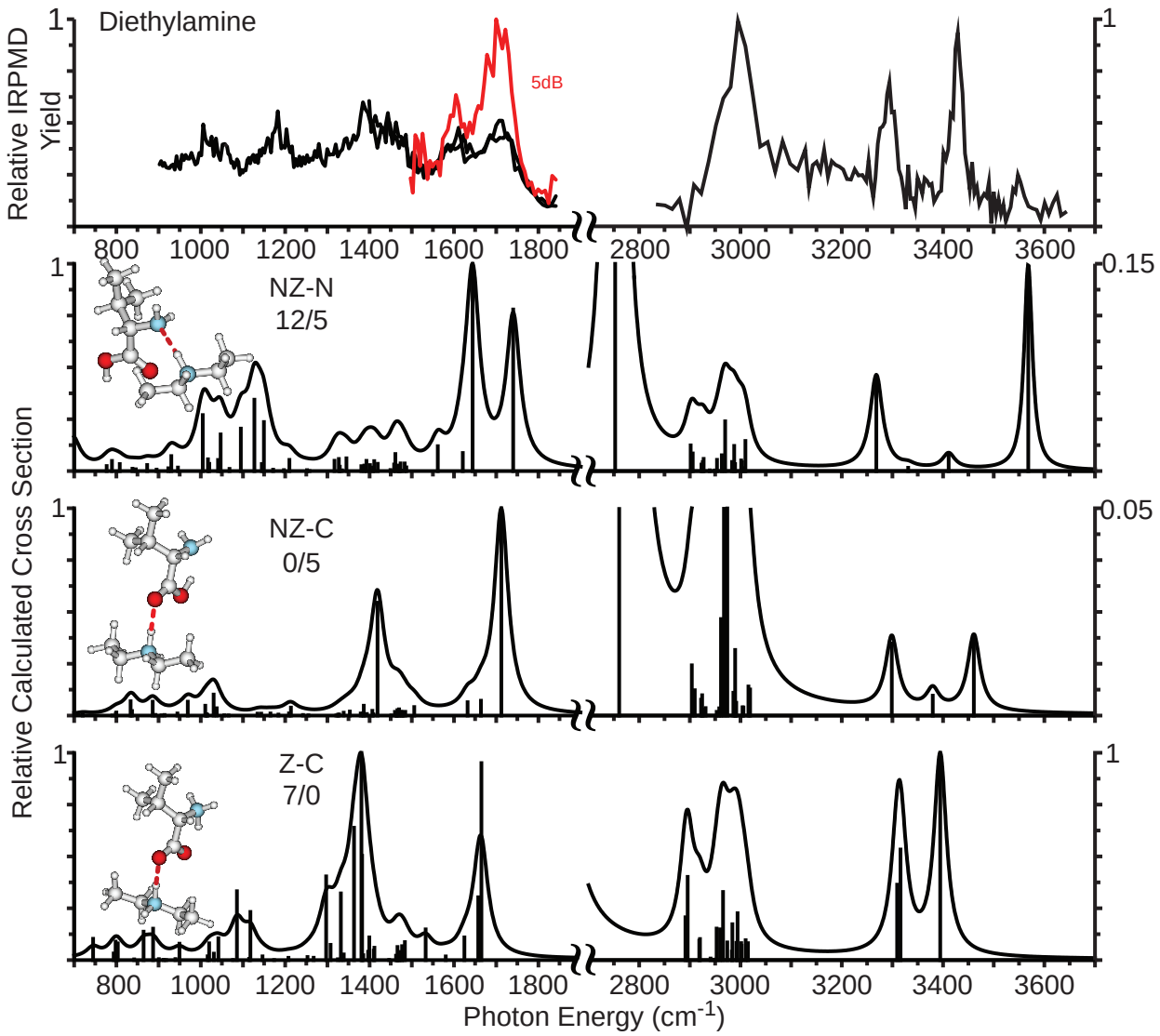

Figure 3.4: IRMPD spectra of Val•H^+•Et_2A from 800–1900 cm^{-1} and 2800–3700 cm^{-1} obtained at 298 K and 351 K, respectively, and calculated absorption spectra for three low energy structures, NZ-N, NZ-C and Z-C at the B3LYP/6-31G++** level of theory. The relative Gibbs free energies at 351 K at the (B3LYP/6-31++G**)/(MP2//B3LYP/6-31++G**) levels of theory are reported.

Chapter 4

Interactions of Mono- and Divalent Metal Ions with Aspartic and Glutamic Acid Investigated with IR Photodissociation Spectroscopy and Theory

Jeremy T. O'Brien, James S. Prell, Jeffrey D. Steill, Jos Oomens, and Evan R. Williams

Journal of Physical Chemistry A, 2008, 112, 10823–10830

4.1 Introduction

Metal ions and solvent molecules play important roles in the structure and reactivity of biomolecules.[1,2] Many proteins require metal ions to fold and become active. Ion-protein interactions are involved in ion transport through cell membranes and in enzymatic catalysis of red-ox reactions. Competitive effects of solvent influence the interactions of metal ions with biomolecules. In the late 1800s, it was recognized that ions varied in their effects on fundamental properties of ionic solutions, such as their ability to denature proteins. Hofmeister ordered ions in their tendency to precipitate proteins or denature proteins,[2] and even today, the origin of this Hofmeister effect is still debated.[3–5]

With mass spectrometry, it is possible to isolate and investigate the structures of cationized biomolecules.[6–50] and investigate how ions and water molecules competitively interact with biomolecules.[18,22,47–49] Such experiments make possible a detailed understanding of competitive effects of ion and solvent interactions with biomolecules. Of particular interest to many groups has been the interaction of metal ions with amino acids and the effects of metal ions on the stability of the zwitterionic form of the amino acid.[10–32,35,46–56] In isolation, all naturally occurring amino acids are nonzwitterionic, even the most basic amino acid, arginine, for which the zwitterionic structure is only 12 – 16 kJ/mol higher in energy.[57–59] The zwitterionic form of an amino acid can be stabilized when a metal ion is attached.[11–32,50–56] The zwitterionic form of arginine, in which the side-chain guanidinium group is protonated and the C-terminus is deprotonated, is most stable when complexed to sodium and the larger alkali metal ions,[11,17,50] and the zwitterionic forms of other amino acids have been reported for both mono-[19,27] and di-cations[14,16,32,53–56]

Either increasing the proton affinity of the proton accepting site[23–25,28,46,60,61] or increasing the acidity of the proton-donating group[60] can potentially stabilize the zwitterionic form of a molecule. For example, the stabilities of the zwitterionic forms of amino acids with aliphatic side chains when complexed with sodium ions are directly related to the proton affinity of the amino acid.[23,24] For amino acids that have one or more heteroatoms in their side chain, such as basic or acidic amino acids, the relation can be much less direct.[11–13,17,28,30,58,59] For example, the charge-solvated forms of lithiated arginine[11,17] and lithiated glycine[52,53] in which the amino acids are nonzwitterionic are both ∼16 kJ/mol more stable than the corresponding zwitterionic forms despite the fact that the proton affinity of arginine is 160 kJ/mol higher than that of glycine.[62] Heteroatoms in the side chain can result in significant stabilization of the charge-solvated structures.[11–13,17,28,30,58,59] The roles of metal ion size, charge state, and amino acid basicity on the propensity for zwitterion formation have

been extensively studied.[11−32,46,52−56] In contrast, the role of gas-phase acidity on amino acid zwitterionic stability is less well known.

The gas-phase acidities (ΔH_{acid}) of the 20 naturally occurring α-amino acids range from ∼1435 kJ/mol for glycine to ∼1350 kJ/mol for aspartic (Asp) and glutamic (Glu) acid, (Scheme 1) the two most acidic amino acids that have side-chain carboxylic acid groups.[63,64]

Scheme 1

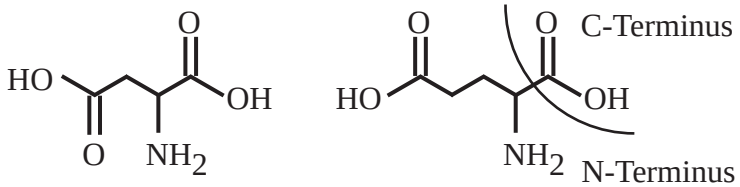

Aspartic Acid Glutamic Acid

By comparison, the gas-phase acidity of propanoic acid (CH_3CH_2COOH) is ∼1454 kJ/mol.[65] This indicates that the intrinsic acidity of the C-terminus is higher than that of the side-chain carboxylic acid group, consistent with calculations which indicate that the C-terminus is preferentially deprotonated in the isolated amino acid.[63,64] The high acidity of Asp and Glu can be attributed to the high stability of the deprotonated forms of these amino acids in which the hydrogen atom of the side-chain carboxylic acid interacts with the C-terminal carboxylate.[63,64]

IR action spectroscopy can provide significant information about the structure of gas-phase ions and has been recently used to elucidate the structures of many cationized amino acids,[11−19,28−31,39] and amino acid complexes.[34,35,40−45] Here the results of IR action spectroscopy in the frequency range of 950 – 1900 cm^{-1} and density functional theory calculations on Asp•M^+, Glu•M^+, M = H, Li, and Cs, Glu•Ca^{2+} and Glu•Ba^{2+} are presented. From these results, information about the effects of mono- and divalent cations on the structures of Asp and Glu and the role of gas-phase acidity on zwitterion stability is obtained.

4.2 Experimental

4.2.1 IR Photodissociation Spectroscopy

All experiments were performed on a 4.7 T Fourier-transform ion cyclotron resonance mass spectrometer. The instrument[66] and experimental methods[31] are described in detail elsewhere. In brief, cationized Asp and Glu were formed by electrospray ionization from a 60/40 water/methanol solution of 2 mM amino acid and 2 mM metal chloride salt infused at a rate of 15-20 μL/min. Precursor ions were mass selected using stored waveform inverse Fourier transforms and subsequently irradiated for 2.5 to 4.5 s using tunable irradiation from the Free-Electron Laser for Infrared eXperiments (FELIX).[67] The same irradiation time was used for each ion and was selected based on the ion stability as indicated by photodissociation yield.

4.2.2 Computations

Low-energy structures of cationized Asp and Glu were generated using Monte Carlo conformational searching and the MMFFs force field as implemented in Macromodel 9.1 (Schrödinger, Inc. Portland, OR). In the initial searches, no constraints were placed on the geometry and 5000 conformers were generated for both nonzwitterionic and zwitterionic forms of Asp•Li^+, Glu•Li^+, Glu•Ca^{2+}, and Glu•Ba^{2+}. The resulting low-energy structures were sorted into different groups with similar metal coordination. Structures for cesiated complexes were generated by metal ion subsititution into lithiated structures prior to geometry optimization. Representative structures from each group were geometry optimized in Q-Chem v. 3.0[68] using hybrid method density functional calculations (B3LYP) with the CRENBL[69] effective core potential for Cs, Ca and Ba and the 6-31++G** basis set for all other atoms. Vibrational frequencies and intensities were calculated using the double harmonic approximation and the analytical Hessian of the energy minimized structures using Q-Chem v. 3.0.[68] Most structures yielded all positive frequency vibrations, but two of the structures for the cesiated species of nonzwitterionic (NZ) Asp and Glu each had two imaginary frequencies < 80 cm^{-1} indicative of torsional modes on a very flat region of the potential energy surface or computational artifacts. In one of these structures, the cesium ion coordinates to the two carbonyl oxygen atoms (NZ O_SO_C; where S indicates the side-chain carbonyl oxygen atom and C indicates the C-terminal carbonyl oxygen atom). The other structure, NZ NO_SO_C, which results in imaginary frequencies is similar, except that the nitrogen of the N-terminus also solvates the cesium ion. Gibbs free energies including zero point energy corrections were determined at 0 K and 298 K. All frequencies were scaled by 0.975. This scaling factor has been used previously in other IR studies in this region to compare experimental photodissociation spectra to spectra calculated at similar levels of theory as used in this study.[13,14,28,29] The frequencies were convolved with a 40 cm^{-1} fwhm Lorentzian distribution which provides a good fit to the observed peak shapes.

4.3 Results and Discussion

Photodissociation of protonated and metal cationized Asp and Glu results in dissociation by several different pathways that depend on the cation (Table 1). Rearrangement reactions resulting in loss of water or formic acid commonly occur. For both Asp•Cs^+ and Glu•Cs^+, bare cesium ion is the only product observed, consistent with a low binding energy for this large cation. For Glu•Ca^{2+} and Glu•Ba^{2+}, both loss of formic acid and MOH^+ are observed. Photodissociation action spectra are obtained from the sum of the photodissociation product ion intensities divided by the total ion intensity measured as a function of photon energy. The laser power is relatively flat from 625 to 1250 cm^{-1} but decreases by ∼3x between 1250 and 1900 cm^{-1}. To roughly account for this change in power, the action spectra are linearly power-corrected.[31] The IR action spectra of Asp•H^+, Asp•Li^+, Asp•Cs^+, Glu•H^+, Glu•Li^+, Glu•Cs^+, Glu•Ca^{2+}, and Glu•Ba^{2+} are shown in Figure 1. Information about the structure of these ions is obtained from comparison among the spectra reported here, comparison to previously reported IR action spectra of cationized amino acids,[12−14,16,19,28−31] and by

comparison to calculated spectra of candidate low-energy structures. The relative Gibbs free energies of these low-energy structures at 0 and 298 K calculated at the B3LYP/CRENBL level of theory for Cs^+, Ba^{2+} and Ca^{2+} and B3LYP/6-31++G** for all other atoms/ions are reported in Table 2.

There are a number of factors that can contribute to differences between IR photodissociation spectra and calculated absorption spectra. Band intensities are calculated using a double harmonic approximation which results in attendant uncertainties in comparing with measured spectra. IR photodissociation spectroscopy is a multiple photon process under these conditions.[70] The IR photodissociation spectrum of naphthalene cation is similar to the measured single-photon linear absorption spectrum.[71] However, several factors can contribute to differences in spectra measured by the two methods. A more complete discussion of the dynamics of IRMPD in these experiments, and their effects on the resulting spectra are reviewed elsewhere.[70]

4.3.1 Asp•H^+ and Glu•H^+

The IR action spectra of protonated Asp and Glu have many common features, including bands centered near 1790, 1710, 1600, 1450, 1300, and 1150 cm^{-1} (Figure 2). In addition, the Glu•H^+ spectrum contains two bands at 1250 and ∼1000 cm^{-1} that are not observed for Asp•H^+. These additional bands are consistent with CH bending modes and C-C stretches associated with the additional CH_2 group in the Glu side chain. The broad photodissociation intensity between 1375 and 1550 cm^{-1} for Glu•H^+ consists of two or more poorly resolved bands whereas the feature for Asp•H^+ is narrower, indicating closer spacing of these bands.

The bands in these spectra can be assigned to vibrational modes based on comparison to the previously reported spectra of protonated and metal cationized amino acids[12–14,28–30] and to the calculated spectra of the lowest-energy structures for both Asp•H^+ and Glu•H^+ (Figure 2). These assignments are given in Table 3. The two peaks between 1700 and 1800 cm^{-1} are consistent with carbonyl stretches. Carbonyl stretches of carboxylic acid groups have been reported previously in this spectral region for protonated arginine[17] and lysine,[28] as well as for many metal-cationized amino acids.[12,14,17,19,29–31]

Protonation at the N-terminus is at least 40 kJ/mol lower in energy than protonation at the carbonyl oxygen of the C-terminus (structures DI and DII, Figure 2). In all the low-energy structures, the protonated nitrogen donates one hydrogen bond to each of the carbonyl oxygen atoms. The H-bond distance to the side-chain and C-terminal carbonyl oxygens is ∼1.5 – 1.6 Å and 2.1 – 2.2 Å, respectively, for these structures, consistent with a stronger hydrogen bond between the protonated N-terminus and the side-chain carbonyl oxygen. This strong hydrogen bond causes a significant red-shift in the carbonyl stretch of the side chain compared to that of the C-terminus. This red shift is greater for Glu•H^+ because the longer side chain provides greater flexibility which enables formation of an even stronger ionic hydrogen bond between the protonated N-terminus and the carbonyl oxygen of the side chain.

The broad feature between 1375 and 1500 cm^{-1} in the spectra of both Asp•H^+ and Glu•H^+ is consistent with previous assignments of hydrogen-bonded NH bends, a free OH

bend of the side-chain carboxylic acid group, and CH bends.[12–14,28–30] Below 1300 cm^{-1}, the most prominent feature in both IR action spectra is a peak centered around 1150 cm^{-1}. A similar band is observed for Gln•Li^+, Lys•Li^+, Ser•Li^+, and Thr•Li^+ and is assigned to the in-plane OH bend of the free hydrogen atom in a carboxylic acid group.[12,13,28,30] For Asp•H^+ and Glu•H^+, both carboxylic acid groups contribute to this feature.

Calculated structures A and B are nearly identical except that in structure A, the hydroxyl oxygen, instead of the carbonyl oxygen, of the C-terminal carboxylic acid group accepts the hydrogen bond. This interaction is less favorable, and structure A is 10 and 14 kJ/mol less stable than structure B for Asp•H^+ and Glu•H^+, respectively. The spacing between carbonyl oxygen stretches in the measured spectra is more consistent with structures B and C. Structures B and C are also very similar and have energies within 3 kJ/mol of each other. Their calculated IR spectra are consistent with the measured IR action spectra. Because these structures are nearly isoenergetic and almost certainly have very low barriers for interconversion, it is likely that both structures are populated and both contribute to the observed IR action spectra. The experimental spectra of Asp•H^+ and Glu•H^+ provide a model for spectroscopic features associated with a protonated N-terminus of Asp and Glu and can be used to identify expected spectral features in possible zwitterionic structures for metal-cationized Asp and Glu.

4.3.2 Asp•Li^+ and Glu•Li^+

The IR action spectra of Asp•Li^+ and Glu•Li^+ are also very similar to each other, but the relative intensities of some bands differ (Figure 3). The bands at ∼1000 and ∼1600 cm^{-1} are substantially more intense in the Glu•Li^+ spectrum, although these features are certainly present in the Asp•Li^+ spectrum. Instead of two distinct bands corresponding to the two carbonyl stretches in the spectra of the protonated species, there is only a single band in the carbonyl stretch region of the lithiated species, indicating that the ionic hydrogen bonds that occur for the protonated amino acids are not present in the lithiated forms. A zwitterionic structure for the amino acid in the metal cationized species should have two distinguishable carbonyl stretch vibrations owing to the presence of both a carboxylate and a carboxylic acid, and can be ruled out based on the single, albeit broad, band in this region.

Three structural families were identified from conformational searching of the lithiated amino acids: a non-zwitterionic (NZ) structure where one oxygen from each of the carboxylic acid groups and the N-terminal nitrogen all coordinate to the metal ion (NZ NO_SO_C; where S indicates the side-chain carbonyl oxygen atom and C indicates the C-terminal carbonyl oxygen atom); an NZ O_SO_C coordinated structure in which the N-terminal nitrogen accepts a hydrogen bond donated by the backbone carboxylic acid group; and the lowest-energy zwitterionic (ZW) structure for both species, ZW OO_C, where the metal ion coordinates to both the oxygen atoms of the deprotonated C-terminus and the protonated N-terminus donates a hydrogen bond to an oxygen atom of the carboxylic acid and carboxylate groups. A similar ZW OO_C structure which instead has a deprotonated side chain was calculated to be ∼6 kJ/mol less stable. This is consistent with the lower ΔH_{acid} of the C-terminus compared with that of the side chain for both amino acids.[63,64]

The band observed in the experimental spectra at ∼1600 cm^{-1} is consistent with an NH_2 scissoring mode in both the NZ NO_SO_C and NZ O_SO_C calculated spectra. The calculated intensity of this vibration is similar for both lithiated species, whereas this band is clearly more intense in the measured spectrum of Glu•Li^+. The band at ∼1000 cm^{-1} is consistent with the out-of-plane wag of the NH_2 group in the NZ NO_SO_C calculated spectrum. This vibration for the NZ O_SO_C structure is calculated to occur at a substantially lower frequency, ∼850 cm^{-1}. The relative Gibbs free energies at 298 K of the three calculated structures indicate that the NZ NO_SO_C structure is lowest in energy for both Asp•Li^+ and Glu•Li^+; the NZ O_SO_C structure is higher by 33 and 28 kJ/mol, respectively, and the zwitterionic structures are even higher. The relative intensities of the ∼1000 cm^{-1} band, the overall excellent agreement between the measured and calculated spectra, and the calculated relative energies all indicate that both Asp•Li^+ and Glu•Li^+ adopt an NZ NO_SO_C coordinated structure similar to the lowest-energy structures reported for lithiated glutamine,[13] serine,[12] and threonine,[30] which also have oxygen atom containing side chains.

4.3.3 Asp•Cs^+ and Glu•Cs^+

The IR action spectra of Asp•Cs^+ and Glu•Cs^+ are very similar to each other and consist of three distinct, broad bands centered at ∼1760, 1400, and 1150 cm^{-1} (Figure 4). These similar spectra indicate that the difference in the length of the side chain plays little role in the structure adopted by each amino acid when complexed with cesium. However, the calculated energies and spectra of candidate low-energy structures indicate that Asp•Cs^+ and Glu•Cs^+ adopt different structures, although the difference is very subtle. As was the case for lithium, the carbonyl stretches are not resolved, resulting in a relatively broad band at ∼1760 cm^{-1}. This band is blue-shifted from the corresponding band in the lithiated spectra by ∼20 cm^{-1}. A similar shift has been observed between the lithiated and cesiated IR action spectra of glutamine,[13] tryptophan,[29] serine,[12] and threonine,[30] consistent with less transfer of electron density for the larger cation. As for the lithiated species, zwitterionic forms of the cesiated species should have two different carbonyl stretch features due to the presence of both a carboxylic acid and a carboxylate group and can be ruled out by the position of the single broad band in this region. In addition, the NH bending modes around 1400 cm^{-1} in the spectra of the cesiated species do not match the features observed for the protonated species indicating that the N-terminus is not protonated and hence the cesiated amino acids are not zwitterionic.

The most apparent difference between the cesiated and lithiated IR action spectra is the absence of distinct bands at 1000 and 1600 cm^{-1} in the spectra of the cesiated species, whereas these features are clearly present in the spectra of the lithiated species. These bands are consistent with NH bends of an amine coordinating with a metal ion (*vide supra*). The absence of these bands in the Cs^+ spectra indicates that the nitrogen is not coordinating directly to the cesium ion.

The same structural families identified for the lithiated species were also calculated to be stable for Cs^+, but two additional conformational families were identified: an NZ O_SOO_C structure in which the cesium coordinates to both oxygens of the C-terminal carboxylic acid

group and the side-chain carbonyl oxygen and an NZ OO_S structure in which the metal ion coordinates to both oxygens of the side-chain carboxylic acid that also donates a hydrogen bond to the N-terminus. The NZ O_SOO_C structure is calculated to be unstable for the lithiated species and isomerizes during energy minimization to an NZ O_SO_C coordinated structure. The NZ O_SOO_C structure is lowest in energy for Asp•Cs^+, whereas the ZW OO_C structure is calculated to be the most stable form of Glu•Cs^+. However, the IR action spectrum shows no significant photodissociation indicative of the carbonyl stretch associated with a carboxylate group at 1675 cm^{-1}, and the experimental features below 1500 cm^{-1} do not match the calculated spectrum of the zwitterionic structure (Figure 4). For both Asp and Glu, a zwitterionic structure with a deprotonated side chain spontaneously transferred a proton from the protonated N-terminus to the side chain upon geometry optimization, resulting in a non-zwitterionic side-chain coordinated structure NZ OO_S. The OH bend of the hydrogen-bonded side-chain carboxylic acid is calculated to occur at ∼1540 cm^{-1} with significant intensity. These NZ OO_S structures can be ruled out by the absence of this feature in the IR action spectra and the absence of a strong band at ∼1400 cm^{-1} in the calculated spectra.

The NZ O_SOO_C structure of Asp•Cs^+ is calculated to have an intense band corresponding to the OH bend of the side-chain carboxylic acid at ∼1150 cm^{-1}, whereas this feature is much weaker in the calculated spectrum of the NZ O_SO_C structure. The intensity of the experimentally observed dissociation at 1150 cm^{-1} is substantial and indicates the presence of NZ O_SOO_C or NZ NO_SO_C structures for Asp. The absence of a distinct band at 1000 cm^{-1}, observed in the lithiated spectra and calculated NZ NO_SO_C structure, indicates that this structure is absent or contributes only minimally to the spectrum of Asp•Cs^+. The calculated spectra contain an NH_2 scissoring mode at ∼1600 cm^{-1} for all three non-zwitterion structures, suggesting that the out-of-plane NH_2 wag at 1000 cm^{-1} is more sensitive to metal ion coordination with the nitrogen. On the basis of these comparisons, the IR action spectrum is most consistent with an NZ O_SOO_C structure, although contribution from NZ O_SO_C or NZ NO_SO_C structures cannot be ruled out.

For Glu•Cs^+, the IR action spectrum is most consistent with the calculated spectrum of an NZ O_SO_C structure (Figure 4), which has three distinct bands centered at ∼1760, 1385 and 1140 cm^{-1} that match very well with the observed bands. However, other structures may also be present. The NZ O_SO_C and NZ O_SOO_C forms of Glu•Cs^+ differ only by a small displacement of the large cesium cation and almost certainly have a low barrier to interconversion. Thus, both of these structures are likely present. The calculated spectrum of the NZ O_SOO_C structure lacks a distinct peak at ∼1140 cm^{-1} because the OH bend which occurs at that frequency in the NZ NO_SO_C and NZ O_SO_C structures instead couples with CH and NH twists, resulting in a distribution of weak bands. The calculated NZ NO_SO_C spectrum matches two of the experimental features but lacks a strong band at ∼1400 cm^{-1}. The photodissociation intensity at ∼1000 cm^{-1} is consistent with a population of NZ O_SOO_C, and NZ NO_SO_C structures may also be present and contribute to photodissociation in this region. All three of these structures, NZ O_SO_C, NZ O_SOO_C, and NZ NO_SO_C, have similar calculated spectra and likely contribute to the observed spectrum.

4.3.4 Glu•Ba^{2+} and Glu•Ca^{2+}

In the IR action spectra of both Glu•Ba^{2+} and Glu•Ca^{2+} (Figure 5), two bands are observed in the carbonyl stretch region centered at ∼1600 and 1660 cm^{-1} and are attributed to the carbonyl stretches of a carboxylate and a carboxylic acid, respectively. The carboxylic acid carbonyl stretch is red-shifted from the corresponding band observed for H^+, Li^+, and Cs^+, and this shift can be attributed to greater transfer of electron density to the divalent cation compared to the monovalent ions. The remaining features of the spectra are very similar to those observed in the IR action spectrum of Glu•H^+: a broad band centered at ∼1440 cm^{-1} and three smaller bands at ∼1290, 1340, and 1160 cm^{-1}. The experimental band at ∼1440 cm^{-1}, corresponding to NH bends, is both higher in frequency and substantially broader than similar features observed in the IR action spectra of the lithiated and cesiated complexes. However, the width and frequency of this feature are similar to those observed in the protonated complexes, consistent with structures for both Glu•Ba^{2+} and Glu•Ca^{2+} that have a protonated N-terminus, providing additional evidence of zwitterionic structures.

A ZW O_SOO_C structure is calculated to be the most stable for both Glu•Ba^{2+} and Glu•Ca^{2+} (Table 2). Geometry optimization calculations were performed on a similar structure with a deprotonated side chain. However, no local minimum on the potential energy surface was found for this structure. The calculated spectra of the ZW O_SOO_C, NZ NO_SO_C, and NZ O_SO_C structures are all similar, but the measured frequencies of the two carbonyl bands are closest to those calculated for the ZW O_SOO_C structures. For Glu•Ca^{2+}, the NZ NO_SO_C structure is calculated to be nearly isoenergetic with ZW O_SOO_C. However, both the frequencies of the carbonyl stretches and width of the NH bending bands near 1450 cm^{-1} in the experimental spectrum are more consistent with the calculated spectrum of the ZW O_SOO_C structure. The NZ O_SO_C and ZW OO_C structures are at least 39 kJ/mol higher in energy than the ZW O_SOO_C structure for Glu•Ca^{2+} and at least 12 kJ/mol higher for Glu•Ba^{2+}. The poor agreement with the measured spectra and these energies suggest that there is no significant contribution from ZW OO_C or NZ O_SO_C structures to the ion population.

Interestingly, the NZ O_SOO_C structure is not stable for these complexes. For Glu•Ca^{2+}, this structure isomerizes to the similar, but zwitterionic, structure ZW O_SOO_C (Figure 5), during geometry optimization. For Glu•Ba^{2+}, the ZW O_SOO_C structure does not converge nor does it isomerize during energy minimization, indicating the potential energy surface is very flat in this region.

4.3.5 Comparing Glu to Gln

The IR action spectra of Gln•M^+, M = Li, Cs, and Gln•Ba^{2+} were recently reported,[13,14] and the structures of these complexes have essentially the same metal ion interactions to the amino acid as those determined for Glu. The spectra of the monocationized Gln complexes have two distinct carbonyl stretches separated by ∼60 cm^{-1}. By comparison, FTIR absorption spectra of gas-phase acetic acid, acetamide, pentanoic acid and pentanamide indicate that the intrinsic frequency of an amide carbonyl stretch is about 40 – 50 cm^{-1} lower than the carbonyl stretch of the corresponding carboxylic acid.[72] The carbonyl stretch of isolated

alanine is at 1785 cm^{-1},[73] ~10 cm^{-1} higher than the corresponding band for propanoic acid.[60] These molecules should provide an indication of the intrinsic difference in carbonyl stretches of the C-terminus and side-chain carboxylic acid groups, respectively, in Glu. These results are consistent with the single, wide band in the IR action spectra of monocationized Glu. For Gln•Ba^{2+}, bands at 1430, 1590 and 1650 cm^{-1} are very similar in frequency and shape to those observed for Glu•Ba^{2+} and Glu•Ca^{2+}, consistent with a similar structure for all three species.[13]

Glu is ~40 kJ/mol more acidic than Gln, and because they adopt similar structures in metal cationized complexes,[13,63,64] the effects of gas-phase acidity on the stabilities of their zwitterionic structures can be directly compared. For Li^+, the lowest-energy zwitterionic form is 32 and 33 kJ/mol higher in energy than the lowest-energy non-zwitterionic form for Glu and Gln, respectively. For Cs^+, the zwitterionic form is calculated to be 4 kJ/mol more stable for both. Thus, the lower ΔH_{acid} of Glu compared to Gln has virtually no effect on the relative zwitterionic stabilities for these monocation complexes. The reason for this is that the metal cations prevent the side chain of Glu from interacting with the C-terminus and disrupt the interaction that is responsible for the high acidity of Glu.

In all the lowest-energy non-zwitterionic structures, the carbonyl oxygen of the side chain interacts directly with the metal ion. Results from Armentrout and co-workers show that the binding affinity of Na^+ to Gln is 14 ± 1 kJ/mol higher than to Glu.[20] For K^+, this difference is 9 ± 1 kJ/mol.[21] These results indicate that an amide group is more effective at stabilizing charge than a carboxylic acid group. This effect does not appear to be significant in preferentially stabilizing the non-zwitterionic form of Gln compared to Glu with either Li^+ or Cs^+.

For Ba^{2+}, the lowest-energy zwitterionic structure is 17 and 2 kJ/mol more stable than the lowest-energy non-zwitterionic structure for Glu and Gln, respectively. In contrast to the results for the monovalent ions, the zwitterionic form is preferentially stabilized for Glu. The difference in the charge solvating ability of the amide vs. the carboxylic acid should be greater for a dication than for a monocation due to greater transfer of electron density to the dication. For Li^+ and Cs^+, the lowest-energy zwitterionic structure is ZW OO_C, but for Ba^{2+}, the ZW O_SOO_C in which the side chain coordinates directly to the divalent metal ion is most stable. Thus, the side-chain carbonyl oxygen interacts with Ba^{2+} in both the lowest-energy zwitterionic and non-zwitterionic forms of both Glu and Gln. The greater zwitterionic stability of Glu•Ba^{2+} compared to Gln•Ba^{2+} can be attributed to a greater relative stabilization of the non-zwitterionic structure of Gln•Ba^{2+} owing to effects of improved charge solvation by the amide vs. the acid, rather than effects of intrinsic gas-phase acidity of the deprotonation site. This charge solvation effect may be lower for the zwitterionic form because there is transfer of electron density from the negatively charged carboxylate group to the metal dication, lowering the effective charge state of the metal ion.

4.4 Conclusions

Infrared photodissociation spectroscopy of mono- and divalent cations coordinated to Asp and Glu provides detailed structural information about the metal binding interaction

to these two acidic amino acids. For the protonated, lithiated, and cesiated species, both amino acids are nonzwitterionic, whereas with Ca^{2+} and Ba^{2+}, Glu is zwitterionic. On the basis of these results, Asp cationized with Ca^{2+} and Ba^{2+} is expected to be zwitterionic as well. The IR action spectra of the protonated species indicate spectral features associated with a protonated N-terminus and are useful for identifying potential zwitterionic structures for metal cationized species. The experimental spectra of both lithiated species are most consistent with an NZ NO_SO_C structure, whereas for the cesiated species, an NZ O_SOO_C and an NZ O_SO_C structure is adopted by Asp and Glu, respectively. The IR action spectra of Asp•M^+ and Glu•M^+ for each M investigated are very similar to each other, indicating that the longer side chain of Glu has only subtle effects on structure.

Cationized Gln has nearly the same metal ion interactions as does Glu and the relative stabilities of the non-zwitterionic and zwitterionic forms are nearly the same for both Li^+ and Cs^+, despite Glu being ∼40 kJ/mol more acidic.[63,64] For Glu•Ba^{2+}, the relative stability of the zwitterionic form is 15 kJ/mol greater than that for Gln•Ba^{2+}, due to the greater charge stabilization of the nonzwitterionic form by an amide vs. a carboxylic acid group. These results indicate that the relative zwitterionic stability is not directly related to gas-phase acidity for these cationized amino acids.

4.5 References

(1) Bellissent-Funel, M. C. *J. Mol. Liq.* **2000**, 84, 39-52.

(2) Hofmeister, F. *Arch. Exp. Pathol. Pharmakol.* **1888**, 24, 247-260.

(3) Para, G.; Jarek, E.; Warszynski, P. *Adv. Colloid Interface Sci.* **2006**, 122, 39-55.

(4) Thomas, A. S.; Elcock, A. H. *J. Am. Chem. Soc.* **2007**, 129, 14887-14898.

(5) Zhou, H. X. *Proteins: Struct., Funct., Bioinf.* **2005**, 61, 69-78.

(6) Rodgers, M. T.; Armentrout, P. B. *Acc. Chem. Res.* **2004**, 37, 989-998.

(7) Rodgers, M. T.; Armentrout, P. B. *J. Am. Chem. Soc.* **2000**, 122, 8548-8558.

(8) Kaltashov, I. A.; Zhang, M. X.; Eyles, S. J.; Abzalimov, R. R. *Anal. Bioanal. Chem.* **2006**, 386, 472-481.

(9) Veenstra, T. D. *Biophys. Chem.* **1999**, 79, 63-79.

(10) Ruan, C. H.; Rodgers, M. T. *J. Am. Chem. Soc.* **2004**, 126, 14600-14610.

(11) Bush, M. F.; O'Brien, J. T.; Prell, J. S.; Saykally, R. J.; Williams, E. R. *J. Am. Chem. Soc.* **2007**, 129, 1612-1622.

(12) Armentrout, P. B.; Rodgers, M. T.; Oomens, J.; Steill, J. D. *J. Phys. Chem. A* **2008**, 112, 2248-2257.

(13) Bush, M. F.; Oomens, J.; Saykally, R. J.; Williams, E. R. *J. Phys. Chem. A* **2008**, *accepted*.

(14) Bush, M. F.; Oomens, J.; Saykally, R. J.; Williams, E. R. *J. Am. Chem. Soc.* **2008**, 130, 6463-6471.

(15) Bush, M. F.; Prell, J. S.; Saykally, R. J.; Williams, E. R. *J. Am. Chem. Soc.* **2007**, 129, 13544-13553.

(16) Dunbar, R. C.; Polfer, N. C.; Oomens, J. *J. Am. Chem. Soc.* **2007**, 129, 14562-14563.

(17) Forbes, M. W.; Bush, M. F.; Polfer, N. C.; Oomens, J.; Dunbar, R. C.; Williams, E. R.; Jockusch, R. A. *J. Phys. Chem. A* **2007**, 111, 11759-11770.

(18) Kamariotis, A.; Boyarkin, O. V.; Mercier, S. R.; Beck, R. D.; Bush, M. F.; Williams, E. R.; Rizzo, T. R. *J. Am. Chem. Soc.* **2006**, 128, 905-916.

(19) Kapota, C.; Lemaire, J.; Maitre, P.; Ohanessian, G. *J. Am. Chem. Soc.* **2004**, 126, 1836-1842.

(20) Heaton, A. L.; Moision, R. M.; Armentrout, P. B. *J. Phys. Chem. A* **2008**, 112, 3319-3327.

(21) Heaton, A. L.; Armentrout, P. B., *J. Phys. Chem. B, submitted for publication, 2008*

(22) Jockusch, R. A.; Lemoff, A. S.; Williams, E. R. *J. Am. Chem. Soc.* **2001**, 123, 12255-12265.

(23) Wyttenbach, T.; Witt, M.; Bowers, M. T. *J. Am. Chem. Soc.* **2000**, 122, 3458-3464.

(24) Lemoff, A. S.; Bush, M. F.; Williams, E. R. *J. Am. Chem. Soc.* **2003**, 125, 13576-13584.

(25) Lemoff, A. S.; Bush, M. F.; O'Brien, J. T.; Williams, E. R. *J. Phys. Chem. A* **2006**, 110, 8433-8442.

(26) Talley, J. M.; Cerda, B. A.; Ohanessian, G.; Wesdemiotis, C. *Chem.-Eur. J.* **2002**, 8, 1377-1388.

(27) Lemoff, A. S.; Bush, M. F.; Williams, E. R. *J. Phys. Chem. A* **2005**, 109, 1903-1910.

(28) Bush, M. F.; Forbes, M. W.; Jockusch, R. A.; Oomens, J.; Polfer, N. C.; Saykally, R. J.; Williams, E. R. *Journal of Physical Chemistry A* **2007**, 111, 7753-7760.

(29) Polfer, N. C.; Oomens, J.; Dunbar, R. C. *Phys Chem Chem Phys* **2006**, 8, 2744-2751.

(30) Rodgers, M. T.; Armentrout, P. B.; Oomens, J.; Steill, J. D. *J. Phys. Chem. A* **2008**, 112, 2258-2267.

(31) Polfer, N. C.; Oomens, J.; Moore, D. T.; von Helden, G.; Meijer, G.; Dunbar, R. C. *J. Am. Chem. Soc.* **2006**, 128, 517-525.

(32) Strittmatter, E. F.; Lemoff, A. S.; Williams, E. R. *J. Phys. Chem. A* **2000**, 104, 9793-9796.

(33) Oh, H.; Breuker, K.; Sze, S. K.; Ge, Y.; Carpenter, B. K.; McLafferty, F. W. *Proc. Natl. Acad. Sci. U. S. A.* **2002**, 99, 15863-15868.

(34) Oh, H. B.; Lin, C.; Hwang, H. Y.; Zhai, H. L.; Breuker, K.; Zabrouskov, V.; Carpenter, B. K.; McLafferty, F. W. *J. Am. Chem. Soc.* **2005**, 127, 4076-4083.

(35) Rajabi, K.; Fridgen, T. D. *J. Phys. Chem. A* **2008**, 112, 23-30.

(36) Baker, E. S.; Manard, M. J.; Gidden, J.; Bowers, M. T. *J. Phys. Chem. B* **2005**, 109, 4808-4810.

(37) Barran, P. E.; Polfer, N. C.; Campopiano, D. J.; Clarke, D. J.; Langridge-Smith, P. R. R.; Langley, R. J.; Govan, J. R. W.; Maxwell, A.; Dorin, J. R.; Millar, R. P.; Bowers, M. T. *Int. J. Mass Spectrom.* **2005**, 240, 273-284.

(38) Baker, E. S.; Gidden, J.; Ferzoco, A.; Bowers, M. T. *Phys Chem Chem Phys* **2004**, 6, 2786-2795.

(39) Stearns, J. A.; Mercier, S.; Seaiby, C.; Guidi, M.; Boyarkin, O. V.; Rizzo, T. R. *J. Am. Chem. Soc.* **2007**, 129, 11814-11820.

(40) Stearns, J. A.; Guidi, M.; Boyarkin, O. V.; Rizzo, T. R. *J. Chem. Phys.* **2007**, 127, 154322.

(41) Polfer, N. C.; Oomens, J.; Dunbar, R. C. *Chemphyschem* **2008**, 9, 579-589.

(42) Kong, X. L.; Tsai, I. A.; Sabu, S.; Han, C. C.; Lee, Y. T.; Chang, H. C.; Tu, S. Y.; Kung, A. H.; Wu, C. C. *Angew. Chem., Int. Ed.* **2006**, 45, 4130-4134.

(43) Simon, A.; MacAleese, L.; Maitre, P.; Lemaire, J.; McMahon, T. B. *J. Am. Chem. Soc.* **2007**, 129, 2829-2840.

(44) Wu, R.; McMahon, T. B. *J. Mass Spectrom.* **2008**, 10.1002/jms.1449.

(45) Wu, R. H.; McMahon, T. B. *J. Am. Chem. Soc.* **2007**, 129, 4864-+.

(46) Wyttenbach, T.; Witt, M.; Bowers, M. T. *Int. J. Mass Spectrom.* **1999**, $182-183$, 243-252.

(47) Lemoff, A. S.; Wu, C. C.; Bush, M. F.; Williams, E. R. *J. Phys. Chem. A* **2006**, 110, 3662-3669.

(48) Lemoff, A. S.; Williams, E. R. *J. Am. Soc. Mass Spectrom.* **2004**, 15, 1014-1024.

(49) Jockusch, R. A.; Lemoff, A. S.; Williams, E. R. *J. Phys. Chem. A* **2001**, 105, 10929-10942.

(50) Jockusch, R. A.; Price, W. D.; Williams, E. R. *J. Phys. Chem. A* **1999**, 103, 9266-9274.

(51) Ai, H. Q.; Bu, Y. X.; Han, K. L. *J. Chem. Phys.* **2003**, 118, 10973-10985.

(52) Hoyau, S.; Ohanessian, G. *Chem.-Eur. J.* **1998**, 4, 1561-1569.

(53) Hoyau, S.; Pelicier, J. P.; Rogalewicz, F.; Hoppilliard, Y.; Ohanessian, G. *Eur. J. Mass Spectrom.* **2001**, 7, 303-311.

(54) Remko, M.; Rode, B. M. *J. Phys. Chem. A* **2006**, 110, 1960-1967.

(55) Belcastro, M.; Marino, T.; Russo, N.; Toscano, M. *J. Mass Spectrom.* **2005**, 40, 300-306.

(56) Constantino, E.; Rodriguez-Santiago, L.; Sodupe, M.; Tortajada, J. *J. Phys. Chem. A* **2005**, 109, 224-230.

(57) Ling, S. L.; Yu, W. B.; Huang, Z. J.; Lin, Z. J.; Haranczyk, M.; Gutowski, M. *J. Phys. Chem. A* **2006**, 110, 12282-12291.

(58) Julian, R. R.; Beauchamp, J. L.; Goddard, W. A. *J. Phys. Chem. A* **2002**, 106, 32-34.

(59) Rak, J.; Skurski, P.; Simons, J.; Gutowski, M. *J. Am. Chem. Soc.* **2001**, 123, 11695-11707.

(60) Strittmatter, E. F.; Williams, E. R. *Int. J. Mass Spectrom.* **2001**, 212, 287-300.

(61) Strittmatter, E. F.; Wong, R. L.; Williams, E. R. *J. Phys. Chem. A* **2000**, 104, 10271-10279.

(62) Hunter, E. P. L.; Lias, S. G. *J. Phys. Chem. Ref. Data* **1998**, 27, 413-656.

(63) Jones, C. M.; Bernier, M.; Carson, E.; Colyer, K. E.; Metz, R.; Pawlow, A.; Wischow, E. D.; Webb, I.; Andriole, E. J.; Poutsma, J. C. *Int. J. Mass Spectrom.* **2007**, 267, 54-62.

(64) Li, Z.; Matus, M. H.; Velazquez, H. A.; Dixon, D. A.; Cassady, C. J. *Int. J. Mass Spectrom.* **2007**, 265, 213-223.

(65) Caldwell, G.; Renneboog, R.; Kebarle, P. *Can. J. Chem.* **1989**, 67, 611-618.

(66) Valle, J. J.; Eyler, J. R.; Oomens, J.; Moore, D. T.; van der Meer, A. F. G.; von Helden, G.; Meijer, G.; Hendrickson, C. L.; Marshall, A. G.; Blakney, G. T. *Rev. Sci. Instrum.* **2005**, 76, 023103.

(67) Oepts, D.; Vandermeer, A. F. G.; Vanamersfoort, P. W. *Infrared Phys. Technol.* **1995**, 36, 297-308.

(68) Shao, Y. *et al. Phys Chem Chem Phys* **2006**, 8, 3172-3191.

(69) Christiansen-Ross-Ermler-Nash-Bursten Large (CRENBL) Ross, R. B.; Powers, J. M.; Atashroo, T.; Ermler, W. C.; Lajohn, L. A.; Christiansen, P. A. *J. Chem. Phys.* **1990**, 93, 6654-6670.

(70) Oomens, J.; Sartakov, B. G.; Meijer, G.; Von Helden, G. *Int. J. Mass Spectrom.* **2006**, 254, 1-19.

(71) Oomens, J.; van Roij, A. J. A.; Meijer, G.; von Helden, G. *Astrophys. J.* **2000**, 542, 404-410.

(72) FTIR spectra obtained from NIST Webbook URL: webbook.nist.gov/chemistry/

(73) Linder, R.; Seefeld, K.; Vavra, A.; Kleinermanns, K. *Chem. Phys. Lett.* **2008**, 453, 1-6.

4.6 Tables and Figures

Aspartic Acid		**Glutamic Acid**	
Cation	Products (m/z)	Cation	Products (m/z)
H^+	—H_2O (116)	H^+	—H_2O (130)
	—formic acid (88)		—formic acid (102)
	—acetic acid (74)		—H_2O, formic acid (84)
Li^+	$H_2CCHNH_2{\bullet}Li^+$ (50)	Li^+	—H_2O (136)
	$H_2NCH_2CHCO{\bullet}Li^+$ (78)		—formic acid (108)
	—formic acid (94)		—H_2O, formic acid (90)
Cs^+	Cs^+ (133)	Cs^+	Cs^+ (133)
		Ca^{2+}	—formic acid (70.5)
			$CaOH^+$ (57)
			H_2NCO^+ (44)
		Ba^{2+}	$BaOH^+$ (155)
			—H_2O (133.5)
			—formic acid (119.5)
			—$BaOH^+$, formic acid (84)

Table 4.1: Photodissociation Products of Protonated and Cationized Aspartic and Glutamic Acid

structure	$Asp•H^+$	$Glu•H^+$
A	11/10	13/14
B	1/2	2/3
C	0/0	0/0
D	42/45	58/60

structure	$Asp•Li^+$	$Glu•Li^+$	$Asp•Cs^+$	$Glu•Cs^+$	$Glu•Ca^{2+}$	$Glu•Ba^{2+}$
NZ O_SOO_C			0/0	9/12		
NZ NO_SO_C	0/0	0/0	7/10	13/12	1/1	17/17
NZ O_SO_C	31/31	27/28	11/18	1/4	51/50	43/38
ZW OO_C	46/43	34/32	11/14	0/0	37/39	14/12
NZ OO_S			2/2	10/11		
ZW O_SOO_C					0/0	0/0

Table 4.2: Relative Gibbs free energies at 0/298 K in kJ/mol calculated with B3LYP using CRENBL effective core potential for Cs, Ba and Ca and 6-31++G** for all other atoms.

IRMPD freq. (cm^{-1})	assignment	structure CI calc. freq. (cm^{-1})
1789	$COOH_C$ asym. stretch	1783
1744	$COOH_S$ asym. stretch	1722
1593	NH_3 scissor	1627
1370–1500	NH_3 umbrella	1439
	NH_3 umbrella/OH_s bend	1409
	OH_C bend/CH wag	1392
1050–1250	OH_S bend	1172
	OH_C bend	1149
	CH_2 twist/$OH_{C/S}$ bends	1122

Table 4.3: IRMPD band assigments for Asp•H^+

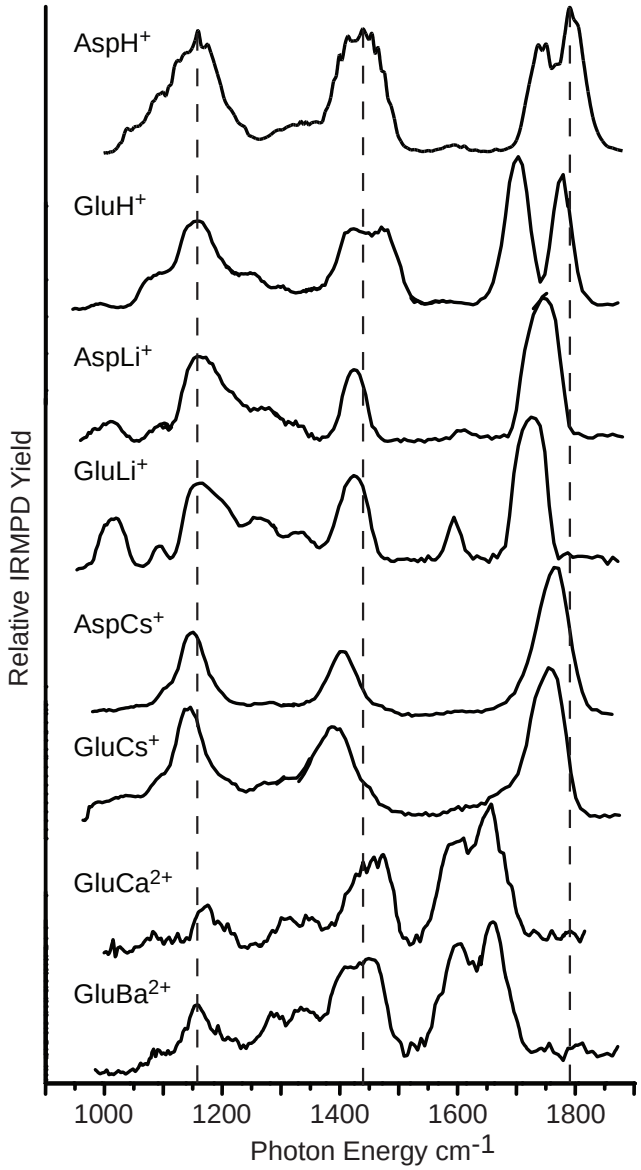

Figure 4.1: IRMPD action spectra of Asp•M^+, Glu•M^+, M = H, Li, and Cs, Glu•Ca^{2+} and Glu•Ba^{2+}.

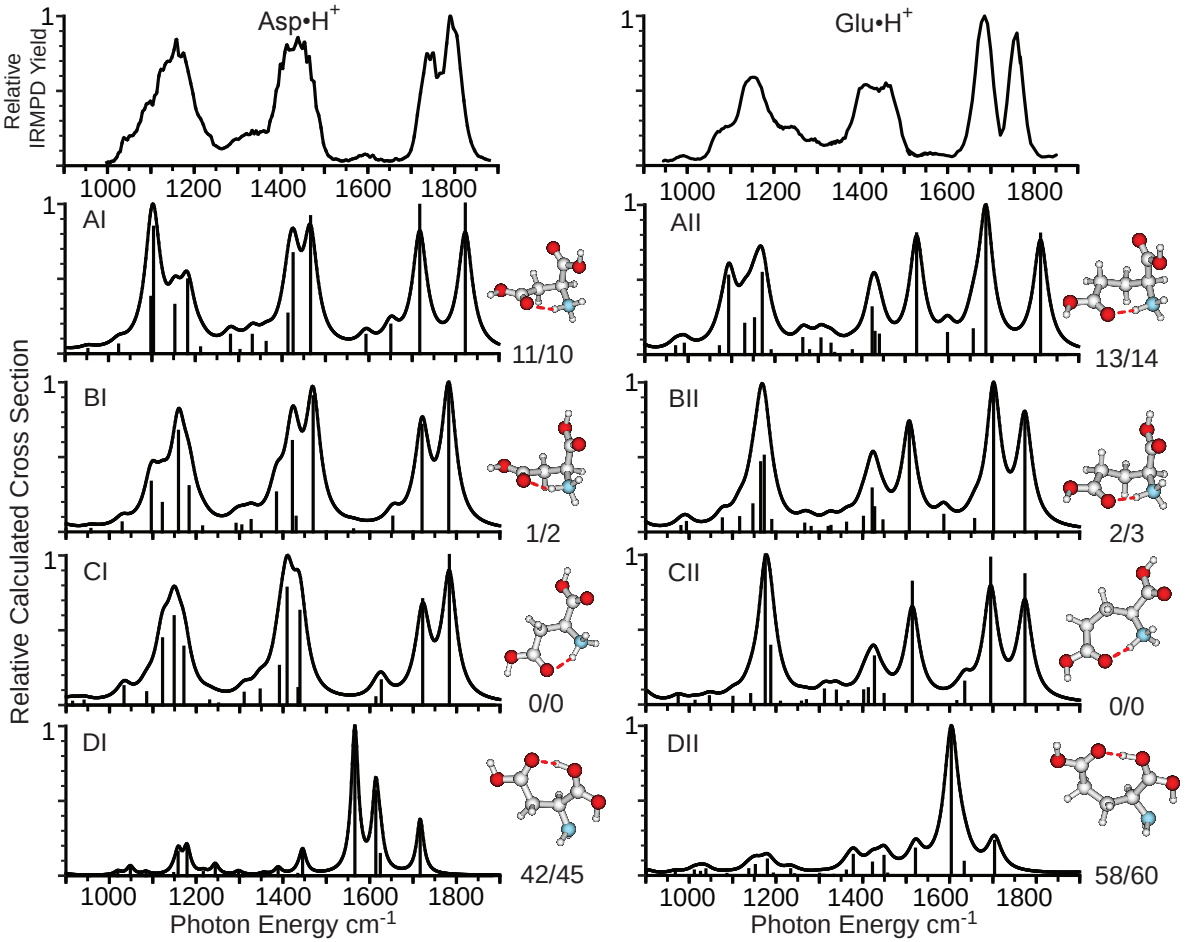

Figure 4.2: IRMPD action spectra of Asp•H^+ (left) and Glu•H^+ (right) obtained with 2.5 s laser irradiation and B3LYP/6-31++G** calculated spectra of candidate low-energy structures (frequencies scaled by 0.975). Energies are Gibbs free energies at 0 K / 298 K in kJ/mol.

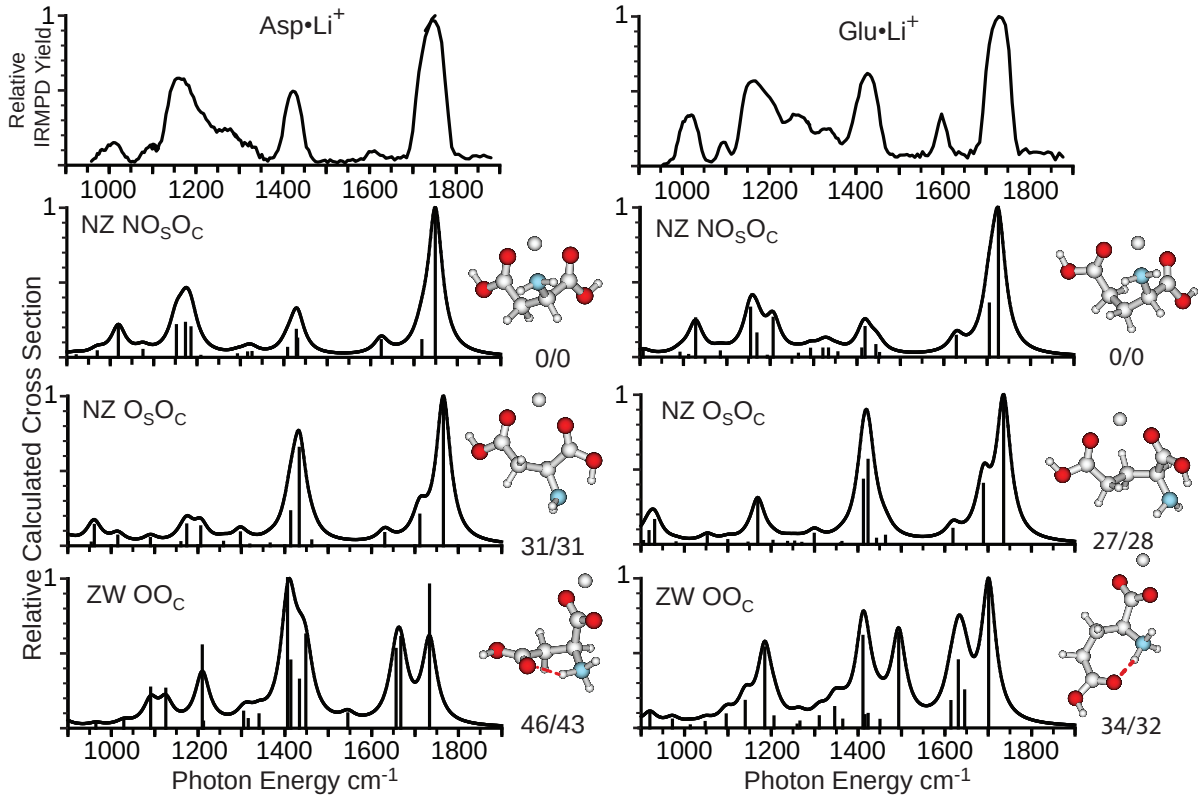

Figure 4.3: IRMPD action spectra of Asp•Li^+ (left) and Glu•Li^+ (right) obtained with 4.5 s laser irradiation and B3LYP/6-31++G** calculated spectra of candidate low-energy structures (frequencies scaled by 0.975). Calculated frequencies have been scaled by 0.975. Energies are Gibbs free energies at 0 K / 298 K in kJ/mol.

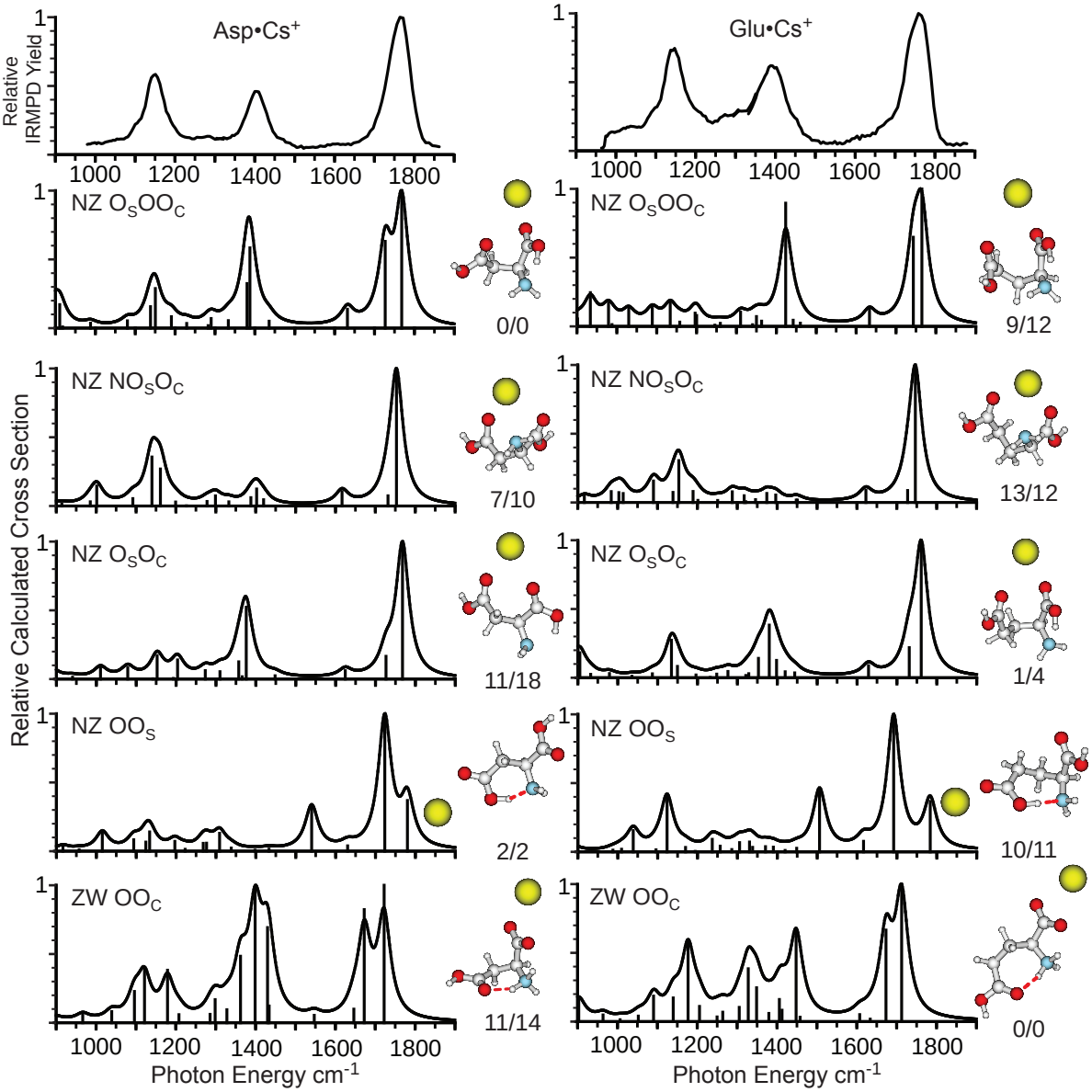

Figure 4.4: IRMPD action spectra of Asp•Cs^+ (left) and Glu•Cs^+ (right) obtained with 2.5 s laser irradiation and B3LYP/6-31++G** calculated spectra of candidate low-energy structures, the CRENBL effective core potential was used for Cs^+ (frequencies scaled by 0.975). Energies are Gibbs free energies at 0 K / 298 K in kJ/mol.

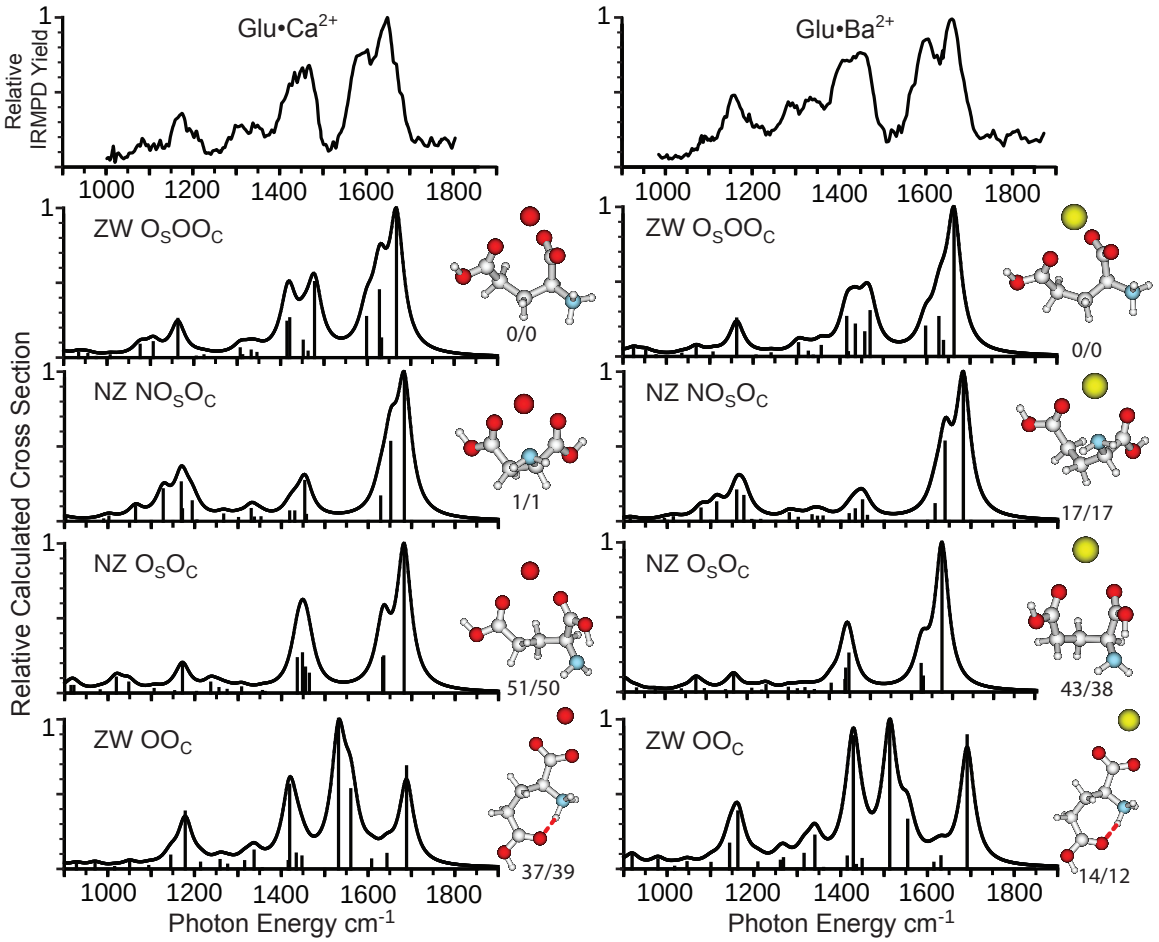

Figure 4.5: IRMPD action spectra of Glu•Ca^{2+} (left) and Glu•Ba^{2+} (right) obtained with 3.5 s laser irradiation and B3LYP/6-31++G** calculated spectra of candidate low-energy structures, the CRENBL effective core potential was used for Ba^{2+} (frequencies scaled by 0.975). Energies are Gibbs free energies at 0 K / 298 K in kJ/mol.

Chapter 5

Effects of Anions on the Zwitterion Stability of Glu, His and Arg Investigated by IRMPD Spectroscopy and Theory

This chapter is reproduced with permission from the American Chemical Society.

Jeremy T. O'Brien, James S. Prell, Giel Berden, Jos Oomens, and Evan R. Williams

International Journal of Mass Spectrometry, 2010, 297, 116–123

5.1 Introduction

Ions are important in many aspects of biology, including protein structure and complex assembly,[1–3] neuron signaling,[4,5] immune response,[6] and pH regulation.[7,8] Ion-protein interactions occur during ion transport through cell membranes and play a critical role in regulating ion concentrations in the body. For example, cystic fibrosis is a life-threatening condition caused by defects in a protein that transports chloride ions across cell membranes.[9] Ions also affect protein solubility. The effects of ions on protein stability were first measured in the 1880's, and the ordering of ions based on their ability to precipitate proteins is known as the Hofmeister series.[10,11] The effects of anions on protein solubility in aqueous solutions are generally stronger than those of cations, although solvent effects may play a significant role in this difference. The precise chemical origins of the Hofmeister series are still debated today.[12–16] Understanding the interactions of ions and proteins in solution is a complex problem that is complicated by effects of solvation, counter-ions, and protein structure.

Infrared multiple photon dissociation (IRMPD) spectroscopy has been used to probe the structures of ionized complexes in the gas phase and is potentially a powerful tool for understanding ion-protein interactions. An important advantage of this technique is the ability to investigate the structures of biomolecules in isolation, where complicating structural effects of solvent and counter-ions are absent. The interactions of metal cations with amino acids, the building blocks of proteins, have been extensively investigated using IRMPD spectroscopy.[17–38] IRMPD spectra have been reported for amino acids complexed with both mono- [19–38] and divalent cations.[17,18,38–31] In isolation, all naturally occurring amino acids are nonzwitterionic, but the zwitterionic form can be preferentially stabilized by the addition of a metal cation. Effects of metal ion size[19–25,28–30,32–34] charge state,[17,18,28–31,39] and amino acid basicity/acidity[19–21,30,40–44] on the relative stability of zwitterionic structures have been extensively studied. These studies indicate that for some amino acids, zwitterionic structures are preferentially stabilized with increasing metal ion size[23–25,28,32] and higher charge state[17,18,28,30] and with increasing amino acid basicity,[19–21,30,40–44] although other factors can compete to stabilize nonzwitterionic forms.[20,21,43] Trp,[18] His,[28] Arg, Gln, Pro, Ser, Val,[17] and Glu[30] complexed with Ba^{2+} are zwitterionic, but nonzwitterionic structures have been reported for some doubly charged complexes, including His•Ca^{2+}[28] and Asn•Ba^{2+}.[29]

In contrast to results for cations, much less is known about anion interactions with amino acids and to what extent they stabilize their zwitterionic forms. Attachment of an excess electron can stabilize the zwitterionic form of Arg.[45,46] Complexes of the dianion of oxalic or malonic acid with the zwitterionic form of glycine were investigated computationally and

were each found to be metastable with relatively low barriers to dissociation.[47] IRMPD spectra of deprotonated amino acids (Asp, Cys, Glu, Phe, Ser, Trp, and Tyr) were recently reported.[48] These spectra are dominated by bands corresponding to carboxylate stretching modes, and for Glu and Asp, the IRMPD spectra have very broad, poorly resolved features which are attributed to the sharing of a proton between the side chain and C-terminal carboxylate groups.

Here, we report the first IRMPD spectra of anionized amino acids, Glu•X^-, His•X^- and Arg•X^-, where X = Cl, Br or I in the spectral region 850 – 1900 cm^{-1}. These amino acids constitute the extremes of gas-phase acidity and basicity values for the naturally occurring amino acids and therefore are expected to have a high propensity to form zwitterionic structures. Effects of anion size on the zwitterion stability of these amino acids are investigated using comparison to IRMPD spectra of corresponding metal cationized complexes and hybrid density functional theory to aid in spectral interpretation.

5.2 Experimental

5.2.1 IRMPD Spectroscopy

All experiments were performed using a 4.7 T Fourier-transform ion cyclotron resonance mass spectrometer and a free electron laser (FELIX) which provides intense tunable infrared radiation in the mid-IR (850 – 1900 cm^{-1}). Descriptions of the instrument[49] and experimental parameters[31] are presented elsewhere. Ions were generated by electrospray ionization from 20/80 water/methanol solutions of Glu, His, or Arg and LiCl, $BaBr_2$, or NaI at 1 – 2 mM concentrations of the amino acid and halide salt. Solutions were infused at a rate of 10 – 20 μL/min. All chemicals were obtained from Sigma-Aldrich, Steinheim, Germany. Precursor complexes were isolated using stored waveform inverse Fourier transforms[50] and subsequently irradiated for 2.5 – 3.5 s using tunable radiation from FELIX with a macropulse rate of 5 Hz. A single irradiation time was used for each complex and was selected to produce extensive, but not complete, photodissociation at the peak intensity of each spectrum.

5.2.2 Computations

Candidate low-energy structures of Glu•Cl^-, His•Cl^-, and Arg•Cl^- were generated using Monte Carlo conformational searching and the MMFFs force field as implemented in *Macromodel 9.7* (Schrodinger, Inc. Portland, OR). At least 10,000 conformations were identified for each complex. Low-energy conformers were then grouped into families with similar structures and representative conformers from each family were selected for quantum mechanical geometry optimization in *Q-Chem v. 3.1*.[51] Structures with Br^- and I^- were generated by halide ion substitution into the chloridated structures. Geometries of the resulting structures were optimized at the B3LYP/6–31+G** level of theory using the CRENBL basis set and effective core potential for Br^- and I^-.[52,53]

Vibrational frequencies and intensities were calculated using the double-harmonic approximation and the analytical Hessian of the energy-minimized structures using *Q-Chem*

v. 3.1. Each of the resulting structures was found to have all real harmonic vibrational frequencies at this level of theory indicating that they are local minima on the potential energy surface. Zero-point energies and 298 K enthalpies and entropies were calculated using unscaled harmonic vibrational frequencies, and 298 K relative Gibbs free energies were obtained using these data. Calculated infrared absorption spectra are plotted with frequencies scaled by 0.975, a factor found to provide reasonable agreement between experimental spectra and calculated spectra at this level of theory in other IRMPD studies of amino acid complexes in this spectral region.[19–21,29,30,37,39–41,54] The intensities are convolved with a 40 cm^{-1} full width at half maximum (fwhm) Lorentzian profile to approximate the experimental peak shapes.

5.3 Results

5.3.1 Fragmentation

IRMPD of Glu•X^-, His•X^- and Arg•X^-, where X = Cl, Br, or I, results predominantly in the formation of X^- or loss of HX. For Arg•Cl^-, a minor product corresponding to the loss of (CN_2H_3 + Cl) was also observed, presumably resulting from subsequent dissociation of the primary product ion. Formation of Cl^- was not observed, whereas for the iodated amino acids, I^- was the primary (Glu) or only (His and Arg) product ion formed. Based on anion size, the binding energy of I^- should be less than that of Cl^-, so I^- should be more readily lost from the amino acids. In addition, HCl has a weaker gas-phase acidity (1372 kJ/mol),[55] compared to HI (1293.7 kJ/mol),[56] which should favor formation and loss of HCl. The IRMPD reaction pathways of each precursor are given in Table 1. By comparison, IRMPD of protonated and metal cationized Arg and Glu results in loss of water and other neutrals, and for cesiated complexes, loss of Cs^+.[30,32]

5.3.2 Spectroscopy

The IRMPD spectral intensity at a given frequency is calculated as a yield from the measured intensities of the precursor and product ions, I_{prec} and I_{prod}, respectively, corrected for the frequency dependent laser power $P(\omega)$.

$$\text{IRMPD spectral intensity (yield)} = (P(\omega))^{-1} \times (\sum I_{prod})/(\sum I_{prod} + I_{prec})$$

An IRMPD spectrum of each precursor ion is reported as the IRMPD spectral intensity as a function of laser frequency, normalized to the peak intensity of the most intense band. IRMPD spectra obtained using this photodissociation yield method are less directly comparable to linear absorption spectra than the laser-induced photodissociation rate constant method as discussed by Prell et al. .[57] However, this method provides spectra that are directly comparable to those reported previously for many cationized or deprotonated amino acids in this spectral region.[17–23,25–34,36–41,54] The IRMPD spectra of Glu•X^-, His•X^- and Arg•X^-, where X = Cl, Br, and I, from ~850 – 1900 cm^{-1} are shown in Fig. 1. Structural information from these spectra is obtained from comparisons to previously reported spectra

of protonated and metal cationized amino acids and from comparisons to calculated spectra of candidate low-energy structures.

The IRMPD spectra of Glu•Cl^-, Glu•Br^-, and Glu•I^- are similar with common features centered at ∼1750 and 1375 cm^{-1} in each spectrum. For Glu•I^- and Glu•Br^-, a weak band is observed at ∼1600 cm^{-1}, and for Glu•I^- there are additional minor bands at ∼1200 and 1040 cm^{-1}. The band at ∼1750 cm^{-1} is narrower for Glu•Cl^- (∼40 cm^{-1} fwhm) than for Glu•Br^- (∼75 cm^{-1} fwhm), and this feature for Glu•I^- consists of two partially resolved peaks at 1755 and 1775 cm^{-1}. The centroid of this feature blueshifts with increasing anion size. These bands correspond to the carbonyl stretching modes of the two carboxylic acid groups of Glu,[30] indicating that Glu is nonzwitterionic in these complexes (vide infra). The band at ∼1375 cm^{-1} for GluCl$^-$ is relatively narrow and appears as a single band whereas for Glu•Br^-, this feature is composed of two poorly resolved bands at ∼1370 and 1400 cm^{-1} and a shoulder from ∼1275 to 1175 cm^{-1}. Bands contributing to this feature for Glu•I^- are not resolved. The weak band observed at ∼1600 cm^{-1} for Glu•I^- and Glu•Br^- is consistent with an NH_2 scissoring bend, and the feature at ∼1375 cm^{-1} for Glu•X^- is similar to that observed for Glu•M^+ and corresponds to hydrogen bonded NH and CH bends.[30]

The IRMPD spectra for His•X^- complexes have many well resolved bands in the region between 850 and 1850 cm^{-1}. The spectra for His•Cl^- and His•Br^- are quite similar in that they both contain the same 10 bands (∼1750, 1600, 1570, 1475, 1410, 1350, 1230, 1190, 1100, 1000 and 915 cm^{-1}) albeit with some small differences in the relative intensities of the bands. The spectrum of His•I^- includes all of these bands and an additional feature at ∼1710 cm^{-1}. Similar to the Glu spectra, the carbonyl stretch near 1750 cm^{-1} blueshifts by ∼10 cm^{-1} with increasing anion size from Cl^- to I^-. The carbonyl stretching bands at ∼1750 cm^{-1} indicate that His is predominantly nonzwitterionic, as does the band at 1710 cm^{-1} which indicates some contribution from an additional structure with a different chemical environment for the carboxylic acid group.[28]

The IRMPD spectra of Arg•Cl^- and Arg•I^- are very similar and each has a broad band, (∼125 cm^{-1} fwhm) centered at ∼1625 cm^{-1} in addition to broad photodissociation below 1500 cm^{-1} with two poorly resolved features at ∼1475 and 1350 cm^{-1} that have low signal-to-noise ratios. There is also a very weak band at ∼1740 cm^{-1}. The band at ∼1625 cm^{-1} corresponds to contributions from the antisymmetric carbonyl stretch of a carboxylate group and hydrogen bonded NH bending modes, consistent with a zwitterionic structure of Arg.[32] This band is close in frequency to the carboxylate stretch band observed at ∼1630 cm^{-1} in the IRMPD spectra of deprotonated Trp, Phe, Tyr and Cys.[48]

5.3.3 Calculated Structures

Representative structures of low-energy conformers for Glu•X^-, His•X^- and Arg•X^- are shown in Fig. 2 – 4, respectively, along with their calculated spectra and relative 0/298 K Gibbs free energies at the B3LYP/6–31+G**/CRENBL level of theory (Table 2). The calculated structures and spectra differ only slightly for the different halide anions. For example, the calculated spectrum of the lowest-energy structure for Glu•Cl^- is nearly indistinguishable from those calculated for the same structure with Br^- and I^-, although there is a slight

blueshift ($\sim$5 – 10 cm^{-1}) in the carbonyl stretches of the carboxylic acids with increasing anion size (Fig. 5), consistent with the measured spectra for these complexes (Fig. 1). A corresponding increase in the OH bond length, indicative of increased carboxylate character, is calculated to occur with decreasing anion size for nonzwitterionic structures where the hydroxyl hydrogen atom interacts with the anion or a strongly basic site. The representative structures and spectra shown in Fig. 2 – 4 are those of the chloridated complexes, and the relative Gibbs free energies (kJ/mol) for all three anions at zero and 298 K are indicated for each structure.

Glu•X^- Structures

Four structural families are identified from conformational searching of Glu•Cl^-: a nonzwitterionic structure, $GluNO_C$, in which the anion interacts with the N-terminus and the OH group of the C-terminus (O_C), and the carboxylic acid group of the side chain donates a hydrogen bond to the N-terminus; $GluO_SO_C$ where both the side chain (O_S) and C-terminal OH groups coordinate to the anion; $GluNO_SO_C$, in which the N-terminus, side chain, and C-terminal OH groups all coordinate to the anion; and GluZW, where the protonated N-terminus of zwitterionic Glu coordinates to the anion, and a hydrogen is shared between C-terminal and side chain carbonyl oxygen atoms. The lowest energy structures are $GluNO_C$ for Br^- and I^- and $GluO_SO_C$ for Cl^-. Structures $GluNO_SO_C$ and GluZW are substantially higher in energy by $\sim$30 and 20 kJ/mol, respectively.

His•X^- Structures

Six structural families are identified from conformational searching of His•Cl^-: five low-energy nonzwitterionic structures and the lowest-energy zwitterionic structure are shown in Fig. 3. The side chain of His has two nitrogen atoms, designated 'pros'(near) and 'tele'(far) to indicate their distance from the tertiary carbon of the imidazole group, and they are abbreviated N_π and N_τ respectively. Each of these nitrogen atoms may bind a hydrogen atom, although not both at the same time without forming a zwitterionic structure. The nonzwitterionic structures are characterized by different coordination of the anion. For the $HisN_\tau$ structure, the anion binds only to the tele-NH group and the pros-nitrogen atom accepts a hydrogen bond from the N-terminus (N_T). This is the lowest energy structure at 298 K for His•Cl^-. The lowest energy structure for His•Br^- and His•I^- is $HisN_TN_\pi$ where the pros-NH and the N-terminus coordinate to the anion and the C-terminus donates a weak hydrogen bond to the N-terminus. $HisN_\pi O$ and $HisN_TN_\pi O$ both have coordination of the C-terminus to the anion along with one or two of the NH groups, respectively. For HisZW, the protonated N-terminus of His coordinates to the anion and the pros-NH donates a hydrogen bond to an oxygen atom of the carboxylate group.

Arg•X^- Structures

Four structural families are identified from conformational searching for Arg•Cl^-: three zwitterionic structures and the lowest energy nonzwitterionic structure are shown in Fig.

4. The un-protonated side chain nitrogen atoms are designated ε, η, and $\eta\prime$, as indicated in Fig. 4, where ε is the secondary amine nitrogen atom, η is the primary imine nitrogen atom, and $\eta\prime$ is the primary amine nitrogen atom. For zwitterionic structures where the side chain is protonated, we retain the η and $\eta\prime$ labels inherited from the un-protonated structures for convenience. For structure ArgZW-A, the ε-NH donates a hydrogen bond to the deprotonated C-terminus and the anion coordinates to the other two NH groups of the protonated side chain. In structure ArgZW-B, the η-NH group of the protonated side chain donates a hydrogen bond to the deprotonated C-terminus, and both the ε- and $\eta\prime$-NH groups coordinate to the anion. These two structures are very similar and nearly isoenergetic. Structure ArgZW-C differs somewhat in that the deprotonated C-terminus accepts two hydrogen bonds, one each from the ε- and $\eta\prime$-NH groups of the protonated side chain, and the anion is coordinated by both the $\eta\prime$- and η-NH groups. Structure ArgNZ-D is nonzwitterionic and is analogous to structure ArgZW-B with a proton transferred from the η-nitrogen to the C-terminus.

5.4 Discussion

5.4.1 Comparison with Cationized Spectra

Cs^+ and Cl^- have nearly the same ionic radii (167 pm),[58] and the carbonyl band in the spectra of Glu•Cs^+ and Glu•Cl^- is remarkably similar in both frequency (1760 and 1755 cm^{-1}, respectively) and peak shape.[30] Similarly, the antisymmetric carbonyl stretch bands of the carboxylate group for Arg•Cs^+ and Arg•Cl^- are close in frequency, centered at ∼1615 and 1625 cm^{-1}, respectively.[32] The similarity of the carbonyl bands in the spectra of cesiated and chloridated Glu and Arg indicate that the sign of the ion's charge plays little role in these vibrational frequencies, although the binding sites of metal cations versus halide anions in these complexes are different. The metal cation in Glu•M^+ and His•M^+ for nonzwitterionic structures attaches to one or more carbonyl oxygen atoms and corresponding free-OH bends are observed at ∼1150 – 1170 cm^{-1}. For Glu•X^- and His•X^-, no hydroxyl bends are evident in the experimental spectra indicating that the OH groups are coordinated to the anion or are hydrogen bonded.

For His•X^-, the bands below 1700 cm^{-1} are especially intriguing because they are not apparent in the IRMPD spectrum of His•Na^+, the only IRPD spectrum reported for alkali metal cationized His.[28] The most intense band in the spectrum of His•Na^+ occurs at ∼1150 cm^{-1} and corresponds to the free-OH bend of the carboxylic acid group. An intense band corresponding to the same mode at ∼1150 cm^{-1} also occurs for HisArg•H^+.[40] Its absence in the anionized spectra is consistent with the OH group donating a hydrogen bond or coordinating to the anion. The bands below 1700 cm^{-1} are unusually sharp and likely correspond to vibrations associated with the rigid imidazole ring.

The band at 1625 cm^{-1} for Arg•X^- and the absence of any intense bands above 1700 cm^{-1} are consistent with predominantly zwitterionic structures of Arg, as observed for Arg•M^+, where M = K, Rb, and Cs.[32] The broad dissociation and poorly resolved bands below 1500 cm^{-1} in the Arg•X^- spectra prohibit further structural conclusions from the experimental

spectra. However, broad dissociation with poorly resolved spectral features has been observed for other amino acid complexes containing strong intramolecular hydrogen bonds.[26,48] The assignment of zwitterionic structures for both Arg•X^- and Arg with an excess electron attached[45,46] indicates that the stabilization of the large dipole of the zwitterionic form by the anion in these zwitterionic structures outcompetes solvation of the anion by hydrogen bonding in nonzwitterionic structures. Evidently, solvation of the charge by hydrogen bonds in these complexes is less effective than the charge solvation by heteroatoms observed for the nonzwitterionic forms of Arg•Li^+ and Arg•Na^+[32] and is likely attributable to the relatively large size of the anions.

The IRMPD spectra for each anionized amino acid are very similar indicating that anion size has little effect on the conformations adopted for each of these complexes. Only the spectrum for His•I^- indicates a clear structural change as a function of ion size. In contrast, effects of ion size on structure have been reported for many metal cationized amino acid complexes, including Glu•M^+,[30] Arg•M^+,[24,32] Lys•M^+,[19] and Met•M^+.[25] For example, the differences observed between the IRMPD spectra of Arg•Li^+ and Arg•Na^+ indicate a switch from a nonzwitterionic structure of Arg when bound to Li to primarily zwitterionic Arg when bound to Na^+.[24,32]

5.4.2 Origins of Carbonyl Stretch Redshifting

The carbonyl band in the IRMPD spectra of both Glu•Cs^+ (1760 cm^{-1}) and Glu•Cl^- (1755 cm^{-1}) is redshifted relative to that of a free carboxylic acid (∼1780 cm^{-1} for gas-phase acetic acid).[59] The carboxylate antisymmetric stretch for Arg•Cs^+(1615 cm^{-1}) and Arg•Cl^- (1625 cm^{-1})[32] is similar to that of benzoate at ∼1630 cm^{-1},[60] which is likely redshifted from that of a free carboxylate due to electron donation from the benzene ring. Further redshifting of carbonyl bands with increasing charge state has also been reported for alkali metal and alkaline earth metal cationized amino acids and peptides, including Glu,[30] His,[28] and Asn.[29] This increasing carbonyl stretch redshift as a function of charge state for metal cationized amino acids and peptides has been attributed to transfer of electron density from the carbonyl to the attached metal ion which increases with increasing metal ion charge state.[30,41]

In the absence of other effects, an attached halide ion would be expected to transfer electron density to the amino acid resulting in a *blueshift* of the carbonyl stretch band, thus the observed carbonyl stretch redshift for the complexes investigated cannot be fully explained by this charge transfer effect. Instead, this carbonyl stretch redshift for both anionized and cationized amino acids and peptides can be primarily attributed to two other factors: the favorable alignment of the dipole moment of the carbonyl with the ion's electric field, and for halidated complexes, partial proton transfer from the carboxylic acid to the halide anion which results in partial carboxylate character. Because cations attach to the complexes close to the carbonyl oxygen whereas anions attach closer to the carbonyl carbon for nonzwitterionic structures, the interaction of the carbonyl dipole moment with the ion's electric field is favorable for ions of either polarity, causing a redshift in the carbonyl stretch frequency, i.e., a Stark effect.

The carbonyl band redshifts for Glu•X^- and His•X^- with decreasing halide ion size by ∼10 cm^{-1} from X = I to X = Cl, and this effect provides additional evidence that the redshift is caused by the electric field of the ion. By comparison, the carbonyl stretch band in the spectrum of Glu•Li^+ is redshifted from the corresponding band for Glu•Cs^+ by ∼20 cm^{-1}. A similar shift has been observed between the lithiated and cesiated spectra of other amino acids, including Gln,[20] Trp,[33] Ser,[23] and Thr.[34] The anion size-dependent shift observed for Glu•X^- and His•X^- is likely smaller than for Glu•M^+ because the halide ions are much larger (Cl^-, Br^- and I^-: 167, 196 and 220 pm) than the alkali metal cations (Li^+ and Cs^+: 76 and 167 pm)[58] and are further away from the carbonyl groups, resulting in a more subtle change in the ion's electrostatic potential as experienced by the carbonyl group. For both anionized and cationized zwitterionic Arg, any change in the frequency of the carboxylate antisymmetric shift with decreasing ion size appears to be obfuscated by contributions from hydrogen bonded NH bending modes that occur in the same region.

The redshift in the carbonyl stretch from that of a neutral carboxylic acid group is in fact slightly *greater* for Glu•Cl^- than for Glu•Cs^+, despite the latter having a much shorter carbonyl-ion distance. Thus, other factors, in addition to the Stark shift, must contribute. Chloride anion is substantially less acidic in the gas phase than are Br^- and I^-, which causes the strength of the interaction between the halide ion and adjacent carboxylic acid hydrogen atom(s) to increase with decreasing halide ion size. This results in increased partial carboxylate character of the carboxylic acid group with decreasing ion size, consistent with the surprisingly large redshifting effects of the halide ions described above. This sharing of the hydrogen atom between the hydroxyl oxygen atom and halide anion is analogous to the sharing of a proton between heteroatoms observed in proton-bound dimeric complexes, where spectral frequencies can be highly sensitive to the difference in proton affinity of the substituents.[61]

5.4.3 Comparisons with Theory

The calculated spectra of the lowest-energy structures are generally consistent with the experimental spectra, although there is evidence for multiple structures for some of these complexes. The carbonyl band in the calculated spectra blueshifts by ∼5 – 10 cm^{-1} with increasing ion size from Cl^- to I^-. For example, the carbonyl band in structure $GluO_SO_C$ occurs at ∼1740, 1745 and 1750 cm^{-1} for Cl^-, Br^- and I^-, respectively (Fig. 5). A corresponding decrease in the hydroxyl OH bond distance with increasing ion size, and hence, decreasing carboxylate character, is calculated for this structure. Similar shifts are observed in the calculated spectra for the other nonzwitterionic structures and are consistent with the experimental spectra of Glu•X^-, which show a ∼10 cm^{-1} blueshift for this band for these same anions. For the zwitterionic structure, GluZW, the carboxylate band is the same for Cl^- and Br^-, but blueshifts by ∼5 cm^{-1} for I^-. Contributions to the experimental spectra from specific low-energy structures are discussed in detail below.

5.4.4 Glu•X^-, X = Cl, Br, and I

The carbonyl stretches of the carboxylic acid groups in Glu•Cl^- have similar frequencies resulting in a single band at ∼1740 cm^{-1} in the calculated spectra of the nonzwitterionic structures, in agreement with the experimental spectra (Fig. 2). The calculated spectra of the zwitterionic structures differ substantially with two carbonyl bands at ∼1660 and 1740 cm^{-1} corresponding to carbonyl stretches of the deprotonated C-terminus and the side chain carboxylic acid, respectively. These calculated spectra support assignment of the experimental spectra to one or more nonzwitterionic structures. The calculated spectrum of $GluO_SO_C$ provides good agreement with the experimental spectrum of Glu•Cl^-. The intense mode predicted at ∼1350 cm^{-1} corresponds to the coupled, in-phase OH bending modes of the two carboxylic acid groups coordinating to the anion and likely contributes to the band observed in the experimental spectra at ∼1375 cm^{-1} for all three anions. The calculated spectrum of $GluNO_C$ differs from that of $GluO_SO_C$ only slightly with a band predicted at ∼1500 cm^{-1} corresponding to the bonded OH bending mode of the side chain carboxylic acid group hydrogen bonded to the N-terminus. This band is not evident in any of the experimental spectra. However, differences in relative intensities between IRMPD and calculated absorption spectra, especially for structures with strong hydrogen bonds, can be attributed to a number of factors, including uncertainties in the calculated intensities and other factors discussed elsewhere.[41] The calculated spectrum of $GluNO_SO_C$ is very similar to that of $GluO_SO_C$, with some differences in the bonded NH/OH bending feature at ∼1350 cm^{-1}. This structure is calculated to be much higher in energy, but contributions from such structures cannot be eliminated based on comparison to the experimental data alone.

5.4.5 His•X^-, X = Cl, Br, and I

No calculated spectrum of a single conformer can account for all of the bands observed in the experimental spectra of His•X^- (Fig. 3). However, the band at ∼1750 cm^{-1} in the IRMPD spectrum of His•X^- is most consistent with a substantial contribution to the ion population from structures like $HisN_TN_\pi$, where the frequency of the carbonyl stretching mode is significantly blueshifted relative to the carbonyl bands of the other nonzwitterionic structures. The frequency of the carbonyl stretch for the zwitterionic structure HisZW is ∼1680 cm^{-1}, supporting assignment of the experimental spectra to nonzwitterionic structures. For His•I^-, the band at ∼1710 cm^{-1} can be attributed to contributions from the other non-zwitterionic structures. For $HisN_\tau$, the hydrogen bond between the C-terminus and the pros-nitrogen atom should be strong due to the excellent alignment and high basicity of the side chain, and the strongly shared hydrogen atom likely gives the carbonyl partial carboxylate character, redshifting the carbonyl stretch. The redshifted carbonyl band at 1710 cm^{-1} is not observed for the other anions indicating minimal contribution from this type of structure in the other complexes. The lower frequency bands are more challenging to assign, but could be more readily identified by measuring IRMPD spectra of His derivatives or by isotopic substitution. The IR spectrum of condensed-phase imidazole, an analogue for the histidine side chain, has many bands between 800 and 1700 cm^{-1} corresponding to CN stretches, ring stretching modes, and NH and CH bends.[62] However, the frequencies of

these modes do not consistently match those observed in the IRMPD spectra of His•X^-, complicating assignment based on these data.

5.4.6 Arg•X^-, X = Cl, and I

The calculated spectra of structures ArgZW-A and ArgZW-B provide reasonable agreement with the broad experimental band at ∼1625 cm^{-1} (Fig. 4). These results are consistent with assignment of Arg•X^- to predominantly zwitterionic structures. The weak band at ∼1740 cm^{-1} may be due to the hydrogen bonded NH bend of the ε nitrogen in ArgZW-A (calculated at ∼1720 cm^{-1}), but this band could also be due to a small population of nonzwitterionic structures, such as ArgNZ-D. Structure ArgZW-C also has a hydrogen bonded NH bend at ∼1690 cm^{-1} that is not observed in the experimental spectra indicating that structure ArgZW-C is not the dominant structure. Bands attributed to this mode have been reported in the IRMPD spectra of alkali metal cationized Arg indicating a difference between the zwitterionic structures adopted for the anionized and cationized complexes. The calculated spectra for structures ArgZW-A and ArgZW-B are very similar. Based on the calculations that indicate that these structures are nearly isoenergetic, it is likely that both are present in the ion population.

5.5 Conclusions

The IRMPD spectra of Glu•X^-, His•X^-, and Arg•X^-, where X = Cl, Br, or I, clearly show whether or not the amino acid adopts a zwitterionic form in these complexes. The spectra of Glu•X^- and His•X^- each have a strong band at ∼1750 cm^{-1} corresponding to the carbonyl stretch of a carboxylic acid indicating that the nonzwitterionic form of the amino acid is dominant. An additional band at ∼1710 cm^{-1} for His•I^- indicates that another structure with a redshifted carbonyl stretch is also present. The broad band at ∼1625 cm^{-1} for Arg•X^-, corresponding to the antisymmetric stretch of a carboxylate group, clearly shows that Arg is zwitterionic in these complexes.

The frequencies of the carbonyl bands are similar for these amino acids with either Cl^- or Cs^+ attached. Thus, the sign of the ion's charge for these similarly sized ions has little effect on the frequency of these diagnostic bands. The coordination of cations to these amino acids is different from that of anions, resulting in a favorable alignment of the dipole moment of the carbonyl stretch with the electric field of ions of either polarity, which causes a redshift in this band, i.e., a Stark effect. The slight redshift (∼10 cm^{-1}) of the carbonyl band at ∼1750 cm^{-1} for Glu•X^- and His•X^- with decreasing anion size is consistent with both a Stark effect and a more subtle effect of greater carboxylate character when smaller halide ions coordinate to the carboxylic acid group. The calculated spectra of the lowest energy structures generally provide good agreement with the experimental spectra. The IRMPD spectra of His•X^- have many sharp bands due to the side chain that do not correspond closely enough in frequency to features observed in the FT-IR spectrum of condensed-phase imidazole or in calculated spectra of low-energy conformers of His•X^- to make unambiguous

assignments. Additional structural information could be obtained by measuring IRMPD spectra of analogous compounds or by isotopic labeling.

5.6 References

(1) Loo, J. A. *Mass Spectrom. Rev.* **1997**, 16, 1-23.

(2) Pidcock, E.; Moore, G. R. *J. Biol. Inorg. Chem.* **2001**, 6, 479-489.

(3) Pyle, A. M. *J. Biol. Inorg. Chem.* **2002**, 7, 679-690.

(4) Frings, S.; Reuter, D.; Kleene, S. J. *Prog. Neurobiol.* **2000**, 60, 247-289.

(5) Misgeld, U.; Deisz, R. A.; Dodt, H. U.; Lux, H. D. *Science* **1986**, 232, 1413-1415.

(6) Mayeno, A. N.; Curran, A. J.; Roberts, R. L.; Foote, C. S. *J. Biol. Chem.* **1989**, 264, 5660-5668.

(7) Chesler, M. *Physiol. Rev.* **2003**, 83, 1183-1221.

(8) Russell, J. M.; Boron, W. F. *Nature* **1976**, 264, 73-74.

(9) Riordan, J. R.; Rommens, J. M.; Kerem, B. S.; Alon, N.; Rozmahel, R.; Grzelczak, Z.; Zielenski, J.; Lok, S.; Plavsic, N.; Chou, J. L.; Drumm, M. L.; Iannuzzi, M. C.; Collins, F. S.; Tsui, L. C. *Science* **1989**, 245, 1066-1072.

(10) Hofmeister, F. *Arch. Exp. Pathol. Pharmacol.* **1888**, 24, 247-260.

(11) Kunz, W.; Henle, J.; Ninham, B. W. *Curr. Opin. Colloid Interface Sci.* **2004**, 9, 19-37.

(12) Chen, X.; Yang, T.; Kataoka, S.; Cremer, P. S. *J. Am. Chem. Soc.* **2007**, 129, 12272-12279.

(13) Freire, M. G.; Neves, C. M. S. S.; Silva, A. M. S.; Santos, L. M. N. B. F.; Marrucho, I. M.; Rebelo, L. P. N.; Shah, J. K.; Maginn, E. J.; Coutinho, J. A. P. *J. Phys. Chem. B* **2010**, 114, 2004-2014.

(14) Pegram, L. M.; Record, M. T. *J. Phys. Chem. B* **2007**, 111, 5411-5417.

(15) Smith, J. D.; Saykally, R. J.; Geissler, P. L. *J. Am. Chem. Soc.* **2007**, 129, 13847-13856.

(16) Uejio, J. S.; Schwartz, C. P.; Duffin, A. M.; Drisdell, W. S.; Cohen, R. C.; Saykally, R. J. *Proc. Natl. Acad. Sci. U. S. A.* **2008**, 105, 6809-6812.

(17) Bush, M. F.; Oomens, J.; Saykally, R. J.; Williams, E. R. *J. Am. Chem. Soc.* **2008**, 130, 6463-6471.

(18) Dunbar, R. C.; Polfer, N. C.; Oomens, J. *J. Am. Chem. Soc.* **2007**, 129, 14562-14563.

(19) Bush, M. F.; Forbes, M. W.; Jockusch, R. A.; Oomens, J.; Polfer, N. C.; Saykally, R. J.; Williams, E. R. *J. Phys. Chem. A* **2007**, 111, 7753-7760.

(20) Bush, M. F.; Oomens, J.; Saykally, R. J.; Williams, E. R. *J. Phys. Chem. A* **2008**, 112, 8578-8584.

(21) Bush, M. F.; Oomens, J.; Williams, E. R. *J. Phys. Chem. A* **2009**, 113, 431-438.

(22) Armentrout, P. B.; Armentrout, E. I.; Clark, A. A.; Cooper, T. E.; Stennett, E. M. S.; Carl, D. R. *J. Phys. Chem. B* **2010**, 114, 3927-3937.

(23) Armentrout, P. B.; Rodgers, M. T.; Oomens, J.; Steill, J. D. *J. Phys. Chem. A* **2008**, 112, 2248-2257.

(24) Bush, M. F.; O'Brien, J. T.; Prell, J. S.; Saykally, R. J.; Williams, E. R. *J. Am. Chem. Soc.* **2007**, 129, 1612-1622.

(25) Carl, D. R.; Cooper, T. E.; Oomens, J.; Steill, J. D.; Armentrout, P. B. *Phys. Chem. Chem. Phys.* **2010**, 12, 3384-3398.

(26) Drayss, M. K.; Blunk, D.; Oomens, J.; Gao, B.; Wyttenbach, T.; Bowers, M. T.; Schäfer, M. *J. Phys. Chem. A* **2009**, 113, 9543-9550.

(27) Drayss, M. K.; Blunk, D.; Oomens, J.; Schäfer, M. *J. Phys. Chem. A* **2008**, 112, 11972-11974.

(28) Dunbar, R. C.; Hopkinson, A. C.; Oomens, J.; Siu, C. K.; Siu, K. W. M.; Steill, J. D.; Verkerk, U. H.; Zhao, J. F. *J. Phys. Chem. B* **2009**, 113, 10403-10408.

(29) Heaton, A. L.; Bowman, V. N.; Oomens, J.; Steill, J. D.; Armentrout, P. B. *J. Phys. Chem. A* **2009**, 113, 5519-5530.

(30) O'Brien, J. T.; Prell, J. S.; Steill, J. D.; Oomens, J.; Williams, E. R. *J. Phys. Chem. A* **2008**, 112, 10823-10830.

(31) Polfer, N. C.; Oomens, J.; Moore, D. T.; von Helden, G.; Meijer, G.; Dunbar, R. C. *J. Am. Chem. Soc.* **2006**, 128, 517-525.

(32) Forbes, M. W.; Bush, M. F.; Polfer, N. C.; Oomens, J.; Dunbar, R. C.; Williams, E. R.; Jockusch, R. A. *J. Phys. Chem. A* **2007**, 111, 11759-11770.

(33) Polfer, N. C.; Oomens, J.; Dunbar, R. C. *Phys. Chem. Chem. Phys.* **2006**, 8, 2744-2751.

(34) Rodgers, M. T.; Armentrout, P. B.; Oomens, J.; Steill, J. D. *J. Phys. Chem. A* **2008**, 112, 2258-2267.

(35) Kamariotis, A.; Boyarkin, O. V.; Mercier, S. R.; Beck, R. D.; Bush, M. F.; Williams, E. R.; Rizzo, T. R. *J. Am. Chem. Soc.* **2006**, 128, 905-916.

(36) Kapota, C.; Lemaire, J.; Maitre, P.; Ohanessian, G. *J. Am. Chem. Soc.* **2004**, 126, 1836-1842.

(37) Polfer, N. C.; Oomens, J.; Dunbar, R. C. *ChemPhysChem* **2008**, 9, 579-589.

(38) Polfer, N. C.; Paizs, B.; Snoek, L. C.; Compagnon, I.; Suhai, S.; Meijer, G.; von Helden, G.; Oomens, J. *J. Am. Chem. Soc.* **2005**, 127, 8571-8579.

(39) Prell, J. S.; Flick, T. G.; Oomens, J.; Berden, G.; Williams, E. R. *J. Phys. Chem. A* **2010**, 114, 854-860.

(40) Prell, J. S.; O'Brien, J. T.; Steill, J. D.; Oomens, J.; Williams, E. R. *J. Am. Chem. Soc.* **2009**, 131, 11442-11449.

(41) Prell, J. S.; Demireva, M.; Oomens, J.; Williams, E. R. *J. Am. Chem. Soc.* **2009**, 131, 1232-1242.

(42) Wyttenbach, T.; Witt, M.; Bowers, M. T. *J. Am. Chem. Soc.* **2000**, 122, 3458-3464.

(43) Julian, R. R.; Jarrold, M. F. *J. Phys. Chem. A* **2004**, 108, 10861-10864.

(44) Lemoff, A. S.; Bush, M. F.; Williams, E. R. *J. Am. Chem. Soc.* **2003**, 125, 13576-13584.

(45) Skurski, P.; Rak, J.; Simons, J.; Gutowski, M. *J. Am. Chem. Soc.* **2001**, 123, 11073-11074.

(46) Xu, S. J.; Zheng, W. J.; Radisic, D.; Bowen, K. H. *J. Chem. Phys.* **2005**, 122, 091103.

(47) Kass, S. R. *J. Am. Chem. Soc.* **2005**, 127, 13098-13099.

(48) Oomens, J.; Steill, J. D.; Redlich, B. *J. Am. Chem. Soc.* **2009**, 131, 4310-4319.

(49) Valle, J. J.; Eyler, J. R.; Oomens, J.; Moore, D. T.; van der Meer, A. F. G.; von Helden, G.; Meijer, G.; Hendrickson, C. L.; Marshall, A. G.; Blakney, G. T. *Rev. Sci. Instrum.* **2005**, 76, 023103.

(50) Marshall, A. G.; Wang, T. C. L.; Ricca, T. L. *J. Am. Chem. Soc.* **1985**, 107, 7893-7897.

(51) Shao, Y. *et al. Phys. Chem. Chem. Phys.* **2006**, 8, 3172-3191.

(52) Hurley, M. M.; Pacios, L. F.; Christiansen, P. A.; Ross, R. B.; Ermler, W. C. *J. Chem. Phys.* **1986**, 84, 6840-6853.

(53) Lajohn, L. A.; Christiansen, P. A.; Ross, R. B.; Atashroo, T.; Ermler, W. C. *J. Chem. Phys.* **1987**, 87, 2812-2824.

(54) Dunbar, R. C.; Steill, J. D.; Polfer, N. C.; Oomens, J. *J. Phys. Chem. B* **2009**, 113, 10552-10554.

(55) Martin, J. D. D.; Hepburn, J. W. *J. Chem. Phys.* **1998**, 109, 8139-8142.

(56) Hanstorp, D.; Gustafsson, M. *J. Phys. B-At. Mol. Opt. Phys.* **1992**, 25, 1773-1783.

(57) Prell, J. S.; O'Brien, J. T.; Williams, E. R. *J. Am. Soc. Mass Spectrom.* **2010**, 21, 800-809.

(58) Shannon, R. D. *Acta Crystallogr. Sect. A* **1976**, 32, 751-767.

(59) Coblentz Society, Inc., "Evaluated Infrared Reference Spectra" in NIST Chemistry WebBook, NIST Standard Reference Database Number 69, Eds. P.J. Linstrom and W.G. Mallard, National Institute of Standards and Technology, Gaithersburg MD, 20899, http://webbook.nist.gov, (retrieved May 5, 2010).

(60) Oomens, J.; Steill, J. D. *J. Phys. Chem. A* **2008**, 112, 3281-3283.

(61) Roscioli, J. R.; McCunn, L. R.; Johnson, M. A. *Science* **2007**, 316, 249-254.

(62) Marcia Cordes, d. N. D.; Walter, J. L. *Spectrochim. Acta, Part A* **1968**, 24, 237-252.

5.7 Tables and Figures

Anion	Glutamic Acid		Histidine	Arginine	
Cl^-	-HCl		-HCl	-HCl	-(CN_2H_3+Cl) (15%)
Br^-	-HBr (75%)	Br^- (25%)	Br^-	N/A	N/A
I^-	-HI (80%)	I^- (20%)	I^-	I^-	

Table 5.1: IRMPD products of anionized amino acid complexes.

Structure	Cl^-	Br^-	I^-
Glu			
$GluNO_C$	7.0/6.2	0/0	0/0
$GluO_SO_C$	0/0	5.6/5.3	8.9/10.5
$GluNO_SO_C$	29.8/31.3	23.3/23.8	28.0/24.5
GluZW	22.8/20.0	19.0/18.2	18.3/19.0
His			
$HisN_\tau$	1.8/0	10.3/8.9	7.0/6.6
$HisN_TN_\pi$	0/2.1	0/0	0/0
HisZW	19.2/17.6	21.0/22.7	24.8/22.3
$HisN_\pi O$	6.9/8.5	6.3/5.5	12.8/17.3
$HisN_TN_\pi O$	9.8/11.3	10.2/13.4	14.1/18.3

Structure	Cl^-	I^-
Arg		
A	0.1/0	0.1/0
B	0/3.8	0/3.8
C	4.5/12.7	2.1/8.9
D	4.9/8.5	1.1/5.0

Table 5.2: Relative Gibbs free energies (kJ/mol) of low-energy structures at 0/298 K calculated at the B3LYP/6–31+G**/CRENBL level of theory.

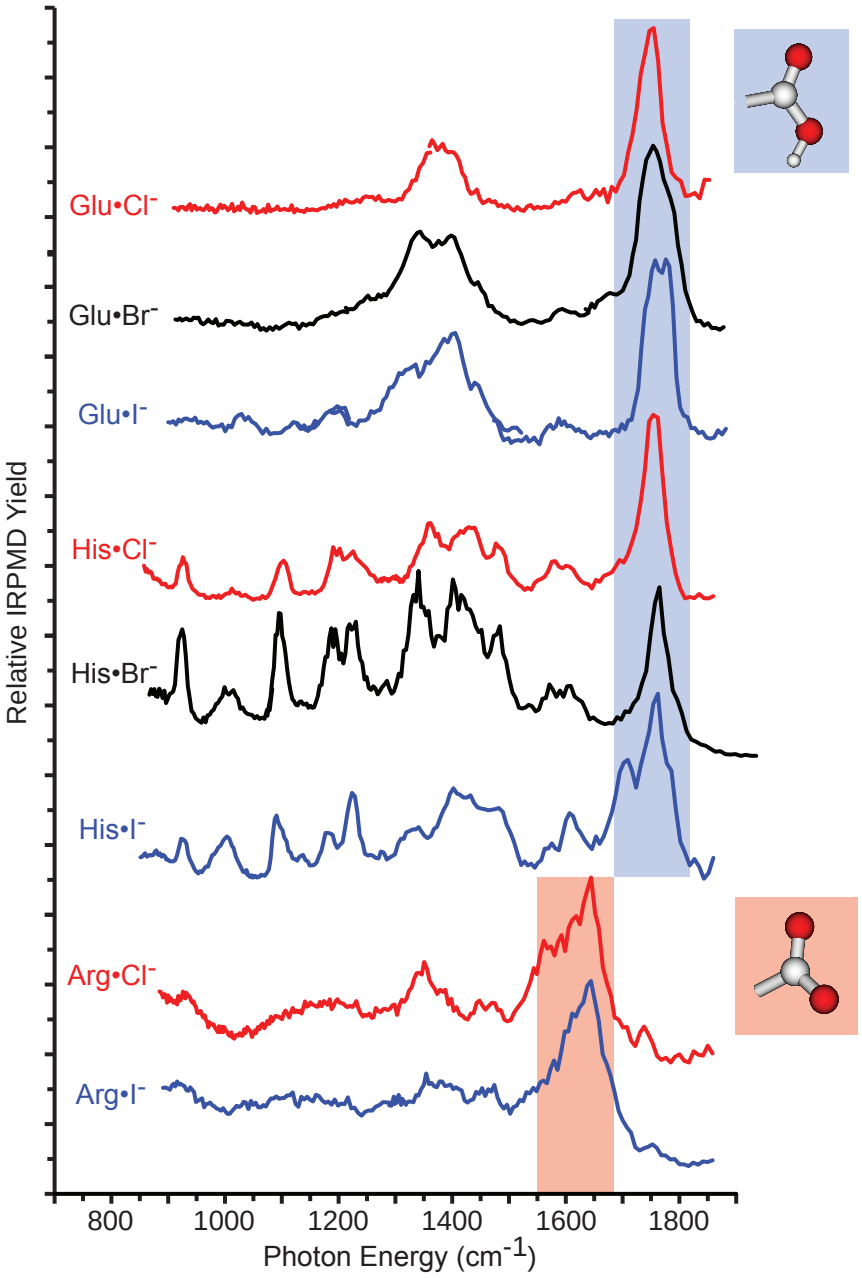

Figure 5.1: IRMPD spectra of Glu•X^-, His•X^- and Arg•X^-, X = Cl^-, Br^-, or I^- at 298 K. Diagnostic carbonyl stretching bands indicating nonzwitterionic (1685 – 1825 cm^{-1}) or zwitterionic (1550 – 1685 cm^{-1}) forms of the amino acids in these complexes are indicated on the spectra.

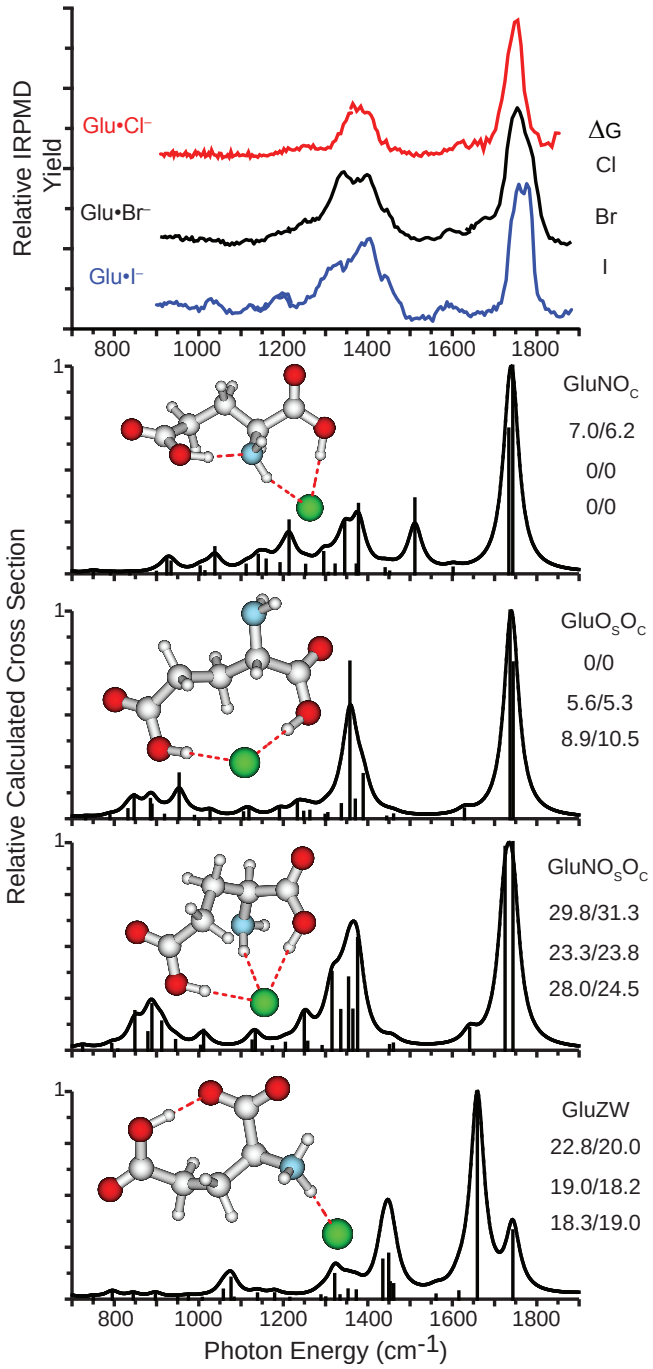

Figure 5.2: Measured IRMPD spectra of Glu•X$^-$, X = Cl$^-$, Br$^-$, or I$^-$ (top), and calculated low-energy structures and spectra for Glu•Cl$^-$. Relative Gibbs free energies in kJ/mol at 0/298 K calculated using the B3LYP/6–31+G**/CRENBL level of theory are indicated for each structure and anion.

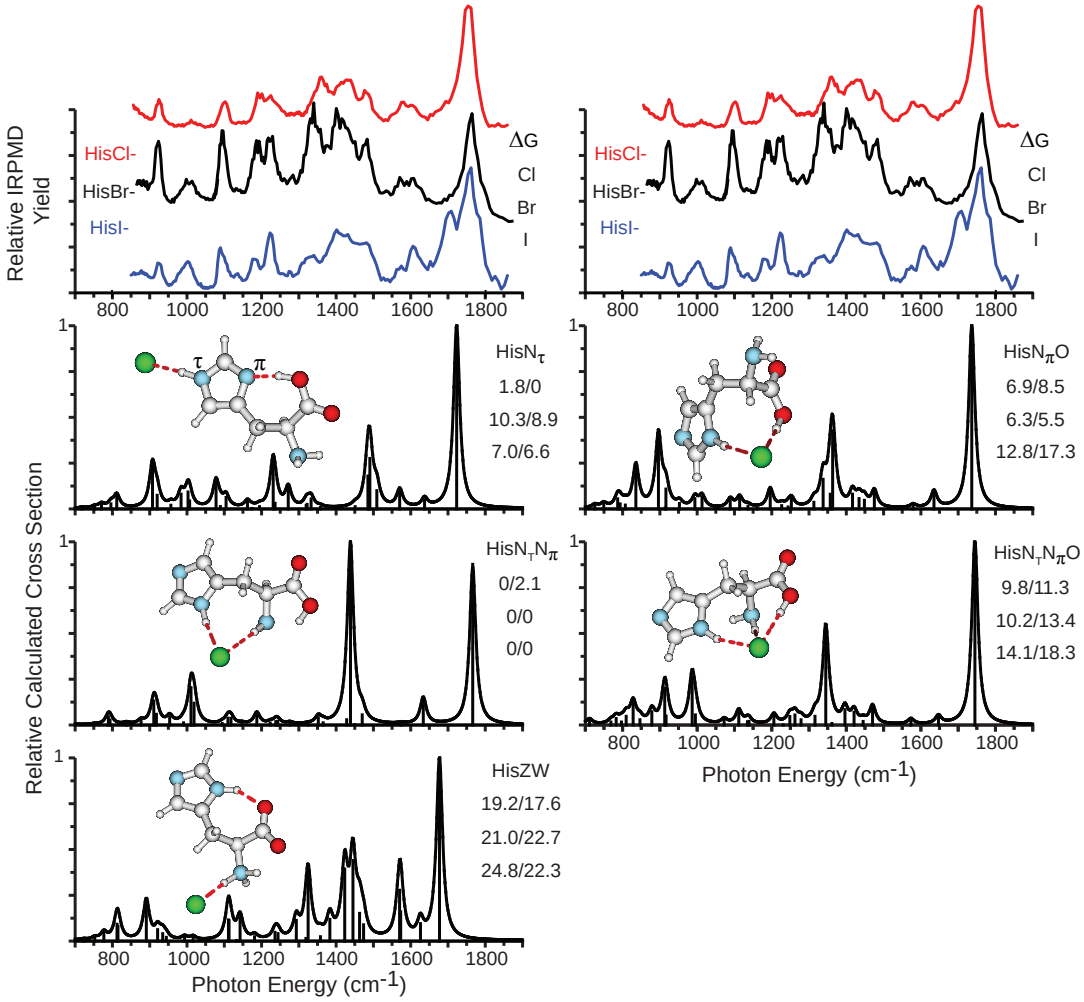

Figure 5.3: Measured IRMPD spectra of His•X$^-$, X = Cl$^-$, Br$^-$, or I$^-$ (top), and calculated low-energy structures and spectra for His•Cl$^-$. Relative Gibbs free energies in kJ/mol at 0/298 K calculated using the B3LYP/6–31+G**/CRENBL level of theory are indicated for each structure and anion.

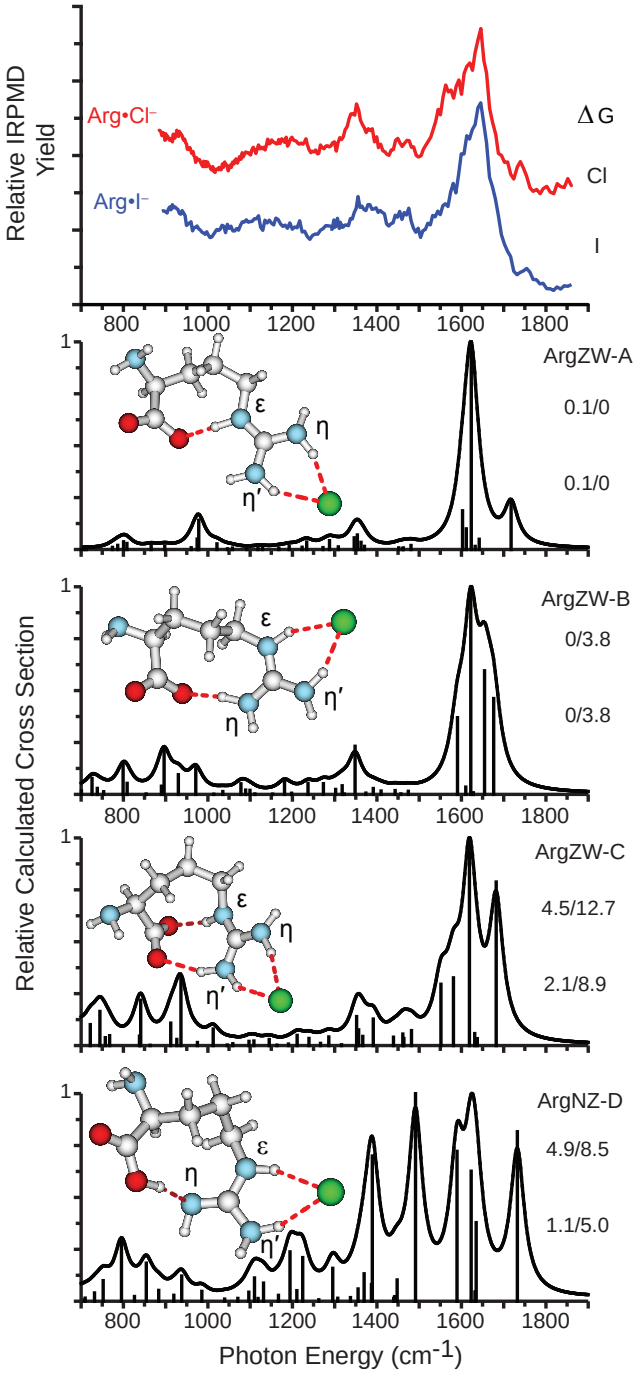

Figure 5.4: Measured IRMPD spectra of Arg•X^-, X = Cl^-, or I^- (top), and calculated low-energy structures and spectra for Arg•Cl^-. Relative Gibbs free energies in kJ/mol at 0/298 K calculated using the B3LYP/6–31+G**/CRENBL level of theory are indicated for each structure and anion.

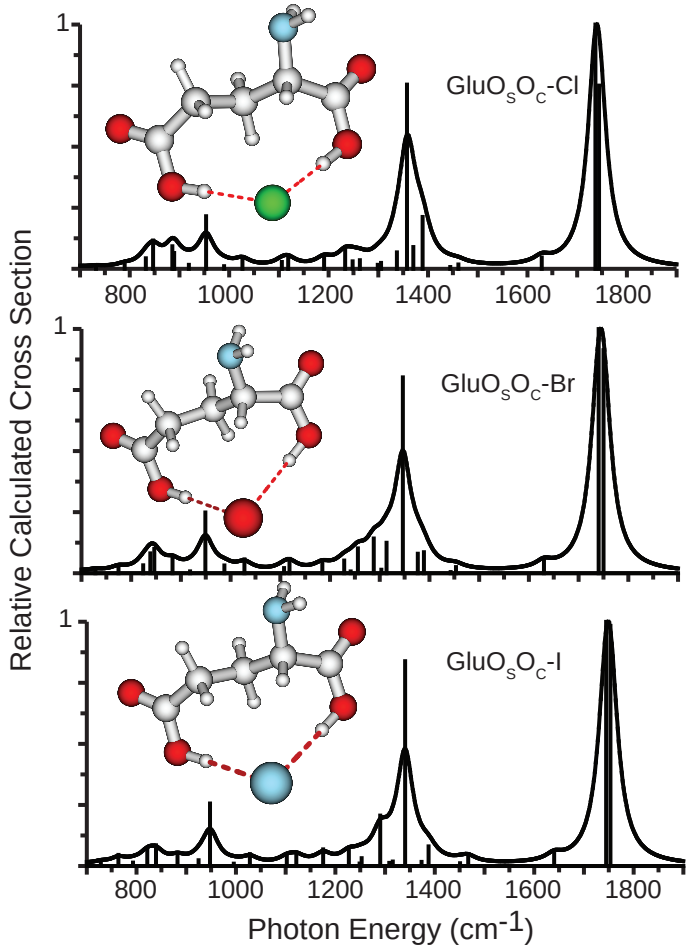

Figure 5.5: $GluO_SO_C$ structures and spectra for Glu complexed with Cl^-, Br^-, and I^- calculated using the B3LYP/6–31+G**/CRENBL level of theory.

Chapter 6

Hydration of Gaseous Copper Dications Probed by IR Action Spectroscopy

Jeremy T. O'Brien, and Evan R. Williams

Journal of Physical Chemistry A, 2008, 112, 5893–5901

6.1 Introduction

Copper plays an important role in many biochemical processes, such as the activity of many enzymes,[1–4] and is an essential element for human health. For example, abnormal regulation of cellular copper is connected to neurodegenerative diseases,[3,4] including Alzheimer's disease.[3] Redox properties of copper and copper complexes have been extensively studied, but some basic properties, such as the coordination number (CN) in water, are not unambiguously known. Cu^+ salts have low solubility in water ($K_{sp} < 10^{-7}$) which limits some solution-phase studies. By comparison, Cu^{2+} salts are readily dissolved in water and can be studied using a variety of methods. It is widely assumed that Cu^{2+} has a CN of six, although coordination numbers ranging from 4 to 6 have been indicated from results of X-ray absorption spectroscopy,[2,5–7] neutron diffraction,[8,9] infrared spectroscopy[7], and computational studies.[9–13] Hydration of Cu^{2+} is especially interesting because the d^9 electronic configuration results in Jahn-Teller distortion characterized by two elongated axial bonds in octahedral structures. Ambiguity about the structure of the first solvation shell has been attributed in part to structural assumptions in the fitting procedures necessary to analyze X-ray absorption spectra and the inability to distinguish axial Cu-O from overlapping Cu-H correlations in neutron diffraction studies.[9] There may be no clearly preferred structure, but rather rapidly interconverting structures that have coordination numbers ranging from 4 to 6.[5]

Insights into the hydration of ions in solution can potentially be obtained by investigating hydrated clusters in the gas phase[14–39] Structures can be examined as a function of cluster size to reveal evidence for shell formation or other uniquely stable structures, such as clathrates for some protonated and other ion-containing water clusters.[18,19] Electrospray ionization (ESI) has made possible the production of hydrated metal dications and even trications[40] for a wide variety of metal ions. $Cu^{2+}(H_2O)_n$ was first produced by ESI,[41] but these clusters can also be produced using a pick-up technique in which water molecules are condensed onto neutral copper atoms and subsequently are ionized by electron impact.[33,42] The dissociation of hydrated divalent ions has been extensively investigated.[24–33,42–44] In general, activation of hydrated divalent ions results in sequential loss of water molecules for larger clusters, but a charge separation reaction typically occurs for small clusters in which H_3O^+ and the corresponding hydrated metal hydroxide with a single charge is produced. The cluster size at which the transition between these two reaction pathways is observed depends on ion identity as well as on activation conditions.[30] A salt-bridge mechanism in which proton transfer occurs from the first solvation shell to a water molecule in the second shell has been

proposed for the charge-separation reaction[43], and both experimental and computational data supporting this mechanism for several hydrated ions have been reported.[36–39]

Duncombe et al. investigated both the formation and dissociation of $Cu^{2+}(H_2O)_n$ and $Cu^{2+}(NH_3)_n$ and found that these clusters with eight ligands are the most abundant in the mass spectrum. For $Cu^{2+}(H_2O)_n$, water loss occurs for clusters with $n \geq 7$ whereas charge separation occurs for $n = 6 - 8$.[30,33,44] In contrast to results for some other hydrated divalent metal ions,[36–38,43] both mono- and dihydrated H_3O^+ is produced in the charge separation reaction. A salt-bridge mechanism analogous to that of Beyer et al.,[43] but in which a second water molecule coordinates to the H_3O^+ before charge separation occurs has been proposed.[39] On the basis of their results for gas-phase clusters, Duncombe et al. concluded that $Cu^{2+}(H_2O)_8$ was of "special significance" and that the structure of this ion may play an important role in aqueous solution.[33] Density functional theory calculations reported by Berces et al. on clusters with $n = 3 - 8$ indicate that the CN of $Cu^{2+}(H_2O)_n$ is 4 and that the first solvation shell for clusters containing up to eight water molecules is square planar.[45] The stability of $Cu^{2+}(H_2O)_8$ was attributed to each of the four water molecules in the second shell accepting two hydrogen bonds from the four water molecules in the inner shell and it was concluded that the gas-phase shell development does not properly reflect that in solution when a limited number of solvent molecules are considered.[45]

Information about ion-water interactions and coordination numbers can be obtained from infrared (IR) action spectroscopy of hydrated ions,[16–23,46–49] although this method has only recently been applied to investigating shell structures of hydrated metal dications.[20] The frequencies of OH stretching vibrations can shift substantially with changes in the hydrogen bonding of the water molecule, making this method especially well suited for structural elucidation of hydrated ions. For example, the IR action spectrum of $Cu^+(H_2O)_3Ar$ has a bonded OH feature that is clearly observed at 2980 cm^{-1}, a > 600 cm^{-1} shift from the free-OH stretching region of 3600 – 3700 cm^{-1}, indicating that even with only three water molecules, one of the water molecules coordinating to the metal ion donates a hydrogen bond to a second-shell water molecule.[48]

Here, structures of $Cu^{2+}(H_2O)_n$, $n = 6 - 12$, are probed using IR action spectroscopy, blackbody infrared radiative dissociation (BIRD), and hybrid density functional theory. From these studies, new insights into the hydration of copper dication and its shell structures are obtained.

6.2 Experimental

6.2.1 Mass Spectrometry

All experiments were performed on a 2.75 T Fourier transform ion cyclotron resonance mass spectrometer.[20,40,50] Distributions of $Cu^{2+}(H_2O)_n$ were produced by nano-electrospray ionization of a 4 mM aqueous solution of $CuSO_4$ (Fischer Scientific, Waltham, MA). These clusters were introduced into the mass spectrometer and were trapped in a cylindrical ion cell that is surrounded by a copper jacket cooled to 215 K by a regulated flow of liquid nitrogen.[27] The copper jacket temperature was allowed to equilibrate for at least 8 h prior

to the experiments. Ions were accumulated in the cell for 4 – 6 s during which time dry N_2 gas ($\sim 10^{-6}$ Torr) was pulsed into the vacuum chamber using a piezoelectric valve to enhance trapping and thermalization of the ions. A mechanical shutter was subsequently closed to prevented further ion accumulation and residual gases were pumped out for 6 – 10 s resulting in a base pressure of $\sim 10^{-8}$ Torr prior to ion isolation.

$Cu^{2+}(H_2O)_7$ was the smallest cluster observed directly by ESI under a wide range of source conditions. $Cu^{2+}(H_2O)_6$ was formed by collisionally activating larger clusters using a frequency sweep or chirp excitation waveform (200 μs, 2000 Hz/μs, $\sim$250 V_{pk-pk}) that increased the average velocity of all trapped ions with $m/z > 90$. This excitation was repeated nine times with a 300 ms delay between each chirp to maximize the intensity of $Cu^{2+}(H_2O)_6$. Dry N_2 was pulsed into the chamber ($\sim 10^{-6}$ Torr) during this time to enhance collisional activation, and residual gases were then pumped out for 10 s prior to isolation of this ion.

The cluster of interest was isolated using a stored waveform inverse Fourier transform. To obtain IR action spectra, the isolated clusters were irradiated using tunable IR light produced by an optical parametric oscillator/amplifier (OPO/OPA) system (LaserVision, Bellevue, WA) pumped by the fundamental of a Nd:YAG laser (Continuum Surelight I-10, Santa Clara, CA) at a 10 Hz repetition rate. Laser irradiation times were varied from 1 to 20 s to improve the dynamic range and the signal-to-noise of the IR spectrum. Typically, 1 or 3 s irradiation times were used for frequencies in the free-OH stretch region (3600 – 3750 cm^{-1}) of the IR spectrum; otherwise, a 20 s irradiation time was used. From the abundances of the precursor and product ions, dissociation rates as a function of the IR laser frequency were obtained. These dissociation rates were corrected for the BIRD background dissociation, the differences in laser power at different frequencies, and the duration of laser irradiation. To obtain unimolecular dissociation rate constants for both laser photodissociation at a specific frequency and for BIRD,[24–27] ions were exposed to radiation for up to 50 s, and these data were fit to first-order kinetics. All data were acquired using a "MIDAS"[51] modular data system.

6.2.2 Computational Chemistry

Candidate low-energy structures were identified using conformational searching and previously reported low-energy structures.[45] Initial structures were generated using 10,000 step Monte Carlo conformational searching as implemented in Macromodel 8.1 (Schrödinger, Inc., Portland, OR) using the MMFF94 force field. The conformation searching generated primarily structures with CN = 6. To obtain structures with CN = 4 and 5 similar to those reported previously,.[45] water molecules were manually rearranged from structures with CN = 6.

These candidate structures were geometry optimized, and the self consistent field energy was calculated with B3LYP hybrid density functional calculations using the LACV3P**++ basis set as implemented in Jaguar v. 6.5 (Schrödinger, Inc., Portland, OR). Harmonic vibrational frequencies and intensities were calculated using the numerical derivatives of the LACV3P**++ energy-minimized Hessian. All structures yielded positive frequency modes,

indicating that they are local-minimum structures. The energies reported are the relative Gibbs free energies at 215 K, the temperature of the copper jacket in the experimental measurements, and include zero-point energy corrections. Relative electronic energies are reported for comparison to previous results for $Cu^{2+}(H_2O)_6$. Structures were energy-minimized, and vibrational frequencies and intensities were calculated for the low-energy structures of $Cu^{2+}(H_2O)_6$ at the BP86/LACV3P**++ level of theory. All vibrational frequencies are scaled by 0.956 which has been shown previously to provide good agreement with experimental IR spectra in the free-OH region.[22] To approximate temperature and other broadening effects, the calculated line spectra are convolved using 15 and 50 cm^{-1} full width at half max (fwhm) Lorentzian distributions for the nonbonded and bonded features, respectively.

6.3 Results and Discussion

6.3.1 Ion Formation

Electrospray ionization of a 4 mM solution of aqueous $CuSO_4$ results in broad distributions of $Cu^{2+}(H_2O)_n$, $CuOH^+(H_2O)_n$, and $H^+(H_2O)_n$. A typical ESI spectrum is shown in Figure 1. The size and width of these distributions depend on ion source and other instrumental parameters and can generally be shifted to the cluster size of interest by adjusting these parameters.[40] Although $Cu^{2+}(H_2O)_8$ can be made the base peak in the spectrum, its abundance does not stand out from that of its neighboring clusters under a wide range of conditions (Figure 1). $Cu^{2+}(H_2O)_7$ is the smallest dication copper cluster observed, consistent with earlier results of hydrated dication copper ions formed by ESI.[41] Clusters as small as $Cu^{2+}(H_2O)_2$ were observed by Duncombe et al. with the pick-up technique,[33] and clusters with n between 1 and 6 have been produced by collisional activation of $Cu^{2+}(H_2O)_{n>6}$.[30,33,44] In order to form $Cu^{2+}(H_2O)_6$ in this experiment, the broad distribution of ions trapped in the Fourier transform ion cyclotron resonance (FT/ICR) cell are collisionally activated using a series of frequency sweep or chirp excitation pulses. No smaller hydrated Cu^{2+} clusters were observed over a wide range of conditions.

6.3.2 Ion Fragmentation and Stability

BIRD spectra of isolated $Cu^{2+}(H_2O)_n$, $n = 7$ – 9, measured at a cell temperature of 298 K and at 20, 25, and 0.5 s reaction times for $n = 7$, 8, and 9, respectively, are shown in Figure 2. BIRD of isolated $Cu^{2+}(H_2O)_n$, $n = 9$ – 12, results in consecutive loss of a neutral water molecules [Reaction 1].

$$Cu^{2+}(H_2O)_n \rightarrow Cu^{2+}(H_2O)_{n-1} + H_2O \quad n = 9\text{–}12 \tag{6.1}$$

For $n = 6$ and 7, a charge-separation reaction takes place resulting in formation of protonated water clusters and the corresponding hydrated $(CuOH)^+$ [Reaction 2].

$$Cu^{2+}(H_2O)_n \rightarrow CuOH^+(H_2O)_{n-k-2} + H_3O^+(H_2O)_k \quad n = 6, 7; \quad k = 1, 2 \tag{6.2}$$

For $Cu^{2+}(H_2O)_8$, fragment ions from both reactions are formed in roughly equal proportions (Figure 2). These results are consistent with the metastable fragmentation pathways reported by Duncombe et al., although in that study, some neutral water loss from $Cu^{2+}(H_2O)_7$ was also observed.[33] By comparison, $Cu^{2+}(H_2O)_n$, $n = 1 - 6$, can be produced by collisional activation of $Cu^{2+}(H_2O)_{n>6}$.[30,33,44] With the relatively long time scale of these BIRD experiments, low-energy dissociation processes are favored compared to activating ions by energetic collisions. Thus, formation of $CuOH(H_2O)_n^+$ under the lower-energy activation conditions of BIRD used here indicates that loss of a water molecule is entropically favored over the charge-separation reaction, consistent with previous results for $SO_4^{2-}(H_2O)_n$.[52]

Dissociation rate constants in the zero-pressure limit[53–55] were obtained from BIRD spectra as a function of reaction times up to 50 s at 215 K. The temperature of 215 K was chosen so that the lifetimes of $Cu^{2+}(H_2O)_{10-12}$ are sufficiently long that IR action spectra can be readily measured. These rate constants as a function of cluster size are shown in Figure 3. For $n \geq 8$, the BIRD rate constant increases with cluster size. This can be attributed both to a decrease in water-binding energy[24–29], and an increase in the rate of absorption of blackbody radiation[54] with increasing cluster size. Surprisingly, the trend in ion stability reverses at $n = 8$, where the $n = 7$ and $n = 6$ clusters are progressively *less* stable. This can be attributed to a lower barrier for the charge separation reaction versus water loss as well as to possible ion structure effects. The higher stability of the $n = 7$ compared to $n=6$ cluster indicates that the barrier for the charge-separation reaction decreases with cluster size over this range.

The stabilities of these clusters alone do not provide significant insights into structures. Additional studies aimed at determining water-binding energies or entropies may provide more useful insights into shell structures.

6.3.3 IR Action Spectroscopy and Free-OH Stretches

Infrared action spectra from ~2800 to 3800 cm^{-1} for $Cu^{2+}(H_2O)_{6-12}$ measured with the ion cell temperature at 215 K are shown in Figure 4. The spectra for $Cu^{2+}(H_2O)_{6-9}$ each have two bands in the high-frequency region at ~3600 cm^{-1} and ~3660 cm^{-1}, consistent with the respective symmetric (ν_{sym}) and asymmetric (ν_{asym}) free-OH stretch frequencies of water molecules that do not donate any hydrogen bonds (acceptor-only molecules). Dangling-OH stretch frequencies from water molecules that donate a single hydrogen bond can also contribute to the band at ~3660 cm^{-1}. These bands can be readily identified as free-OH stretches on the basis of comparison to previously reported IR action spectra of hydrated metal ion clusters, such as $Ca^{2+}(H_2O)_{4-9}$,[20] $Ni^+(H_2O)_{1-5}$,[21] $Cs^+(H_2O)_{1-5}$,[23] and $H_3O^+(H_2O)_{3-8}$.[15–17] The frequencies of these vibrations are substantially red shifted from those of an isolated water molecule (3649 cm^{-1} and 3731 cm^{-1} respectively)[56] or free-OH stretches of $Ni^+(H_2O)Ar_2$ (3623 cm^{-1} and 3696 cm^{-1})[21] because of partial electron transfer from the water molecules to the cation which leads to weaker O-H bonding and lower frequency vibrations.[21] These peaks for $Cu^{2+}(H_2O)_{6-12}$ blue shift with increasing cluster size because the magnitude of the electron transfer per water molecule decreases. Similar trends have been observed in the spectra of both $H_3O^+(H_2O)_n$[17,18] and $Ca^{2+}(H_2O)_n$[20].

In contrast, spectra of $Cu^{2+}(H_2O)_{10-12}$ have four distinct features in this region which become more pronounced with increasing cluster size. All of these features are characteristic of different free-OH stretching vibrations in hydrated clusters, and these hydrogen bonding motifs are illustrated in Figure 5.[15–20] These bands can be assigned on the basis of previously reported IR action spectra of $H_3O^+(H_2O)_{7-20}$[15–19] and the calculated spectra of low-energy structures (vide infra). The peaks at ∼3640 cm^{-1} and ∼3725 cm^{-1} are consistent with the free-OH ν_{sym} and ν_{asym}, respectively, of water molecules that accept a single hydrogen bond, that is, single acceptor (A) molecules. The band at ∼3660 cm^{-1} is due to the ν_{asym} of water molecules that accept two hydrogen bonds and donate one, that is, acceptor-acceptor-donors (AAD). The band at ∼3690 cm^{-1} is the ν_{asym} of water molecules that accept two hydrogen bonds (AA), blue-shifted from the corresponding vibration in the smaller clusters.

6.3.4 Hydrogen-Bonded OH Stretches

Two bands corresponding to hydrogen-bonded stretches are identified in the $Cu^{2+}(H_2O)_n$ IR action spectra: a very broad band from ∼3300 to 3600 cm^{-1} that is clearly present for n = 8 – 12 and a second broad feature (∼3000 to 3300 cm^{-1}) in the spectra of $Cu^{2+}(H_2O)_{10-12}$. Weak photodissociation occurs for $Cu^{2+}(H_2O)_{6,7}$ in the region between ∼3200 and 3500 cm^{-1}. Similarly broad OH bonded features have been observed in the IR spectra of $Cu^+(H_2O)_n$,[48] $Ni^+(H_2O)_n$,[21] $Ca^{2+}(H_2O)_n$,[20] and $H_3O^+(H_2O)_n$.[16–19] On the basis of earlier studies, the very broad feature centered near 3500 cm^{-1} for the larger clusters is assigned to the hydrogen bonded OH stretches of double-donor (DD) water molecules. The photodissociation between 3300 and 3500 cm^{-1} for $Cu^{2+}(H_2O)_{6,7}$ is consistent with DD water molecules indicating that some population of the clusters contain at least two water molecules in the second solvation shell. The band centered around 3100 cm^{-1} in the larger clusters coincides with the appearance of the AAD ν_{asym} free-OH peak and is consistent with results from protonated water clusters for which a band in the same region is assigned to the hydrogen-bonded ν_{sym} OH stretches of AAD water molecules.[18]

6.3.5 Comparison to Divalent Calcium

Some useful insights into the structures of $Cu^{2+}(H_2O)_n$ can be obtained by comparing data for hydrated divalent calcium, which has a larger ionic radius (1.00 Å, CN = 6) compared to that for copper (0.73 Å, CN = 6).[57] IR action spectra of $Cu^{2+}(H_2O)_6$ and $Ca^{2+}(H_2O)_{6,7}$ are shown in Figure 6. The relative intensities of the ν_{sym} and ν_{asym} free-OH stretches of $Cu^{2+}(H_2O)_6$ more closely resembles those of $Ca^{2+}(H_2O)_7$ than those of $Ca^{2+}(H_2O)_6$. $Ca^{2+}(H_2O)_6$ has an octahedral structure (CN = 6) on the basis of BIRD,[24–26] guided ion beam,[29] spectroscopic[20] and computational[20,29] results. Some of these studies indicate that $Ca^{2+}(H_2O)_7$ also has a CN = 6 although a heptacoordinated structure is not ruled out.[25] Spectroscopic evidence indicates the presence of at least two different structures of this ion in which an outer shell water molecule accepts either one (A) or two (AA) hydrogen bonds from inner-shell water molecules.[20]

The free-OH stretches in the $Cu^{2+}(H_2O)_6$ spectrum are red-shifted by ∼10 cm^{-1} compared to the corresponding bands in the $Ca^{2+}(H_2O)_6$ spectrum. This indicates greater

electron transfer from the water molecules to the Cu^{2+}, consistent with the smaller size and therefore greater charge density of Cu^{2+}. The intensity of the ν_{sym} band relative to that of the ν_{asym} band for $Cu^{2+}(H_2O)_6$ is substantially smaller than that for $Ca^{2+}(H_2O)_6$ and is much closer to that of $Ca^{2+}(H_2O)_7$. The significantly lower intensity of ν_{sym} compared to ν_{asym} has been observed in many other action spectra of large hydrated clusters.[18–21,48] The relative intensities of these bands are related to the structure of the cluster and to the extent of hydrogen bonding[17–21,34] and for $Ca^{2+}(H_2O)_n$[20] and $Ni^{+}(H_2O)_n$,[21] are indicative of the onset for second shell formation. This ratio for the $Cu^{2+}(H_2O)_6$ also suggests that one or more water molecules are in the second shell, although structural differences between $Cu^{2+}(H_2O)_n$ and $Ca^{2+}(H_2O)_n$ will almost certainly affect this ratio as well.

A region of the spectrum that is potentially more indicative of water molecules in a second shell is the lower frequency region between 3000 and 3500 cm^{-1}, which corresponds to the OH stretching region of inner-shell water molecules involved in hydrogen bonding to outer-shell water molecules. Some photodissociation in this region is observed for $Cu^{2+}(H_2O)_6$, although the intensity is very low. By comparison, significantly more photodissociation in this region is observed for $Ca^{2+}(H_2O)_7$ than for $Ca^{2+}(H_2O)_6$, although the photodissociation intensity in this region for $Ca^{2+}(H_2O)_7$ is much less than that expected on the basis of calculated absorption spectra for structures containing a second-shell water molecule.[20]

The laser photodissociation rate at 3450 cm^{-1} for $Cu^{2+}(H_2O)_6$ is only about 2 times higher than the BIRD rate. To ascertain if this laser-induced photodissociation is significant and indicates the presence of a second-shell water molecule or molecules, data were acquired as a function of time for reaction times up to 50 s. The data for $Cu^{2+}(H_2O)_6$ were acquired at 215 K, the temperature at which the spectra were obtained. The data for $Ca^{2+}(H_2O)_6$ were acquired at both 296 (data not shown) and at 335 K (Figure 7). The latter temperature was chosen so that the BIRD rate would be comparable to that for $Cu^{2+}(H_2O)_6$ at 215 K. Measurement of laser photodissociation kinetics under conditions where the BIRD rates of the two ions are comparable should compensate for the different dissociation energies of these two ions so that absorption of one or more laser generated photons should produce comparable dissociation despite the different dissociation energies. These data are fit to first-order kinetics, and the rate constants are reported in Table 1.

Laser photodissociation data, obtained under the same conditions as the BIRD data and at 3450 and 3655 cm^{-1} for $Cu^{2+}(H_2O)_6$ and at 3450 and 3610 cm^{-1} for $Ca^{2+}(H_2O)_6$ are shown in Figure 7. The two higher frequencies are where maximum photodissociation occurs in the IR action spectrum of each cluster. The lower frequency corresponds to an approximate maximum in the hydrogen-bonding band in the $Cu^{2+}(H_2O)_8$ spectrum, the smallest cluster in which a distinct hydrogen-bonding feature is clearly observed. These data fit first-order kinetics, and laser-induced photodissociation rate constants are obtained from the difference of the total dissociation and BIRD rate constants. These values are given in Table 1.

From the ratio of the laser-induced photodissociation rate constants at the two photon energies, a comparison of the relative extent of fragmentation that occurs in the hydrogen-bonding region of the spectrum of $Cu^{2+}(H_2O)_6$ to that of $Ca^{2+}(H_2O)_6$ is obtained (Table 1). For $Ca^{2+}(H_2O)_6$, the laser-induced photodissociation rate constant at 3450 cm^{-1} is $\sim$ 450 times smaller than that at 3610 cm^{-1}. In sharp contrast, this rate constant for $Cu^{2+}(H_2O)_6$

at 3450 cm^{-1} is 60 times smaller than that where maximum dissociation occurs. Thus, there is ∼8 times more relative dissociation in the hydrogen-bonding region for $Cu^{2+}(H_2O)_6$ compared to that for $Ca^{2+}(H_2O)_6$. These data indicate the presence of hydrogen bonding for the $Cu^{2+}(H_2O)_6$ cluster and illustrate the advantage of the high signal-to-noise ratio that is possible in these experiments for identifying weak, but structurally significant, features.

For the $Ca^{2+}(H_2O)_6$ data at 295 K, the laser-induced photodissociation rate contant at 3450 cm^{-1} is almost 1000 times smaller than that at 3610 cm^{-1}. The lower dissociation efficiency at the lower temperature and frequency suggests that some of the photodissociation can be attributed to absorption of more than one photon under these conditions. By increasing the temperature, a greater fraction of the population can be dissociated upon absorption of a single photon.

6.3.6 Computations

More detailed structural information can be obtained by comparing the experimentally measured IR action spectra to calculated absorption spectra of candidate low-energy structures. The relative electronic energies as well as Gibbs free energies at the temperature of the spectroscopy experiments (215 K) are reported in Table 2 for $Cu^{2+}(H_2O)_n$, $n = 6 - 8$, 10. The lowest-energy structure for each cluster size is found to be very similar to those identified by Bérces et al. who used the BP86 density functional and Slater function basis sets.[45] The only minor structural differences are the orientations of some water molecules; tetrahedral bonding of water molecules is favored by the BP86 functional whereas more planar bonding is favored by B3LYP.[45] However, the energy differences between different structures are substantially smaller at the B3LYP/LACV3P**++ level of theory. Relative electronic energies from calculations for $Cu^{2+}(H_2O)_6$ at the BP86/LACV3P**++ level of theory are compared to those reported by Bérces et al[45] (Table 2). These values are within 10 kJ/mol of the previously reported values,[45] but the energy differences between structures with B3LYP/LACV3P**++ are substantially lower. This indicates that although the ordering of the stabilities of the different structures is nearly the same, the magnitude of the energetic differences depends strongly on the density functional used.

For all these clusters, structures with a CN = 4 were found to be most stable. For all but $Cu^{2+}(H_2O)_8$, structures with a CN = 5 are ∼10 kJ/mol less stable at 215 K. Structures with CN = 6 are more than 20 kJ/mol less stable. As noted previously for $Cu^{2+}(H_2O)_8$,[33,45] there is a clear preference for a CN = 4 structure because of an especially favorable hydrogen bond network.

6.3.7 Comparisons to Experimental Data

Vibrational frequencies and intensities were calculated for the low-energy structures at the B3LYP/LACV3P**++ level of theory for comparison to the experimentally measured IR action spectra. The calculated vibrational frequencies are scaled by 0.956, a factor found previously to provide good agreement between measured and calculated spectra in the free-OH stretch region.[22] The calculated line spectra are convolved with Lorentzian peak shapes with 15 cm^{-1} fwhm for non-bonded features and 50 cm^{-1} for bonded features. Because of

the very large conformational spaces of these ions, comparisons with only a limited number of structures that illustrate important bonding motifs are presented. Also, there are uncertainties associated with comparing calculated absorption spectra at zero K using the double-harmonic approximation with IR action spectra measured at 215 K.

For $Cu^{2+}(H_2O)_6$, the two lowest-energy structures, 6AI and 6AII, each have a square planar inner shell with the two second shell water molecules each accepting two hydrogen bonds from the inner shell (Figure 8). The second shell water molecules in 6AI occupy adjacent double acceptor sites whereas these molecules in structure 6AII are opposite one another. The calculated spectra of these structures are different because of the presence of a double-donor water molecule in the former. The ν_{asym} and ν_{sym} associated with double donor water molecules are calculated to occur in the 3300–3400 cm^{-1} region whereas those of single donors are calculated to be between 3100 cm^{-1} and 3300 cm^{-1}. Structures 6B (CN = 5) and 6C (CN = 6) are, respectively, $\sim$ 9 and 22 kJ/mol less stable than 6AI at 215 K. The calculated spectra of structures 6AI and 6AII match the experimental spectrum well in the free-OH region, though subtle differences exist. These bands for structure 6C are 30 cm^{-1} higher and there are no hydrogen-bonding features whereas the experimental data has significant, albeit low-intensity, photodissociation between 3100 and 3500 cm^{-1}. These results indicate that structures with a CN = 4 provide the best match to the experimental spectrum, but minor contributions from other structures cannot be ruled out.

The photodissociation intensity between 3100 and 3500 cm^{-1} relative to features in the free-OH region is much lower than predicted by the calculated absorption spectra. Even for larger clusters with significant hydrogen bonding, such as $Cu^{2+}(H_2O)_8$, the relative peak intensity of the hydrogen-bonded features is substantially weaker than calculations predict. This discrepancy has been observed previously in the water loss IR action spectra of other clusters[15,19,20] and has been attributed to several factors including the broadness of hydrogen-bonded bands relative to free-OH bands. OH stretching bands can broaden considerably when involved in hydrogen bonding, thereby reducing the peak intensity of these bands relative to those of the free-OH stretches.[20,21,48,58] However, even the integrated photodissociation intensity of these bands does not account for the discrepancy, indicating that other factors, such as lower photon energy, calculation uncertainties, and anharmonicity, also play a role.

For $Cu^{2+}(H_2O)_7$, the free-OH region matches well with that calculated for 7A (Figure 9), the lowest-energy structure in these calculations, although the ν_{asym} and ν_{sym} bands are calculated to be $\sim$10 cm^{-1} lower in frequency. The lack of distinct bands below 3550 cm^{-1} in the measured action spectrum precludes any more detailed comparison to the calculated absorption spectra.

The free-OH region of the measured spectrum of $Cu^{2+}(H_2O)_8$ matches well with that calculated for 8A (Figure 10), although the calculated ν_{asym} and ν_{sym} bands are about 10 cm^{-1} lower in frequency as was the case for 7A for $Cu^{2+}(H_2O)_7$. These bands for 7A are calculated to blue shift by $\sim$20 cm^{-1} for 8A. This same shift is observed in the experimental action spectra of these two ions, consistent with structures with CN = 4 for both cluster sizes. This shift indicates that less charge transfer occurs at $n = 8$ compared to $n = 6$ and 7, and coincides with the change in fragmentation from charge separation to water loss. In

the hydrogen-bonded region of $Cu^{2+}(H_2O)_8$, broad photodissociation occurs from ∼3200 to 3600 cm^{-1} without distinct features which is somewhat surprising given the large energetic preference calculated for 8A.

Calculated spectra of some low-energy $Cu^{2+}(H_2O)_{10}$ structures are shown in Figure 11. Structure 10A matches well with the experimental spectrum in the free-OH region. The experimentally observed peaks at ∼3715 and ∼3630 cm^{-1} match the free-OH ν_{asym} and ν_{sym} of single acceptors in 10A, indicating the presence of water molecules in a third solvation shell. The band observed at ∼3690 cm^{-1} corresponds to the free-OH ν_{asym} of double acceptor water molecules and the peak at ∼3660 cm^{-1} matches the ν_{asym} of the two AAD water molecules in 10A. These four bands become progressively more distinct for $Cu^{2+}(H_2O)_{11}$ and $Cu^{2+}(H_2O)_{12}$ suggesting continued filling of the third solvation shell. The band at 3100 cm^{-1} corresponds with the hydrogen-bonded ν_{sym} of the AAD molecules in 10A and becomes more prominent in the spectra of $Cu^{2+}(H_2O)_{11}$ and $Cu^{2+}(H_2O)_{12}$ further indicating the presence of additional third-shell water molecules in these larger clusters.

An exhaustive conformational search of $Cu^{2+}(H_2O)_{10}$ was not performed because of the many low-energy conformations possible and the difficulty associated with identifying these conformers. Many structures similar to 10A with CN = 4 are expected to be low in energy and should have similar calculated absorption spectra. The calculated spectrum of 10B with CN = 5 and a single third-shell water molecule is also consistent with the experimental spectrum, although the higher frequency region is not as good a match as that for 10A. Structure 10C with a CN = 6 is substantially higher in energy and does not have a low-frequency band attributable to third-shell water molecules. For a structure with CN = 6 to have a third-shell water molecule, a net loss of two hydrogen bonds would be necessary. Such structures are expected to be substantially higher in energy. From these calculated spectra, the experimental results for $Cu^{2+}(H_2O)_{10-12}$ are found to support the formation of a third solvent shell and are consistent with a CN = 4 although contributions of structures with CN = 5 and even 6 cannot be ruled out.

6.4 Conclusions

Structures of $Cu^{2+}(H_2O)_n$, n = 6 – 12, were investigated using IR action spectroscopy, blackbody infrared radiative dissociation, and density functional calculations on select cluster sizes. Results from BIRD show that cluster stability decreases with increasing size above n = 8, but this trend is reversed for the smaller clusters where $Cu^{2+}(H_2O)_8$ is the most stable and $Cu^{2+}(H_2O)_6$ is the least stable. This reversal in stability coincides with a change in the dominant fragmentation pathway from loss of a water molecule for clusters with $n \geq 9$ to a charge-separation reaction producing protonated water clusters and the corresponding singly charged hydrated metal hydroxide for $n \leq 7$. These results indicate a lower dissociation barrier for the latter reaction pathway that decreases with decreasing cluster size.

Results from density functional theory calculations for $Cu^{2+}(H_2O)_n$, n = 6 – 8 and 10, indicate that the lowest-energy structures have a coordination number of 4, although structures with a CN = 5 are within about 10 kJ/mol for all clusters except $Cu^{2+}(H_2O)_8$. The structure of the latter cluster is square planar with each of the four second shell water molecules

accepting two hydrogen bonds from the inner-shell water molecules. These lowest-energy structures are essentially the same as those identified previously,[33] but the energy differences between these structures and those with higher coordination numbers are significantly lower with the B3LYP/LACV3P**++ level of theory.

IR action spectra provide evidence for hydrogen bonding in each of these clusters and the results for $Cu^{2+}(H_2O)_n$, n = 6 – 8, are consistent with structures with CN = 4, although structures with higher CN may contribute to these spectra. New spectral features for $Cu^{2+}(H_2O)_n$, n = 10 – 12, attributable to single acceptor and acceptor-acceptor-donor water molecules indicate the onset of the formation of a third solvation shell.

The axial bonding sites of Cu^{2+} are unfavorable even in the larger clusters investigated, although structures with a CN = 5 are calculated to be close in energy and such structures may contribute substantially to the measured IR action spectra for the larger clusters. With the exception of $Cu^{2+}(H_2O)_8$, which has a clear preference for a CN = 4, the relative energy differences between CN = 4 and 5 for the other gas-phase clusters are not so pronounced. The propensity to form a third solvent shell at such a small cluster size indicates that the energy differences between different CN in solution may not be large. Experiments on even larger clusters may provide additional insights of the interactions of Cu^{2+} in bulk solution.

6.5 References

(1) Zeng, L.; Miller, E. W.; Pralle, A.; Isacoff, E. Y.; Chang, C. J. *J. Am. Chem. Soc.* **2006**, 128, 10-11.

(2) Frank, P.; Benfatto, M.; Szilagyi, R. K.; D'Angelo, P.; Della Longa, S.; Hodgson, K. O. *Inorg. Chem.* **2005**, 44, 1922-1933.

(3) Barnham, K. J.; Masters, C. L.; Bush, A. I. *Nat. Rev. Drug Discovery* **2004**, 3, 205-214.

(4) Waggoner, D. J.; Bartnikas, T. B.; Gitlin, J. D. *Neurobiol. Disease* **1999**, 6, 221-230.

(5) Chaboy, J.; Muñoz-Páez, A.; Merkling, P. J.; Marcos, E. S. *J. Chem. Phys.* **2006**, 124, 064509.

(6) Garcia, J.; Benfatto, M.; Natoli, C. R.; Bianconi, A.; Fontaine, A.; Tolentino, H. *Chem. Phys.* **1989**, 132, 295-307.

(7) Beagley, B.; Eriksson, A.; Lindgren, J.; Persson, I.; Pettersson, L. G. M.; Sandström, M.; Wahlgren, U.; White, E. W. *J. Phys.: Condens. Matter* **1989**, 1, 2395-2408.

(8) Salmon, P. S.; Neilson, G. W. *J. Phys.: Condens. Matter* **1989**, 1, 5291-5295.

(9) Pasquarello, A.; Petri, I.; Salmon, P. S.; Parisel, O.; Car, R.; Tóth, E.; Powell, D. H.; Fischer, H. E.; Helm, L.; Merbach, A. E. *Science* **2001**, 291, 856-859.

(10) Amira, S.; Spångberg, D.; Hermansson, K. *Phys. Chem. Chem. Phys.* **2005**, 7, 2874-2880.

(11) Schwenk, C. F.; Rode, B. M. *J. Chem. Phys.* **2003**, 119, 9523-9531.

(12) Schwenk, C. F.; Rode, B. M. *ChemPhysChem* **2003**, 4, 931-943.

(13) Schwenk, C. F.; Rode, B. M. *J. Am. Chem. Soc.* **2004**, 126, 12786-12787.

(14) Kolaski, M.; Lee, H. M.; Choi, Y. C.; Kim, K. S.; Tarakeshwar, P.; Miller, D. J.; Lisy, J. M. *J. Chem. Phys.* **2007**, 126, 074302.

(15) Jiang, J. C.; Wang, Y. S.; Chang, H. C.; Lin, S. H.; Lee, Y. T.; Niedner-Schatteburg, G.; Chang, H. C. *J. Am. Chem. Soc.* **2000**, 122, 1398-1410.

(16) Headrick, J. M.; Diken, E. G.; Walters, R. S.; Hammer, N. I.; Christie, R. A.; Cui, J.; Myshakin, E. M.; Duncan, M. A.; Johnson, M. A.; Jordan, K. D. *Science* **2005**, 308, 1765-1769.

(17) Yeh, L. I.; Okumura, M.; Myers, J. D.; Price, J. M.; Lee, Y. T. *J. Chem. Phys.* **1989**, 91, 7319-7330.

(18) Miyazaki, M.; Fujii, A.; Ebata, T.; Mikami, N. *Science* **2004**, 304, 1134-1137.

(19) Shin, J. W.; Hammer, N. I.; Diken, E. G.; Johnson, M. A.; Walters, R. S.; Jaeger, T. D.; Duncan, M. A.; Christie, R. A.; Jordan, K. D. *Science* **2004**, 304, 1137-1140.

(20) Bush, M. F.; Saykally, R. J.; Williams, E. R. *ChemPhysChem* **2007**, 8, 2245-2253.

(21) Walters, R. S.; Pillai, E. D.; Duncan, M. A. *J. Am. Chem. Soc.* **2005**, 127, 16599-16610.

(22) Kamariotis, A.; Boyarkin, O. V.; Mercier, S. R.; Beck, R. D.; Bush, M. F.; Williams, E. R.; Rizzo, T. R. *J. Am. Chem. Soc.* **2006**, 128, 905-916.

(23) Weinheimer, C. J.; Lisy, J. M. *J. Chem. Phys.* **1996**, 105, 2938-2941.

(24) Rodriguez-Cruz, S. E.; Jockusch, R. A.; Williams, E. R. *J. Am. Chem. Soc.* **1998**, 120, 5842-5843.

(25) Rodriguez-Cruz, S. E.; Jockusch, R. A.; Williams, E. R. *J. Am. Chem. Soc.* **1999**, 121, 8898-8906.

(26) Rodriguez-Cruz, S. E.; Jockusch, R. A.; Williams, E. R. *J. Am. Chem. Soc.* **1999**, 121, 1986-1987.

(27) Wong, R. L.; Paech, K.; Williams, E. R. *Int. J. Mass Spectrom.* **2004**, 232, 59-66.

(28) Blades, A. T.; Jayaweera, P.; Ikonomou, M. G.; Kebarle, P. *Int. J. Mass Spectrom. Ion Processes* **1990**, 102, 251-267.

(29) Carl, D. R.; Moision, R. M.; Armentrout, P. B. *Int. J. Mass Spectrom.* **2007**, 265, 308-325.

(30) Shvartsburg, A. A.; Siu, K. W. M. *J. Am. Chem. Soc.* **2001**, 123, 10071-10075.

(31) Stace, A. J. *Phys. Chem. Chem. Phys.* **2001**, 3, 1935-1941.

(32) Stace, A. J. *J. Phys. Chem. A* **2002**, 106, 7993-8005.

(33) Duncombe, B. J.; Duale, K.; Buchanan-Smith, A.; Stace, A. J. *J. Phys. Chem. A* **2007**, 111, 5158-5165.

(34) Pankewitz, T.; Lagutschenkov, A.; Niedner-Schatteburg, G.; Xantheas, S. S.; Lee, Y. T. *J. Chem. Phys.* **2007**, 126, 074307.

(35) Beyer, M. K. *Mass Spectrom. Rev.* **2007**, 26, 517-541.

(36) Faherty, K. P.; Thompson, C. J.; Aguirre, F.; Michne, J.; Metz, R. B. *J. Phys. Chem. A* **2001**, 105, 10054-10059.

(37) Thompson, C. J.; Husband, J.; Aguirre, F.; Metz, R. B. *J. Phys. Chem. A* **2000**, 104, 8155-8159.

(38) Beyer, M. K.; Metz, R. B. *J. Phys. Chem. A* **2003**, 107, 1760-1762.

(39) Cox, H.; Stace, A. J. *J. Am. Chem. Soc.* **2004**, 126, 3939-3947.

(40) Bush, M. F.; Saykally, R. J.; Williams, E. R. *Int. J. Mass Spectrom.* **2006**, 253, 256-262.

(41) Cheng, Z. L.; Siu, K. W. M.; Guevremont, R.; Berman, S. S. *J. Am. Soc. Mass Spectrom.* **1992**, 3, 281-288.

(42) Stace, A. J.; Walker, N. R.; Firth, S. *J. Am. Chem. Soc.* **1997**, 119, 10239-10240.

(43) Beyer, M.; Williams, E. R.; Bondybey, V. E. *J. Am. Chem. Soc.* **1999**, 121, 1565-1573.

(44) Stone, J. A.; Vukomanovic, D. *Int. J. Mass Spectrom.* **1999**, 187, 227-229.

(45) Bérces, A.; Nukada, T.; Margl, P.; Ziegler, T. *J. Phys. Chem. A* **1999**, 103, 9693-9701.

(46) Bush, M. F.; Saykally, R. J.; Williams, E. R. *J. Am. Chem. Soc.* **2007**, 129, 2220-2221.

(47) Fridgen, T. D.; McMahon, T. B.; MacAleese, L.; Lemaire, J.; Maitre, P. *J. Phys. Chem. A* **2004**, 108, 9008-9010.

(48) Iino, T.; Ohashi, K.; Inoue, K.; Judai, K.; Nishi, N.; Sekiya, H. *J. Chem. Phys.* **2007**, 126, 194302.

(49) Zhou, J.; Santambrogio, G.; Brümmer, M.; Moore, D. T.; Wöste, L.; Meijer, G.; Neumark, D. M.; Asmis, K. R. *J. Chem. Phys.* **2006**, 125, 111102.

(50) Bush, M. F.; O'Brien, J. T.; Prell, J. S.; Saykally, R. J.; Williams, E. R. *J. Am. Chem. Soc.* **2007**, 129, 1612-1622.

(51) Senko, M. W.; Canterbury, J. D.; Guan, S. H.; Marshall, A. G. *Rapid Commun. Mass Spectrom.* **1996**, 10, 1839-1844.

(52) Wong, R. L.; Williams, E. R. *J. Phys. Chem. A* **2003**, 107, 10976-10983.

(53) Price, W. D.; Schnier, P. D.; Jockusch, R. A.; Strittmatter, E. F.; Williams, E. R. *J. Am. Chem. Soc.* **1996**, 118, 10640-10644.

(54) Price, W. D.; Williams, E. R. *J. Phys. Chem. A* **1997**, 101, 8844-8852.

(55) Dunbar, R. C.; McMahon, T. B. *Science* **1998**, 279, 194-197.

(56) Herzberg, G. *Molecular Spectra and Molecular Structure II. Infrared and Raman Spectra of Polyatomic Molecules*; Van Nostrand: New York, 1945.

(57) Shannon, R. D.; Prewitt, C. T. *Acta Crystallogr., Sect. B: Struct. Sci.* **1969**, 25, 925-946.

(58) Pimentel, G. C.; McClellan, A. L. *The Hydrogen Bond*; Freeman: San Francisco, CA, 1960.

6.6 Tables and Figures

	k_{max} (s^{-1})	k_{3450} (s^{-1})	k_{BIRD} (s^{-1})	BIRD corrected k_{max}/ k_{3450}
$Cu^{2+}(H_2O)_6$	0.22 $\pm$ 0.01	8.1 x 10^{-3} $\pm$ 4 x 10^{-4}	4.6 x 10^{-3} $\pm$ 2 x 10^{-4}	61
$Ca^{2+}(H_2O)_6$ (296 K)	0.15 $\pm$ 0.008	1.6 x10^{-4} $\pm$ 8 x 10^{-6}	4.0 x 10^{-5} $\pm$ 5 x 10^{-6}	954
$Ca^{2+}(H_2O)_6$ (335 K)	0.26 $\pm$ 0.004	3.8 x10^{-3} $\pm$ 1 x 10^{-4}	3.2 x10^{-3} $\pm$ 1 x 10^{-4}	433

Table 6.1: Dissociation rate constants (s^{-1}) for $Cu^{2+}(H_2O)_6$ and $Ca^{2+}(H_2O)_6$ at a copper jacket temperatures of 215 K for $Cu^{2+}(H_2O)_6$ and both 296 and 335 K for $Ca^{2+}(H_2O)_6$, obtained from the slopes of the Figure 7 data; the laser frequency of k_{max} is 3655 cm^{-1} and 3610 cm^{-1} for $Cu^{2+}(H_2O)_6$ and $Ca^{2+}(H_2O)_6$ respectively.

	B3LYP		BP86	
	LACV3P**++		LACV3P**++	Slater
Structure	relative Gibbs free energies	relative electronic energies	relative electronic energies	previous work[a]
6AI	0	1	0	0
6AII	3	0	3	13
6B	9	13	22	29
6C	22	37	61	71
7A	0	0		
7B	11	15		
7C	38	46		
8A	0	0		
8B	21	21		
8C	40	53		
10A	0	0		
10B	10	5		
10C	32	31		

Table 6.2: Relative Gibbs free energies (kJ/mol) at 215 K and relative electronic energies for select structures of $Cu^{2+}(H_2O)_n$, n = 6–8 and 10, from B3LYP/LACV3P**++ calculations and relative electronic energies from BP86 calculations.

[a] From reference 45

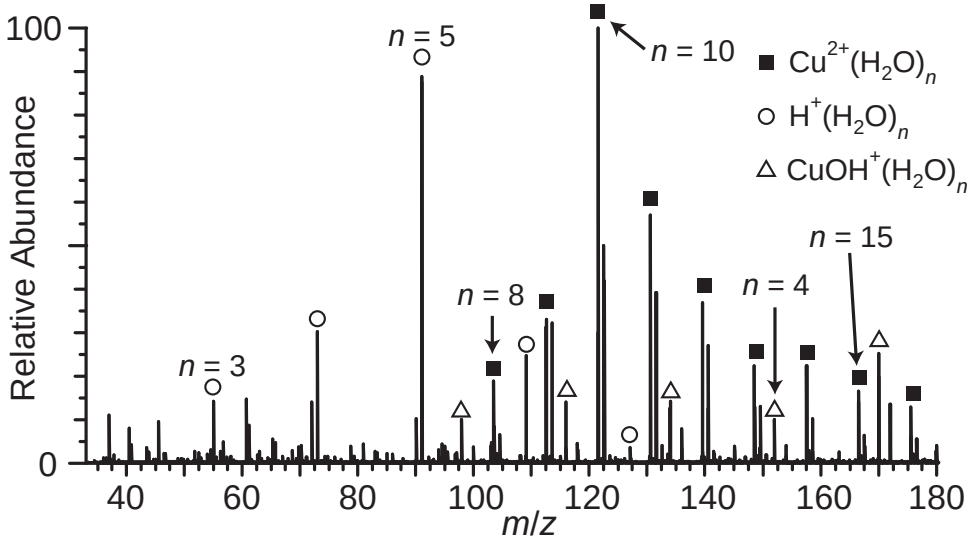

Figure 6.1: Representative electrospray ionization mass spectrum of a 4 mM aqueous $CuSO_4$ solution with the copper jacket that surrounds the ion cell at 215 K. Distributions of $Cu^{2+}(H_2O)_n$, $CuOH^+(H_2O)_n$ and $H_3O^+(H_2O)_n$ are indicated on the spectrum.

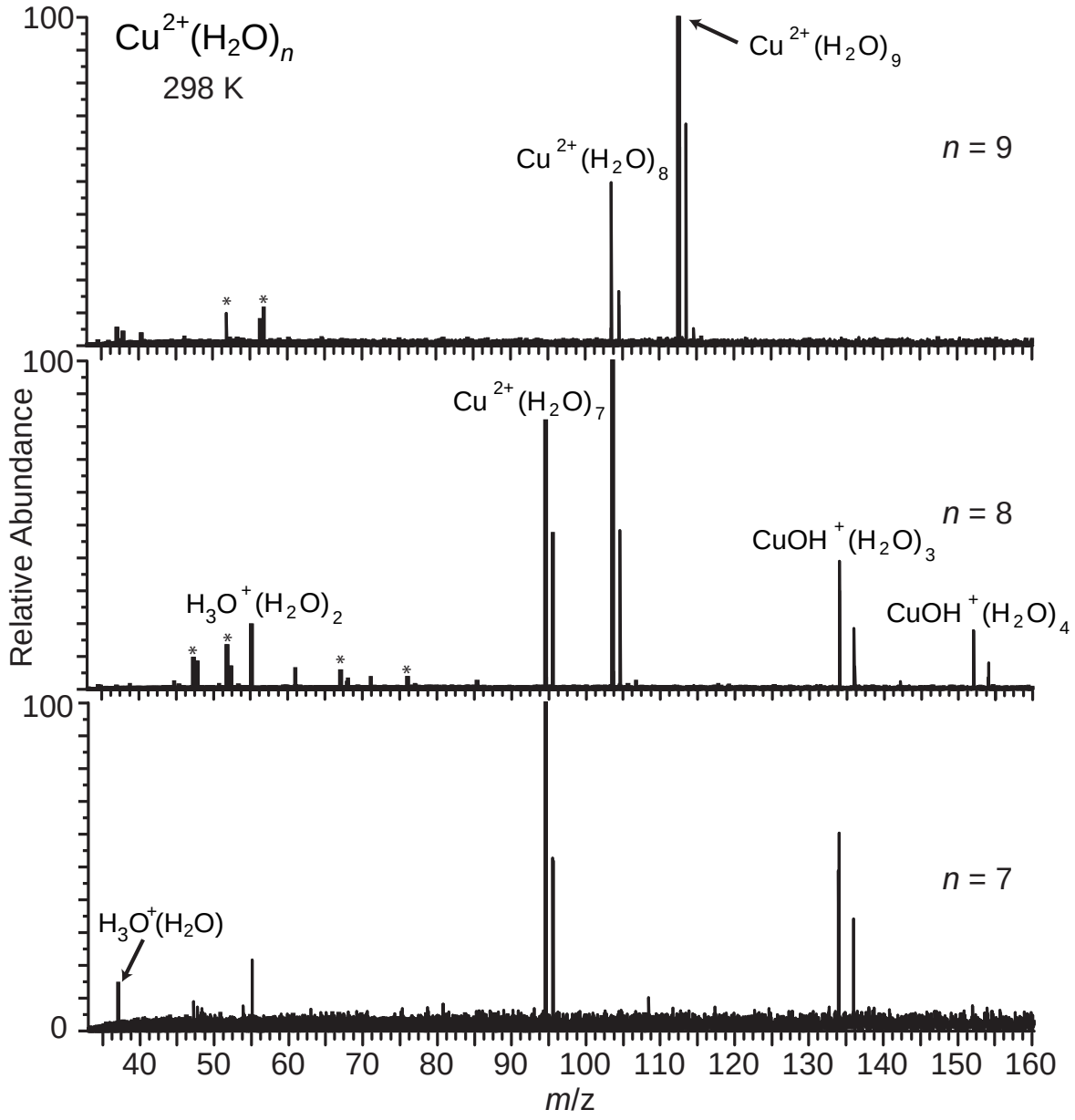

Figure 6.2: BIRD spectra of isolated $Cu^{2+}(H_2O)_n$, $n = 7$–9, measured with a copper jacket temperature of 298 K and 20, 25 and 0.5 s reaction times, respectively for $n = 7$, 8 and 9 respectively. Harmonics of the fundamental frequencies of trapped ions are marked with a "*".

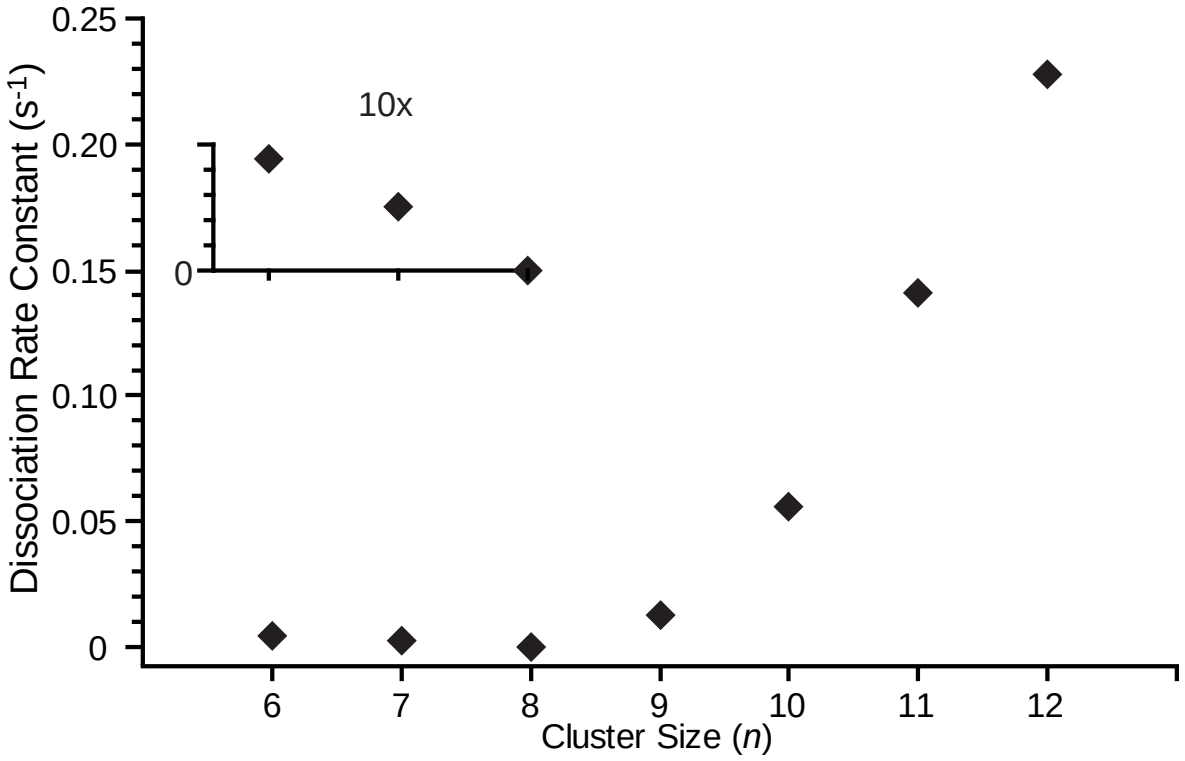

Figure 6.3: BIRD rate constants of $Cu^{2+}(H_2O)_n$, $n = 6$ –12, with a copper jacket temperature of 215 K.

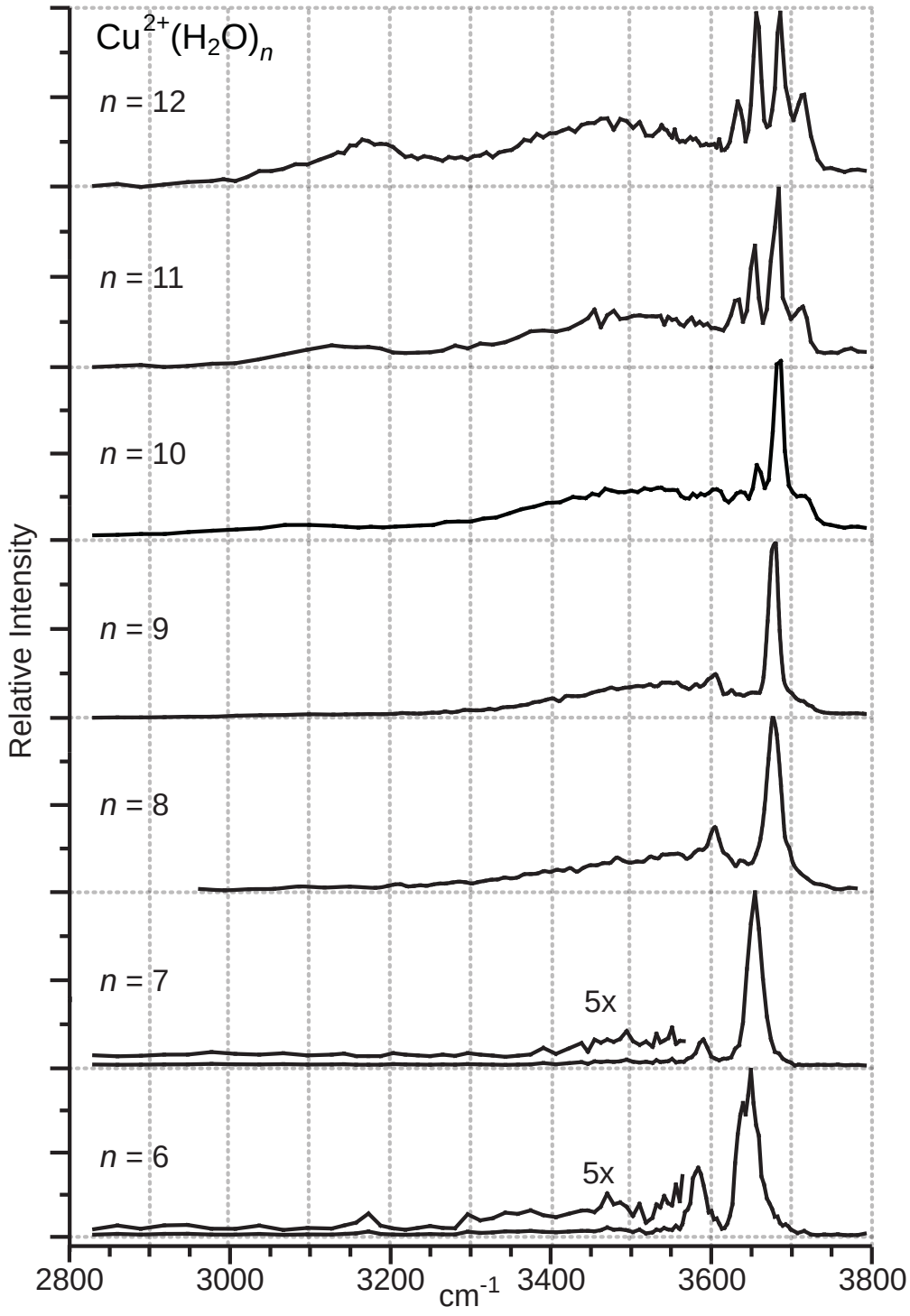

Figure 6.4: Infrared action spectra of $Cu^{2+}(H_2O)_n$, $n = 6$–12, obtained with a copper jacket temperature of 215 K. The cluster size (n) is indicated for each spectrum.

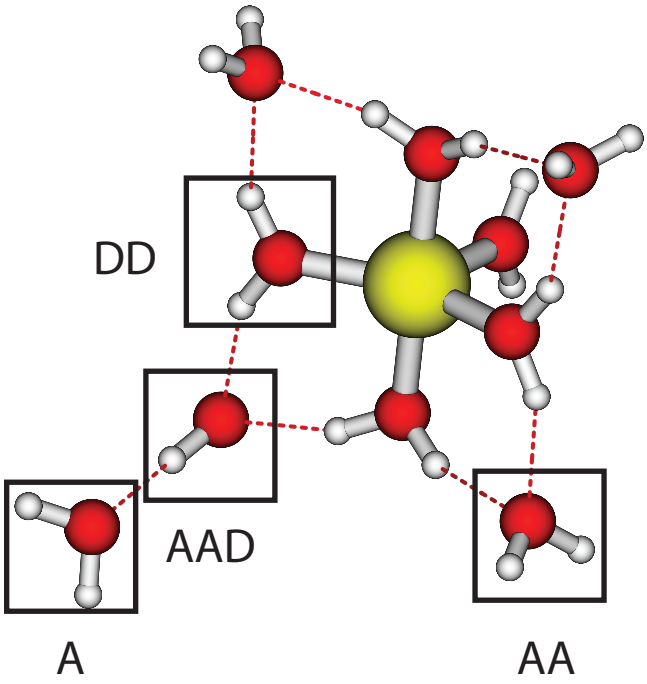

Figure 6.5: Hydrogen bonding motifs; A = single acceptor, AA = double acceptor, DD = double donor, AAD = acceptor acceptor donor

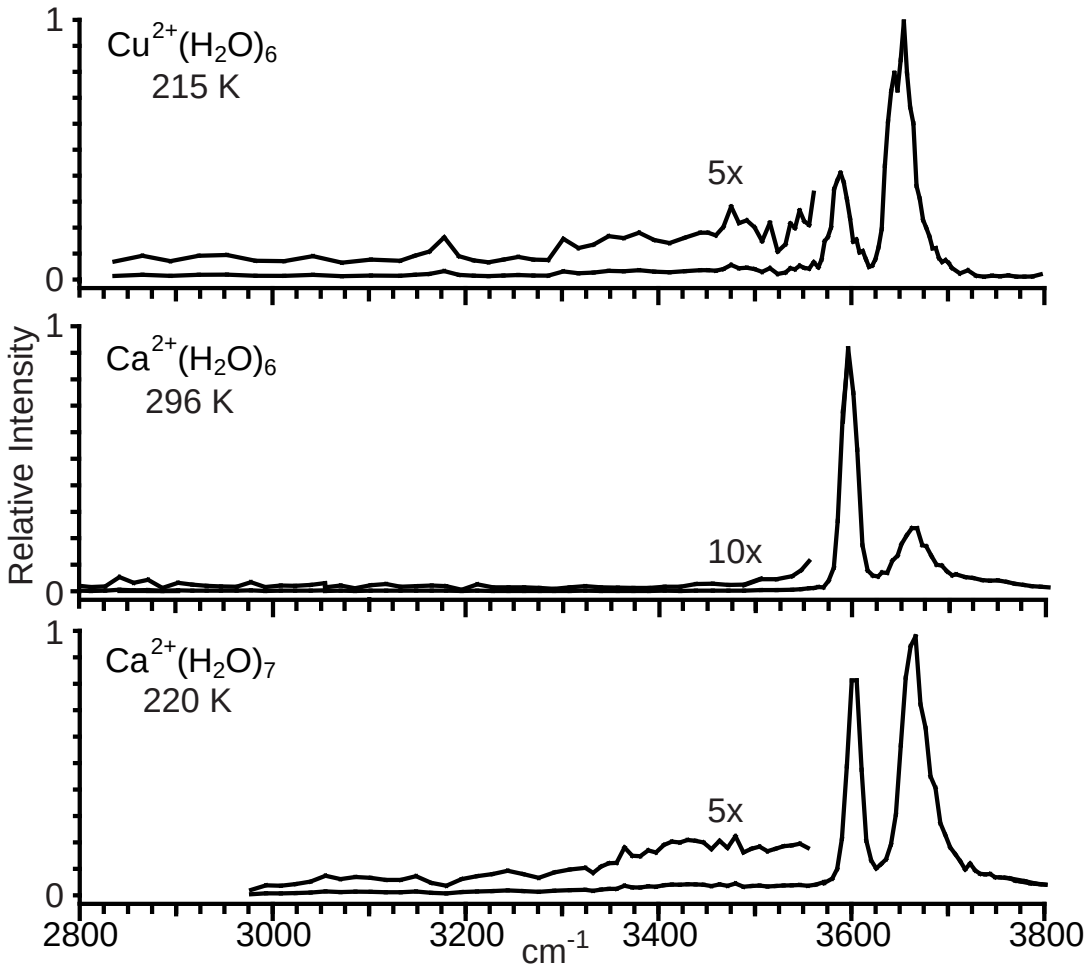

Figure 6.6: Infrared action spectra of $Cu^{2+}(H_2O)_6$, $Ca^{2+}(H_2O)_6$, and $Ca^{2+}(H_2O)_7$ measured at the indicated temperature. The hydrated divalent calcium spectra are replotted from reference 20.

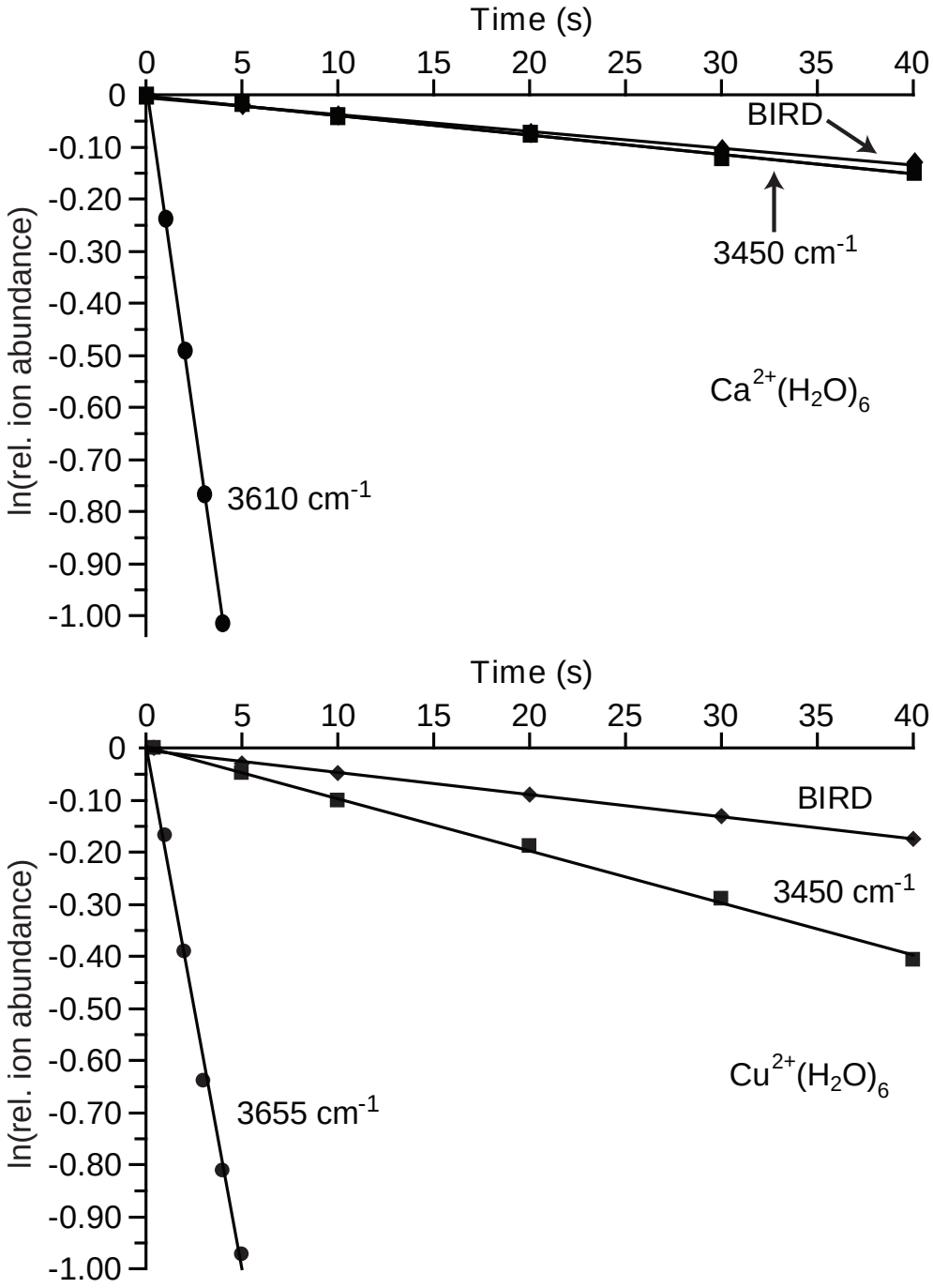

Figure 6.7: BIRD and laser photodissociation data at the frequencies indicated in the plots for $Cu^{2+}(H_2O)_6$ and $Ca^{2+}(H_2O)_6$ with a copper jacket temperature of 215 K and 335 K respectively.

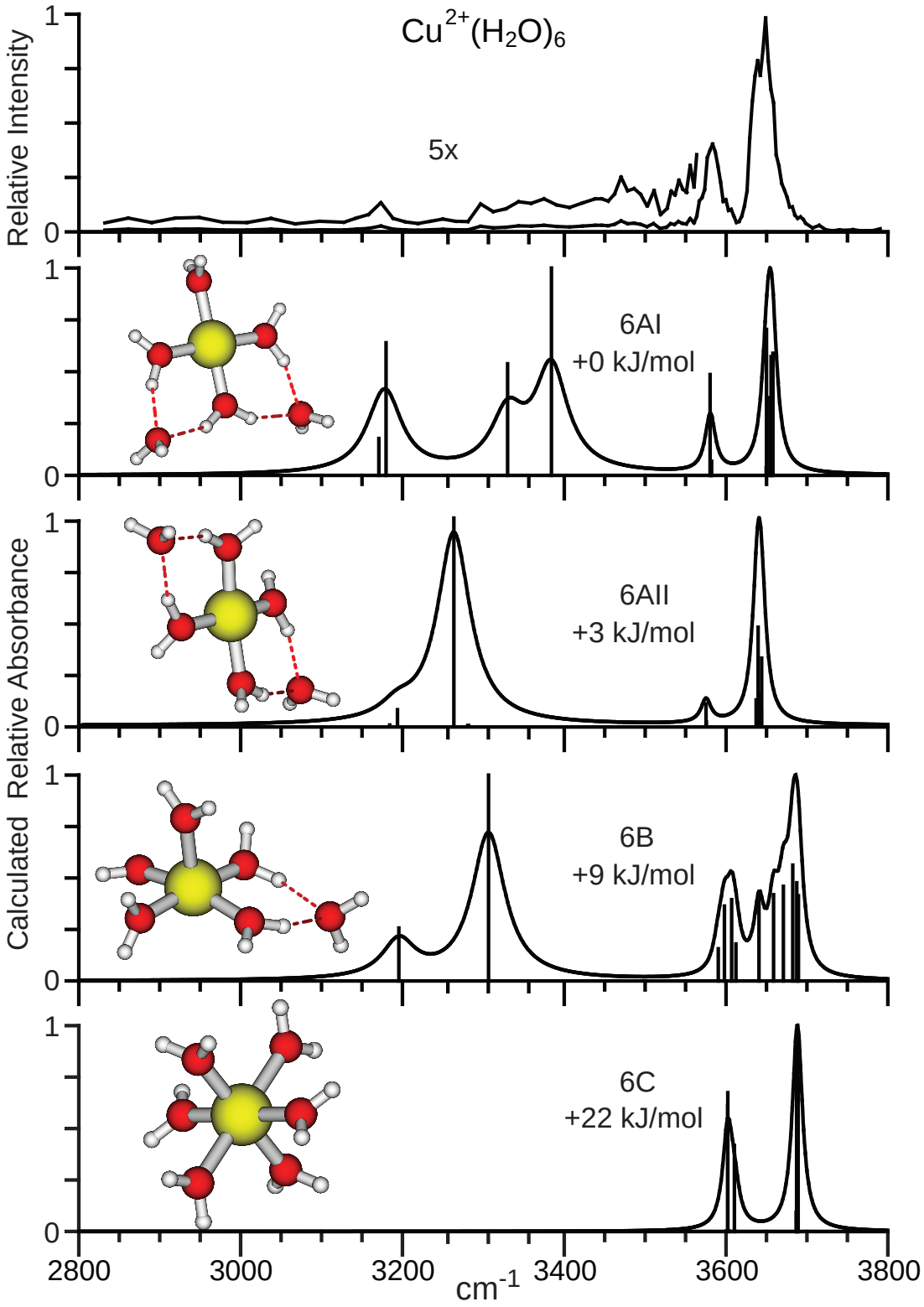

Figure 6.8: Infrared action spectrum of $Cu^{2+}(H_2O)_6$ obtained with a copper jacket temperature of 215 K and the spectra for four low-energy conformers (6AI – 6C) from B3LYP/LACV3P**++ calculations.

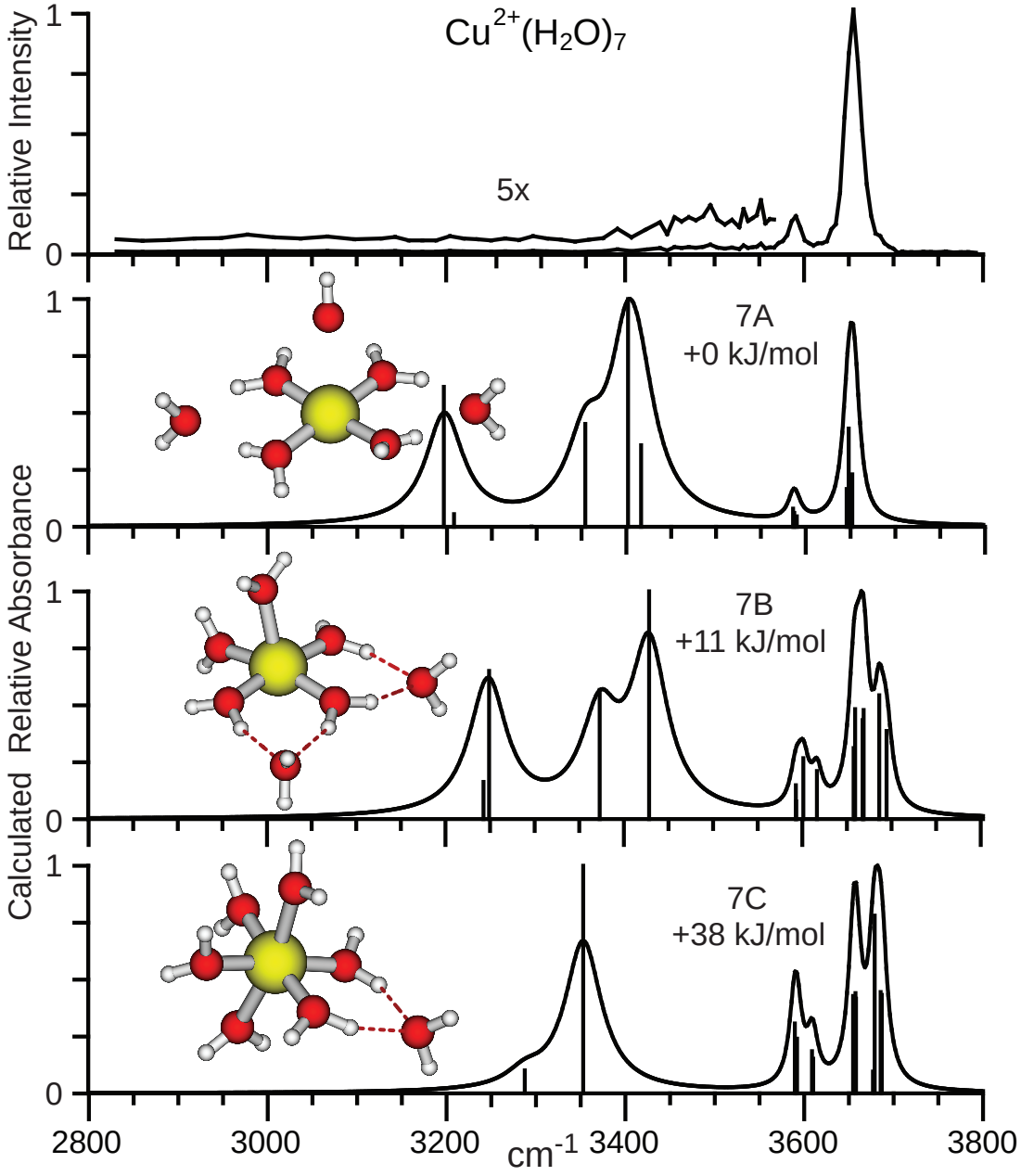

Figure 6.9: Infrared action spectrum of $Cu^{2+}(H_2O)_7$ obtained with a copper jacket temperature of 215 K and the spectra for three low-energy conformers (7A – 7C) from B3LYP/LACV3P**++ calculations.

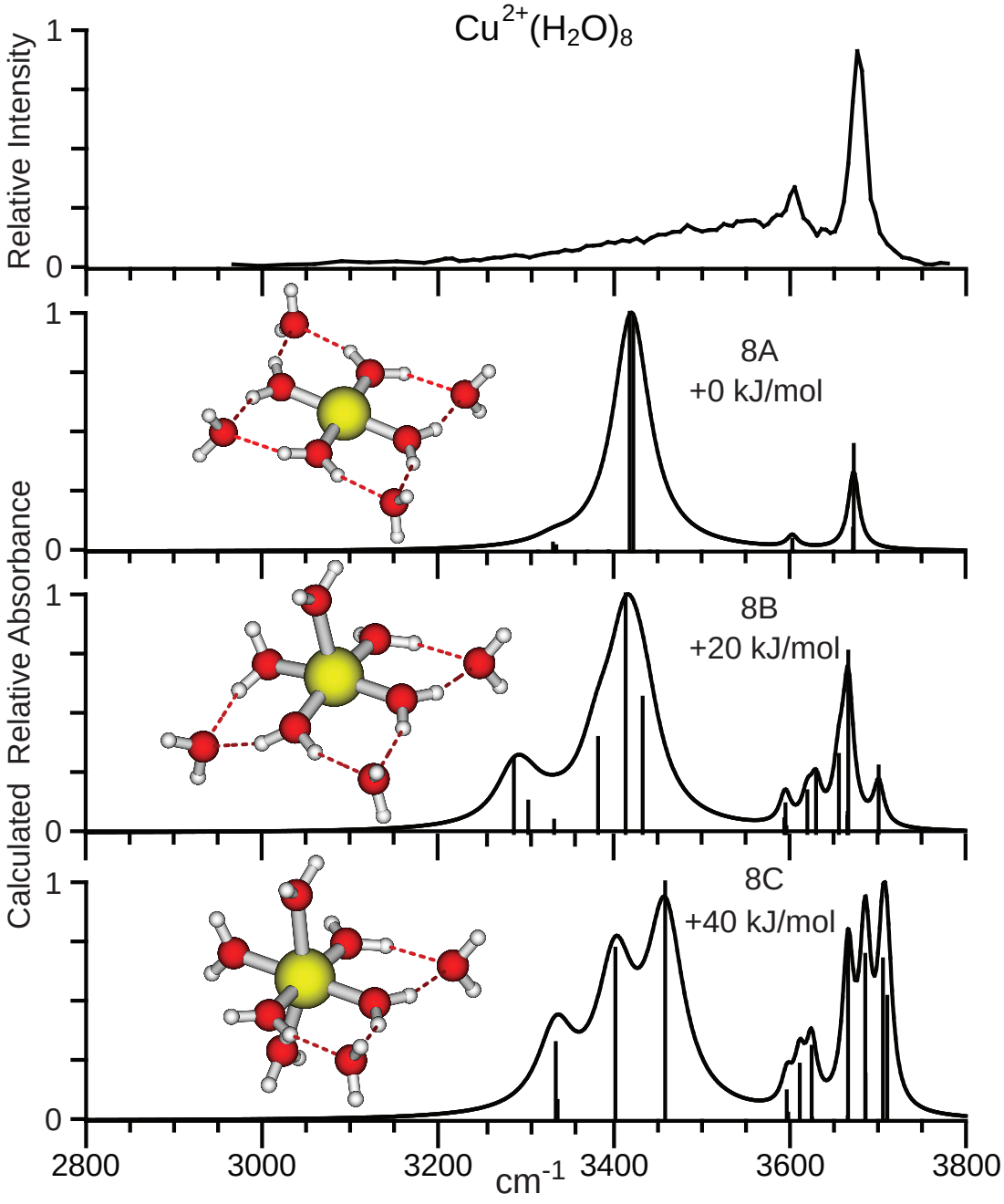

Figure 6.10: Infrared action spectrum of $Cu^{2+}(H_2O)_8$ obtained with a copper jacket temperature of 215 K and the spectra for three low-energy conformers (8A – 8C) from B3LYP/LACV3P**++ calculations.

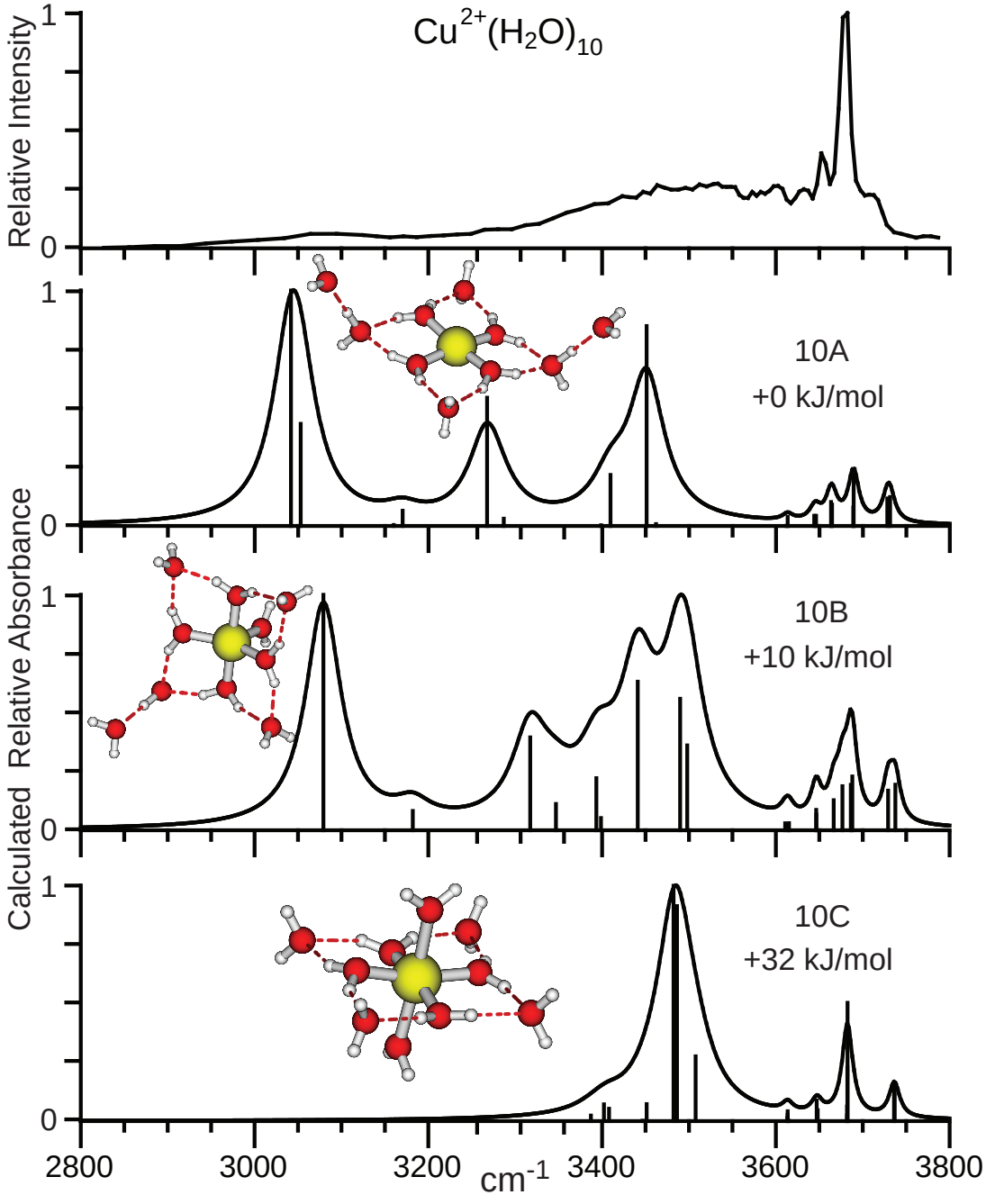

Figure 6.11: Infrared action spectrum of $Cu^{2+}(H_2O)_{10}$ obtained with a copper jacket temperature of 215 K and the spectra for three low-energy conformers (10A – 10C) from B3LYP/LACV3P**++ calculations.

Chapter 7

Coordination Numbers of Hydrated Divalent Transition Metal Ions Investigated with IRPD Spectroscopy

This chapter is reproduced with permission from the American Chemical Society.

Jeremy T. O'Brien, and Evan R. Williams

Journal of Physical Chemistry A, 2011, 112, 14612–14619

7.1 Introduction

Transition metal ions are necessary for many biological processes, including oxygen transport,[1] DNA transcription,[2–4] and the activation/function of proteins and enzymes.[3,5-8] Mn, Fe, Co, Cu, and Zn are essential for both plant and animal life, but concentrations of these metals *in vivo* must be tightly regulated due to their toxicity at elevated levels.[9,10] Ni also has important biological roles complexing with enzymes in microorganisms and plants.[11,12] These metals are used heavily in industry, and toxic levels of metal ions, such as Zn^{2+}, can accumulate quickly in the environment. In addition to industrial sources, automobiles can produce transition metal pollution as indicated by isotopic analysis of zinc pollution in urban aerosols, which identified traffic as the primary source.[13] Transition metals also have significant pharmaceutical applications in metallo-protein complexes, such as zinc finger arrays.[5,14,15] Detailed understanding of the hydration structure and aqueous reactivity of transition metal ions can provide insight into the roles and transport of these metals in biological systems and can enable a more sophisticated design of metallo-protein complexes.

The coordination of water to transition metal ions in solution has been investigated using many techniques including; X-ray absorption/diffraction,[16–22] neutron scattering,[21,23,24] NMR,[21,25,26] IR and Raman spectroscopy,[21,27–29] and computational chemistry.[21,22,30,31] On the basis of these studies, the dominant hydration structure assigned is regular octahedral with an average coordination number (CN) = ∼6 for all divalent transition metal ions except Cu and Cr. Aqueous Cu^{2+} and Cr^{2+} are typically assigned to octahedral hydration structures distorted by Jahn-Teller effects due to their d^9 and d^4 electronic structure, respectively. These solution-phase techniques typically require ion concentrations >1 M, well above biological levels, and the presence of counterions can complicate interpretation of these data.

Gas-phase studies of hydrated ion clusters have the advantage that effects of counterions can be eliminated and ion hydration can be investigated at low effective concentration. Structures and reactivities can be measured as a function of cluster size and ion identity to reveal detailed differences in solvation shells or the presence of uniquely stable structures, such as clathrates.[32,33] Activation of hydrated divalent metal ions generally results in sequential loss of water molecules for large clusters, but a charge-separation reaction can occur for small clusters resulting in the formation of a singly charged hydrated metal hydroxide and the corresponding protonated water cluster. The cluster size at which charge separation is energetically favored over water loss varies significantly depending on ion identity and activation conditions.[34,35] A salt-bridge mechanism in which proton transfer occurs between

the first solvation shell and a water molecule in the second shell has been proposed for the charge separation reaction,[36] and both experimental and computational results supporting this mechanism have been reported.[35–41]

The hydration of divalent metal ions has been investigated using many gas-phase techniques including; blackbody infrared radiative dissociation (BIRD),[42–45] collision induced dissociation,[34,46,47] high pressure mass spectrometry,[48,49] and also guided ion beam mass spectrometry.[50–53] These studies provide thermodynamic values, such as the sequential hydration enthalpies ($\Delta H°_{n-1,n}$) and entropies ($\Delta S°_{n-1,n}$), from which structural information, such as the formation of a second solvent shell, can be inferred. However, these measurements are indirect probes of structure and do not typically indicate the presence of multiple structures with different CN.

IRPD spectroscopy is a more direct probe of hydrated ion structure and can provide detailed insight into the structures and average CNs of hydrated transition metal ions. The frequencies of OH stretching modes can shift significantly with changes in their hydrogen-bonding environment making this technique especially well-suited for the structural investigation of hydrated ions. IRPD spectra have been reported for many singly-,[54–63] doubly-,[60–68] and triply-charged[62,69,70] hydrated metal ions, including the divalent transition metal ions Cu^{2+} and Zn^{2+}. The IRPD spectra for $Cu^{2+}(H_2O)_{6-12}$ support a CN = 4 for $n = 6$ – 8 and indicate the presence of water molecules in a third solvation shell for $n \geq 10$.[67] The spectra for $Zn^{2+}(H_2O)_{6-12}$ indicate a primary CN = 5 for these clusters with contributions from structures with CN = 6.[68]

Here we investigate the structures of $M^{2+}(H_2O)_{5-8}$, M = Mn, Fe, Co, and Ni using IRPD spectroscopy, BIRD, and comparisons to the previously reported results for hydrated Cu^{2+} and Zn^{2+} clusters. BIRD and laser-induced photodissociation rate constants are obtained using multiple irradiation times to provide more precise comparisons of the average structures and CNs of these hydrated ions.

7.2 Experimental

All experiments were performed on a home-built 2.75 T Fourier-transform ion cyclotron resonance mass spectrometer coupled with a tunable OPO/OPA laser system. The instrument and experimental set-up are described in detail elsewhere.[71] Briefly, hydrated metal ion clusters are generated by nanoelectrospray ionization of 2 – 6 mM aqueous solutions of transition metal salts using borosilicate capillaries pulled to an inner tip diameter of $\sim$1 μm. A platinum wire is inserted into the capillary so that it is in contact with the solution, and a voltage of $\sim$ +600 V relative to the entrance of the mass spectrometer is applied to the wire. The resulting nanospray generated ions are guided through five stages of differential pumping to an ion cell surrounded by a temperature controlled copper jacket. The copper jacket is cooled using a regulated flow of liquid nitrogen or heated using a resistively heated blanket surrounding the vacuum chamber. The temperature of the copper jacket is equilibrated for at least 8 hrs prior to each experiment. Ions are accumulated for 3 - 6 s and are trapped and thermalized with the aid of a pulse of dry nitrogen gas ($\sim 10^{-6}$ Torr). After a 6 - 12 s delay, pressure in the ion cell returns to $<10^{-8}$ Torr, and the ion of interest is

isolated using a stored inverse Fourier transform waveform. Photodissociation is achieved by irradiating the isolated precursor ions with tunable light from an OPO/OPA laser system (LaserVision, Bellevue, WA, U.S.A.) pumped by a 1064 cm^{-1} Nd:YAG laser (Continuum Surelite I-10, Santa Clara, CA, U.S.A.) at a 10 Hz repetition rate for 2 – 30 s.

IRPD spectra are obtained from the photodissociation rate constants $k_{\mathrm{D}}(\hbar\omega,\, t_{irr})$ where $\hbar\omega$ is the photon energy, and t_{irr} is the irradiation time.

$$k_D\left(\hbar\omega\right) = ln\left\{\frac{A_{prec}\left(\hbar\omega, t_{irr}\right)}{A_{prec}\left(\hbar\omega, t_{irr}\right) + \sum A_{prod}\left(\hbar\omega, t_{irr}\right)}\right\}/t_{irr}$$

A_{prec} and A_{prod} are the relative ion abundances of the precursor and fragmentation product ions, respectively. Fragmentation due to blackbody infrared radiative dissociation (BIRD) is measured in the absence of laser irradiation, and the BIRD dissociation rate constant is subtracted from $k_{\mathrm{D}}(\hbar\omega,\, t_{irr})$ to obtain laser-induced photodissociation rate constants, which are plotted versus photon energy to obtain the IRPD spectrum of the isolated precursor ion. All IRPD spectra are corrected for frequency-dependent variations in laser power.

7.3 Results

7.3.1 Ion fragmentation

$M^{2+}(H_2O)_{5-8}$, where M = Mn, Fe, Co, Ni, Cu, and Zn, were fragmented by laser-induced photodissociation (2800 – 3800 cm^{-1}) and by BIRD. Two dissociation pathways are observed; sequential loss of water molecules, which occurs exclusively at larger cluster size, and charge separation to form singly charged metal hydroxide clusters and the corresponding protonated water cluster, which occurs at smaller cluster size. At 215 K, laser-induced photodissociation of $Fe^{2+}(H_2O)_{7-8}$, $Co^{2+}(H_2O)_{7-8}$, and $M^{2+}(H_2O)_{5-8}$, M = Mn and Ni, results solely in sequential loss of water molecules, as does BIRD of clusters with $n = 8$. For Fe^{2+} with 5 and 6 water molecules, ∼80% and 35%, respectively, of the photodissociation products are formed via charge separation. For Co^{2+} with 5 and 6 water molecules, these percentages are ∼90 and 70%, respectively. BIRD of Co^{2+} and Fe^{2+} with 5 water molecules results exclusively in charge separation. No product ions from BIRD of clusters with $n = 6 - 7$ and Mn and Ni clusters with $n = 5$ are formed at 215 K for up to 120 s. In order to more directly compare the laser-induced photodissociation kinetics for each of the hydrated metal ions, the copper jacket temperature was adjusted so that the BIRD rate constant for each $M^{2+}(H_2O)_6$ complex was roughly the same as those reported for $Cu^{2+}(H_2O)_6$ and $Zn^{2+}(H_2O)_6$ at 215 K.[67,68] Laser-induced dissociation of $Mn^{2+}(H_2O)_6$ and $Ni^{2+}(H_2O)_6$ at 305 and 331 K, respectively, results in predominately sequential water loss. Charge separation products formed at these temperatures arise from BIRD. The fragmentation channels for all the hexa-hydrated ions are summarized in Table 1.

7.3.2 Spectroscopy

IRPD spectra of $M^{2+}(H_2O)_{5-7}$ at 215 K, where M = Mn, Fe, Co, Ni, Cu, and Zn in the spectral region of 2800 – 3800 cm^{-1} are shown in Figures 1 – 3 for clusters with 5 – 7 water molecules, respectively. Spectra of $M^{2+}(H_2O)_8$ covering the free-OH spectral region (from 3550 – 3800 cm^{-1}) are shown in Figure 4. Spectra of $Mn^{2+}(H_2O)_6$ and $Ni^{2+}(H_2O)_6$, acquired at 305 and 331 K, respectively, are shown in Figure 5 along with the corresponding 215 K spectra. $Cu^{2+}(H_2O)_5$ and $Zn^{2+}(H_2O)_5$ clusters were not formed in these experiments. The dissociative charge separation reaction becomes dominant for these metal ions with six water molecules attached, resulting in formation of $MOH^+(H_2O)_{n\leq 4}$ instead. The IRPD spectra for Cu^{2+} and Zn^{2+} have been reported previously.[67,68]

Each IRPD spectrum has bands at ∼3600 cm^{-1} and ∼3660 cm^{-1}. The band at ∼3600 cm^{-1} is attributed to the symmetric (ν_{sym}) stretch mode of water molecules that do not donate any H-bonds, i.e., acceptor-only water molecules. The band at ∼3660 cm^{-1} corresponds to the antisymmetric stretch mode of acceptor only water molecules, although the free-OH stretch of water molecules that donate a single hydrogen bond also contributes for clusters with $n \geq 7$ (vide infra). These bands in the IRPD spectra of Ni, Co, Mn, and Fe are similar in frequency, shape, and relative intensity for clusters with $n = 5$ and also with $n = 6$. For $n = 7$, the relative intensity of the ν_{sym} band for Co is significantly lower than for Mn, Fe and Ni. Free-OH stretches of water molecules that donate a single H-bond may also contribute to the band at ∼3660 cm^{-1}. The free-OH bands in these spectra are significantly red-shifted from the ν_{sym} and ν_{asym} of an isolated water molecule which occur at 3657 and 3756 cm^{-1}, respectively. Two effects contribute to this redshift: partial electron transfer from the water molecules to the metal ion which, for smaller hydrates, leads to weaker O-H bonding and lower frequency vibrations, and the effect of the ion's electric field on the stretching frequencies of the water molecules, i.e., a vibrational Stark shift. These bands blueshift by ∼20 – 25 cm^{-1} with increasing cluster size from $n = 5$ to $n = 8$.

The IRPD spectra of clusters with $n = 7$ each have a broad (∼150 cm^{-1} fwhm), weak band that occurs in the H-bonding region (2800 – 3500 cm^{-1}) centered near 3400 cm^{-1} for all metal ions except Cu^{2+} where it is broader and slightly blue shifted with no distinct maximum. No bands in this spectral region are apparent in the spectra of clusters with $n < 7$, although laser-induced photodissociation does occur to some extent for some of these clusters in this spectral region (vide infra). These H-bonded bands are assigned to inner-shell water molecules that donate one or two H-bonds to double acceptor, second shell water molecules. This assignment is based on broad, weak bands observed in this spectral region for other hydrated metal ions.[64–68] These bands indicate that water molecules populate a second solvation shell in some of the ions at this cluster size.

To investigate effects of temperature, spectra of $Mn^{2+}(H_2O)_6$ and $Ni^{2+}(H_2O)_6$ were measured at 305 and 331 K, respectively, and these spectra, normalized to the free-OH ν_{sym} bands, are compared to the low temperature (215 K) spectra in Figure 5. These temperatures were selected so that the BIRD rate constants for each cluster are comparable to those reported previously for Cu^{2+} and Zn^{2+} at 215 K.[67,68] At higher temperature, both free-OH bands are broader, but the free-OH ν_{asym} band broadens more resulting in a higher relative integrated intensity. A similar temperature broadening was observed for $Mg^{2+}(H_2O)_6$.[64] For

$Mn^{2+}(H_2O)_6$, the free-OH ν_{asym} band has broad shoulders on each side, consistent with the superposition of two ν_{asym} bands of different width. In addition, a peak in the H-bonding region at ∼3400 cm^{-1} is apparent in the higher temperature spectrum of $Mn^{2+}(H_2O)_6$ but not for Ni^{2+}.

7.3.3 Photodissociation Kinetics

Photodissociation data measured at a single laser frequency over a range of irradiation times provide more accurate dissociation rate constants than data acquired at a single laser irradiation time as was used to measure the IRPD spectra. These kinetics data can be used to determine the extent to which laser-induced dissociation occurs even when a distinct band may not appear in the IRPD spectrum. For example, no H-bonding bands are apparent in the IRPD spectra for $M^{2+}(H_2O)_6$. However, bands due to H-bonded stretches are broad and can be weak for hydrated clusters in the size range where population of a second solvation shell starts to occur. This can be attributed to the lower energy of photons in this region and small populations of clusters with second shell structures. To determine the extent to which any H-bonds may occur in these clusters, dissociation rate constants are obtained at the laser frequency where maximum photodissociation occurs in the IRPD spectrum for each cluster (k_{max}) and in the H-bonded region (k_{HB}). The frequency used to obtain k_{HB} is determined by the center of the band observed in the H-bonding region for larger hydrates (∼3400 cm^{-1} for Mn, Fe, Co, Ni and Zn, ∼3450 cm^{-1} for Cu and Ca). The laser-induced photodissociation rate constants are obtained by subtracting the BIRD rate constant (k_{BIRD}) from k_{max} and k_{HB}.

For $M^{2+}(H_2O)_6$, M = Mn, Fe, Co and Ni at 215 K, BIRD and laser irradiation at 3400 cm^{-1} results in no product ions for irradiation times up to 120 s. The barriers to dissociation at 215 K are sufficiently high and the internal energy of these small clusters sufficiently low that weak absorption in the H-bonding region may not result in measurable dissociation on the time scale of these experiments owing to the necessity to absorb multiple photons and competitive effects of radiative emission. In order to increase the initial internal energy of the clusters so that laser photon absorption results in measurable dissociation for these clusters within 120 s, the temperature of the copper jacket surrounding the ion cell was increased so that the BIRD rate constant for each complex at the elevated temperature is roughly equivalent to those reported previously for $Cu^{2+}(H_2O)_6$ and $Zn^{2+}(H_2O)_6$ at 215 K.[67,68]

The ratio of product ion abundances resulting from charge separation/water loss (I_{CS}/I_{WL}) for BIRD of the $M^{2+}(H_2O)_6$ clusters and the temperature at which the BIRD rate constants are similar to those of Cu^{2+} and Zn^{2+} at 215 K vary for the different metal ions (Table 1). The temperature required for both $Fe^{2+}(H_2O)_6$ and $Co^{2+}(H_2O)_6$ (263 K) is much lower than for the Mn^{2+} and Ni^{2+} complexes (305 and 331 K, respectively) indicating relatively lower barriers to dissociation for Fe^{2+} and Co^{2+}. BIRD of the Mn^{2+} cluster at 305 K results in mostly loss of water (∼40% charge separation) whereas mostly charge separation (∼90%) occurs for the Ni^{2+} cluster at 331 K. BIRD of the Fe^{2+} and Co^{2+} clusters at 263 K results exclusively in charge separation. The ordering of these metals from highest to lowest percent products from charge separation for BIRD of the $M^{2+}(H_2O)_6$ cluster is Fe, Co > Ni > Mn

(Table 1). $Zn^{2+}(H_2O)_6$ and $Cu^{2+}(H_2O)_6$ dissociate only by charge separation and similar BIRD rates are observed at substantially lower temperature than the other metal ion clusters (215 K).

From these dissociation data, k_{BIRD}, k_{max} at ∼3600 cm^{-1} and k_{HB} at 3400 cm^{-1} are obtained from linear fits to dissociation data measured for irradiation times up to 120 s (Table 2). The error reported is one standard deviation in the slope of the linear fit. These kinetic data for $Mn^{2+}(H_2O)_6$ and $Ni^{2+}(H_2O)_6$ at 305 and 331 K, respectively, are shown in Figure 6. Significant dissociation attributable to irradiation at 3400 cm^{-1} occurs for $Mn^{2+}(H_2O)_6$ whereas no dissociation above BIRD occurs for $Ni^{2+}(H_2O)_6$ at this photon energy. The relative extent of fragmentation in the H-bonding region for each metal ion is obtained from the ratio of the laser-induced photodissociation rate constants at the two laser frequencies (Table 2). For Ni^{2+}, k_{BIRD} and k_{HB} are the same within error and the laser-induced photodissociation in the H-bonding region is more than 3000x smaller than that measured at ∼3600 cm^{-1} (Figure 6). For Fe^{2+}, Co^{2+} and Ca^{2+}, k_{HB} is greater than k_{BIRD}, but photodissociation in the H-bonding region is ∼400 times smaller than at k_{max}. For Mn^{2+}, Cu^{2+}, and Zn^{2+}, relative photodissociation in the H-bonding region is 8 - 10 times greater than that observed for Fe^{2+}, Co^{2+} and Ca^{2+}.

7.4 Discussion

7.4.1 Relative Integrated Intensities of Free OH-Stretches

The relative intensities of the free-OH ν_{sym} and ν_{asym} bands change with cluster size and can provide information about hydration structure. For $M^{2+}(H_2O)_5$, where M = Mn, Fe, Co, and Ni, the ν_{asym} band at ∼3660 cm^{-1} is very weak and broad relative to the ν_{sym} band at ∼3600 cm^{-1} (Figure 1). In contrast, the corresponding bands in the spectra of $M^{2+}(H_2O)_8$ are reversed in intensity; the lower frequency ν_{sym} band is much less intense relative to theν_{asym} band in the spectra of these larger clusters (Figure 4). H-bonding due to second shell water molecules results in depletion of the ν_{sym} band relative to the ν_{asym} band because the free-OH stretches of water molecules that donate a single H-bond occur at nearly the same frequency as ν_{asym} for acceptor only water molecules, however the frequency of the bonded stretch is significantly redshifted thereby removing intensity from the ν_{sym} band. The relative intensities of these bands are therefore related to the structures and extent of H-bonding of the clusters and can indicate the onset of second-shell formation as observed for hydrated metal ion complexes containing Ni^+,[59] Ca^{2+},[65] Zn^{2+},[68] and Cu^{2+}.[67] The relative intensities of the ν_{sym} and ν_{asym} bands for $Cu^{2+}(H_2O)_6$ and $Zn^{2+}(H_2O)_6$ (Figure 2) are much closer to those observed for Mn, Fe, Co, and Ni with $n = 7$ (Figure 3) than for $n = 6$ consistent with lower CNs for Cu and Zn.

To obtain a more quantitative measure of how the intensities of the ν_{sym} andν_{asym} bands change as a function of cluster size and metal ion, the ratio of the integrated areas of these two bands (A_{asym}/A_{sym}) were obtained by fitting the experimental data with Gaussian lineshapes. The ratios A_{asym}/A_{sym} are plotted as a function of cluster size for each of the metal ions at 215 K in Figure 7. The ratio A_{asym}/A_{sym} increases with increasing cluster

size for each metal ion. At each size, the ratios for clusters containing Mn, Fe, Co and Ni are similar suggesting that the average CNs for these ions are comparable. A_{asym}/A_{sym} for $Ni^{2+}(H_2O)_{6-8}$, is consistently the lowest of the metal ion complexes at each cluster size indicating that Ni^{2+} has the highest average CN. For $Cu^{2+}(H_2O)_{6-8}$, A_{asym}/A_{sym} is significantly greater than for any of the other ions consistent with a CN = 4, previously reported for Cu^{2+}. For $n = 6$ and 8, A_{asym}/A_{sym} for Zn^{2+} is below that of Cu^{2+} and significantly above the other metal ions indicating Zn^{2+} has an intermediate CN, consistent with a value of five reported previously. For $n = 7$, the ratio for Zn^{2+} is similar to the other transition metals, perhaps indicating a more significant contribution from structures with higher CN than for the $n = 6$ and 8 complexes. Previous IRPD and computational results indicate these hydrated Zn clusters predominantly have CN = 5, although structures with CN = 6 may contribute as well.[68]

7.4.2 Hydrogen Bonding Region

Photodissociation in the H-bonding region is a somewhat more direct probe of second shell structure than the relative areas of the free-OH bands. The IRPD spectra for $M^{2+}(H_2O)_{5-7}$, M = Mn, Fe, Co and Ni each have a band in this region for clusters with $n = 7$, but not $n = 5$ or 6. However, photodissociation kinetics data indicate that for $n = 6$, all metal ions except Ni^{2+} have some laser-induced dissociation in the H-bonding region (Table 2). The absence of measurable photodissociation in this region for Ni^{2+} indicates a CN = 6. For Fe^{2+}, Co^{2+} and Ca^{2+}, the relative extent of laser-induced photodissociation in the H-bonding region is greater than that for Ni^{2+}, but small compared to that for Cu^{2+} and Zn^{2+}, consistent with a predominant population of structures with a CN = 6 and a small population containing second shell water molecules, i.e., an average CN slightly below six for Fe^{2+}, Co^{2+} and Ca^{2+}.

7.4.3 Temperature Effects

The spectra of $Ni^{2+}(H_2O)_6$ at both low (215 K) and high temperature (331 K) are similar. There is a slight increase in the width of the free-OH bands at higher temperature, consistent with rotational broadening and a slight increase in its relative integrated intensity of the ν_{asym} band compared to the ν_{sym} band (Figure 5). There is no laser-induced photodissociation in the hydrogen bonding region above the background dissociation from BIRD at either temperature (Figures 5, 6 and Table 2). Thus, these results indicate that $Ni^{2+}(H_2O)_6$ has a CN = 6 at both temperatures, with no contributions from structures with lower CN. In contrast, there is a subtle change in the spectra of $Mn^{2+}(H_2O)_6$ with temperature that suggests a slight change in the average CN for this ion. There is measurable photodissociation in the H-bonded region of $Mn^{2+}(H_2O)_6$ at higher temperature (305 K) (Figure 5 and 6) consistent with some population of structures with water molecules in the second solvation shell, i.e., CN < 6. The absence of this band at lower temperature may be due to a reduction of the population that has CN < 6 or it may be due to the inability of photodissociation to effectively compete with radiative emission for this low intensity band (vide infra). However, both the shape and relative integrated intensity of the free-OH ν_{asym} band indicates an increasing population of structures with outer shell water molecules at higher temperature.

To determine how the relative intensities of the free-OH bands change at higher temperature, A_{asym}/A_{sym} for each of the metal ions with 6 water molecules was obtained (Table 3). The relative integrated intensity of the ν_{sym} band for $Mn^{2+}(H_2O)_6$ increases almost the same amount as $Ni^{2+}(H_2O)_6$ at higher temperature (Table 3), but this band is best fit by at least two Gaussian peaks of differing width, which suggests an increased population of structures with CN < 6. The widths of the two Gaussian bands are ∼32 and 77 cm^{-1} indicating contributions from two ion populations with different structures. The width of ∼32 cm^{-1} is similar to that observed in the lower temperature spectra of Mn, Fe, Co and Zn with 6 water molecules whereas a width of ∼77 cm^{-1} is similar to that observed for the same metal ions with 5 water molecules consistent with some population of structures with CN < 6.

7.4.4 Hydrolysis

The charge separation reactions that occur to various extents for the smaller clusters is related to the hydrolysis of these metal ions in solution: $M^{2+}{}_{(aq)} + 2H_2O \rightarrow MOH^+{}_{(aq)} + H_3O^+{}_{(aq)}$. BIRD of $M^{2+}(H_2O)_6$, M = Mn, Fe, Co and Ni, at the elevated temperatures produces primarily charge separation products for all metals except Mn (Table 1). The ordering of these metals from greatest to least percent charge separation products is Cu, Zn, Fe, and Co > Ni > Mn. With laser photodissociation, the extent to which charge separation occurs decreases for all metal ions and follows the trend Cu, Zn > Fe > Co > Mn > Ni. This greater propensity for sequential water molecule loss with more internal energy deposition is consistent with the loss of a water molecule being entropically favored over the charge separation reaction, as has been reported previously for Cu^{2+}, Zn^{2+}, and $SO_4{}^{2-}$.[51,67,72]

The trend in the extent to which charge separation occurs for these different metal ions roughly parallels the trend in the aqueous hydrolysis constants where Zn^{2+} and Cu^{2+} have the greatest propensity to hydrolyze and Mn^{2+} and Ni^{2+} the least (Table 1).[73] In the gas phase, the charge separation reaction likely goes through a salt-bridge intermediate in which a metal hydroxide is formed by proton transfer to a water molecule in a second solvation shell, followed by the separation of protonated water or water cluster and the corresponding singly-charged hydrated metal hydroxide. Interestingly, the trend in charge separation propensity for the $M^{2+}(H_2O)_6$ clusters parallels the trends in average CN values for these metal ions, where Cu^{2+} and Zn^{2+}, which have average CN values of 4 and 5 respectively, have the greatest propensity for charge separation, and Ni^{2+}, which has a CN = 6 and no evidence for a population of lower CN structures has the least charge separation propensity with laser-induced dissociation. The presence of one or more water molecules that are already in a second solvation shell should reduce the energy required to form a salt-bridge intermediate compared to structures where all water molecules are in the inner shell and additional energy is required to promote a water molecule to the second solvation shell.

7.5 Conclusions

IRPD spectroscopy of $M^{2+}(H_2O)_{5-8}$, where M = Mn, Fe, Co, Ni, and photodissociation kinetics for clusters with $n = 6$, combined with previously reported results for Ca, Cu, and

Zn provide valuable insight into the shell structures and average CN values for these ions. Although computational chemistry can be useful in interpreting IRPD spectra of hydrated metal ions, there are often significant discrepancies between calculated and experimental frequencies and intensities that complicate detailed spectral interpretation. In addition, calculated relative energies for different structures can be strongly dependent on the level of theory used.[64,68] Structural information deduced from these spectroscopic data can thus be determined more reliably by comparisons to those of other hydrated metal ions.

The IRPD spectra and the integrated free-OH intensities, A_{asym}/A_{sym}, for $M^{2+}(H_2O)_{5-8}$, where M = Mn, Fe, Co, Ni, indicate that at 215 K, Ni has the highest average CN with no evidence for structures where a water molecule is in a second solvation shell for $Ni^{2+}(H_2O)_6$, indicating a CN = 6. Clusters containing Mn, Fe and Co have similar shell structure and average CN at each cluster size. Comparisons with the previously reported IRPD spectra for hydrated Cu^{2+} and Zn^{2+} indicate that at 215 K, the extent of second shell structures for Mn, Fe, Co and Ni clusters is less than for Cu (CN = 4) and Zn (CN = 5) suggesting an average CN > 5 for these metal ions. Photodissociation kinetics for complexes with 6 water molecules measured at higher temperatures (263 – 331 K) where the BIRD rate constants are comparable, provide a more accurate measure of the extent of H-bonding than the IRPD spectra and these data indicate a CN = 6 for Ni and an average CN slightly less than six for Fe, Co and Mn.

There is no indication that the structure or average CN of $Ni^{2+}(H_2O)_6$ depends on temperature. However, a decrease in average CN from 215 K to 305 K is apparent for $Mn^{2+}(H_2O)_6$ from the extent of H-bonding determined from photodissociation kinetics which is much closer to that for Zn and Cu than to that for Fe and Co. Subtle changes in the IRPD spectrum of $Mn^{2+}(H_2O)_6$ at 305 K are consistent with this decrease in average CN.

The trend in charge separation propensity for $M^{2+}(H_2O)_6$, M = Mn, Fe, Co, Ni, Cu and Zn correlates with trends in the average CN and with the aqueous hydrolysis constants for these metal ions. These results are consistent with a salt-bridge intermediate for the dissociative charge separation reaction where the presence of second shell water molecules reduces the energy required to form the salt bridge intermediate. The correlation of the gas-phase reactivity of these hydrated clusters with the hydrolysis constants of the metal ions indicates a close relationship between the gas-phase hydration of these metal ions and their hydration in aqueous solution.

References

(1) Wriggleworth, J. M.; Baum, H. *The biochemical function of iron*; Academic Press: London, 1980.

(2) O'Halloran, T. V. *Science* **1993**, *261*, 715-725.

(3) Vallee, B. L.; Falchuk, K. H. *Physiol. Rev.* **1993**, *73*, 79-118.

(4) Pyle, A. M. *J. Biol. Inorg. Chem.* **2002**, *7*, 679-690.

(5) Berg, J. M.; Shi, Y. G. *Science* **1996**, *271*, 1081-1085.

(6) Kobayashi, M.; Shimizu, S. *Eur. J. Biochem.* **1999**, *261*, 1-9.

(7) Jackson, G. S.; Murray, I.; Hosszu, L. L. P.; Gibbs, N.; Waltho, J. P.; Clarke, A. R.; Collinge, J. *Proc. Natl. Acad. Sci. U. S. A.* **2001**, *98*, 8531-8535.

(8) Waldron, K. J.; Rutherford, J. C.; Ford, D.; Robinson, N. J. *Nature* **2009**, *460*, 823-830.

(9) Valko, M.; Morris, H.; Cronin, M. T. D. *Curr. Med. Chem.* **2005**, *12*, 1161-1208.

(10) Stohs, S. J.; Bagchi, D. *Free Radical Biol. Med.* **1995**, *18*, 321-336.

(11) Mobley, H. L. T.; Island, M. D.; Hausinger, R. P. *Microbiol. Rev.* **1995**, *59*, 451-480.

(12) *Nickel and Its Surprising Impact in Nature*; Sigel, A.; Sigel, H.; Sigel, R. K. O., Eds.; Wiley: West Sussex, 2007.

(13) Gioia, S.; Weiss, D.; Coles, B.; Arnold, T.; Babinski, M. *Anal. Chem.* **2008**, *80*, 9776-9780.

(14) Segal, D. J.; Dreier, B.; Beerli, R. R.; Barbas, C. F. *Proc. Natl. Acad. Sci. U. S. A.* **1999**, *96*, 2758-2763.

(15) Blancafort, P.; Segal, D. J.; Barbas, C. F. *Mol. Pharmacol.* **2004**, *66*, 1361-1371.

(16) Frank, P.; Benfatto, M.; Szilagyi, R. K.; D'Angelo, P.; Della Longa, S.; Hodgson, K. O. *Inorg. Chem.* **2005**, *44*, 1922-1933.

(17) Chaboy, J.; Muñoz-PÁez, A.; Merkling, P. J.; Marcos, E. S. *J. Chem. Phys.* **2006**, *124*, 064509.

(18) Garcia, J.; Benfatto, M.; Natoli, C. R.; Bianconi, A.; Fontaine, A.; Tolentino, H. *Chem. Phys.* **1989**, *132*, 295-307.

(19) Kuzmin, A.; Obst, S.; Purans, J. *J. Phys.: Condens. Matter* **1997**, *9*, 10065-10078.

(20) Chen, Y. S.; Fulton, J. L.; Partenheimer, W. *J. Solution Chem.* **2005**, *34*, 993-1007.

(21) Ohtaki, H.; Radnai, T. *Chem. Rev.* **1993**, *93*, 1157-1204.

(22) D'Angelo, P.; Barone, V.; Chillemi, G.; Sanna, N.; Meyer-Klaucke, W.; Pavel, N. V. *J. Am. Chem. Soc.* **2002**, *124*, 1958-1967.

(23) Howell, I.; Neilson, G. W. *J. Mol. Liq* **1997**, *73-4*, 337-348.

(24) Herdman, G. J.; Neilson, G. W. *J. Mol. Liq* **1990**, *46*, 165-179.

(25) Fratiello, A.; Kubo, V.; Peak, S.; Sanchez, B.; Schuster, R. E. *Inorg. Chem.* **1971**, *10*, 2552-2557.

(26) Matwiyoff, N. A.; Darley, P. E. *J. Phys. Chem.* **1968**, *72*, 2659-2661.

(27) Rudolph, W. W.; Pye, C. C. *Phys. Chem. Chem. Phys.* **1999**, *1*, 4583.

(28) Kanno, H. *J. Phys. Chem.* **1988**, *92*, 4232-4236.

(29) Bergstrom, P. A.; Lindgren, J. *Inorg. Chem.* **1992**, *31*, 1529-1533.

(30) Schwenk, C. F.; Loeffler, H. H.; Rode, B. M. *J. Am. Chem. Soc.* **2003**, *125*, 1618-1624.

(31) Rode, B. M.; Schwenk, C. F.; Hofer, T. S.; Randolf, B. R. *Coord. Chem. Rev.* **2005**, *249*, 2993-3006.

(32) Miyazaki, M.; Fujii, A.; Ebata, T.; Mikami, N. *Science* **2004**, *304*, 1134-1137.

(33) Shin, J. W.; Hammer, N. I.; Diken, E. G.; Johnson, M. A.; Walters, R. S.; Jaeger, T. D.; Duncan, M. A.; Christie, R. A.; Jordan, K. D. *Science* **2004**, *304*, 1137-1140.

(34) Shvartsburg, A. A.; Siu, K. W. M. *J. Am. Chem. Soc.* **2001**, *123*, 10071-10075.

(35) Cooper, T. E.; Armentrout, P. B. *J. Phys. Chem. A* **2009**, *113*, 13742-13751.

(36) Beyer, M.; Williams, E. R.; Bondybey, V. E. *J. Am. Chem. Soc.* **1999**, *121*, 1565-1573.

(37) Beyer, M. K.; Metz, R. B. *J. Phys. Chem. A* **2003**, *107*, 1760-1762.

(38) Cox, H.; Stace, A. J. *J. Am. Chem. Soc.* **2004**, *126*, 3939-3947.

(39) Faherty, K. P.; Thompson, C. J.; Aguirre, F.; Michne, J.; Metz, R. B. *J. Phys. Chem. A* **2001**, *105*, 10054-10059.

(40) Thompson, C. J.; Aguirre, F.; Husband, J.; Metz, R. B. *J. Phys. Chem. A* **2000**, *104*, 9901-9905.

(41) Chen, X. J.; Wu, G. H.; Wu, B. H.; Duncombe, B. J.; Stace, A. J. *J. Phys. Chem. B* **2008**, *112*, 15525-15528.

(42) Rodriguez-Cruz, S. E.; Jockusch, R. A.; Williams, E. R. *J. Am. Chem. Soc.* **1998**, *120*, 5842-5843.

(43) Rodriguez-Cruz, S. E.; Jockusch, R. A.; Williams, E. R. *J. Am. Chem. Soc.* **1999**, *121*, 8898-8906.

(44) Rodriguez-Cruz, S. E.; Jockusch, R. A.; Williams, E. R. *J. Am. Chem. Soc.* **1999**, *121*, 1986-1987.

(45) Wong, R. L.; Paech, K.; Williams, E. R. *Int. J. Mass Spectrom.* **2004**, *232*, 59-66.

(46) Blades, A. T.; Jayaweera, P.; Ikonomou, M. G.; Kebarle, P. *J. Chem. Phys.* **1990**, *92*, 5900-5906.

(47) Blades, A. T.; Jayaweera, P.; Ikonomou, M. G.; Kebarle, P. *Int. J. Mass Spectrom. Ion Processes* **1990**, *102*, 251-267.

(48) Peschke, M.; Blades, A. T.; Kebarle, P. *J. Phys. Chem. A* **1998**, *102*, 9978-9985.

(49) Peschke, M.; Blades, A. T.; Kebarle, P. *J. Am. Chem. Soc.* **2000**, *122*, 10440-10449.

(50) Carl, D. R.; Chatterjee, B. K.; Armentrout, P. B. *J. Chem. Phys.* **2010**, *132*, 044303.

(51) Cooper, T. E.; Carl, D. R.; Armentrout, P. B. *J. Phys. Chem. A* **2009**, *113*, 13727-13741.

(52) Carl, D. R.; Moision, R. M.; Armentrout, P. B. *Int. J. Mass Spectrom.* **2007**, *265*, 308-325.

(53) Cooper, T. E.; Armentrout, P. B. *Chem. Phys. Lett.* **2010**, *486*, 1-6.

(54) Inokuchi, Y.; Ohshimo, K.; Misaizu, F.; Nishi, N. *J. Phys. Chem. A* **2004**, *108*, 5034-5040.

(55) Kolaski, M.; Lee, H. M.; Choi, Y. C.; Kim, K. S.; Tarakeshwar, P.; Miller, D. J.; Lisy, J. M. *J. Chem. Phys.* **2007**, *126*, 074302.

(56) Miller, D. J.; Lisy, J. M. *J. Am. Chem. Soc.* **2008**, *130*, 15381-15392.

(57) Miller, D. J.; Lisy, J. M. *J. Chem. Phys.* **2006**, *124*, 024319.

(58) Patwari, G. N.; Lisy, J. M. *J. Chem. Phys.* **2003**, *118*, 8555-8558.

(59) Walters, R. S.; Pillai, E. D.; Duncan, M. A. *J. Am. Chem. Soc.* **2005**, *127*, 16599-16610.

(60) Carnegie, P. D.; Bandyopadhyay, B.; Duncan, M. A. *J. Chem. Phys.* **2011**, *134*.

(61) Carnegie, P. D.; Bandyopadhyay, B.; Duncan, M. A. *J. Phys. Chem. A* **2008**, *112*, 6237-6243.

(62) Prell, J. S.; O'Brien, J. T.; Williams, E. R. *J. Am. Chem. Soc.* **2011**, *133*, 4810-4818.

(63) Carnegie, P. D.; Bandyopadhyay, B.; Duncan, M. A. *J. Phys. Chem. A* **2011**, *115*, 7602-7609.

(64) Bush, M. F.; O'Brien, J. T.; Prell, J. S.; Wu, C. C.; Saylkally, R. J.; Williams, E. R. *J. Am. Chem. Soc.* **2009**, *131*, 13270-13277.

(65) Bush, M. F.; Saykally, R. J.; Williams, E. R. *ChemPhysChem* **2007**, *8*, 2245-2253.

(66) Bush, M. F.; Saykally, R. J.; Williams, E. R. *J. Am. Chem. Soc.* **2008**, *130*, 15482-15489.

(67) O'Brien, J. T.; Williams, E. R. *J. Phys. Chem. A* **2008**, *112*, 5893-5901.

(68) Cooper, T. E.; O'Brien, J. T.; Williams, E. R.; Armentrout, P. B. *J. Phys. Chem. A* **2010**, *114*, 12646-12655.

(69) Bush, M. F.; Saykally, R. J.; Williams, E. R. *J. Am. Chem. Soc.* **2008**, *130*, 9122-9128.

(70) Donald, W. A.; Leib, R. D.; Demireva, M.; O'Brien, J. T.; Prell, J. S.; Williams, E. R. *J. Am. Chem. Soc.* **2009**, *131*, 13328-13337.

(71) Bush, M. F.; O'Brien, J. T.; Prell, J. S.; Saykally, R. J.; Williams, E. R. *J. Am. Chem. Soc.* **2007**, *129*, 1612-1622.

(72) Wong, R. L.; Williams, E. R. *The Journal of Physical Chemistry A* **2003**, *107*, 10976-10983.

(73) Burgess, J. *Metal Ions in Solution*; Ellis Horwood: Chichester, England, 1978.

7.6 Tables and Figures

$M^{2+}(H_2O)_6$	Temperature (K)	BIRD Products I_{CS}/I_{WL} (%)	Laser Products I_{CS}/I_{WL} (%)	Hydrolysis Constant at 298 K
Mn	215	Not observed	0/100	-10.46
Fe	"	"	35/65	-9.5
Co	"	"	70/30	-9.65
Ni	"	"	0/100	-9.86
Cu	"	"	100/0	<-8
Zn	"	"	100/0	-8.96
Mn	305	40/60	15/85	-10.46
Fe	263	100/0	45/55	-9.5
Co	263	100/0	29/71	-9.65
Ni	331	89/11	4/96	-9.86

Table 7.1: Dissociation products formed via charge separation (CS) and water loss (WL) from BIRD and laser-induced photodissociation (3600 cm^{-1}) at the temperature listed and corresponding metal ion hydrolysis constants at 298 K (ref. 73)

$M^{2+}(H_2O)_6$	Temp (K)	$k_{\max}$ (10^{-3} s^{-1})	k_{HB} (s^{-1})	k_{BIRD} (s^{-1})	$\frac{k_{max}-k_{BIRD}}{k_{HB}-k_{BIRD}}$
Mn	305	197 ± 1	5.0 ± 0.2	2.34 ± 0.09	73
Fe	263	160 ± 10	0.99 ± 0.03	0.584±0.004	392
Co	263	87± 2	0.78 ± 0.02	0.59± 0.02	454
Ni	331	96± 3	3.9 ± 0.2	3.9 ± 0.1	3070
Cu	215	220± 10	8.1 ± 0.4	4.6 ± 0.2	61
Zn	215	114± 4	18.3 ± 0.2	16.0 ± 0.4	42
Ca	335	256± 4	3.8 ± 0.1	3.2 ± 0.1	421

Table 7.2: Dissociation rate constants (s^{-1}) for $Cu^{2+}(H_2O)_6$ and $Ca^{2+}(H_2O)_6$ at a copper jacket temperatures of 215 K for $Cu^{2+}(H_2O)_6$ and both 296 and 335 K for $Ca^{2+}(H_2O)_6$, obtained from the slopes of the Figure 7 data; the laser frequency of k_{max} is 3655 cm^{-1} and 3610 cm^{-1} for $Cu^{2+}(H_2O)_6$ and $Ca^{2+}(H_2O)_6$ respectively.

$M^{2+}(H_2O)_6$	A_{asym}/A_{sym}
Mn	0.81
Mn (305 K)	1.09
Fe	0.83
Co	0.87
Ni	0.46
Ni (331 K)	0.72
Cu	2.79
Zn	2.17

Table 7.3: Relative integrated free-OH band intensities A_{asym}/A_{sym} from the IRPD spectra of $M^{2+}(H_2O)_6$ at 215 K except where noted.

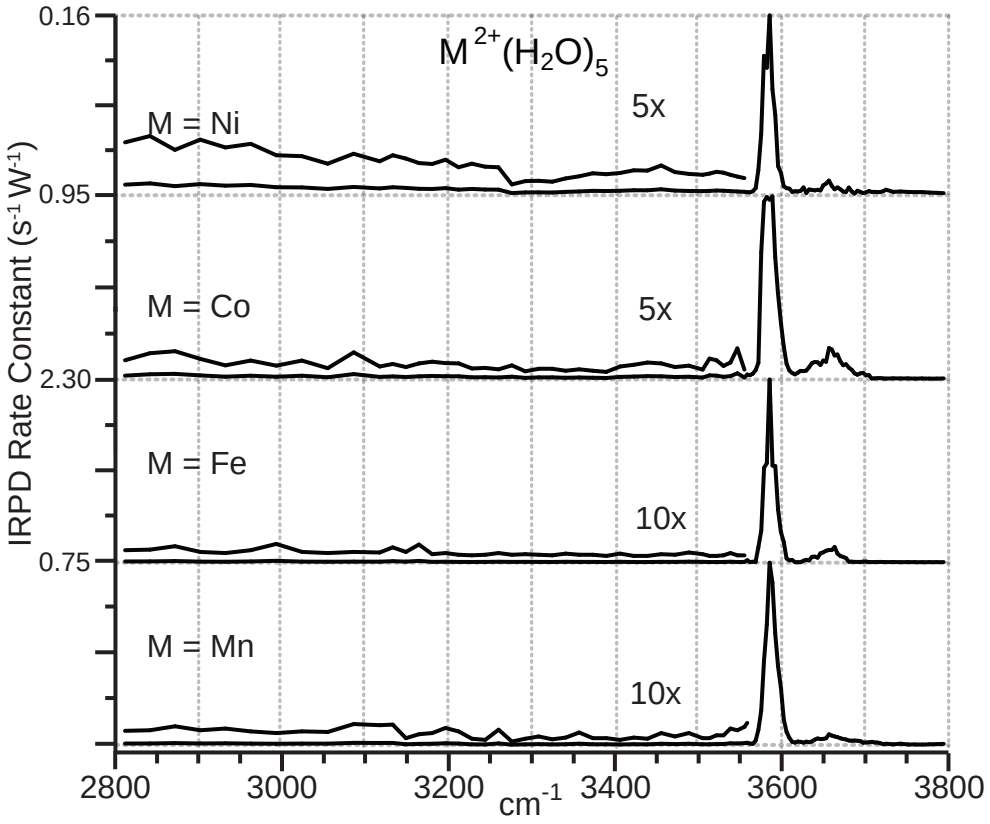

Figure 7.1: IRPD spectra of $M^{2+}(H_2O)_5$ from 2800 – 3800 cm^{-1} at 215 K.

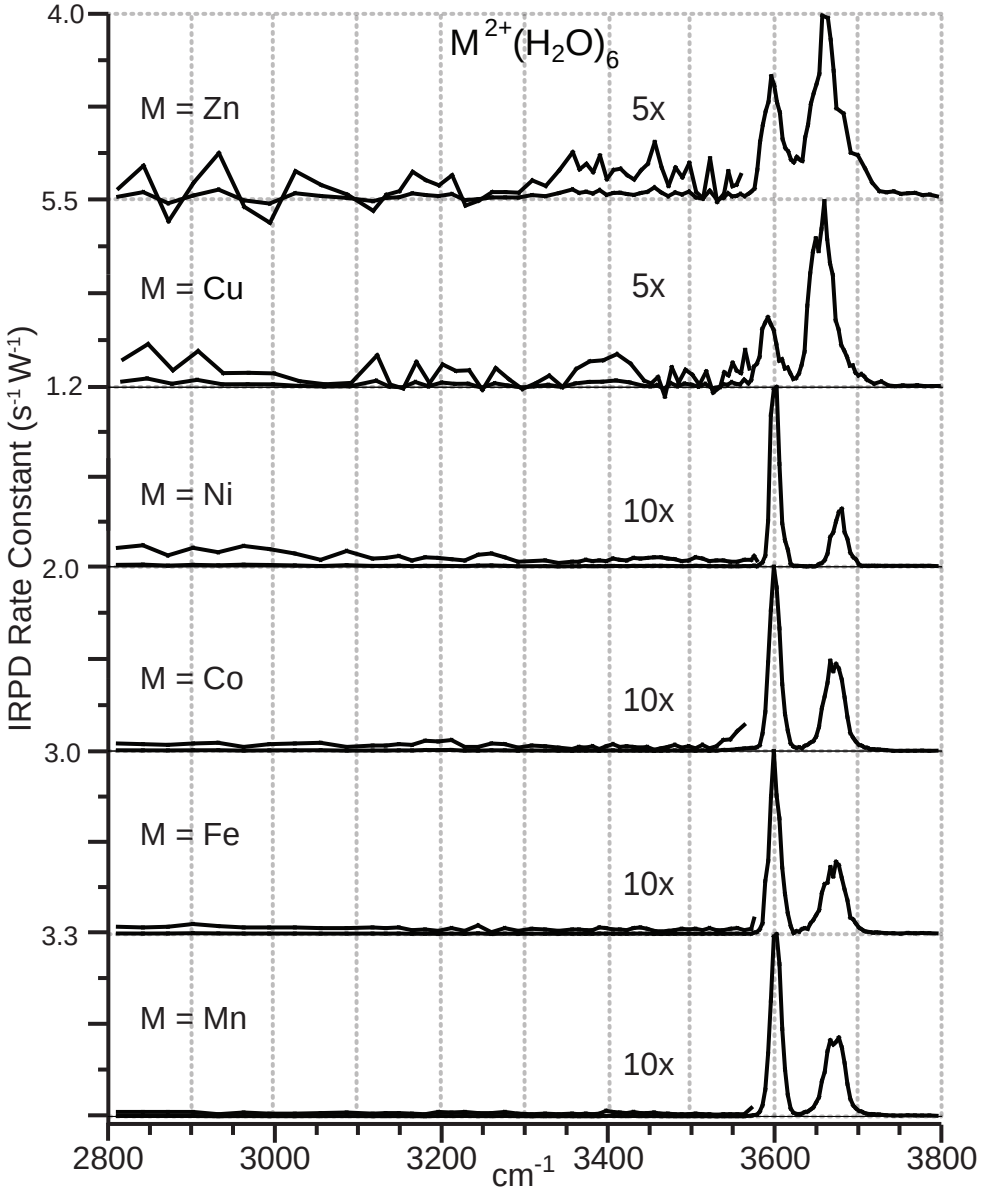

Figure 7.2: IRPD spectra of $M^{2+}(H_2O)_6$ from 2800 – 3800 cm^{-1} at 215 K.

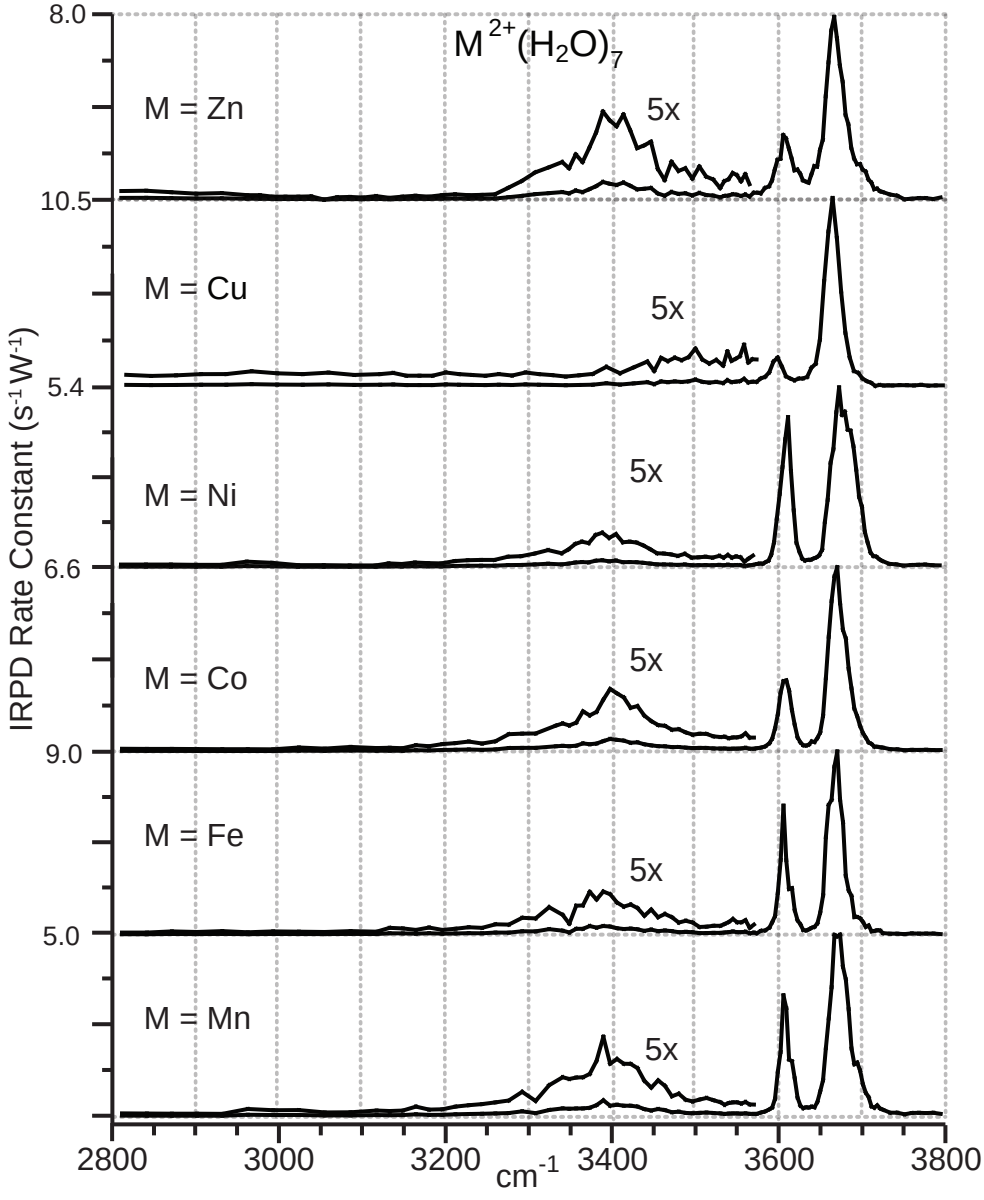

Figure 7.3: IRPD spectra of $M^{2+}(H_2O)_7$ from 2800 – 3800 cm^{-1} at 215 K.

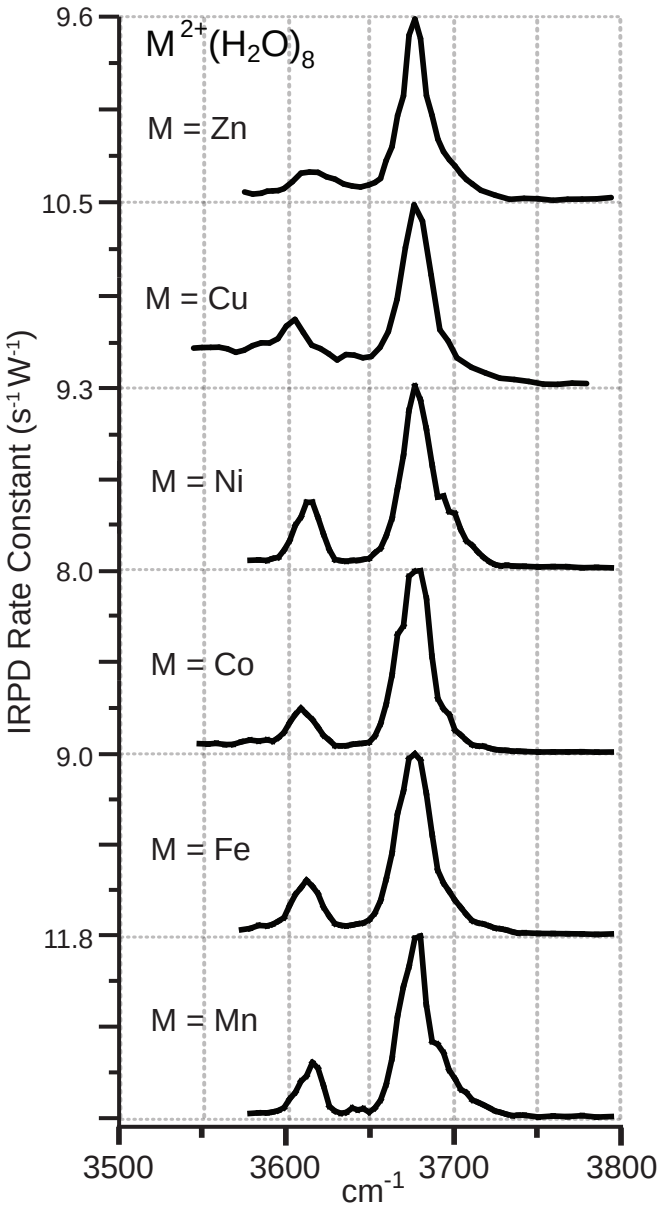

Figure 7.4: IRPD spectra of $M^{2+}(H_2O)_8$ from 3600 – 3800 cm^{-1} at 215 K.

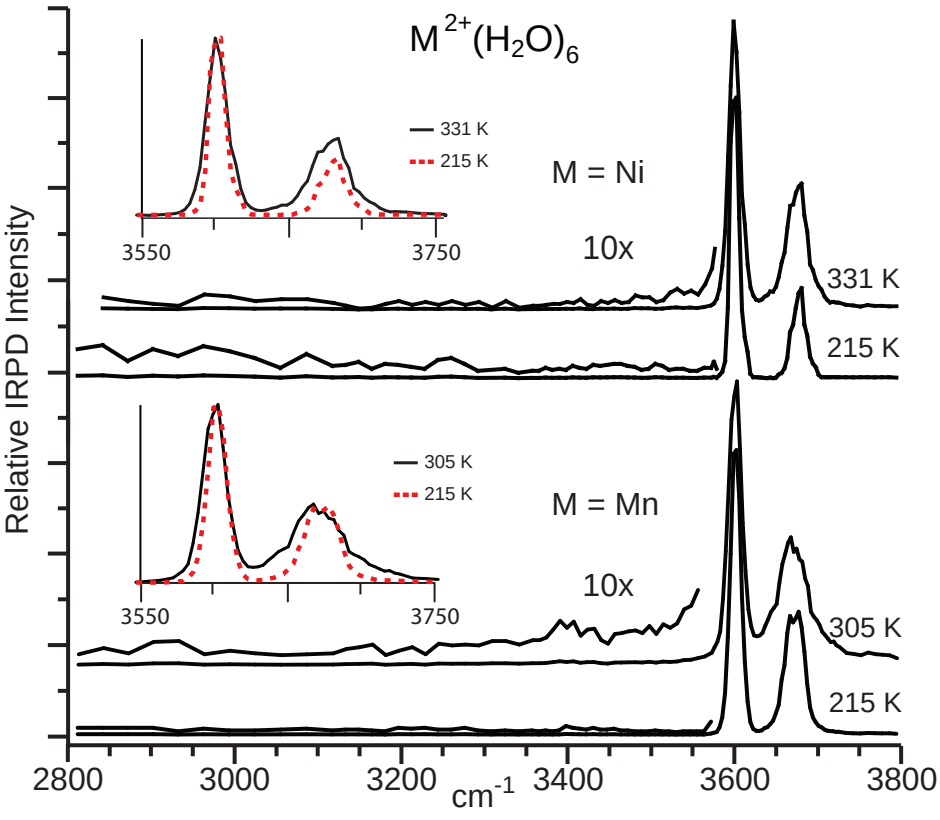

Figure 7.5: Comparison of higher temperature IRPD spectra of $Ni^{2+}(H_2O)_6$ and $Mn^{2+}(H_2O)_6$ (331 K and 305 K, respectively) to spectra acquired at 215 K. Inset shows overlay of the spectra in the free-OH region.

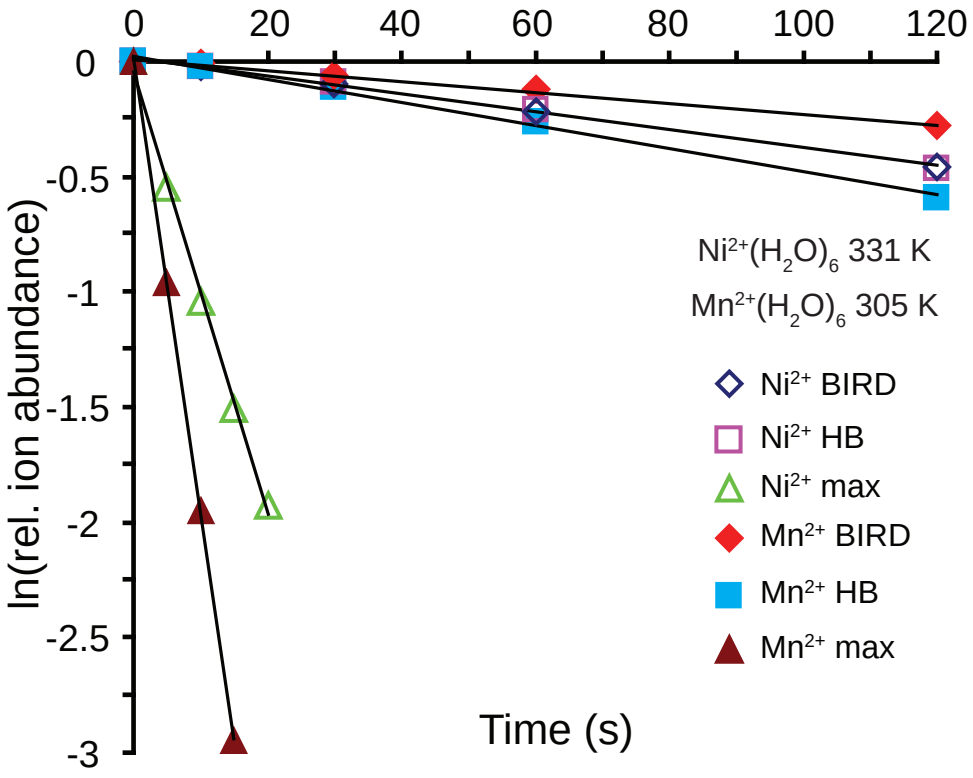

Figure 7.6: BIRD and laser photodissociation kinetics data at ∼3600 (max) and 3400 cm^{-1} (HB) for $Ni^{2+}(H_2O)_6$ and $Mn^{2+}(H_2O)_6$ at 331 K and 305 K, respectively.

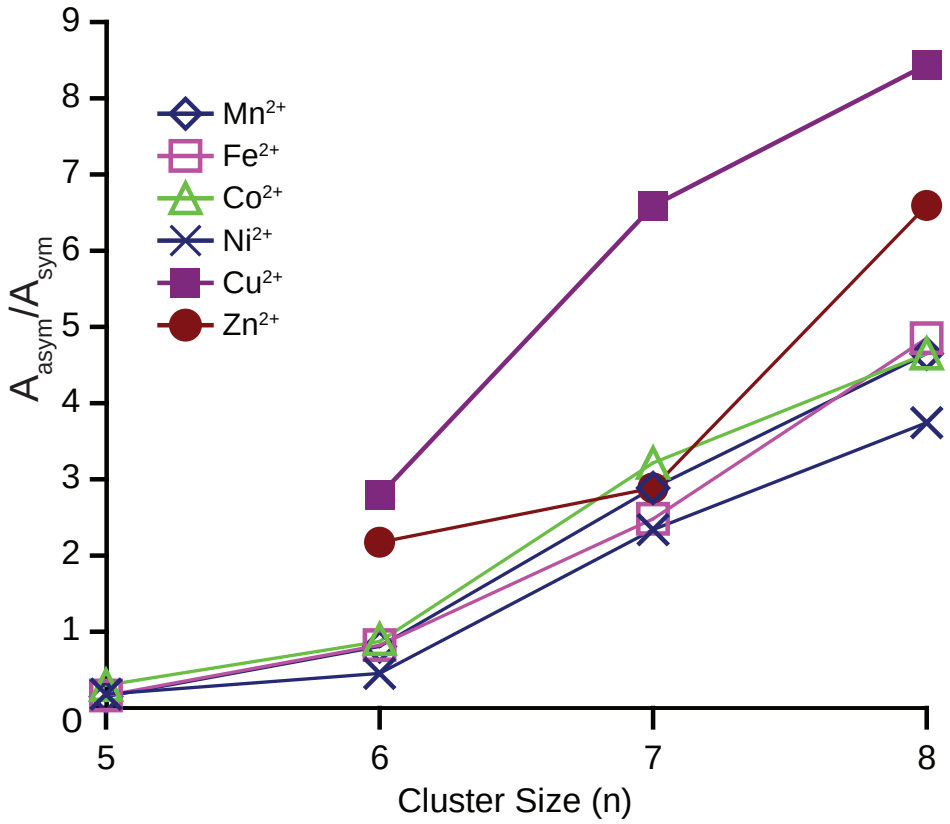

Figure 7.7: Ratios of the integrated areas of the free-OH ν_{sym} and ν_{asym} (A_{asym}/A_{sym}) bands in the IRPD spectra of $M^{2+}(H_2O)_{5-8}$ at 215 K as a function of cluster size.

Chapter 8

Sulfate Ion Patterns Water At Long Distance

Jeremy T. O'Brien, James S. Prell, Matthew F. Bush, and Evan R. Williams

Journal of the American Chemical Society, 2010, 132, 8248–8249

8.1 Introduction

In 1888, F. Hofmeister reported an ordering for salts based on their ability to precipitate hen egg albumin in aqueous solution.[1] This "Hofmeister series" that ranks how ions affect protein solubility is remarkably reproducible for a wide variety of proteins and salts, with anions generally having a stronger effect than cations. Among the anions, sulfate in particular has a strong ability to decrease protein solubility placing it at the kosmotropic (structure maker) end of the Hofmeister scale. In contrast, ions such as ClO_4^-or SCN^- are chaotropes (structure breakers) on the opposite end of the Hofmeister scale and these ions increase protein solubility. Hofmeister effects have been extensively investigated using a number of methods, including X-ray absorption spectroscopy,[2] nuclear magnetic resonance,[3] sum-frequency generation (SFG) spectroscopy,[4] and computational chemistry.[5] Despite significant progress, the precise chemical origins of the Hofmeister series are still debated over 120 years later. Evidence supporting both direct ion-protein interactions and long-range effects of ions on solvent structure has been reported,[2–6] but no clear consensus has been reached as to what extent either of these effects are responsible for the Hofmeister series. Although it is widely accepted that ions can have a very significant structuring effect on water molecules in the first solvation shell, the dynamic nature of liquid water presents a significant challenge in determining long-range structural effects beyond the first solvation shell. Ascribing ion-induced structural effects to a specific ion can also be complicated by counter-ions, which are always present in bulk salt solutions.

Effects of salts on water structure at interfaces have also been investigated, and rankings for how ions affect surface tension[6] and ion interfacial affinities[4] that are very similar to the Hofmeister series have been reported. Surface-sensitive methods, such as SFG, can provide information about the orientation of water molecules near surfaces, and effects of ions on these interfacial water molecules have been observed. For example, the intensity of the SFG signal in the frequency region 3000 – 3600 cm^{-1} for sodium salt solutions with different anions at an aqueous/polymer interface correlates with the Hofmeister series.[4] However, even phase-resolved SFG spectra can be difficult to interpret in terms of the water surface structure.[7,8]

Infrared photodissociation (IRPD) spectroscopy of gas-phase hydrated ions is a more direct probe of vibrational resonances than non-linear spectroscopic methods. In many cases, IRPD spectra closely resemble linear absorption spectra and can provide detailed information about both the interior *and* surface hydrogen bond structure of water in these complexes.[9–11] This technique is especially well suited for investigating how ions affect water

structure because the frequencies of OH stretching vibrations are highly sensitive to their hydrogen bonding environment. The structures of small, hydrated sulfate clusters have been investigated recently using both photo-electron[12] and IRPD spectroscopy.[10,11] For sulfate ions surrounded by up to 14 water molecules, the ion patterns nearby water molecules such that each hydrogen atom interacts with the sulfate ion or the oxygen atom of another water molecule.[10–12] In contrast, many water molecules at the surface of bulk solutions are oriented so that a hydrogen atom protrudes from the surface and is not part of a hydrogen bond, i.e., such water molecules have a "free-OH" group. An important question in measuring the ability of sulfate to pattern the water hydrogen bond network and thus a benchmark for studying Hofmeister series effects is: at what size does the surface of hydrated sulfate clusters exhibit these free-OH groups?

8.2 Results and Discussion

Here, we report the IRPD spectra of $SO_4^{2-}(H_2O)_n$ clusters with up to 80 water molecules measured at 130 K (**Figure 1**). IRPD spectra are acquired using a 2.7 T Fourier-transform ion cyclotron resonance mass spectrometer by measuring the frequency-dependent, laser-induced photodissociation rate constant of a mass-selected cluster(s).[13] Hydrated sulfate ions are generated from a 4 mM solution of $MgSO_4$ (Fisher Scientific, Pittsburgh, PA) by nanoelectrospray ionization and are trapped in a cylindrical ion cell surrounded by a copper jacket cooled to 130 K with a regulated flow of liquid nitrogen.[14] The clusters of interest are isolated using stored waveform inverse Fourier transform excitations. A single cluster size is isolated for the spectrum of $SO_4^{2-}(H_2O)_{36}$, and an ensemble of five adjacent cluster sizes is isolated for all other spectra. Each spectrum in Figure 1 is labeled with the weighted-average cluster size. The ions are photodissociated with IR radiation from a tunable 10 Hz OPO/OPA laser system (LaserVision, Bellevue, WA) for 1.5 – 5 s (15 – 50 pulses). For all of the clusters studied, sequential loss of water molecules is the only dissociation pathway observed. Under these conditions, absorption of a single photon increases the photodissociation rate, although absorption of more than one photon can also occur. IRPD spectra are obtained by plotting the laser-induced photodissociation rate constant versus the photon energy of the laser radiation. The photodissociation rate constants are calculated using the ensemble average method[15] which makes possible IRPD spectroscopy of large, hydrated clusters with improved signal-to-noise. All photodissociation rate constants are corrected for dissociation due to blackbody radiation and frequency-dependent variations in laser power.

There is a broad, intense feature from ~3100 to 3700 cm^{-1} in the IRPD spectra of $SO_4^{2-}(H_2O)_n$at all cluster sizes, which corresponds to hydrogen-bonded OH groups (**Figure 1**). At smaller cluster sizes, the maximum in this band is blue-shifted from the hydrogen-bonded OH-stretch absorption of bulk water.[16] This indicates less optimal water-water binding in these clusters presumably due to strong patterning of the first solvation shell by the ion. With increasing cluster size, the shape and central frequency of this band approaches those of the OH-stretch absorption spectrum of bulk water. No band above ~3700 cm^{-1} is observed in the spectra of $SO_4^{2-}(H_2O)_{36}$ and $SO_4^{2-}(H_2O)_{43}$, indicating that each surface

water molecule donates two hydrogen bonds. Although a number of factors can affect band intensities, these results indicate that the vast majority of the cluster populations do not have free-OH groups. For $SO_4^{2-}(H_2O)_n$, $n > 43$, a new band appears at ∼3710 cm^{-1} that grows in intensity with increasing cluster size. This band corresponds to free-OH groups of water molecules at the nanodrop surface. The increasing relative intensity of this band with increasing cluster size is consistent with additional water molecules adopting a more intrinsic structure at the nanodrop surface. A similar effect for the hydrated electron is observed at a much smaller cluster size.[17]

The frequency of the free-OH band in the IRPD spectra of the clusters is slightly blue-shifted from a band in SFG spectra of pure water[18] (∼3700 cm^{-1}) and a band observed near 3700 cm^{-1} in vibrational predissociation spectra of neutral water clusters,[19] which are attributed to free-OH groups at the liquid-air interface and cluster surface, respectively. The slight blue shift in this band compared to that for neutral water clusters or at the air/water interface is consistent with a Stark shift in this frequency as a result of the electric field at the surface of these clusters that contain sulfate dianion. This blue shift decreases slightly (less than 3 cm^{-1} from $n = 47$ to 80) with increasing cluster size, consistent with decreasing electric field strength at the surface due to improved ion solvation for larger clusters.

The appearance of the free-OH band at ∼3710 cm^{-1} indicates that intrinsic water-water interactions begin to dominate over the ion-induced structure for cluster sizes greater than ∼43, which is equivalent to a bulk sulfate concentration of ∼1.3 M. These free-OH groups belong to water molecules *in the third or higher solvation shells* of the sulfate dianion, indicating that an individual sulfate ion patterns water molecules to a distance much farther than the first solvation shell. Despite the significant patterning effects of the sulfate dianion the hydrogen-bonded feature in these spectra is similar to both that of bulk water and that observed in the IRPD spectra of large, hydrated Ca^{2+} complexes.[9] This indicates that the patterning of the hydrogen-bond network does not significantly affect the local environment of fully hydrogen bonded water molecules, a conclusion that is supported by results from MD simulations of hydrated anions, which indicate that despite substantial perturbations of the spatial pattern of water molecules in outer solvation shells, the number and typical strength of hydrogen bonds are remarkably unaffected.[5] These results are also supported by spectroscopy experiments, which indicate that ions do not substantially affect the reorientation time of water molecules beyond the first solvation shell.[20] The results of these studies have been interpreted by some as evidence that ion-induced solvent structure effects are not the dominant factor behind the Hofmeister series. However, it appears unlikely that rotational dynamics of bulk water molecules reflect the presence or absence of large scale patterning of the hydrogen-bond network.

IRPD spectroscopy provides a unique measure of the water patterning ability of sulfate and this technique has many advantages over condensed-phase methods for investigating the effects of ions on water structure. The free-OH band is sensitive to subtle changes in the patterning of the water hydrogen bond network and is more structurally informative than the bonded-OH region. By investigating these long-range patterning effects for other ions, new insight into the origins of the Hofmeister series could be obtained.

8.3 References

(1) Hofmeister, F. *Arch. Exp. Pathol. Pharmacol.* **1887**, *24*, 247-260.

(2) Uejio, J. S.; Schwartz, C. P.; Duffin, A. M.; Drisdell, W. S.; Cohen, R. C.; Saykally, R. J. *Proc. Natl. Acad. Sci. U. S. A.* **2008**, *105*, 6809-6812.

(3) Freire, M. G.; Neves, C. M. S. S.; Silva, A. M. S.; Santos, L. M. N. B. F.; Marrucho, I. M.; Rebelo, L. P. N.; Shah, J. K.; Maginn, E. J.; Coutinho, J. A. P. *J. Phys. Chem. B* **2010**, *114*, 2004-2014.

(4) Chen, X.; Yang, T.; Kataoka, S.; Cremer, P. S. *J. Am. Chem. Soc.* **2007**, *129*, 12272-12279.

(5) Smith, J. D.; Saykally, R. J.; Geissler, P. L. *J. Am. Chem. Soc.* **2007**, *129*, 13847-13856.

(6) Pegram, L. M.; Record, M. T. *J. Phys. Chem. B* **2007**, *111*, 5411-5417.

(7) Tian, C. S.; Shen, Y. R. *Chem. Phys. Lett.* **2009**, *470*, 1-6.

(8) Noah-Vanhoucke, J.; Smith, J. D.; Geissler, P. L. *J. Phys. Chem. B* **2009**, *113*, 4065-4074.

(9) Bush, M. F.; Saykally, R. J.; Williams, E. R. *J. Am. Chem. Soc.* **2008**, *130*, 15482-15489.

(10) Bush, M. F.; Saykally, R. J.; Williams, E. R. *J. Am. Chem. Soc.* **2007**, *129*, 2220-2221.

(11) Zhou, J.; Santambrogio, G.; Brummer, M.; Moore, D. T.; Meijer, G.; Neumark, D. M.; Asmis, K. R. *J. Chem. Phys.* **2006**, *125*, 111102.

(12) Wang, X. B.; Sergeeva, A. P.; Yang, J.; Xing, X. P.; Boldyrev, A. I.; Wang, L. S. *J. Phys. Chem. A* **2009**, *113*, 5567-5576.

(13) Bush, M. F.; O'Brien, J. T.; Prell, J. S.; Saykally, R. J.; Williams, E. R. *J. Am. Chem. Soc.* **2007**, *129*, 1612-1622.

(14) Wong, R. L.; Paech, K.; Williams, E. R. *Int. J. Mass Spectrom.* **2004**, *232*, 59-66.

(15) Prell, J. S.; O'Brien, J. T.; Williams, E. R. *J. Am. Soc. Mass Spectrom.* **2010**, *21*, 800-809.

(16) Freda, M.; Piluso, A.; Santucci, A.; Sassi, P. *Appl. Spectrosc.* **2005**, *59*, 1155-1159.

(17) Hammer, N. I.; Roscioli, J. R.; Bopp, J. C.; Headrick, J. M.; Johnson, M. A. *J. Chem. Phys.* **2005**, *123*, 244311.

(18) Ji, N.; Ostroverkhov, V.; Tian, C. S.; Shen, Y. R. *Phys. Rev. Lett.* **2008**, *100*, 096102.

(19) Andersson, P.; Steinbach, C.; Buck, U. *Eur. Phys. J. D* **2003**, *24*, 53-56.

(20) (a) Omta, A. W.; Kropman, M. F.; Woutersen, S.; Bakker, H. J. *Science* **2003**, *301*, 347-349. (b) Omta, A. W.; Kropman, M. F.; Woutersen, S.; Bakker, H. J. *J. Chem. Phys.* **2003**, *119*, 12457-12461.

8.4 Figure

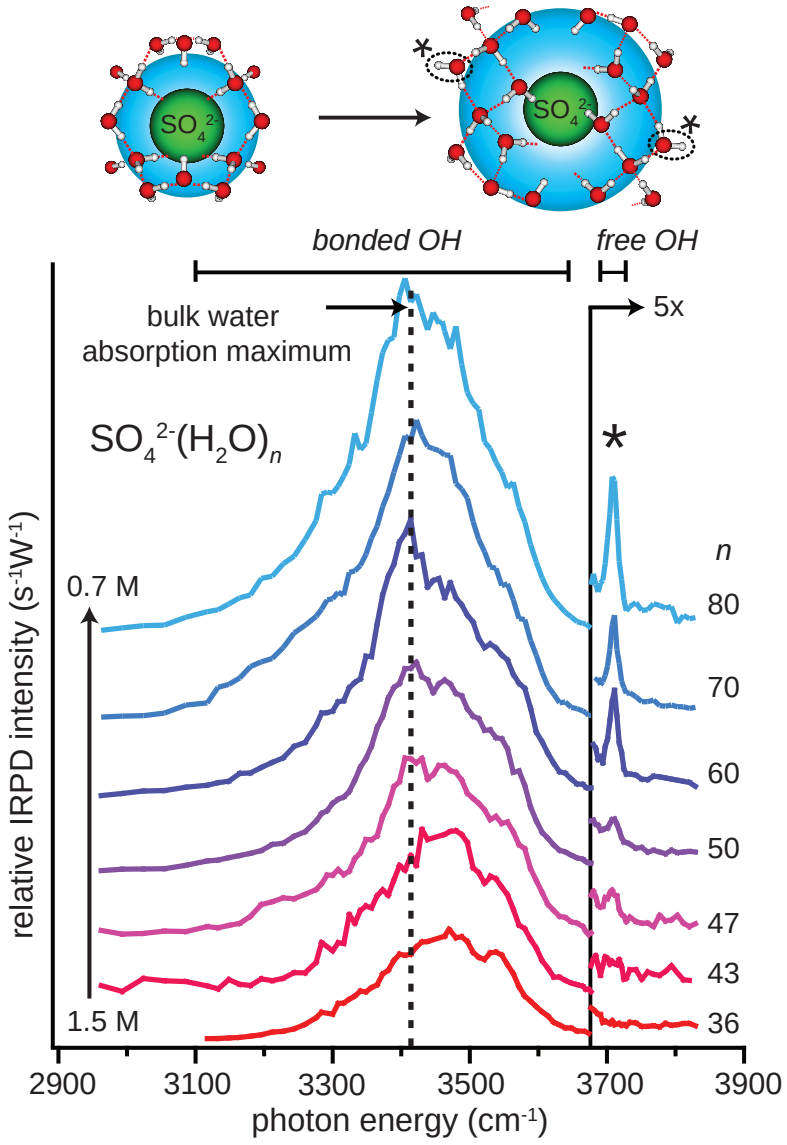

Figure 8.1: Ensemble average IRPD spectra of $SO_4^{2-}(H_2O)_n$ with up to 80 water molecules obtained at 130 K. The band at $\sim$ 3710 cm^{-1} (*) for n > 43 corresponds to outer-shell water molecules with "free" OH groups similar to those at the bulk water surface, indicating that sulfate ion has a long-range effect on water structure. Equivalent molarity of SO_4^{2-} is indicated. Bulk water absorption maximum is from Ref. 16.

Chapter 9

Effects of Ions on Hydrogen-bonding Water Networks in Large Aqueous Nanodrops

9.1 Introduction

The effects of interactions between ions, proteins, and water have been debated for over 120 years since Franz Hofmeister first ordered ions by their tendency to precipitate hen egg albumin in aqueous solutions.[1–3] This "Hofmeister series", which ranks how ions affect protein solubility, is remarkably reproducible for a wide variety of salts and proteins and has been observed for other chemical properties, such as salt solubilities,[4] cloud points of nonionic surfactants,[5] and transport through ion channels.[6] Hofmeister series effects have been investigated using a number of methods, including X-ray absorption spectroscopy,[7] nuclear magnetic resonance,[8] sum-frequency generation (SFG) spectroscopy,[9] computational chemistry,[10,11] and static vibrational spectroscopy.[11,12] Results supporting both direct ion-protein interactions[4,7–10,13] and effects of ions on solvent structure[11,14–17] have been reported, but no clear consensus has been reached as to what extent either of these effects are responsible for the Hofmeister series, and the physical origin of this ordering is still debated.[4,7–20]

Recent results from static vibrational spectroscopy,[11,12] femtosecond spectroscopy,[21–24] and terahertz dielectric relaxation spectroscopy[23,24] indicate that ions do not strongly affect the hydrogen bond (H-bond) network of water beyond the first solvation shell for salt solutions with high ionic strengths (2 – 12 M). Bakker and co-workers reported, based on water reorientation dynamics, that ion-water interactions only extend beyond the first solvation shell in solutions where both ion and counter-ion are strongly hydrated (i.e. $MgSO_4$).[23,24] They suggest that the physical origin of the Hofmeister series is related to cooperative structure-making effects between ions and charges present on biomolecules.[24]

The effects of salts on water structure at aqueous interfaces have also been linked to the Hofmeister series due to the large dielectric difference at both the liquid-vapor and the protein-water interfaces.[14] Linear spectroscopies have poor sensitivity to surface water molecules due to the overwhelming signal from the bulk. Sum-frequency generation (SFG) spectroscopy is a second-order optical technique and it is sensitive to the structure of the first few layers of water molecules at the liquid-vapor interface. Results from SFG,[25,26] electrospray ionization,[20] and molecular dynamics simulations[27] indicate that some ions, including Br^- and I^- are highly surface active,[25,27] whereas other ions, including Cl^- [25] and $SO_4{}^{2-}$,[26] have lower surface activity, suggesting that the ranking for ion surface activities is similar to the Hofmeister series.

Gas-phase studies of hydrated ion clusters have the advantage that the effects of a single ion or electron on water structure can be investigated as a function of hydration extent for up to hundreds of water molecules attached,[28–31] and any competing effects of counter-ions can be eliminated. The structures of many gas-phase ion complexes, including hydrates of small mono-[16,31–50], di-[15,16,47–57] and tri-valent[16,28,58] ions have been have been investigated using infrared photodissociation (IRPD) spectroscopy. Under readily achievable experimental conditions, absorption of a single IR photon by a hydrated ion can induce a measurable increase in the rate of dissociation resulting in IRPD spectra that closely resemble linear absorption spectra. Thus, IRPD spectroscopy can be a more direct probe of vibrational resonances than non-linear spectroscopic methods, such as SFG, and can provide detailed information about both the interior and surface H-bond structure of water in clusters. The

hydrogen-stretch region (∼2300 – 4000 cm^{-1}) is especially useful for investigating how ions affect water structure because the frequencies of OH stretching modes are very sensitive to their H-bonding environment. IRPD spectra of small hydrated ion clusters[33–57] indicate that many ions can have strong effects on the structure of water molecules in the first solvation shell, but with some ions, such as tetramethylammonium[32] and Cs^+,[37] water-water hydrogen bonding is favored over ion-water interactions and these ions have little effect on the hydration structure. Results from IRPD spectroscopy of hydrated $SO_4{}^{2-}$ indicate that the dianion strongly affects water structure even beyond the second solvation shell for clusters with up to 80 water molecules attached, and contrast sharply with conclusions from condensed phase femtosecond spectroscopy studies.[15] Recent results from IRPD spectroscopy of seventeen different hydrated ions with charge states between -1 and +3 at fixed cluster size (35 – 37 water molecules) show spectral differences attributable to various extents of ion-induced patterning of the water network that extends to the surface of the clusters, providing further evidence of long-range ion effects on hydration structure.[16]

Here, we present results from IRPD spectroscopy of $M(H_2O)_{\sim 250}$ where M = La^{3+}, Ca^{2+}, Na^+, I^-, and $SO_4{}^{2-}$ in the spectral region of 2800 - 3800 cm^{-1} measured at 133 K. To our knowledge, these are the largest mass-selected ionic clusters for which IRPD spectra have been reported. These spectra indicate that ion-induced patterning of the water network extends to the surface of these nanodrops and that the surface free-OH stretch frequency depends on ion charge state. Effects of ion polarity and charge state are investigated and compared to results for smaller hydrated ions as well as to condensed-phase results.

9.2 Experimental

All experiments were performed on a home-built 7.0 T Fourier-transform ion cyclotron resonance (FT/ICR) mass spectrometer coupled with a tunable OPO/OPA laser system. The instrument and experimental set-up, which previously included a 2.75 T magnet, are described in detail elsewhere.[59] Briefly, hydrated ion clusters are generated by nanoelectrospray ionization of 2 – 6 mM aqueous solutions using borosilicate capillaries pulled to an inner tip diameter of ∼1 μm that are filled with the solution of interest. A platinum wire is inserted into the capillary so that it is in contact with the solution, and a voltage of ∼ +600 V relative to the entrance of the mass spectrometer is applied to the wire. Hydrated ions are guided through five stages of differential pumping to an ion cell surrounded by a temperature controlled copper jacket, cooled using a regulated flow of liquid nitrogen to 133 K. The temperature of the copper jacket is equilibrated for at least 8 hrs prior to each experiment. Ions are accumulated for 3 - 6 s and thermalized with the aid of a pulse of dry nitrogen gas (∼10^{-6} Torr). After a 6 – 12 s delay, the pressure in the ion cell returns to <10^{-8} Torr and the ions of interest are isolated using a stored inverse Fourier transform waveform.

IRPD spectra are obtained using the ensemble average method, which improves the signal-to-noise ratio of IRPD spectra compared to spectra measured for an individual ion.[60] Ensembles of hydrated ions containing 245 – 255 water molecules are isolated and irradiated with tunable light from an OPO/OPA laser system (LaserVision, Bellevue, WA, U.S.A.) pumped by a 1064 cm^{-1} Nd:YAG laser (Continuum Surelite I-10, Santa Clara, CA, U.S.A.)

at a 10 Hz repetition rate for 0.5 – 1 s. Background dissociation due to blackbody infrared radiative dissociation (BIRD) and changes in the initial ensemble distribution are remeasured approximately every 10 minutes. BIRD rate constants (k_{BIRD}) are measured in the absence of laser irradiation and calculated from the measured ion abundances.

$$k_{BIRD} = \frac{\langle n(t)\rangle - \langle n(0)\rangle}{t}$$

$\langle n(t)\rangle$ is the abundance-weighted average number of water molecules in the ensemble after exposure to the 133 K blackbody field for time t. Laser-induced photodissociation rate constants (k_{IRPD}) are calculated similarly where t_{irr} is the laser irradiation time, and$\hbar\omega$ is the laser photon energy.

$$k_{IRPD}(\hbar\omega, t_{irr}) = \frac{\langle n(\hbar\omega, t_{irr})\rangle - \langle n(0)\rangle}{t_{irr}} - k_{BIRD}$$

k_{IRPD} is plotted versus photon energy to obtain the average IRPD spectrum of the isolated ensemble of hydrated ions. All ensemble IRPD spectra are corrected for frequency-dependent variations in laser power by scaling each k_{IRPD} value by the laser power at that energy.

Calculated structures of $Ca^{2+}(H_2O)_{250}$ and $SO_4{}^{2-}(H_2O)_{250}$ are obtained in order to compare the average number of free-OH groups present in each cluster. After an initial geometry relaxation using molecular mechanics, canonical ensemble molecular dynamics is used to generate 1000 structures for each hydrated ion cluster at 133 K using Impact 5.6 (Schrodinger, LLC, Portland, OR). Every atom is assigned an electrostatic charge, +0.41/-0.82 e, for hydrogen and oxygen, respectively and the ion is assigned its full formal charge. The projection E_i of the local electric field at a given hydrogen atom (H_i) onto a unit vector in the OH_i direction is calculated based on contributions from the ion and the hydrogen and oxygen atoms of all other water molecules. The distribution of E_i values obtained is bi-modal corresponding to contributions from free-OH and bonded-OH groups. The average number of free-OH groups is obtained from the histogram of E_i values for all 1000 structures. A similar technique has been applied previously to calculate infrared absorption spectra of hydrated ion clusters containing 36 water molecules.[16]

9.3 Results and Discussion

9.3.1 Hydrated Ion Formation.

Under "soft" instrumental conditions, a broad distribution of hydrated ions can be formed using electrospray ionization from aqueous solutions and trapped in the cooled ion cell of a FT/ICR mass spectrometer. A typical mass spectrum of $La^{3+}(H_2O)_n$ measured under such conditions with as many as 500 water molecules attached is shown in Figure 1, illustrating the much larger clusters that can be detected with a 7.0 T magnet compared to previous results with a 2.7 T magnet on this same instrument. Because of the wide range of clusters produced and the limited ion storage capabilities of the cell, the abundance of any individual cluster is relatively low. In addition, the blackbody infrared radiative dissociation (BIRD)

rate for large clusters is high, which makes it challenging to isolate and measure the IRPD spectrum of a single cluster size with a high signal-to-noise (S/N) ratio. IRPD spectra were measured using the ensemble average method[60] with an initial distribution of clusters with ∼245 – 255 water molecules. In addition to increasing S/N ratios, this method has the advantage that the potential influence of a single "magic" number cluster on the IRPD spectra is significantly reduced, although such effects are likely to be negligible for clusters of this size.

9.3.2 Spectroscopy.

IRPD spectra of $M(H_2O)_{\sim 250}$ at 133 K, where M = La^{3+}, Ca^{2+}, Na^+, I^-, and $SO_4{}^{2-}$ in the spectral region of 2800 – 3800 cm^{-1} are shown in Figures 2 and 3. The spectrum for each ion has a broad feature that extends from 2950 to 3675 cm^{-1}, which is attributable to H-bonded OH groups. There is also a narrow band near 3700 cm^{-1}, which is due to free-OH stretches of water molecules that accept two H-bonds and donate one H-bond (defined as an AAD water molecule). A small shoulder band is present at slightly higher frequencies, near 3720 cm^{-1}, for each ion except $SO_4{}^{2-}$ and is due to water molecules that accept and donate a single H-bond (AD water molecules). The centroids of the H-bonded features and the free-OH bands vary between 3300 and 3400 cm^{-1} and 3697 to 3705 cm^{-1}, respectively. The spectra of these clusters are similar owing to the large number of water molecules and the similar local H-bonding environments for many of the water molecules. However, even at this large cluster size (roughly equivalent to a bulk single ion concentration of 200 mM), there are distinct spectral differences that indicate the various extents to which ions can affect the H-bonding network of water molecules, even for those molecules that are remote from the ion.

The IRPD spectra of the $M(H_2O)_{\sim 250}$ nanodrops more closely resemble the IR absorbance spectra of liquid water or amorphous ice than crystalline ice.[61] In the absence of an ion, the nanodrop's freezing point is estimated from the Gibbs-Thomson equation and an approximate diameter of 2.4 nm to be ∼234 K. Results from IR spectroscopy of water droplets in a supersonic expansion indicate that onset of freezing occurs at ∼202 K for a 3.2 nm droplet.[62] The presence of an ion in the nanodrop should further reduce the freezing point. Binding enthalpies of water molecules to hydrated clusters containing divalent metal ions with up to 124 water molecules measured under similar conditions indicate that the clusters may have some ice-like structure.[30] Thus, the nanodrops in our experiments may be more like amorphous ice than liquid water.

9.3.3 IRPD Spectral Fitting.

In order to more directly compare the IRPD spectra, each spectrum was fit by three optimized Gaussian lineshapes with two peaks in the bonded-OH spectral region (2900 – 3600 cm^{-1}) and one smaller peak near 3700 cm^{-1}. Using only one Gaussian lineshape in the H-bonding region results in a significantly worse fit and three lineshapes provide only slightly improved fitting over two. H-bonded features in absorption,[26] Raman,[26] and SFG[63,64] spectra

have also been fit with two dominant lineshapes and have often been interpreted as corresponding to "ice-like" and "liquid-like" water molecules for the lower and higher frequency bands, respectively. However, more recent studies[11,65] indicate that water molecules adopt a continuum of H-bonding environments and that a two-state (or multi-state) interpretation of these spectra is misleading. Spectral fitting is used here solely for the purpose of more directly comparing the IRPD spectra of different ions. The experimental data and fits to these data for Ca^{2+} and $SO_4{}^{2-}$ are shown in Figure 4. From the optimized Gaussian lineshapes, peak centroids, intensities, and widths are obtained and these parameters for the spectrum of each ion are given in Table 1. The free-OH band frequency is red-shifted systematically over a 7 cm^{-1} range and increases in intensity by a factor of three with increasing positive charge state of the ion in the nanodrop. The frequencies of the two lineshapes fit to the bonded-OH feature each vary by less than 75 cm^{-1} with ion identity. Recent computational models[11,66] for infrared and Raman spectroscopy of aqueous solutions indicate that the spectral region from 3500 - 3600 cm^{-1} is associated with water molecules that are less strongly H-bonded than those at lower frequencies. There is a slight red-shift in the centroid of the H-bonded feature with increasing charge state for the cation spectra and this shift is consistent with the greater polarization of interior water molecules for the more highly charged ions.

9.3.4 Integrated Band Intensities.

The IRPD intensity at a given wavelength depends on many factors, including the laser power, the absorption cross section at that frequency, the number of labile surface water molecules, and the dissociation barrier for the loss of a water molecule from the cluster. The internal energy of these clusters is sufficiently high at 133 K that the absorption of even a single photon will result in an increased dissociation rate, although absorption of many photons occurs over the irradiation times used in these experiments. Under these conditions, the IRPD spectra should resemble linear absorption spectra so that the intensity of the bands are roughly proportional to both the oscillator strength and the number of oscillators.

The integrated intensities of these spectra obtained from the fits to the IRPD data as a function of charge state are given in Figure 5. The total integrated intensity of clusters with Na^+ and I^- are similar indicating that the absorption cross sections and the dissociation barriers for these clusters are similar. The integrated intensities for Ca^{2+}, La^{3+}, and $SO_4{}^{2-}$ containing nanodrops are higher than those for the monovalent ions. The binding energy of a water molecule in $M^{z+/-}(H_2O)_{250}$, calculated using a continuous Thomson liquid-drop model,[67] is 9.52, 9.58, and 9.67 kcal/mol for singly, doubly and triply-charged ions, respectively. Although the dissociation barrier increases slightly with charge state, the clusters containing multivalent ions dissociate more readily. The similar dissociation observed for the monovalent ions indicates that the polarity of the ion does not, in the absence of any significant structural effects, have a strong effect on the absorption cross sections of water in these clusters.

9.3.5 Ion Effects on Free-OH Stretch Frequency and Intensity.

The frequency of the free-OH band in each spectrum varies nearly linearly with the charge state of the ion in the nanodrop, decreasing from 3704.5 cm^{-1} for $SO_4^{2-}(H_2O)_{\sim 250}$ to 3697.1 cm^{-1} for $La^{3+}(H_2O)_{\sim 250}$ (Figure 6A). A line fit to all these data results in a slope of ∼1.5 cm^{-1} per unit charge. A similar linear dependence of the frequency of the free-OH band with charge state was reported previously for ions with ∼36 water molecules attached, but the slope for these smaller clusters is ∼10x greater.[16] The near linear dependence of frequency with ion charge state is consistent with a Stark effect owing to the electric field at the nanodrop surface that is caused by the ion. The much smaller dependence for clusters with 250 compared to those with 36 water molecules is consistent with a lower electric field strength at the surface of the larger nanodrops due to improved ion solvation and greater average distances between the surface water molecules with free-OH groups and the ion in the nanodrop.

As was the case for the clusters with 36 water molecules, the data for the cations are significantly more linear than when the anion data is included.[16] This indicates that the orientation of water molecules at the surface of the clusters that contain cations is similar for each charge state, but differs slightly from those at the surface of clusters that contain anions. This suggests that the polarity of the ion in the droplet results in differences in water structure that propagates out to water molecules that are at the surface of these clusters. The relative integrated area of the free-OH band to the H-bonded band determined from the fitted lineshapes for each of the ions also depends on charge state (Figure 6B). The relative intensity of this band increases as a function of increasing positive charge of the ion in the nanodrop. This increasing intensity for bands with nearly the same frequency suggests that there are greater populations of AAD water molecules for the more positively charged nanodrops indicating that ion induced patterning of the hydration structure of these clusters extends to the surface.

Although neutral nanodrops cannot be probed in these experiments, an estimate of the free-OH stretch of surface water molecules in a neutral aqueous nanodrop can be obtained by extrapolating the data for charged nanodrops to zero charge. Extrapolation of the cation and anion data to zero charge results in values of 3699.3 and 3700.1 cm^{-1}, respectively, which should be lower and upper bounds for the free-OH band frequency of a similarly sized neutral water cluster. These values are slightly lower than our previously estimated range for the neutral AAD free-OH band frequency (3704.9 - 3709.7 cm^{-1}) obtained from the IRPD spectra of clusters with 36 water molecules.[16] The discrepancy between the extrapolation at small and large cluster size indicates that the structure of water at the surface of the smaller ion-containing clusters differs slightly from that of the larger clusters. The value of the free-OH stretch frequency of water on a neutral droplet obtained from the data for the larger clusters is nearly the same as the AAD free-OH band frequencies measured for protonated water clusters (3699.1 cm^{-1}, for $H^+(H_2O)_{200}$)[31] and for large neutral water clusters generated in supersonic expansions, 3693 and 3710 cm^{-1} for cluster sizes ∼16.5 nm and ∼1 nm, respectively.[68] It is also consistent with the estimates of bulk water AAD free-OH band frequencies obtained from SFG experiments at room temperature (3690 - 3705 cm^{-1})[26,63,69,70] which also show evidence of two types of surface water molecules, although the origin of the band assigned to AD water

molecules is debated. The free-OH band measured in SFG experiments is very broad (∼50 cm^{-1}) and the SFG band frequency and lineshape depend on the polarization and angle of incidence of the incoming laser beams resulting in a concomitant uncertainty in determining the true free-OH stretch band frequency of a surface water molecule precisely from these measurements. The differing fits for cations and anions suggest that there is a slight effect of the ion polarity on the water molecule orientation at the surface of these very large hydrated clusters, but this effect is relatively small and does not likely significantly affect our estimate of the free-OH stretch frequency of surface water molecules in an uncharged nanodrop of this size.

9.3.6 Spectra of Hydrated Monovalent Ions.

The IRPD spectra of $Na^+(H_2O)_{\sim 250}$ and $I^-(H_2O)_{\sim 250}$ are similar with only very subtle differences in the free-OH and H-bonded bands (Figure 7). The intensity of the free-OH band is slightly greater for Na^+ than for I^- whereas the H-bonded band is marginally greater for I^-. Because the integrated intensities of these spectra are essentially the same, this difference in the free-OH band intensity suggests that there are slight differences in the structure of surface water molecules for nanodrops containing Na^+ compared to those containing I^-. In contrast, the free-OH band intensity for Na^+ is approximately double that for I^- for clusters with 36 water molecules,[16] indicating that the structure of water at the surface of the smaller nanodrops depends more strongly on the ion polarity. The similarity of the spectra with ∼250 water molecules is consistent with the polarity of the ion having a negligible effect on the transition intensities or the H-bonding network for the majority of water molecules in these larger nanodrops.

Ions of opposite polarity tend to orient water molecules that coordinate directly to the ions differently. Weakly interacting ions, such as tetramethylammonium, have only a small effect on the orientation of solvating water molecules.[32] For most cations, adjacent water molecules align so that the OH groups point away from the ion whereas for anions, the H atoms generally interact with the anion or oxygen atoms of other water molecules so that the OH groups point inwards, or are at least tangent to the ion. This difference in hydration orientation can cause substantial differences in the IRPD spectra of many small hydrated cation and anion clusters, especially in the free-OH spectral region. A free OH-band occurs for cations at all cluster sizes. In contrast, there is no free-OH band for many smaller hydrated anion clusters, including I^-, Cl^-, and Br^- with three water molecules.[40] For sulfate dianion, no free-OH band is observed with up to 43 water molecules indicating that this ion can affect the structure of water well past the first and second solvent shells.[15] Although differences in the H-bonding structure of water may persist past the first and even second solvent shells for nanodrops containing Na^+ and I^- as well, any differences for the majority of water molecules in clusters with 250 water molecules are small.

9.3.7 Spectra of Hydrated Divalent Ions.

In contrast to the results for the monovalent ions, there are significant spectral differences between the IRPD spectra of $Ca^{2+}(H_2O)_{\sim 250}$ and $SO_4{}^{2-}(H_2O)_{\sim 250}$ (**Figure 4**). For Ca^{2+},

the free-OH band intensity is ∼2× greater than that for SO_4^{2-}. Assuming that the polarity of the ion has little effect on the transition dipoles moments of the surface water molecules, as appears to be the case for the singly charged ions, the greater intensity of this band for Ca^{2+} indicates that there are significantly more free-OH groups at the surface compared to droplets containing SO_4^{2-}. Structures obtained from the molecular dynamics simulations are consistent with these results. Based on 1000 calculated structures for each hydrated ion, ∼5% of OH groups in nanodrops with SO_4^{2-} are free-OH groups whereas this number is ∼10% for Ca^{2+}, consistent with the ∼2× more intense free-OH band in the IRPD spectrum of $Ca^{2+}(H_2O)_{\sim 250}$ compared to that for $SO_4^{2-}(H_2O)_{\sim 250}$.

There are also significant differences in the H-bonded region of the spectra for these two ions. For SO_4^{2-}, the dissociation intensity at ∼3480 cm^{-1} is ∼50% greater than the intensity at ∼3300 cm^{-1} whereas the intensities for Ca^{2+} at these energies are within 5% of each other. To confirm the differences in band intensities obtained from the spectral fits, accurate photodissociation rate constants for these two ions were measured at 3340 cm^{-1} and 3475 cm^{-1} (Figure 8). Dissociation rate constants (k_{3340}, k_{3475}, k_{BIRD}) are obtained from linear fits to the dissociation data measured for irradiation times up to 1.25 s (Table 2). Laser-induced dissociation rate constants are determined by subtracting the BIRD rate constant k_{BIRD} from the photodissociation rate constants, k_{3340} and k_{3475}. Consistent with the analysis based on the Gaussian fits to the IRPD spectra, the laser-induced dissociation rate constant at 3475 cm^{-1} for SO_4^{2-} is ∼2× greater than that at 3340 cm^{-1}. For Ca^{2+}, the laser-induced dissociation rate constant at 3475 cm^{-1} is within 5% of the value for 3340 cm^{-1}.

The differences observed in the H-bonded region indicates that the structure of water in the interior of the droplets differs when the nanodrop contains SO_4^{2-} vs. Ca^{2+}. For cations, the red-shift in the centroid of the fully H-bonded feature indicates greater polarization of the interior water molecules with increasing charge state. However, the spectra for I^- and SO_4^{2-} indicate the opposite trend and the faster dissociation at ∼3480 cm^{-1} for SO_4^{2-} indicates an increased population of more weakly H-bonded water molecules relative to those in the Ca^{2+} hydrated clusters. This difference is likely due to the competition between ion-induced water patterning and intrinsic water-water interactions. For cations, both the ion-induced patterning and intrinsic water-water interactions orient water molecules such that OH groups tend to point away from the ion. However, as indicated by the increasing free-OH band intensity with increasing cluster size in IRPD spectra of SO_4^{2-} clusters with ∼43 – 80 water molecules,[15] anion-induced patterning of water molecules competes with the intrinsic water-water interactions, orienting molecules close to the ion such that the OH groups point inward. This competition may result in a strain on the H-bond network and a larger population of more weakly H-bonded water molecules for anions with extensive ion-induced water patterning.

9.3.8 Hydrated Trivalent Ions.

Although nanodrops containing positively charged trivalent ions that exist in bulk solution can be readily formed and probed with IRPD spectroscopy, nanodrops containing small

trivalent anions have not yet been observed. Thus, we are unable to directly compare the IRPD spectra of trivalent ions of opposite polarity. However, we can draw some conclusions about the effects of ion valency from the comparison of the IRPD spectra of $La^{3+}(H_2O)_{\sim 250}$ with those of the other ions. The free-OH band for La^{3+} is the most intense of any of the ions (Figure 3), consistent with this cluster having the largest number of water molecules with a free-OH stretch. The total integrated area (A_{total}) over both the bonded and free O-H stretch regions for La^{3+} is greater than that for the monovalent ions and for Ca^{2+}, but is close to that for $SO_4{}^{2-}$ (Figure 5). For hydrated La^{3+} clusters, the water molecules are more tightly bound than for Na^+ at equivalent cluster size. However, A_{total} for La^{3+} is greater than for Na^+, the opposite of the order expected based on the slightly lower water binding energy for Na^+. This indicates that the difference in A_{total} may be the result of differences in the H-bonding network of water molecules in these clusters. At some cluster size, the interactions between the majority of water molecules should not depend on the identity of the ion in the cluster. The similarity of the IRPD spectra of $M(H_2O)_{\sim 250}$, M = Na^+ and I^- indicates that the majority of water molecules are not significantly affected by these ions whereas the spectra for M = La^{3+}, Ca^{2+}, and $SO_4{}^{2-}$ indicate that much larger water clusters are required for this to be the case for multivalent ions.

9.4 Conclusions

The IRPD spectra of aqueous nanodrops consisting of ∼250 water molecules and either $SO_4{}^{2-}$, I^-, Na^+, Ca^{2+} or La^{3+} were measured to determine the effect of the ion on the H-bonded structure of water both in the interior of the droplet and at the droplet surface. Free-OH stretches corresponding to water molecules at the nanodrop surface that accept two H-bonds and donate a single H-bond red-shift with increasingly positive charge, consistent with a Stark effect as a result of the ion's electric field at the droplet surface. A small difference between this Stark shift for droplets containing anions compared to those that contain cations is consistent with a subtle difference in the orientation of water molecules at the surface of the nanodrops containing ions of opposite polarity. A clear trend in increasing intensity of this peak with increasing positive charge on the nanodrop is consistent with more water molecules with free-OH stretches at the surfaces of the more positively charged nanodrops.

The spectra of nanodrops with Na^+ and I^- are very similar, which indicates that the H-bonding network of the majority of water molecules is very similar for these monovalent ions despite differences that likely exist in the first and possibly second solvation shells. In contrast, the IRPD spectra of nanodrops containing $SO_4{}^{2-}$ and Ca^{2+} are significantly different both in the free-OH stretch region and in the H-bonding region. These results indicate that these divalent ions can affect not only the H-bonding network of water molecules in the interior, but also at the surface of the droplet itself. The number of water molecules in the first solvation shell of either ion is relatively small compared to the overall number of water molecules. In addition, the differences in the H-bonding region occurs in the higher frequency region of the spectrum where inner shell water molecules should not contribute significantly. Thus, these results provide compelling evidence that these ions affect the

structure of fully H-bonded water molecules well past the first solvation shell.

In contrast to conclusions from many other studies, these results indicate that ions can have a significant and readily measured effect on the structure of water, even for water molecules that are remote from the ion. Although our earlier studies showed that SO_4^{2-} can significantly affect the structure of water at the surface of droplets with as many as 43 water molecules,[15] which is well past the second solvation shell, this effect is expected to be mitigated in dilute bulk solution because of H-bonding to other water molecules that are even more remote from the ion. The results here for clusters with $\sim$250 water molecules show that the H-bonding network of water molecules in the second or even third solvation shell that are fully H-bonded, *as they would be in bulk solution*, are also affected. These results provide new insights into ion hydration and how ions may affect various physical properties, including Hofmeister effects.

These are the largest mass selected ionic clusters for which IRPD spectra have been reported to date. Additional studies on even larger ion-containing nanodrops made possible by the higher magnetic field strength of the FT/ICR apparatus should provide even more detailed information about ion-water interactions. For example, what is the size of a nanodrop where ions no longer measurably affect the H-bonding structure of surface water molecules? How does the presence of a counter-ion in the nanodrop affect the H-bonding network of water? We anticipate the answers to these and many other interesting questions will be forthcoming.

9.5 References

(1) Hofmeister, F. *Archiv for Experimentelle Pathologie und Pharmakologie* **1888**, *24*, 247-260.

(2) Hofmeister, F. *Arch. Exp. Pathol. Pharmacol.* **1888**, *24*, 247-260.

(3) Kunz, W.; Henle, J.; Ninham, B. W. *Curr. Opin. Colloid Interface Sci.* **2004**, *9*, 19-37.

(4) Collins, K. D. *Biophys. J.* **1997**, *72*, 65-76.

(5) Schott, H. *J. Colloid Interface Sci.* **1973**, *43*, 150-155.

(6) Grigorjev, P. A.; Bezrukov, S. M. *Biophys. J.* **1994**, *67*, 2265-2271.

(7) Uejio, J. S.; Schwartz, C. P.; Duffin, A. M.; Drisdell, W. S.; Cohen, R. C.; Saykally, R. J. *Proc. Natl. Acad. Sci. U. S. A.* **2008**, *105*, 6809-6812.

(8) Freire, M. G.; Neves, C. M. S. S.; Silva, A. M. S.; Santos, L. M. N. B. F.; Marrucho, I. M.; Rebelo, L. P. N.; Shah, J. K.; Maginn, E. J.; Coutinho, J. A. P. *J. Phys. Chem. B* **2010**, *114*, 2004-2014.

(9) Chen, X.; Yang, T.; Kataoka, S.; Cremer, P. S. *J. Am. Chem. Soc.* **2007**, *129*, 12272-12279.

(10) Algaer, E. A.; van der Vegt, N. F. A. *J. Phys. Chem. B* **2011**, *115*, 13781-13787.

(11) Smith, J. D.; Saykally, R. J.; Geissler, P. L. *J. Am. Chem. Soc.* **2007**, *129*, 13847-13856.

(12) Lin, Y. S.; Auer, B. M.; Skinner, J. L. *J. Chem. Phys.* **2009**, *131*, 144511.

(13) Collins, K. D. *Methods* **2004**, *34*, 300-311.

(14) Pegram, L. M.; Record, M. T. *J. Phys. Chem. B* **2007**, *111*, 5411-5417.

(15) O'Brien, J. T.; Prell, J. S.; Bush, M. F.; Williams, E. R. *J. Am. Chem. Soc.* **2010**, *132*, 8248-8249.

(16) Prell, J. S.; O'Brien, J. T.; Williams, E. R. *J. Am. Chem. Soc.* **2011**, *133*, 4810-4818.

(17) Flick, T. G.; Merenbloom, S. I.; Williams, E. R. *J. Am. Soc. Mass Spectrom.* **2011**, *22*, 1968-1977.

(18) Baldwin, R. L. *Biophys. J.* **1996**, *71*, 2056-2063.

(19) Cacace, M. G.; Landau, E. M.; Ramsden, J. J. *Q. Rev. Biophys.* **1997**, *30*, 241-277.

(20) Cheng, J.; Vecitis, C. D.; Hoffmann, M. R.; Colussi, A. J. *J. Phys. Chem. B* **2006**, *110*, 25598-25602.

(21) Omta, A. W.; Kropman, M. F.; Woutersen, S.; Bakker, H. J. *J. Chem. Phys.* **2003**, *119*, 12457-12461.

(22) Omta, A. W.; Kropman, M. F.; Woutersen, S.; Bakker, H. J. *Science* **2003**, *301*, 347-349.

(23) Tielrooij, K. J.; Garcia-Araez, N.; Bonn, M.; Bakker, H. J. *Science* **2010**, *328*, 1006-1009.

(24) Tielrooij, K. J.; van der Post, S. T.; Hunger, J.; Bonn, M.; Bakker, H. J. *J. Phys. Chem. B* **2011**, *115*, 12638-12647.

(25) Liu, D. F.; Ma, G.; Levering, L. M.; Allen, H. C. *J. Phys. Chem. B* **2004**, *108*, 2252-2260.

(26) Gopalakrishnan, S.; Jungwirth, P.; Tobias, D. J.; Allen, H. C. *J. Phys. Chem. B* **2005**, *109*, 8861-8872.

(27) Jungwirth, P. *Faraday Discuss.* **2009**, *141*, 9-30.

(28) Donald, W. A.; Leib, R. D.; Demireva, M.; O'Brien, J. T.; Prell, J. S.; Williams, E. R. *J. Am. Chem. Soc.* **2009**, *131*, 13328-13337.

(29) Griffin, G. B.; Young, R. M.; Ehrler, O. T.; Neumark, D. M. *J. Chem. Phys.* **2009**, *131*, 194302.

(30) Donald, W. A.; Leib, R. D.; Demireva, M.; Negru, B.; Neumark, D. M.; Williams, E. R. *J. Phys. Chem. A* **2011**, *115*, 2-12.

(31) Mizuse, K.; Mikami, N.; Fujii, A. *Angew. Chem.-Int. Edit.* **2010**, *49*, 10119-10122.

(32) Prell, J. S.; Williams, E. R. *J. Am. Chem. Soc.* **2009**, *131*, 4110-4119.

(33) Chang, H. C.; Wang, Y. S.; Lee, Y. T. *Int. J. Mass Spectrom.* **1998**, *180*, 91-102.

(34) Choi, J. H.; Kuwata, K. T.; Cao, Y. B.; Okumura, M. *J. Phys. Chem. A* **1998**, *102*, 503-507.

(35) Headrick, J. M.; Diken, E. G.; Walters, R. S.; Hammer, N. I.; Christie, R. A.; Cui, J.; Myshakin, E. M.; Duncan, M. A.; Johnson, M. A.; Jordan, K. D. *Science* **2005**, *308*, 1765-1769.

(36) Iino, T.; Ohashi, K.; Inoue, K.; Judai, K.; Nishi, N.; Sekiya, H. *J. Chem. Phys.* **2007**, *126*, 194302.

(37) Miller, D. J.; Lisy, J. M. *J. Am. Chem. Soc.* **2008**, *130*, 15381-15392.

(38) Miyazaki, M.; Fujii, A.; Ebata, T.; Mikami, N. *Science* **2004**, *304*, 1134-1137.

(39) Nicely, A. L.; Miller, D. J.; Lisy, J. M. *J. Mol. Spectrosc.* **2009**, *257*, 157-163.

(40) Robertson, W. H.; Johnson, M. A. *Annu. Rev. Phys. Chem.* **2003**, *54*, 173-213.

(41) Shin, J. W.; Hammer, N. I.; Diken, E. G.; Johnson, M. A.; Walters, R. S.; Jaeger, T. D.; Duncan, M. A.; Christie, R. A.; Jordan, K. D. *Science* **2004**, *304*, 1137-1140.

(42) Walters, R. S.; Pillai, E. D.; Duncan, M. A. *J. Am. Chem. Soc.* **2005**, *127*, 16599-16610.

(43) Ayotte, P.; Bailey, C. G.; Weddle, G. H.; Johnson, M. A. *J. Phys. Chem. A* **1998**, *102*, 3067-3071.

(44) Ayotte, P.; Weddle, G. H.; Bailey, C. G.; Johnson, M. A.; Vila, F.; Jordan, K. D. *J. Chem. Phys.* **1999**, *110*, 6268-6277.

(45) Beck, J. P.; Lisy, J. M. *J. Chem. Phys.* **2011**, *135*, 044302.

(46) Cabarcos, O. M.; Weinheimer, C. J.; Lisy, J. M.; Xantheas, S. S. *J. Chem. Phys.* **1999**, *110*, 5-8.

(47) Bandyopadhyay, B.; Duncan, M. A. *Chem. Phys. Lett.* **2012**, *530*, 10-15.

(48) Carnegie, P. D.; Bandyopadhyay, B.; Duncan, M. A. *J. Phys. Chem. A* **2008**, *112*, 6237-6243.

(49) Carnegie, P. D.; Bandyopadhyay, B.; Duncan, M. A. *J. Chem. Phys.* **2011**, *134*, 014302.

(50) Carnegie, P. D.; Bandyopadhyay, B.; Duncan, M. A. *J. Phys. Chem. A* **2011**, *115*, 7602-7609.

(51) Bush, M. F.; O'Brien, J. T.; Prell, J. S.; Wu, C. C.; Saylkally, R. J.; Williams, E. R. *J. Am. Chem. Soc.* **2009**, *131*, 13270-13277.

(52) Bush, M. F.; Saykally, R. J.; Williams, E. R. *ChemPhysChem* **2007**, *8*, 2245-2253.

(53) Bush, M. F.; Saykally, R. J.; Williams, E. R. *J. Am. Chem. Soc.* **2007**, *129*, 2220-2221.

(54) Bush, M. F.; Saykally, R. J.; Williams, E. R. *J. Am. Chem. Soc.* **2008**, *130*, 15482-15489.

(55) Cooper, T. E.; O'Brien, J. T.; Williams, E. R.; Armentrout, P. B. *J. Phys. Chem. A* **2010**, *114*, 12646-12655.

(56) O'Brien, J. T.; Williams, E. R. *J. Phys. Chem. A* **2008**, *112*, 5893-5901.

(57) O'Brien, J. T.; Williams, E. R. *J. Phys. Chem. A* **2011**, *115*, 14612-14619.

(58) Bush, M. F.; Saykally, R. J.; Williams, E. R. *J. Am. Chem. Soc.* **2008**, *130*, 9122-9128.

(59) Bush, M. F.; O'Brien, J. T.; Prell, J. S.; Saykally, R. J.; Williams, E. R. *J. Am. Chem. Soc.* **2007**, *129*, 1612-1622.

(60) Prell, J. S.; O'Brien, J. T.; Williams, E. R. *J. Am. Soc. Mass Spectrom.* **2010**, *21*, 800-809.

(61) Schriver-Mazzuoli, L.; Schriver, A.; Hallou, A. *J. Mol. Struct.* **2000**, *554*, 289-300.

(62) Manka, A.; Pathak, H.; Tanimura, S.; Wolk, J.; Strey, R.; Wyslouzil, B. E. *Phys. Chem. Chem. Phys.* **2012**, *14*, 4505-4516.

(63) Du, Q.; Superfine, R.; Freysz, E.; Shen, Y. R. *Phys. Rev. Lett.* **1993**, *70*, 2313-2316.

(64) Du, Q.; Freysz, E.; Shen, Y. R. *Science* **1994**, *264*, 826-828.

(65) Tian, C. S.; Shen, Y. R. *Chem. Phys. Lett.* **2009**, *470*, 1-6.

(66) Yang, M.; Skinner, J. L. *Phys. Chem. Chem. Phys.* **2010**, *12*, 982-991.

(67) Donald, W. A.; Williams, E. R. *J. Phys. Chem. A* **2008**, *112*, 3515-3522.

(68) Buch, V.; Bauerecker, S.; Devlin, J. P.; Buck, U.; Kazimirski, J. K. *Int. Rev. Phys. Chem.* **2004**, *23*, 375-433.

(69) Ji, N.; Ostroverkhov, V.; Tian, C. S.; Shen, Y. R. *Phys. Rev. Lett.* **2008**, *100*, 096102.

(70) Raymond, E. A.; Richmond, G. L. *J. Phys. Chem. B* **2004**, *108*, 5051-5059.

9.6 Tables and Figures

	SO_4^{2-}	I^-	Na^+	Ca^{2+}	La^{3+}
Band 1					
Frequency (cm^{-1})	3330 ± 6	3281 ± 11	3256 ± 14	3305 ± 7	3314 ± 5
Intensity (s^{-1} W^{-1})	0.227 ± 0.005	0.171 ± 0.005	0.162 ± 0.006	0.246 ± 0.004	0.258 ± 0.004
Width (cm^{-1})	191 ± 7	163 ± 11	165 ± 14	185 ± 8	197 ± 7
Band 2					
Frequency (cm^{-1})	3482.4 ± 1.7	3464 ± 4	3459 ± 7	3481 ± 3	3487 ± 2
Intensity (s^{-1} W^{-1})	0.18 ± 0.01	0.18 ± 0.02	0.17 ± 0.02	0.12 ± 0.01	0.13 ± 0.01
Width (cm^{-1})	81 ± 4	98 ± 5	112 ± 6	83 ± 6	72 ± 6
Band 3					
Frequency (cm^{-1})	3704.5 ± 0.8	3702.5 ± 0.7	3698.6 ± 0.7	3697.8 ± 0.4	3697.1 ± 0.3
Intensity (s^{-1} W^{-1})	0.044 ± 0.005	0.046 ± 0.005	0.060 ± 0.006	0.089 ± 0.005	0.126 ± 0.007
Width (cm^{-1})	9 ± 1	9 ± 1	9 ± 1	8.1 ± 0.5	7.7 ± 0.5

Table 9.1: Parameters of Gaussian lineshapes fit to IRPD spectra for $M(H_2O)_{\sim 250}$. Error values are calculated from the scatter of the experimental data about the fitted lineshapes.

$M(H_2O)_{\sim 250}$	k_{3475} (s^{-1})	k_{3340} (s^{-1})	k_{BIRD} (s^{-1})
Ca^{2+}	9.4 ± 0.3	9.1 ± 0.5	1.04 ± 0.03
$SO_4{}^{2-}$	11.1 ± 0.7	6.3 ± 0.3	1.13 ± 0.01

Table 9.2: Dissociation rate constants (s^{-1}) for $Ca^{2+}(H_2O)_{\sim 250}$ and $SO_4{}^{2-}(H_2O)_{\sim 250}$

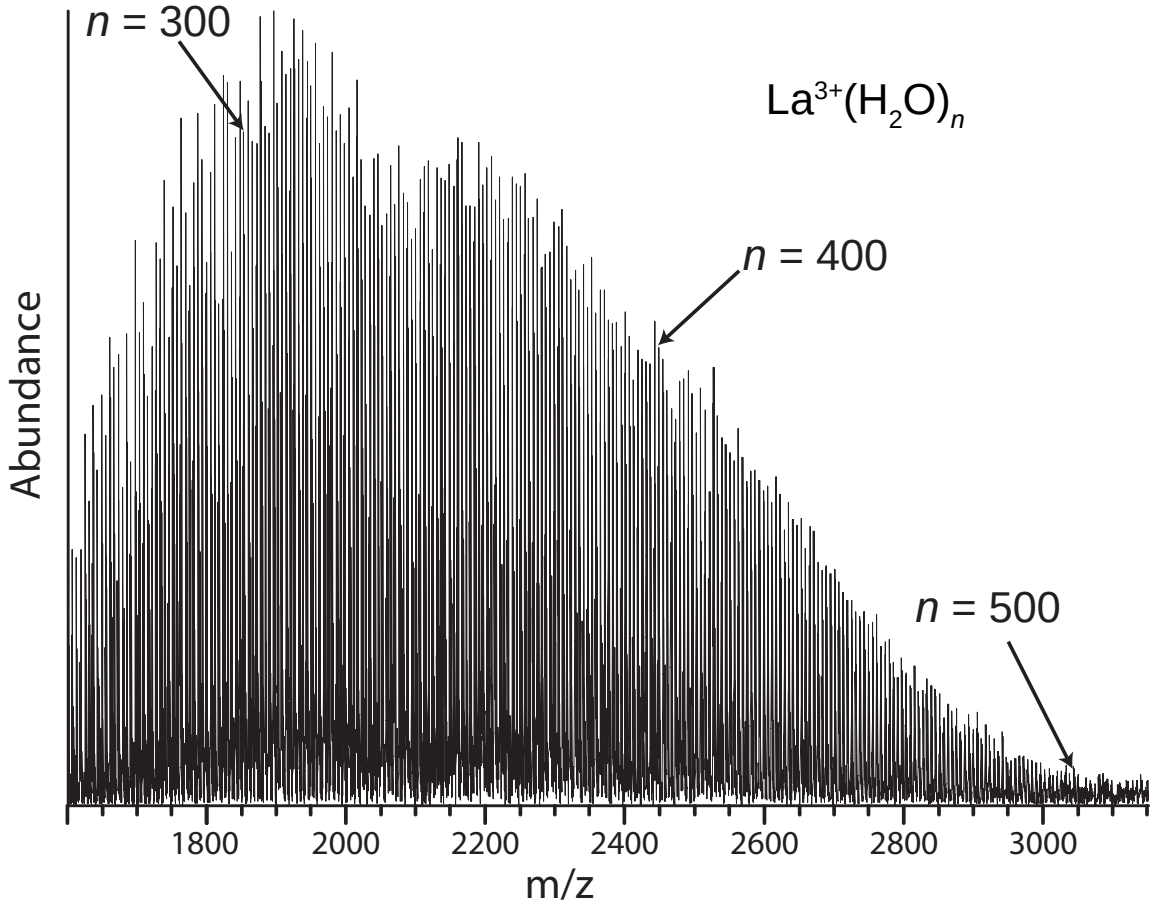

Figure 9.1: Representative electrospray ionization mass spectrum of a 4 mM aqueous $LaCl_3$ solution with the copper jacket surrounding the ion cell at 133 K. $La^{3+}(H_2O)_n$ nanodrops with $\sim$250 – 500 water molecules are observed.

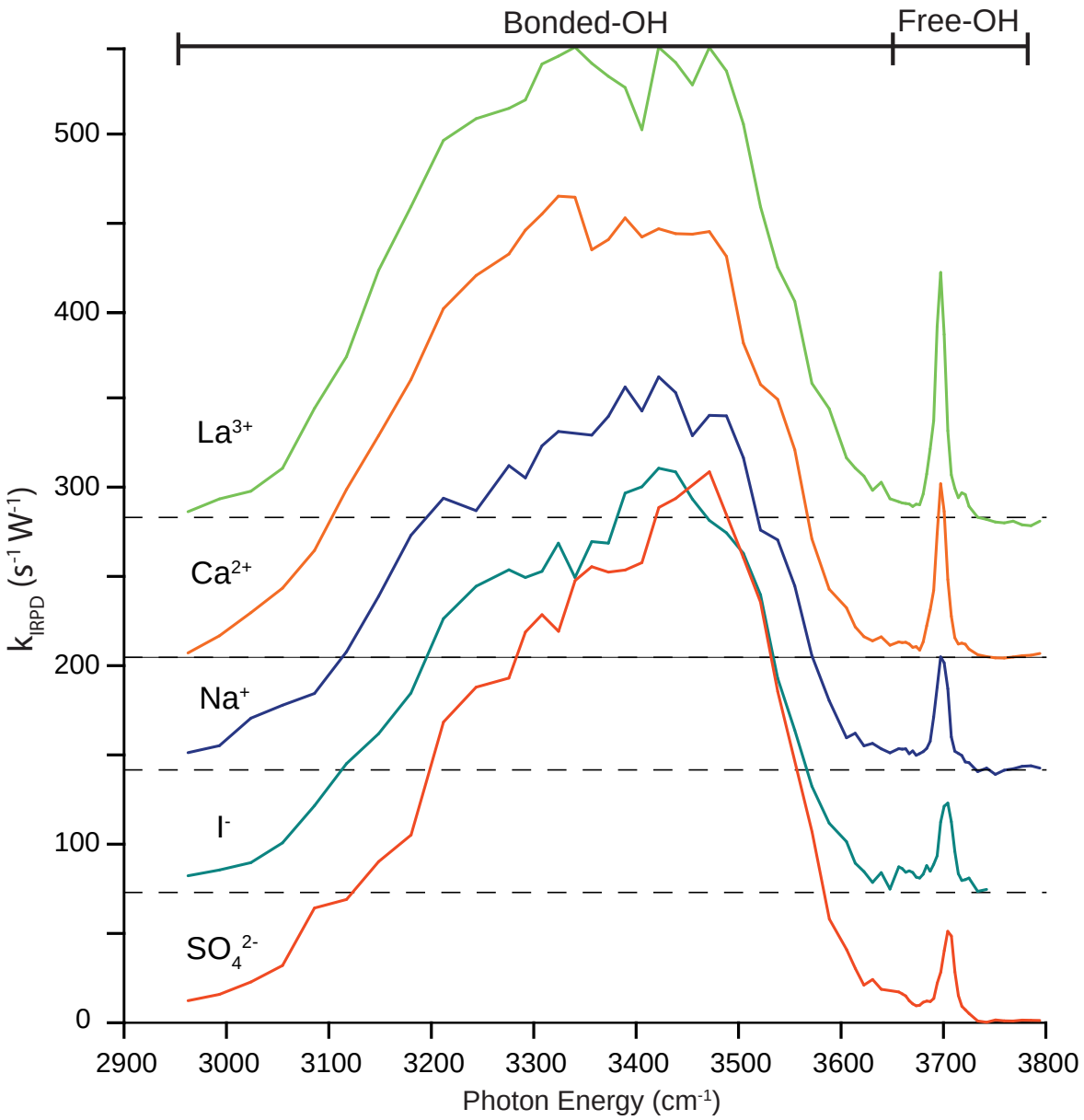

Figure 9.2: Ensemble IRPD spectra of $M(H_2O)_{\sim 250}$, M = La^{3+}, Ca^{2+}, Na^{+}, I^{-}, and SO_4^{2-} at 133 K.

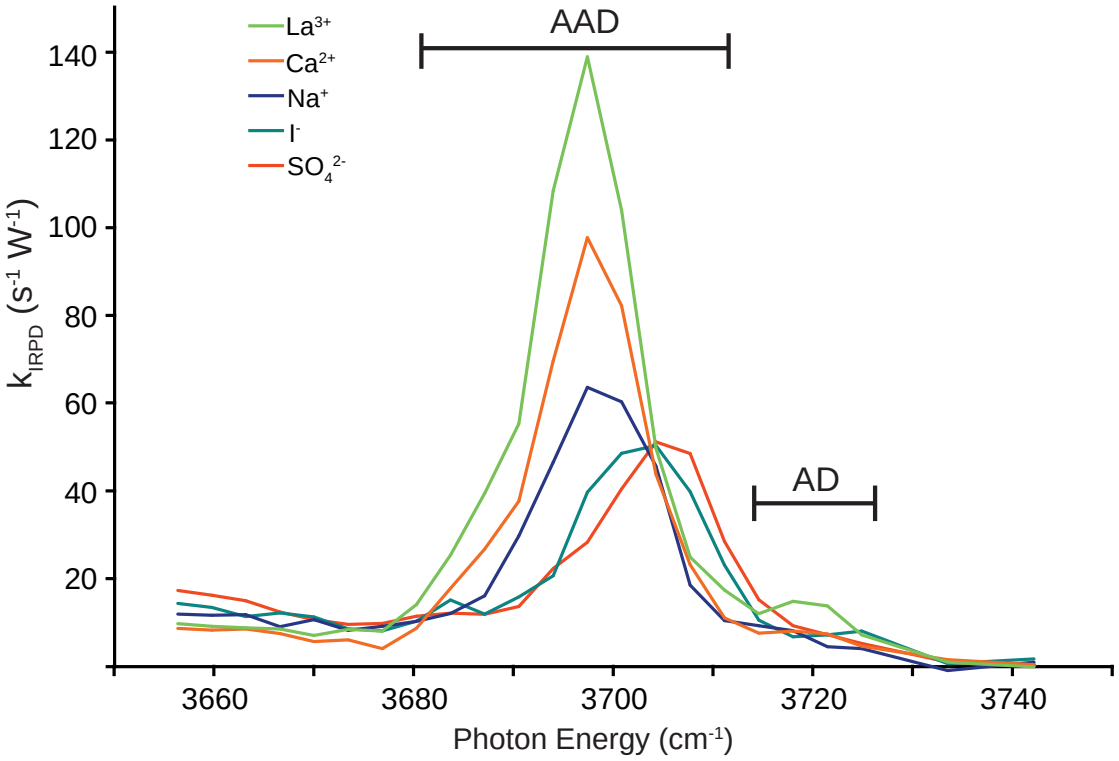

Figure 9.3: Ensemble IRPD spectra in the free-OH region for $M(H_2O)_{\sim 250}$, M = La^{3+}, Ca^{2+}, Na^{+}, I^{-}, and SO_4^{2-} at 133 K.

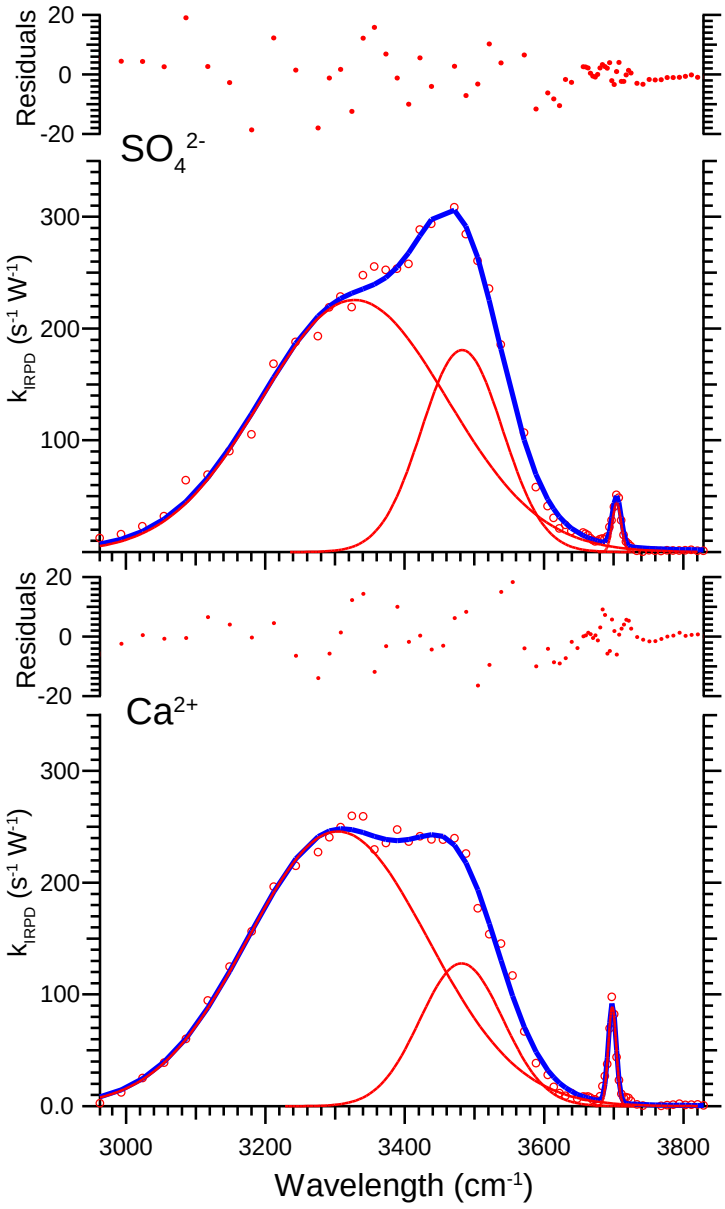

Figure 9.4: IRPD spectra of $M(H_2O)_{\sim 250}$, M = Ca^{2+}, and $SO_4{}^{2-}$ with fitted Gaussian lineshapes and the residual values between the total fit and the experimental data.

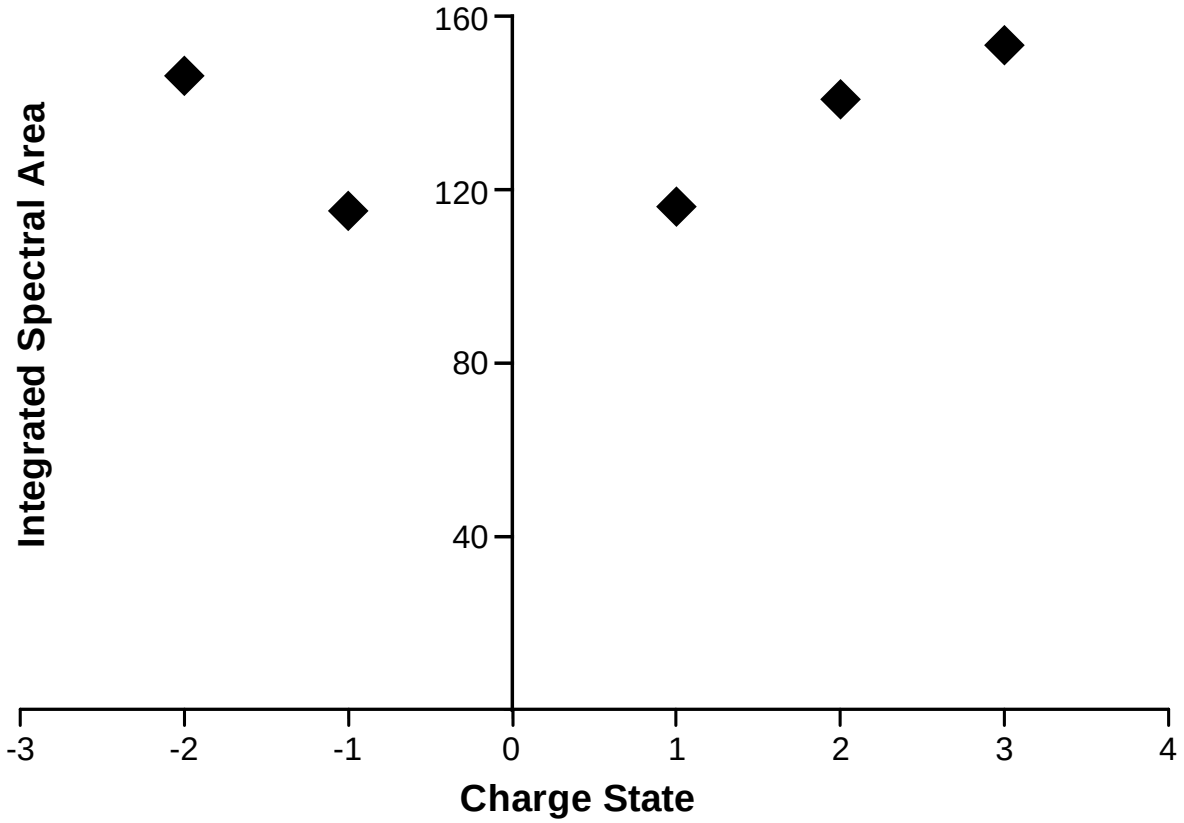

Figure 9.5: Integrated spectral areas from the ensemble IRPD spectra of $M(H_2O)_{\sim 250}$, M = La^{3+}, Ca^{2+}, Na^{+}, I^{-}, and SO_4^{2-} versus ion charge state.

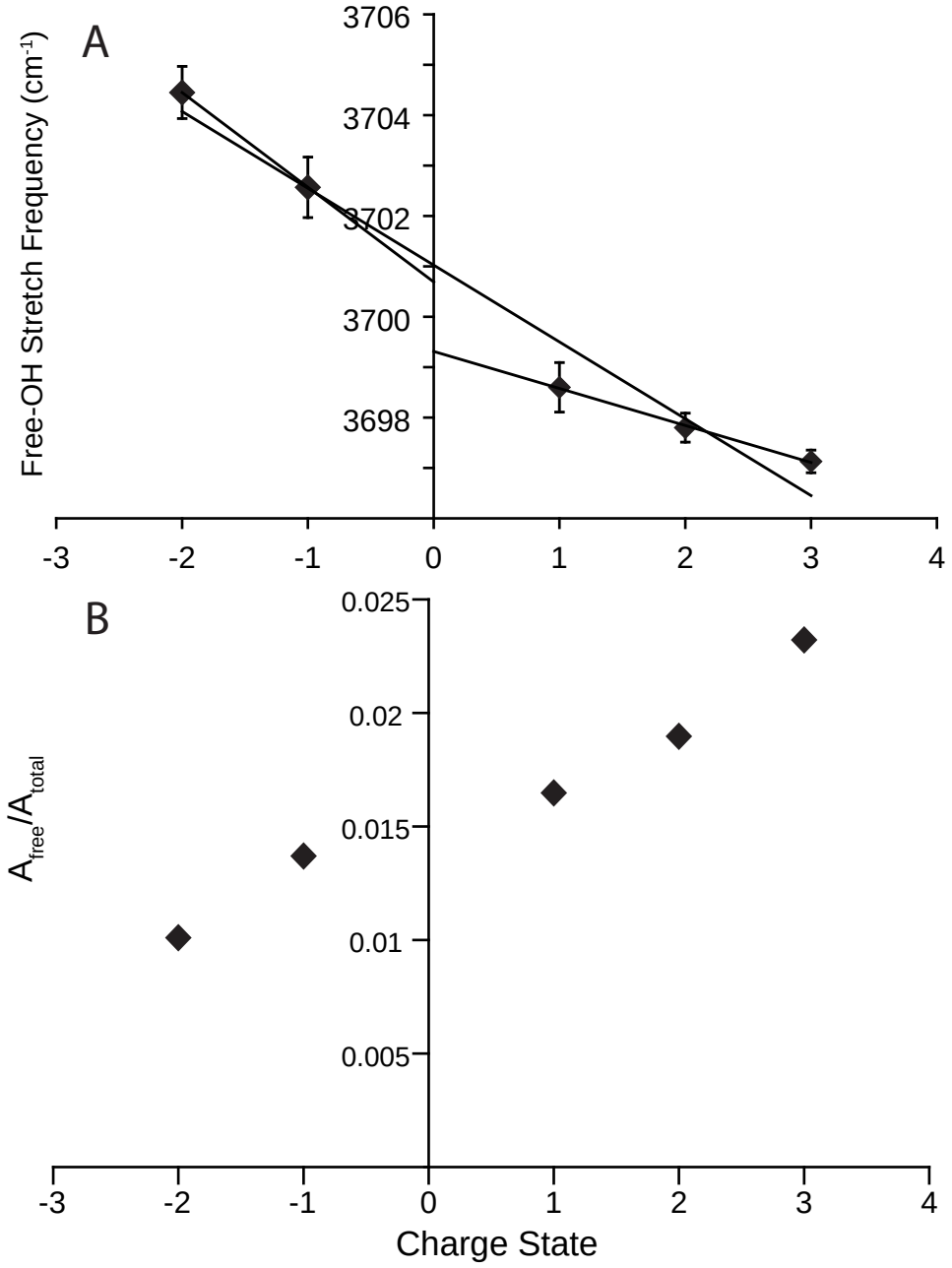

Figure 9.6: (A) Ratios of the free-OH integrated area (A_{free}) to total integrated area (A_{total}) from the ensemble IRPD spectra of $M(H_2O)_{\sim 250}$, M = La^{3+}, Ca^{2+}, Na^{+}, I^{-}, and SO_4^{2-} versus ion charge state. (B) Free-OH stretch frequencies from the ensemble IRPD spectra of $M(H_2O)_{\sim 250}$, M = La^{3+}, Ca^{2+}, Na^{+}, I^{-}, and SO_4^{2-} versus ion charge state. The R-squared values for the fits of the cation and total data sets are 0.9974 and 0.9651, respectively.

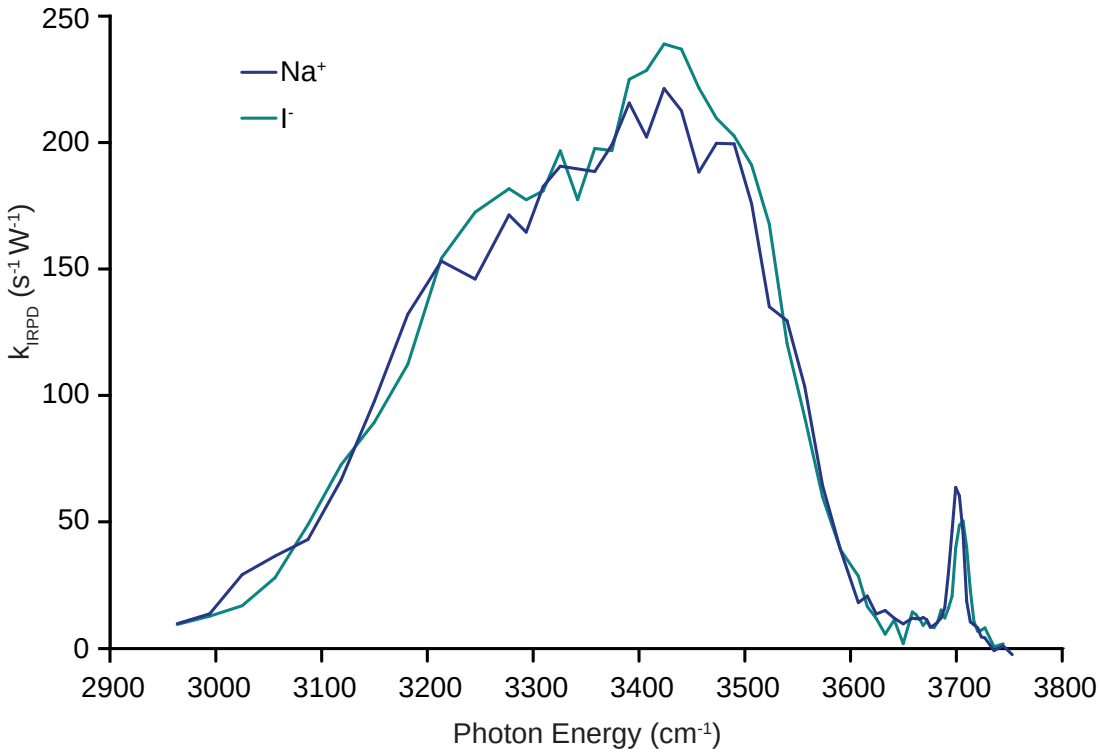

Figure 9.7: Overlay of the ensemble IRPD spectra of $M(H_2O)_{\sim 250}$, M = Na^+, and I^- at 133 K.

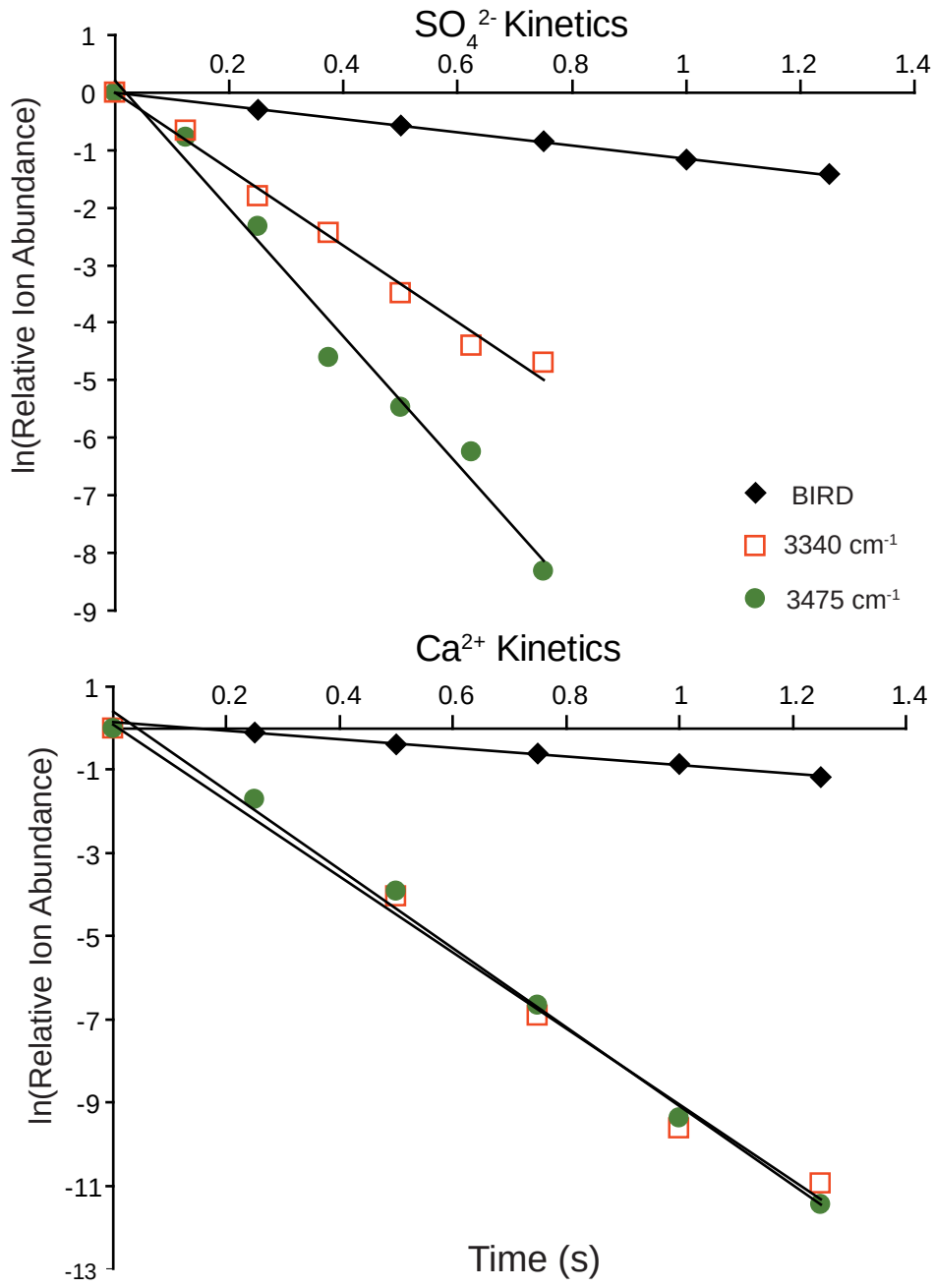

Figure 9.8: BIRD and laser photodissociation data at ∼3340 and 3475 cm^{-1} for $SO_4^{2-}(H_2O)_{\sim 250}$ and $Ca^{2+}(H_2O)_{\sim 250}$ at 133 K.

Chapter 10

Summary and Future Work

This research investigated the effects of non-covalent interactions on the structure and reactivity of ion-biomolecule and ion-water complexes. In Chapter 2, the effects of electron kinetic energy on the internal energy deposited into hydrated ions during ECD experiments was investigated. Varying the electric potential of a heated metal cathode to control the kinetic energy of the generated electrons had no measured effect on the internal energy deposited into ions under typical ECD experimental conditions. These results suggest that some small fraction of electrons are generated with near zero kinetic energy relative to the ions in the cell and so have significantly greater capture cross-sections. It is capture of these low-energy electrons that results in the observed ECD products. Ion nanocalorimetry is a highly sensitive method for determining how much internal energy is deposited into ions upon activation and these results help improve the accuracy with which these values can be obtained for ECD experiments.

In Chapter 3, the structures and reactivities of proton-bound dimers consisting of valine and basic primary and secondary amines were investigated using IRMPD spectroscopy and CID. The spectra indicate a transition in structure with increasing basicity of the amine and that for some of the complexes, an intramolecular hydrogen bond stabilizes a structure where the proton is not shared with the most basic site of valine. This suggests that for some amino acids, their structure in protonated dimers may be different than in isolation which breaks an assumption made in the determination of gas-phase basicities using the kinetic method.

In Chapter 4, the role of gas-phase acidity on the relative zwitterion stabilities of Asp and Glu were investigated using IRMPD spectroscopy and theory. For protonated, lithiated, and cesiated species, both amino acids are nonzwitterionic, whereas with Ca^{2+} and Ba^{2+}, Glu is zwitterionic. Based on comparisons to results for cationized Gln, these experiments indicate that the relative zwitterionic stability is not directly related to gas-phase acidity for these cationized amino acids. In Chapter 5, the role of anions and the effects of halide ion size on zwitterion stability were investigated for Glu, His and Arg. The IRMPD spectra of these amino acids complexed with Cl^-, Br^-, and I^- indicate that both Glu and His are predominantly nonzwitterionic with all three halide ions and whereas Arg is zwitterionic. The coordination of cations to these amino acids is different from anions, resulting in a favorable alignment of the carbonyl stretch dipole moment with the electric field of ions of either polarity causing a redshift in this band, i.e., a Stark shift.

In Chapters 6 and 7, the coordination numbers of hydrated divalent transition metals and the effect of Jahn-Teller distortion on the hydration of Cu^{2+} were investigated with IRPD spectroscopy. The d^9 electronic structure of Cu^{2+} which leads to Jahn-Teller distortion effects observed in bulk solutions also significantly affects the hydration of the metal ion in gas-phase clusters. Based on IRPD of small hydrated clusters, the CN of Cu^{2+} is 4 whereas Mn^{2+}, Fe^{2+}, Co^{2+} and Ni^{2+} have CN > 5 and for Zn^{2+}, CN $= 5$. Interestingly, the trend in average CN for these metal ions correlates with the trend in charge separation propensity and the aqueous hydrolysis constants. This indicates a close relationship between the gas-phase hydration of these metal ions and their hydration in aqueous solution.

Anions orient water molecules differently than cations and the extent of this patterning effect was investigated for hydrated SO_4^{2-} in Chapter 8. IRPD spectra of hydrated SO_4^{2-}

with up to 43 water molecules attached have no clear free-OH band indicating that structure induced by the dianion dominates over the intrinsic water-water interactions which orient water molecules such that surface free-OH groups are present. For the hydrated clusters with 43-80 water molecules, a small free-OH band grows in intensity with increasing cluster size indicating that even with 80 water molecules attached, the SO_4^{2-} ion plays a significant role in the structure of the hydrogen bonding network of the water molecules.

In Chapter 9, the effects of ion charge state on the structure of very large hydrated clusters ($\sim$250 water molecules), or nanodrops, was investigated. The free-OH stretch frequency of surface water molecules is a sensitive probe of the ion's electric field at the surface of these nanodrops. This frequency redshifts with increasingly positive charge of the ion, consistent with a Stark effect. A trend of increasing peak intensity with increasingly positive charge is also observed indicating that there are more water molecules with free-OH groups at the surface of the more positively charged nanodrops. In contrast to conclusions from other studies on bulk solutions, these results indicate that ions can have a significant effect on the structure of water molecules well past the first solvation shell and perhaps beyond the second and third solvation shells as well.

The nature of the effect of ions on structure of the hydrogen bonding network of water molecules was further investigated in Chapter 10 by examining the effects of cluster size on the IRPD spectra in the free-OH region of hydrated ions with ion charge 2- to 3+. The dependence of the free-OH frequency on cluster size appears to change at ~80 and ~100 water molecules for Ca^{2+} and La^{3+}, respectively. Plotting the free-OH band frequencies versus an approximation of $\frac{1}{r^2}$ for the hydrated clusters indicates two linear regions for the mulitvalent cations. These data are consistent with a change in the effective dielectric constant of the nanodrop. The patterning of the solvating water molecules may result in a low dielectric constant correlating with rapid change in the free-OH band frequency with increasing cluster size. However, above a certain cluster size, the free-OH band frequency changes only slowly. This suggests that beyond the range of the ion-induced patterning, water molecules adopt a less organized structure correlating with a high dielectric constant, similar to that of bulk water and proton-disordered forms of ice.

These experiments demonstrate the powerful capabilities of FT/ICR mass spectrometry combined with IR(M)PD spectroscopy and computational chemistry for investigating non-covalent interactions in the gas phase and for providing a bridge between gas-phase cluster ion measurements and solution phase behavior. Recent instrumentation upgrades have made possible experiments on even larger ion-containing nanodrops. Future work will utilize this capability to further investigate the roles of non-covalent interactions and the effects of ions on biomolecule and solvation structure.